Aus dem Adolf-Butenandt Institut der
Ludwig-Maximilians-Universität München
Lehrstuhl: Stoffwechselbiochemie

Vorstand: Prof. Dr. rer. nat. Dr. h.c. Christian Haass

Regulated Intramembrane Proteolysis of NRG1 Type III Mediates Postnatal Peripheral Myelination

Dissertation
zur Erlangung des Doktorgrades der Naturwissenschaften
an der Medizinischen Fakultät
der Ludwig-Maximilians-Universität München

Vorgelegt von

Daniel Fleck

aus Stuttgart

2014

Mit Genehmigung der Medizinischen Fakultät der Universität München

Betreuer: Prof. Dr. rer. nat. Dr. h.c. Christian Haass

Zweitgutachter: Prof. Dr. rer. nat. Gunnar Schotta

Dekan: Prof. Dr. med. Dr. h.c. Maximilian Reiser, FACR, FRCR

Tag der mündlichen Prüfung: 22.06.2015

II

Eidesstattliche Versicherung

Ich erkläre hiermit an Eides statt, dass ich die vorliegende Dissertation selbständig verfasst, mich außer der angegebenen keiner weiteren Hilfsmittel bedient und alle Erkenntnisse, die aus dem Schrifttum ganz oder annähernd übernommen sind, als solche kenntlich gemacht und nach ihrer Herkunft unter Bezeichnung der Fundstelle einzeln nachgewiesen habe.

Ich erkläre des Weiteren, dass die hier vorgelegte Dissertation nicht in gleicher oder in ähnlicher Form bei einer anderen Stelle zur Erlangung eines akademischen Grades eingereicht wurde.

San Francisco, den 03.09. 2014

(Daniel Fleck)

IV

"For a successful technology, reality must take precedence over public relations,

for nature cannot be fooled."

Richard Feynman

"Alles seit je. Nie was anderes. Immer versucht. Immer gescheitert. Einerlei.

Wieder versuchen. Wieder scheitern. Besser scheitern."

Samuel Beckett

Table of contents

Summary

Neuregulin-1 (NRG1) type III is a growth factor on the surface of neurons in the peripheral nervous system (PNS). It is required for initial myelination of nerves by Schwann cells after birth and for remyelination after injury. Neuregulin-1 type III is activated by cleavage (shedding) in its extracellular juxtamembrane region generating a membrane-bound N-terminal fragment (NTF) that contains a bioactive epidermal growth factor (EGF)-like domain. This domain signals to neighboring Schwann cells in a contact-dependent manner prompting the cells to initiate myelination. The β-site APP cleaving enzyme 1 (BACE1) was identified as the enzyme that cleaves NRG1 type III and promotes myelination. Consequently, loss of BACE1 cleavage results in dramatically reduced myelin sheaths around nerves in the PNS of BACE1 knockout mice.

Besides its role in myelination, BACE1, better known as β-secretase, is also involved in the generation of the neurotoxic amyloid β-peptide (Aβ) which is the main component of amyloid plaques in the brain of patients suffering from Alzheimer's disease (AD). The Aβ peptide is derived through sequential cleavage of the amyloid precursor protein APP, first by BACE1 in the extracellular domain and subsequently by the γ-secretase in the transmembrane domain (TMD). Inhibition of BACE1 and γ-secretase is therefore considered a promising therapeutic strategy for AD. However, this approach harbors the risk of mechanism-based side effects due to impaired processing of substrates beside APP such as NRG1 type III which is not only a substrate for BACE1 but like APP is also cleaved in its TMD by the γ-secretase. Adding another layer of complexity, ADAM10 and ADAM17, the so-called α-secretases of AD, also cleave NRG1 type III.

In the first part of this study, the proteolytic processing of NRG1 type III in its ectodomain was investigated in detail. The precise juxtamembrane shedding sites of BACE1, ADAM10 and ADAM17 were determined by mass spectrometry and two novel cleavage sites of BACE1 and ADAM17 N-terminal of the EGF-like domain were discovered. Cleavage at these novel sites by ADAM17 and BACE1 results in the secretion of the EGF-like domain from NRG1 type III as α-sEGF and β-sEGF, respectively. Using novel monoclonal antibodies generated against the identified cleavage sites the processing of NRG1 type III could also be confirmed in primary neurons. The soluble EGF-like domains were found to be functionally active and induced signaling pathways required for myelination in cultured Schwann cells. Furthermore, β-sEGF rescued the myelination deficit in the PNS of a zebrafish model lacking BACE1, thereby demonstrating its activity *in vivo*. Using cell culture and the zebrafish model

Summary

the effects of BACE1- and ADAM17-mediated shedding on the activity of the soluble EGF-like domains were carefully dissected. In contrast to published evidence, however, both the BACE1- as well as the ADAM17-shed sEGF were found to be equally active and to promote myelination *in vivo.* Together this suggests that NRG1 type III dependent myelination is not only controlled by membrane-retained NRG1 type III but also in a contact-independent manner via proteolytic liberation of the EGF-like domain.

The second part of this study investigates the processing of the C-terminal fragment (CTF) which remains after shedding of NRG1 type III. Intramembranous cleavage of the CTF by the γ-secretase was previously shown to release the NRG1 intracellular domain, which acts as transcriptional regulator of proteins involved in neuronal maturation and brain plasticity. Interestingly, a mutation within the TMD of NRG1 type III is associated with an increased risk of schizophrenia linking γ-secretase processing of NRG1 type III to this neurological disorder. Using a novel antibody against the N-terminus of the NRG1 CTF it was possible to detect a NRG1 β-peptide that is secreted during γ-secretase cleavage and could potentially serve as marker for this processing. Moreover, by means of mass spectrometry, the precise cleavage sites within the TMD of NRG1 could be identified. Strikingly, the ε-like cleavage site was found to be located exactly at the position of the schizophrenia-associated mutation providing a possible mechanism for the reported interference of this mutation with γ-secretase cleavage. The evidence presented unambiguously establishes NRG1 type III as a γ-secretase substrate and provides a basis for further investigation of the mechanisms which link its processing to the development of schizophrenia.

In summary and with regard to BACE1 and γ-secretase being prime targets for a potential AD therapy, the results of this work call for further careful investigation of the consequences of altered NRG1 type III signaling due to chronic treatment with inhibitors.

Zusammenfassung

Als Wachstumsfaktor auf der Oberfläche von Neuronen des peripheren Nervensystems (PNS) ist Neuregulin-1 (NRG1) Typ III nach der Geburt essentiell für die Ausbildung der die Nerven umgebenden Myelinscheiden durch Schwann-Zellen sowie zur Re-myelinisierung nach einer Verletzung. Hierfür wird NRG1 Typ III durch proteolytische Spaltung seiner extrazellulären Domäne (so genanntes Shedding) durch die Protease BACE1 (engl. β-site APP cleaving enzyme 1) aktiviert. Dabei entsteht ein membranständiges N-terminales Fragment (NTF), das in kontaktabhängiger Weise durch seine bioaktive, dem Epidermalen Wachstumsfaktor ähnliche (engl. epidermal growth factor, EGF) Domäne die Myelinisierung durch benachbarte Schwann-Zellen einleitet. Folglich führt der Verlust der BACE1-vermittelten Spaltung von NRG1 Type III in BACE1 Knockout-Mäusen zu stark reduzierten Myelinscheiden der peripheren Nerven.

Neben seiner Rolle bei der Myelinisierung ist BACE1, besser bekannt als β-Sekretase, auch an der Bildung des neurotoxischen Amyloid β Peptides (Aβ), Haupt-bestandteil der Amyloidplaques im Gehirn von Alzheimer-Patienten, beteiligt. Das Aβ Peptid entsteht durch die aufeinanderfolgende Spaltung des Amyloid-Vorläufer-Proteins APP (engl. amyloid precursor protein) erst durch BACE1 innerhalb der extrazellulären Domäne und anschließend durch die γ-Sekretase in der Transmembrandomäne (TMD). Die Hemmung von BACE1 und der γ-Sekretase gilt deshalb als vielversprechender Ansatz für die Therapie von Alzheimer. Allerdings könnte dies zu starken Nebenwirkungen führen, weil beispiels-weise NRG1 Typ III wie APP auch von BACE1, der γ-Sekretase sowie von ADAM10 und ADAM17, den α-Sekretasen der Alzheimer Krankheit, prozessiert wird.

Im ersten Teil dieser Studie wurde die proteolytische Prozessierung der Ektodomäne von NRG1 genauer untersucht. Mithilfe massenspektrometrischer Untersuchungen wurden die genauen Schnittstellen von BACE1, ADAM10 und ADAM17 in der extrazellulären membrannahen Region von NRG1 Typ III bestimmt und zusätzlich zwei neue Schnittstellen auf der N-terminalen Seite der EGF-ähnlichen Domäne identifiziert. Die proteolytische Spaltung von NRG1 Typ III durch ADAM17 und BACE1 an diesen zuvor unbekannten Stellen setzt die EGF-ähnliche Domäne von NRG1 Typ III als α-sEGF und β-sEGF frei. Mit neuen gegen die Schnittstellen gerichteter monoklonaler Antikörpern gelang es zudem, die Prozessierung von NRG1 Typ III auch in primären Nervenzellen nachzuweisen. Es wurde gezeigt, dass die löslichen EGF-ähnlichen Domänen funktional sind und die zur Ausbildung von Myelinscheiden notwendigen Signalkaskaden in Schwann-Zellen auslösen. Außerdem

Zusammenfassung

war β-sEGF in der Lage, den Myelinisierungsdefekt im PNS eines BACE1-defizienten Zebrafish-Modells zu beheben, was die Aktivität von β-sEGF *in vivo* bestätigt. Der Einfluss, den das Shedding durch BACE1 und ADAM17 auf die Aktivität der löslichen EGF-ähnlichen Domäne hat, wurde in Zellkultur und im Zebrafish-Modell ausführlich untersucht. Im Widerspruch zu bisher veröffentlichten Daten wurde festgestellt, dass sowohl das von BACE1 als auch das von ADAM17 geschnittene sEGF gleichermaßen aktiv ist und die Ausbildung von Myelinscheiden fördert. Zusammengenommen deutet dies darauf hin, dass die von NRG1 Typ III abhängige Myelinisierung nicht nur von membrangebundenem NRG1 Typ III gesteuert wird, sondern auch auf eine kontaktunabhängige Weise von der durch Proteolyse freigesetzten löslichen EGF-ähnlichen Domäne.

Der zweite Teil dieser Studie befasst sich mit der Prozessierung des durch das Shedding von NRG1 Typ III entstandenen C-terminalen Fragments (CTF). Wie bereits früher gezeigt wurde, führt die Intramembranproteolyse des CTFs durch die γ-Sekretase zur Freisetzung der intrazellulären Domäne von NRG1, die an der Regulierung der neuronalen Reifung und der Plastizität des Gehirns beteiligt ist. Interessanterweise ist eine Mutation innerhalb der TMD von NRG1 Typ III mit einem erhöhten Risiko an Schizophrenie zu erkranken verbunden und stellt damit einen Zusammenhang zwischen der Prozessierung von NRG1 Typ III durch die γ-Sekretase und dieser neurologischen Erkrankung dar. Die Verwendung eines neuen Antikörpers gegen den N-Terminus des NRG1 CTFs ermöglichte es, ein NRG1 β Peptid zu detektieren, das während der Spaltung durch die γ-Sekretase freigesetzt wird und möglicherweise als Biomarker für diese Prozessierung dienen könnte. Des Weiteren konnten massenspektrometrisch die genauen Schnittstellen innerhalb der TMD von NRG1 identifiziert werden. Bemerkenswerterweise liegt die ε-ähnliche Schnittstelle genau an der Position der mit Schizophrenie assoziierten Mutation, was möglicherweise die von dieser Mutation ausgehende Beeinträchtigung der γ-Sekretase-bedingten Spaltung, über die früher schon berichtet wurde, erklären könnte. Die hier vorgelegten Daten zeigen eindeutig, dass NRG1 Typ III ein Substrat der γ-Sekretase ist und bereiten die Grundlage für weiterführende Untersuchungen des Zusammenhangs zwischen der Prozessierung von NRG1 Typ III und der Entwicklung von Schizophrenie.

Vor dem Hintergrund, dass die Hemmung bzw. Modulation von BACE1 und der γ-Sekretase als vielversprechende Strategie zur Behandlung der Alzheimer Krankheit gilt, machen die Ergebnisse dieser Arbeit deutlich, dass es weiterer Untersuchungen der Auswirkungen bedarf, die eine veränderte Signalübertragung von NRG1 Typ III aufgrund der Hemmung dieser beiden Enzyme zur Folge hätte.

1   Introduction

The controlled breakdown of proteins is a fundamental physiological process. Through hydrolytic cleavage of their peptide bonds, proteins may either be disassembled completely for the sake of energy generation or reutilization of their amino acids. In addition to this non-specific breakdown during protein turnover and digestion, proteins may also be cleaved at fewer, more specific sites.

Such limited proteolysis may modify the precursor protein, for example by removing its signal sequence or alter its properties and activity. More than 500 proteases have been identified in humans (Puente et al., 2003) and the coordinated proteolytic processing of numerous substrates plays an important role in many pathways of intra- and intercellular communication (Turk et al., 2012). Through this, proteases are regulators of physiological processes such as inflammation, blood clogging, growth and the combat of pathogens (López-Otín and Bond, 2008). On the other hand deregulated protease activity, altered specificity towards their substrates or cleavage by proteases of pathogens (e.g. viruses), underlay many pathophysiological processes (Turk, 2006; López-Otín and Bond, 2008). This is especially relevant in cancer and viral infections but also in neurodegenerative diseases, like Alzheimer's disease (Turk, 2006; Strooper, 2010). Due to their role in the etiology of many different diseases, proteases have emerged as important drug targets (Turk, 2006). However, therapeutic intervention even with inhibitors highly specific to their target protease still harbors the risk of severe side effects due to the fact that most proteases cleave many different substrates. In addition, even for well investigated proteases and important drug targets such as Alzheimer's β-secretase BACE1, novel substrates are identified continuously (Hemming et al., 2009). Unintended co-inhibition of the cleavage of substrates that are unrelated to the targeted pathology may lead to severe side effects. It is therefore crucial for any successful therapeutic inhibition to determine the importance of the target protease for as many substrates as possible and to reveal its precise function in their proteolytic processing.

1.1   Alzheimer's disease

Alzheimer's disease (AD) starts out insidiously and early symptoms such as forgetfulness or mild impairment of learning are often incorrectly attributed to normal aging or stress. However, as the disease progresses these symptoms worsen and changes in speech and

behavior become apparent (Förstl and Kurz, 1999). In the further course of the disease, cognitive impairments extend to other abilities such as recognition and coordinated movement until, in the final stages of AD, patients are unable to perform even the simplest tasks, becoming completely dependent upon caregivers (Förstl and Kurz, 1999).

Age is the primary risk factor for AD (Querfurth and LaFerla, 2010) which is estimated to currently affect approx. 25 mio people worldwide (Ferri et al., 2005). With every third over 85 years of age suffering from this most prevalent form of dementia and patient numbers estimated to double in the next two decades, Alzheimer's disease constitutes one of the greatest challenges for the health care systems of aging societies (Wimo and Prince, 2010; Kiencke et al., 2011). In view of these facts there is an urgent demand for pharmacological interference with the mechanisms that lead to this form of neurodegeneration and even modest therapeutic advances in delaying the onset and progression would significantly reduce the global burden of the disease (Brookmeyer et al., 2007). In spite of great efforts, however, it is still not possible to cure or even halt AD successfully.

1.1.1 Neuropathological hallmarks

The typical neuropathological hallmarks of AD were first described by Alois Alzheimer over a hundred years ago (Alzheimer, 1907, 1911). He observed extracellular protein aggregates, so called amyloid plaques and neurons filled with intracellular neurofibrillary tangles (NTFs) in the brain of his patient Auguste D.

1.1.1.1 Amyloid plaques

Extracellular, neuritic amyloid plaques (Figure 1 A) are the characteristic feature of AD and mainly consist of amyloid β (Aβ) peptides. Ranging from 37 to 43 amino acids in length, these peptides are derived from the proteolytic processing of the amyloid precursor protein (APP) (Goldgaber et al., 1987; Kang et al., 1987). Among the different Aβ peptides, Aβ42 and Aβ43 are especially prone to aggregation and were shown to be central to the formation of amyloid plaques (Iwatsubo et al., 1994). The plaques are usually surrounded by dystrophic neurites and have directly been associated with neurodegenerative processes in AD. However, there is evidence that much smaller, soluble Aβ aggregates ranging from dimers to oligomers are the actual neurotoxic entity responsible for neuronal dysfunction and later demise (Walsh et al., 2002; Haass and Selkoe, 2007).

Proteolytic cleavage of APP is a physiological process (Haass et al., 1992; Vigo-Pelfrey et al., 1993) and under normal conditions mainly yields Aβ40 and low levels of Aβ42.

A change of this ratio towards Aβ42 or an increase in the total level of Aβ accelerates AD pathology and leads to an earlier onset of the disease (Scheuner et al., 1996). This is especially evident in the rare cases of familial Alzheimer's disease (FAD) with disease onset often as low as 30 years of age (Selkoe, 2001). FAD is caused predominantly by mutations in three genes: APP, presenilin 1 (PS1) and PS2, the latter two being part of the γ-secrease complex which cleaves APP (1.1.3.3). Supporting a central role of Aβ and especially Aβ42 in the pathology of AD, all these mutations either lead to an increase in overall Aβ production or favor the generation of Aβ42 (Selkoe, 1999).

1.1.1.2 Neurofibrillary tangles

Neurofibrillary tangles (Figure 1 B) mainly consist of a hyperphosphorylated form of the protein tau which physiologically stabilizes microtubules and is important for the integrity of axons (Drubin and Kirschner, 1986). In AD, excessive phosphorylation of tau causes the protein to dissociate from the microtubules and to aggregate (Goedert et al., 1992; Friedhoff et al., 1998). As a consequence the stability of the axonal microtubule network is thought to be compromised and eventually the axon and later the neuron degenerate. Previously this loss-of-function has been seen as the main mechanism through which tau contributes to the dysfunction of neurons in AD. Recently, however, evidence has emerged that strengthens an alternative mechanism: Hyperphosphorylated tau was found to mislocalize from the axonal into the somato-dendritic compartment of neurons and to mediate the (postsynaptic) toxicity of Aβ (Roberson et al., 2007; Ittner et al., 2010; Morris et al., 2011).

The reasons for the hyperphosphorylation of tau are not entirely clear yet but it is interesting to note that unlike amyloid plaques, tau pathology is not restricted to AD but is in fact common to various forms of dementia (Lee et al., 2001). Also in contrast to amyloid plaques, the number of NTF correlates well with the loss of synapses and the severity of clinical symptoms and therefore is considered an important pathological marker (Braak and Braak, 1995; Thind and Sabbagh, 2007).
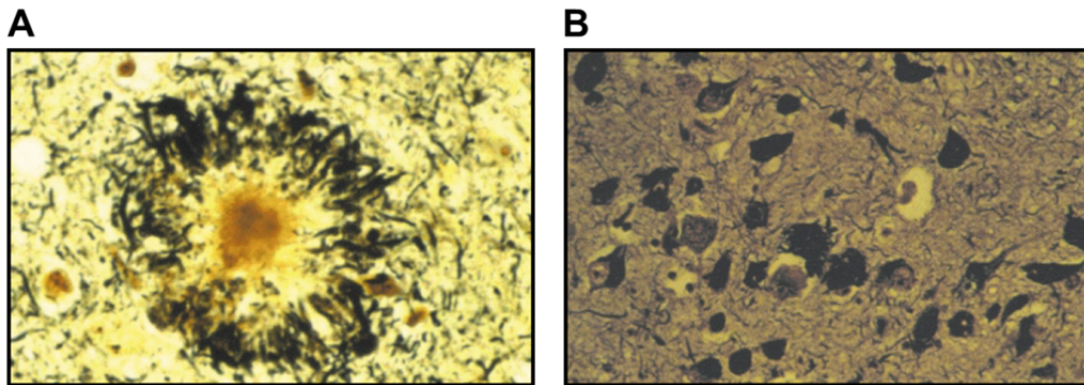
Figure 1. Neuropathological hallmarks of Alzheimer's disease. A) Microscopic image of an amyloid plaque. The central core of the plaque is visible in the middle (brown) and consists of aggregated Aβ fibrils. The plaque is surrounded by dystrophic neurites that are filled with neurofibrillary tangles. **B)** Photomicrograph of neurons filled with neurofibrillary tangles. Silver-staining shows cortical pyramidal neurons with intracellular deposits of hyperphosphorylated tau. Pictures from (Sisodia and St George-Hyslop, 2002).

1.1.1.3 Amyloid cascade

The amyloid cascade hypothesis tries to reconcile the genetic and molecular findings with the neuropathological hallmarks of AD (Hardy and Higgins, 1992). This hypothesis suggests that the altered generation and subsequent aggregation of Aβ initiates a pathological cascade that, through downstream events such as tau dysfunction and NTF formation, oxidative stress and inflammation, finally leads to neuronal dysfunction and dementia. The failure of clinical trials designed on the basis of the amyloid cascade hypothesis as well as its unclear relevance for sporadic AD, however, have raised concerns as to its validity (Hardy, 2009; Golde et al., 2011; Mullane and Williams, 2013). Nonetheless, compared to other hypotheses, the amyloid cascade most completely consolidates experimental observations and therefore remains the most widely accepted hypothesis for the etiology of AD. The recent identification of a mutation in APP which decreases the generation of Aβ and protects against AD (Jonsson et al., 2012) has further strengthened the plausibility of the amyloid cascade hypothesis.

1.1.2 Processing of APP

APP is a ubiquitously expressed type I transmembrane protein comprising a large extra-cellular and a small intracellular domain (Figure 2), whose physiological function is currently not fully understood (Zheng and Koo, 2011). It is processed in a two-step fashion through a mechanism called regulated intramembrane proteolysis (RIP) (Brown et al., 2000) (1.2): First, in a process called shedding, its ectodomain is shortened by a cleavage close to its

transmembrane domain (TMD) and then in a second step, the remaining fragment is removed through proteolysis within the membrane (Figure 2).

Generation of Aβ depends on whether APP is cleaved at the α- or β-site during ectodomain shedding. Cleavage at the β-site by the so called β-secretase initiates the amyloidogenic pathway and releases the majority of the APP ectodomain into the lumen (sAPPβ) while simultaneously generating the N-terminus of the Aβ peptide (Figure 2). In the further course of the amyloidogenic pathway, the resulting β-cleaved C-terminal fragment of APP (β-CTF) is cleaved by the γ-secretase complex, releasing Aβ into the luminal space and the APP intracellular domain (AICD) into the cytoplasm (Haass, 2004). In contrast, shedding by the α-secretase at the α-site located within the Aβ sequence precludes the release of Aβ and mediates the non-amyloidogenic pathway (Figure 2). Such cleavage liberates the slightly longer sAPPα from the membrane and leaves the APP α-CTF for subsequent γ-secretase cleavage. As a result of this pathway the smaller, non-amyloidogenic peptide p3 is released from the cell surface (Fluhrer et al., 2009; Lichtenthaler, 2011).
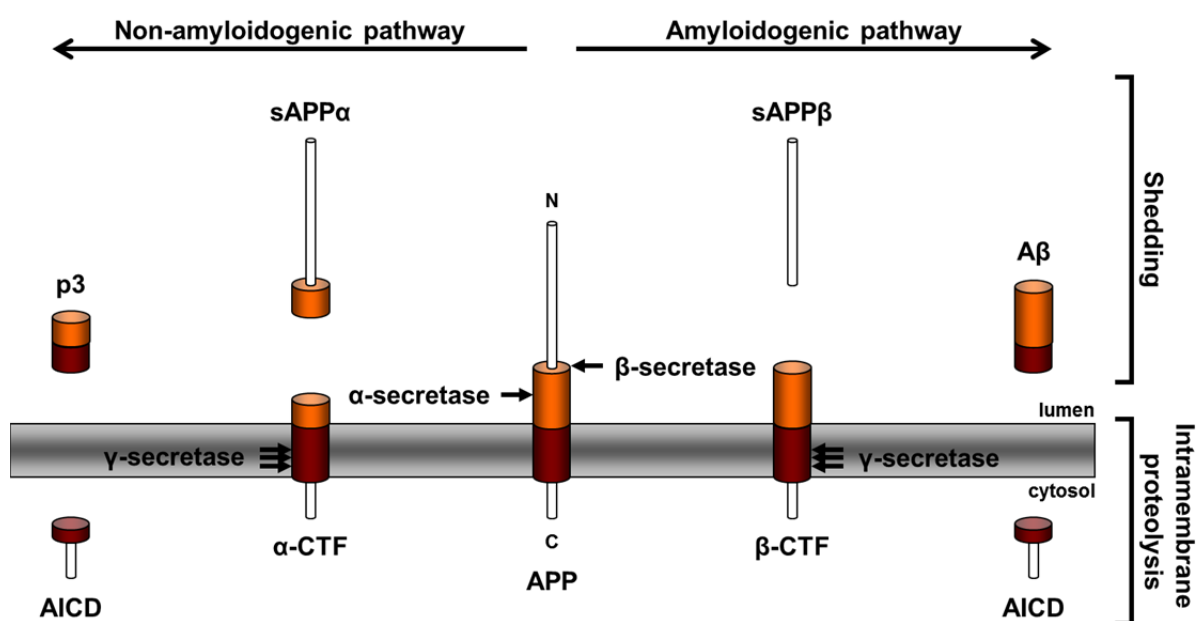
Figure 2. Processing of APP. Schematic overview of the amyloidogenic and non-amyloidogenic processing of APP. Shedding by α- or β-secretase releases the ectodomain into the luminal space. Cleavage of the remaining membrane fragments by the γ-secretase generates the non-amyloidogenic p3 or the aggregation prone Aβ peptide. The intracellular domain is released into the cytosol.

More than 30 mutations leading to familial Alzheimer's disease with early onset have been identified in APP (Cruts et al., 2012). Interestingly, these mutations cluster in three different regions of the APP protein, their location determining their impact on amyloid generation (Selkoe, 1999; St George-Hyslop, 2000): Mutations near the γ-cleavage sites (1.1.3.3) alter the cleavage precision of the γ-secretase thus enhancing the generation of the aggregation prone Aβ42 at the expense of Aβ40 (Suzuki et al., 1994). FAD mutations next to the shedding sites promote the processing of APP at the β-site leading to an increased overall amyloid production. These mutations either directly enhance β-secretase cleavage (Citron et al., 1992) or impair cleavage at the non-amyloidogenic α-site (Kaden et al., 2012). Conversely, a mutation at the β-secretase cleavage site that reduces cleavage was recently found to confer protection against AD (Jonsson et al., 2012).

1.1.3 Alzheimer's disease secretases – APP processing and beyond

Processing of APP occurs sequentially and is mediated by proteolytic cleavages at distinct sites. At least three different protease activities are involved which, before their identities were unambiguously resolved, were referred to as α-, β- and γ-secretase relating to the order of their discovery. Although their precise molecular identity is now known and all of these proteases are involved in the cleavage of many other substrates besides APP, their original names are still in use (Lichtenthaler et al., 2011).

1.1.3.1 α-Secretase

Shedding of APP at the α-site (Figure 2, 1.1.3.3 Figure 3) is mediated by the so called α-secretase (Esch et al., 1990). Several members of the ADAMs (a disintegrin and metalloproteinase) family of proteases cleave APP at this site and of those, ADAM10 and ADAM17 (also called TACE for tumor necrosis factor α converting enzyme) have been discussed most prominently as α-secretases (Buxbaum et al., 1998; Lammich et al., 1999). ADAM10 was identified as the main α-secretase responsible for the constitutive cleavage of APP in neurons (Jorissen et al., 2010; Kuhn et al., 2010). In contrast, under physiological conditions ADAM17 seems to be of minor importance as constitutive α-secretase but instead belongs to the group of regulated α-secretases whose APP shedding activity may be strongly enhanced pharmacologically (Lichtenthaler, 2011).

ADAM10 and ADAM17 are the best characterized and most closely related members of the ADAM family of proteases (Reiss and Saftig, 2009). Both are type I transmembrane proteins with large extracellular and short cytoplasmic domains. Their catalytically active

metalloprotease domain is located within the N-terminal portion of the extracellular domain and harbors a zinc-binding motif with three conserved histidine residues. Expression of both proteases was detected in a broad spectrum of cells and tissues. Interestingly, ADAM10 and ADAM17 are expressed differentially in the CNS with ADAM10 being present in neurons and ADAM17 being predominantly expressed by non-neuronal cells (Kärkkäinen et al., 2000; Marcinkiewicz and Seidah, 2000; Goddard et al., 2001). Within cells, the majority of ADAM10 and ADAM17 is localized to the Golgi apparatus and only a smaller fraction is found at the plasma membrane (Lammich et al., 1999; Schlöndorff et al., 2000).

More than 30 membrane proteins have been identified as substrates for ADAM10 and ADAM17, respectively, and besides their role as α-secretases, ADAM10 and ADAM17 are best known for their involvement in the release of soluble factors like hormones, chemokines and growth-factors (Reiss and Saftig, 2009). These factors are often present as inactive, membrane-bound precursor proteins on the surface of cells and require proteolytic activation. Once cleaved, the biologically active domains are released and signal in an autocrine or paracrine fashion. In addition to the regulation of extracellular signaling pathways, ADAM10- and ADAM17-mediated shedding also triggers numerous intracellular signaling pathways by regulated intramembrane proteolysis (1.2).

Important substrates for ADAM10 include among others notch and ephrins. The crucial role of ADAM10 for notch signaling is demonstrated by the fact that mice lacking ADAM10 die at embryonic day 9.5 (E9.5) and phenocopy many notch knockout (KO) defects (Hartmann et al., 2002). For ADAM17, the tumor necrosis factor α (TNFα) and different members of the epidermal growth factor (EGF) receptor family EGFR/ErbB1 and their ligands (such as transforming growth factor α (TGFα), heparin-binding EGF (HB-EGF) and epiregulin) have been identified as important substrates. Accordingly, ADAM17 KO mice die perinatally and display developmental deficits reminiscent of animals lacking these factors (Peschon et al., 1998; Jackson et al., 2003; Sternlicht et al., 2005). Together with ADAM10, which through cleavage of EGF is also involved in the EGFR/ErbB1 signaling, ADAM17 has additionally been shown to cleave neuregulin-1 (NRG1) (1.3.3).

In summary, both ADAM10 and ADAM17 are able to cleave a broad variety of different transmembrane proteins, with more substrates likely to be identified in the future. Besides their role in AD, these proteases therefore are involved in multiple physiological and pathophysiological processes such as development, signal transduction, inflammation and cancer (Saftig and Reiss, 2011). In this light, the long sought therapeutic strategy for AD involving the pharmacological activation of ADAM10 and ADAM17 to promote the non-

amyloidogenic processing of APP (Fahrenholz, 2007) must be considered carefully and it will be crucial to investigate the many pathways in which these enzymes are involved for potential side effects (Endres and Fahrenholz, 2010; Lichtenthaler, 2011).

1.1.3.2 β-Secretase

The β-secretase or β-site APP cleaving enzyme one (BACE1) mediates the shedding of APP at the β-site (1.1.2 Figure 2, 1.1.3.3 Figure 3). Genetic ablation of BACE1 in mice completely prevents Aβ generation in the brain arguing for BACE1 as the principle and physiologically relevant β-secretase (Cai et al., 2001; Luo et al., 2001). Discovered in 1999 by five independent groups, BACE1 belongs to the pepsin-like family of aspartyl proteases and features a type I transmembrane topology (Hussain et al., 1999; Sinha et al., 1999; Vassar et al., 1999; Yan et al., 1999; Lin et al., 2000). Its active site is localized to the large ectodomain and comprises two D-T/S-G-T/S motifs characteristic of aspartic proteases (Hong et al., 2000). Compared to other aspartic proteases, however, the active site of BACE1 is much larger and less hydrophobic which has severely hindered the development of small molecule inhibitors. In the brain, BACE1 was found to form homodimers which display a higher enzymatic activity than the monomeric enzyme (Westmeyer et al., 2004).

Intracellularly, BACE1 cycles between acidic compartments of the secretory pathway (mainly the trans Golgi network), the plasma membrane and early endosomes, where, owing to its acidic pH optimum, the highest BACE1 activity is observed and Aβ generation occurs (Haass et al., 1993; Koo and Squazzo, 1994; Vassar et al., 1999). In the brain, BACE1 is transported axonally and most likely localizes to presynaptic nerve terminals in neurons (Sheng et al., 2003).

BACE1 is expressed by most cell types but the highest expression and activity levels are found in neurons of the CNS, in motoneurons of the spinal cord and in dorsal root ganglia (DRG) (Sinha et al., 1999; Vassar et al., 1999; Willem et al., 2006). In contrast, BACE1 expression in glial cells is relatively low (Bettegazzi et al., 2010).

Consistent with its importance in nerve development (1.3.4.1) BACE1 levels peak during early postnatal stages when myelination occurs and rapidly decline afterwards (Willem et al., 2006). Interestingly, later in life BACE1 protein levels increase again in the context of AD. About 30% of sporadic AD cases are associated with elevated BACE1 protein but not mRNA levels and several translational control mechanisms were uncovered whose alteration might lead to increased BACE1 activity and consequently Aβ generation in AD (Willem et al., 2009; Dislich and Lichtenthaler, 2012).

The idea of BACE1 inhibition as AD therapy was strongly encouraged by initial reports that found BACE1 KO mice to completely lack Aβ generation while at the same time displaying no overt phenotype (Luo et al., 2001; Roberds et al., 2001). In contrast to these initial reports, however, subsequent in depths analyses of BACE1 KO mice uncovered multiple albeit often subtle phenotypes. These include altered behavior regarding anxiety and exploration as well as features that are considered rodent analogs of schizophrenia such as deficits in social recognition, impaired memory and prepulse inhibition (Harrison et al., 2003; Laird et al., 2005; Savonenko et al., 2008). More dramatic phenotypic changes in some BACE1 KO lines include spontaneous epileptic seizures, increased neonatal lethality and decreased body size due to enhanced insulin sensitivity (Dominguez et al., 2005; Hitt et al., 2010; Meakin et al., 2012). Taken together this suggests a crucial role of BACE1 not only in the nervous system but also in the periphery.

Finally, it was discovered that BACE1 KO mice have severely reduced myelin sheaths around the nerves of the PNS (1.3.4.1.5) and also display retarded remyelination after nerve injury (Hu et al., 2008). While impaired myelination in the PNS was recently confirmed in a zebrafish model lacking BACE1 activity (van Bebber et al., 2013), myelination deficits in the CNS as initially reported by one group (Hu et al., 2006) were not observed (Willem et al., 2006).

BACE1 has been shown to cleave many different proteins *in vitro* (Hemming et al., 2009) but only few have been identified as physiological BACE1 substrates *in vivo*. In addition to APP these include among others the β-subunits 2 and 4 of voltage-gated sodium channels (VGSC), neuregulin-1 (NRG1), and the α-2,6 sialyltransferase (ST6Gal-1) (Dislich and Lichtenthaler, 2012). Overall, however, it has been difficult to associate the lack of proteolytic processing of these individual substrates with the phenotypes observed in BACE1 KO mice. For example, despite being the most studied BACE1 substrate, the physiological consequences of BACE1-mediated APP shedding remain mostly unclear. In contrast to the α-secretase cleavage product sAPPα which rescues most of the phenotypes observed in APP KO mice (such as decreased brain and body weight, deficits in cognition and locomotion), the BACE1-cleaved APP ectodomain sAPPβ fails to compensate for the lack of full-length APP (Ring et al., 2007; Li et al., 2010). Specifically it was demonstrated that sAPPβ is not able to function in the APP-mediated formation of neuromuscular synapses during development and does not rescue postnatal lethality in APP/APLP2 KO animals (Li et al., 2010). Instead, sAPPβ was proposed to regulate the expression of genes such as transthyretin and klotho but the respective receptor(s) as well as the physiological

consequences of this BACE1-mediated APP function remain unclear. Overall, processing by BACE1 seems to be dispensable for the role of APP during development (Li et al., 2010).

The most consistent connection between processing by BACE1 and the respective KO phenotype has been established for NRG1 type III, an isoform of NRG1 expressed in neurons of the PNS (1.3.1). The peripheral hypomyelination of BACE1 KO mice phenocopies mice with heterozygous levels of NRG1 type III and mice lacking its receptors in Schwann cells (Michailov et al., 2004; Taveggia et al., 2005). Furthermore, the uncleaved full-length precursor of NRG1 type III accumulates in BACE1 KO mice while the corresponding cleavage products are diminished (Willem et al., 2006). Together this indicates that the processing of NRG1 type III by BACE1 is required for proper Schwann cell myelination in the PNS and that a lack thereof causes the observed phenotype in BACE1 KO mice (1.3.4.1.5). Interestingly, NRG1 has also been identified as a risk gene for schizophrenia and its signaling is involved in the neuronal plasticity of the CNS (1.3.4.2). Although the molecular details are still unclear, abolished BACE1-dependent NRG1 processing might therefore establish a connection to the schizophrenia-like phenotypes observed in BACE1 KO mice.

In summary, through the cleavage of many different substrates besides APP, BACE1 seems to be involved in numerous processes throughout development and adulthood in both the nervous system and the periphery. With regard to its potential as therapeutic target this suggests that AD therapies based on chronic inhibition of BACE1 are likely to cause mechanism-based toxic side effects. Instead of completely blocking BACE1, rather a modulation or normalization of its activity may therefore be a more favorable intervention strategy (Willem et al., 2009; Vassar and Kandalepas, 2011). Indeed, already partial reduction of BACE1 activity resulted in strongly alleviated plaque burden and synaptic deficits in a mouse model of AD (McConlogue et al., 2007).

1.1.3.3 γ-Secretase

Following shedding at the α- or β-site, the remaining APP CTF is cleaved within its TMD by the γ-secretase (Steiner et al., 2008) (1.1.2 Figure 2, Figure 3). Rather than being a single protein, the γ-secretase is a protein complex consisting of four different transmembrane proteins most likely in a 1:1:1:1 stoichiometry (Sato et al., 2007). The subunits essential and sufficient for a functional γ-secretase complex are: Presenilin 1/2 (PS1/2), nicastrin (NCT), APH-1 (anterior pharynx-defective-1) a/b and PEN-2 (presenilin enhancer-2) (Edbauer et al., 2003; Kimberly et al., 2003). The catalytic subunit presenilin (De Strooper et al., 1998; Herreman et al., 2000; Zhang et al., 2000) exists as two homologs in mammals, PS1 and

PS2 and spans the membrane nine times (Laudon et al., 2005). It belongs to the family of GxGD-type intramembrane aspartyl proteases (Haass and Steiner, 2002) and contains the characteristic active site motif YD and GxGD in its transmembrane domains TMD six and seven, respectively (Wolfe et al., 1999b; Steiner et al., 2000). During maturation of the complex PS undergoes auto-endoproteolysis and is present as a heterodimer consisting of an N-terminal and C-terminal fragment (NTF and CTF) in the active complex (Thinakaran et al., 1996; Fukumori et al., 2010). Importantly, the activity of PS and thus the γ-secretase depends on the assembly of the complex as PS is not fully active by itself. Nicastrin is a type I transmembrane protein and the largest γ-secretase component (Yu et al., 2000) whose ectodomain is controversially discussed to function as a substrate receptor of the γ-secretase complex (Shah et al., 2005; Chávez-Gutiérrez et al., 2008). The function of the seven pass transmembrane protein APH-1 (Fortna et al., 2004) is not well understood. It is required for complex formation, however, and likely acts as an assembly scaffold for the other subunits (Gu et al., 2003; LaVoie et al., 2003). In the model of the stepwise assembly of the active γ-secretase complex (Kaether et al., 2006a; Spasic and Annaert, 2008), APH-1 and nicastrin form an initial dimeric complex that is then joined by the immature presenilin holoprotein to form an inactive trimer still retained in the ER (Kim et al., 2004; Capell et al., 2005). In the final and rate-limiting step, the immature complex then binds PEN-2, the smallest subunit. PEN-2 features a hairpin-like topology (Crystal et al., 2003) and its binding triggers the endoproteolysis of PS and stabilizes the complex (Luo et al., 2003; Prokop et al., 2004). Once assembled, the γ-secretase complex is transported to the plasma membrane and the endosomal/lysosomal compartments which are the sites of its main activity in cells (Kaether et al., 2006b).

The γ-secretase processes its substrates in an unusual stepwise manner that involves cleavage at two major sites within their transmembrane domain (Figure 3). The details of this unconventional proteolytic mechanism have mostly been investigated for the processing of APP and notch but seem to apply for other substrates as well (Lichtenthaler et al., 2011). The first cleavage (called ε-cleavage) occurs close to the cytoplasmic border of the substrate's transmembrane domain and releases the intracellular domain (ICD) of the substrate into the cytosol (Gu et al., 2001; Sastre et al., 2001; Yu et al., 2001; Weidemann et al., 2002; Kakuda et al., 2006) (Figure 3). As shown for APP, the γ-secretase then proceeds with a stepwise cleavage towards the N-terminus of the remaining membrane stub (Qi-Takahara et al., 2005; Zhao et al., 2005). The detection of characteristic intermediate peptides suggest that at least in the case of APP, cleavage occurs after approximately every

third amino acid (Takami et al., 2009). Processing continues until, after cleavage at the so called γ-site, the substrate is short enough to be released from the membrane (Figure 3). Besides APP, also notch (Okochi et al., 2002), CD44 (Lammich et al., 2002), APLP1 and APLP2 (Eggert et al., 2004) as well as a variety of other substrates are similarly processed by the γ-secretase at multiple sites. This suggests that proteolysis in a stepwise manner may be a general mechanism employed by GxGD proteases to reduce the hydrophobicity of their substrates and allow their liberation from the membrane. This stepwise proteolysis and the fact that the intermediate cleavages are heterogeneous in nature also explain the generation and release of different sized peptides by the γ-secretase (e.g. Aβ37-43 in case of APP).

With 185 mutations in PS1 and 13 in PS2, mutations in the catalytic subunits of the γ-secretase account for the vast majority of FAD-linked mutations (Cruts et al., 2012). They all shift the ratio of Aβ42/Aβ40 towards the more toxic and amyloidogenic Aβ42 while usually leaving the total amount of secreted Aβ unchanged.

Due to its role in the generation of Aβ, inhibition of the γ-secretase is considered a promising therapeutic strategy for the prevention and treatment of AD. Indeed, early studies in transgenic mice confirmed the potential of γ-secretase inhibitors (GSIs) in lowering brain Aβ levels (Dovey et al., 2001) and prompted the development and clinical evaluation of a variety of compounds targeting γ-secretase activity (Tomita, 2009; De Strooper et al., 2010). However, besides APP at least 80 additional proteins have been identified as substrates and through their cleavage the γ-secretase complex is involved in many different cellular processes ranging from the regulation of transcription, cell fate and apoptosis to the control of neurite outgrowth and tumorigenesis (Haapasalo and Kovacs, 2011). In this regard, the processing of notch (Fiúza and Arias, 2007; Kopan and Ilagan, 2009) that results in the release of the notch intracellular domain (NICD) into the cytosol is probably one of the most important physiological functions of the γ-secretase (De Strooper et al., 1999) (1.2.2). Generation of the NICD which subsequently translocates into the nucleus and acts as a transcription factor is a crucial event in the notch pathway. Loss of γ-secretase activity during development severely affects embryogenesis in different model organisms and results in a lethal phenotype indistinguishable from deficient notch signaling (Donoviel et al., 1999; Geling et al., 2002). As notch signaling is also required during adulthood, chronic inhibition of γ-secretase in later life has likewise been shown to cause a variety of toxicities that include gastrointestinal, skin and immune system abnormalities (Wong et al., 2004; De Strooper et al., 2010). The side effects resulting from the concomitant inhibition of important γ-secretase substrates beside APP led to the failure of γ-secretase inhibitors in clinical trials and render

Figure 3 Localization of the α-, β- and γ-secretase cleavage sites in APP. The cleavage positions of the proteases are indicated by arrows and the number of residues comprised by the Aβ peptides resulting from γ-cleavage is given. The transmembrane domain of APP is shaded in brown.

their use as AD therapeutics unlikely (Blennow et al., 2013; Doody et al., 2013; Mullane and Williams, 2013).

As an alternative to GSI treatment, γ-secretase modulators (GSM) have been developed (Weggen et al., 2001; Oehlrich et al., 2011). Instead of blocking γ-secretase cleavage, GSMs are designed to favor the generation of shorter Aβ peptides (Aβ37 and 38) over the generation of the aggregation prone Aβ42 while leaving the total level of Aβ unchanged. Unlike inhibitors, GSMs do not block the ε-like cleavage mediated by the γ-secretase but only affect the precision of the γ-cleavage (Figure 3). In this way the release of the substrate's ICD into the cytosol is not compromised which is especially important in the case of notch but may be relevant for other substrates that mediate intracellular signaling as well (1.2.2). Treatment with GSMs is expected to result in much less target-mediated toxicity compared to GSIs and different compounds are being developed (Golde et al., 2010).

Overall, due to its numerous substrates and its various physiological functions, targeting γ-secretase for AD therapy has proven more complicated than initially anticipated. To reduce target-mediated adverse effects it will be crucial to develop potent therapeutics that selectively alter the processing of APP but do not affect the normal turnover of other substrates. It is therefore necessary to identify as many substrates as possible and to closely investigate their cleavage by the γ-secretase as well as the physiological relevance of said processing. In this context it is noteworthy that NRG1 is also a substrate of the γ-secretase and that its impaired intramembranous cleavage is implicated in the dysregulation of cortical development and schizophrenia-like phenotypes in mice (1.3.4.2).

1.2 Regulated intramembrane proteolysis (RIP) and proteases in signaling

The processing of APP (1.1.2) represents a classical example of regulated intramembrane proteolysis (RIP) (Brown et al., 2000). RIP processes type I and type II transmembrane proteins in a sequential way involving a primary extracellular cleavage (shedding) and a secondary cleavage within the boundaries of the cellular membrane (Figure 4). The basic two-step mechanism of RIP is conserved from prokaryotes to mammals and the combination of shedding and intramembrane cleavage has emerged as a novel mechanism of signal transduction (Weihofen and Martoglio, 2003; Landman and Kim, 2004; Lal and Caplan, 2011).

1.2.1 Shedding mediates extracellular signaling

Shedding, the rate-limiting first cleavage during RIP occurs in the juxtamembrane region of the substrate. It releases the substrate's ectodomain into the luminal space and generates a shortened membrane-retained fragment (Figure 4). Shedding which is mediated by membrane-bound proteases, so called sheddases such as the members of the ADAM family of proteases and BACE1, may be triggered by ligand binding (in the case of receptor shedding) but may also occur ligand-independent (e.g. for precursors of signaling factors). Cleavage of the notch receptor (Fiúza and Arias, 2007) represents an example of ligand-induced shedding. Binding of one of its ligands delta/jagged/serrate triggers shedding by ADAM10 or ADAM17 which releases the notch ectodomain and generates a membrane-bound fragment called NEXT (notch extracellular truncated) (Brou et al., 2000; Mumm et al., 2000). A similar ligand-induced receptor shedding was observed for the receptor tyrosine kinase ErbB4 (Carpenter, 2003) which is shed by ADAM17 upon binding of neuregulin-1 (Zhou and Carpenter, 2000). Vice versa, binding to its receptor EphB (Pasquale, 2008) triggers the shedding of the ephrinB ligand and therefore represents an example of receptor-induced ligand shedding (Georgakopoulos et al., 2006). In contrast, shedding of APP (1.1.2) seems to be independent of ligand binding and instead is regulated by intracellular signaling, trafficking, protease expression and activity (Sannerud and Annaert, 2009). Other examples of shedding events that do not require prior interaction with a ligand include the cleavage of many membrane-bound precursors of extracellular signals such as TNFα, Fas ligand and growth factors like TGFα and neuregulin-1 (Reiss and Saftig, 2009) (1.3). Through the processing of these factors and the release of their bioactive domains from the cell surface

sheddases participate in numerous paracrine and autocrine signaling pathways and shedding therefore has emerged as a key mechanism in many biological processes throughout development and adulthood.

1.2.2 Intramembrane cleavage mediates (bi-directional) intracellular signaling

In addition to the classical extracellular signaling, the combination of shedding and intramembrane proteolysis also enables both forward and reverse intracellular signaling. Cleavage of substrates within the boundaries of the cell membrane is catalyzed by so called intramembrane cleaving proteases (I-CLiPs) (Wolfe et al., 1999a) which are multi-spanning transmembrane proteins. The group of I-CLiPs comprises the site-2-protease (S2P) family, the rhomboids and the GxGD family of proteases whose name is derived from the characteristic GxGD active site motif common to all of its members (Haass and Steiner, 2002; Wolfe, 2009). Besides the presenilins which are the best characterized members, the GxGD family also includes the signal peptide peptidase (SPP) and the SPP-like (SPPL) family (Fluhrer et al., 2009).

Intramembrane proteolysis of shortened membrane proteins liberates their cytoplasmic domains into the cytosol which subsequently may participate in signal transduction within the cell. The notch pathway is the most prominent example of such RIP-mediated intracellular forward signaling. After shedding, the remaining NEXT fragment undergoes intramembrane cleavage by the γ-secretase and the notch intracellular domain (NICD) is released into the cytosol (Schroeter et al., 1998; De Strooper et al., 1999). Subsequently, the NICD translocates to the nucleus where it binds to transcription factors and acts as "transcriptional switch" to induce the expression of target genes (Mumm and Kopan, 2000). Likewise, the γ-secretase generated ICD of the receptor ErbB4 (B4-ICD) was shown to act as transcriptional regulator in the nucleus but the precise mechanism and physiological consequences of this non-canonical forward signaling have yet to be determined (Ni et al., 2001).

In addition to the above described forward signaling of receptor ICDs, RIP also mediates intracellular back signaling via the ICD of ligands (Landman and Kim, 2004). The notch ligands jagged and delta for example participate in the canonical forward signaling by binding and activating the notch receptor (Fiúza and Arias, 2007). However, jagged and delta themselves are subject to shedding by an ADAM protease and subsequent intramembrane cleavage by the γ-secretase liberates their ICDs into the cytosol (Bland et al., 2003; LaVoie and Selkoe, 2003; Six et al., 2003). Both ICDs reportedly act as reverse intracellular signals

and localize to the nucleus where the jagged ICD was found to stimulate activator protein-1 (AP-1) mediated transcription normally inhibited by the NICD (LaVoie and Selkoe, 2003). Another protein that seems to be involved in both forward and reverse signaling is APP. In the forward signaling pathway, the APP ectodomain secreted through α-secretase shedding (sAPPα) (1.1.2) was found to convey neurotrophic and neuroprotective effects although the respective receptor(s) remain(s) to be identified (Furukawa et al., 1996; Meziane et al., 1998). The reverse signaling pathway of APP is controversially discussed and its physiological implications are not well understood (Beckett et al., 2012). Nonetheless, reverse signaling of APP is proposed to be mediated by the AICD (1.1.2) which in analogy to the notch ICD was shown to act as a intracellular signal, indirectly activating the transcription of several target genes (Cao and Südhof, 2001, 2004). In addition, RIP also mediates the reverse signaling within the ErbB/neuregulin signaling pathway (1.3.3).

In conclusion, through the combination of extracellular and intramembrane cleavage, RIP processes membrane proteins to release soluble peptides in different cellular compartments. Shedding liberates numerous soluble factors from their membrane-bound precursors and thereby regulates a variety of extracellular paracrine and autocrine signaling pathways. In addition, intramembrane proteolysis generates ICDs within the cell which subsequently may mediate intracellular signal transduction and regulate transcription. In cases where both the extracellular and intracellular domains act as a signal, RIP therefore allows bi-directional signaling by one substrate (Figure 4). Manipulating the "RIPping" of a target protein for therapy (like APP processing in case of AD) therefore harbors the risk to impact on the signaling of many other, unrelated proteins. This is especially relevant when targeting core components of RIP such as the γ-secretase that are involved in many RIP-mediated pathways. The development of a successful AD therapy directed at the proteolysis of APP will therefore depend on detailed knowledge of the processing and signaling of as many RIP substrates as possible.
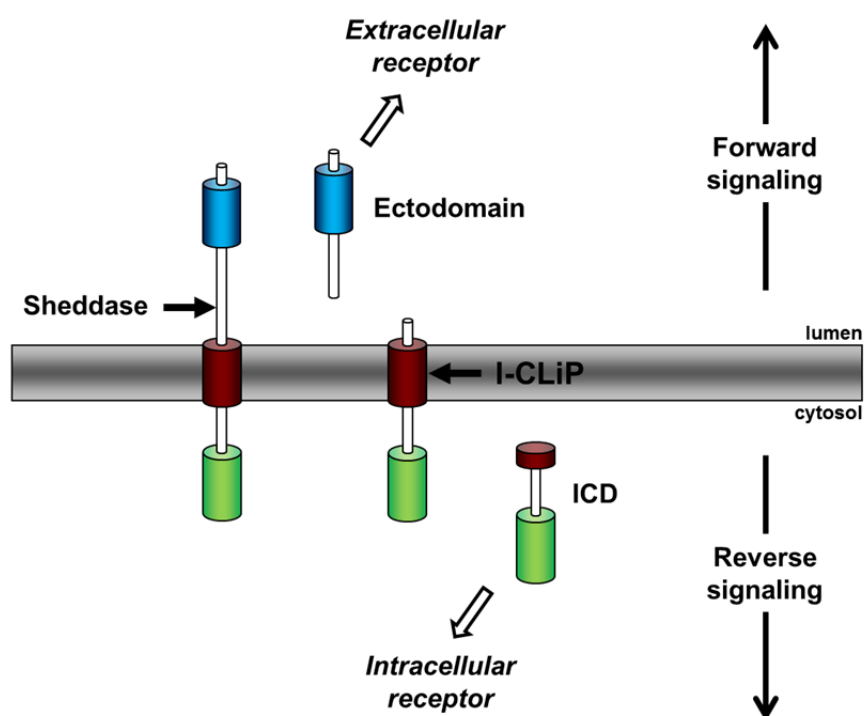
Figure 4. Regulated intramembrane proteolysis (RIP) allows bi-directional signaling. Shedding of a transmembrane protein by a membrane-bound protease (sheddase) generates a (soluble) ectodomain which may act as extracellular forward signal. Intramembrane cleavage of the remaining fragment by an intramembrane-cleaving protease (I-CLiP) liberates the intracellular domain (ICD) which subsequently may mediate intracellular reverse signaling. Shedding is the rate-limiting step of RIP and either occurs constitutively or is triggered by signals such as ligand binding.

1.3 Neuregulin-1

The growth factor neuregulin-1 was identified as one of the most important physiological substrates of BACE1 and abolished or reduced BACE1-mediated processing of NRG1 in mice causes defects in the peripheral nervous system (PNS) and probably also in the central nervous system (CNS) (1.1.3.2, 1.3.4.1.5). As NRG1 is also cleaved by the γ-secretase inducing an intracellular signal cascade (1.3.3.3), its processing represents a typical example of RIP-mediated signaling.

1.3.1 The neuregulin family

The neuregulin (NRG) gene family in vertebrates comprises four genes (NRG1-4) that encode the related growth factors neuregulin-1-4. While the sequences of NRG1 and NRG2 share a higher degree of homology, NRG3 and NRG4 seem to be only distantly related to NRG1 (Buonanno and Fischbach, 2001). The usage of different promoters and excessive

splicing generates numerous NRG isoforms but almost all are synthesized as type I transmembrane precursor proteins and require proteolytic processing to achieve full activity. As a common and family defining feature, all NRGs share an epidermal growth factor (EGF)-like domain in their extracellular portion which binds to and activates ErbB receptor tyrosine kinases (RTKs). The NRG EGF-like domains comprise approx. 50 residues and contain three pairs of conserved cysteine residues that, through the formation of disulfide bridges, are responsible for the domains' typical tertiary structure and biological activity. As of yet there are no criteria that clearly define a neuregulin EGF-like domain. However, all NRGs share conserved residues within the domain that clearly distinguishes the NRG family members from other members of the EGF-like family such as EGF, TGFα or HB-EGF (Buonanno and Fischbach, 2001). As another common family feature, neuregulins collectively only signal through ErbB2, 3 and 4 receptors but do not activate ErbB1 (Yarden and Sliwkowski, 2001; Mei and Xiong, 2008).

NRG1 is the most broadly expressed family member and has been detected during development and adulthood in neural cells (neurons and glia) of both the CNS and PNS, as well as in other organs such as the heart, liver, kidney, spleen and lung (Orr-Urtreger et al., 1993; Wen et al., 1994). Although in contrast to NRG1 only very little is known about the functions of NRG2-4 their distinct temporal and spatial expression patterns suggest different and non-redundant roles. NRG2 is expressed in the heart during embryogenesis but later its expression is restricted to the brain and the spinal cord with only low levels in lung and liver (Busfield et al., 1997; Chang et al., 1997). In contrast, NRG3 seems to be exclusively expressed in the CNS and PNS during both development and adulthood (Zhang et al., 1997), whereas NRG4 expression is restricted to non-neural tissue and was observed in adult skeletal muscle and especially pancreas (Harari et al., 1999).

1.3.2 Neuregulin-1 – A growth factor that comes in multiple isoforms

Neuregulin-1 is the best characterized member of the NRG family and was identified in the early 1990s (Falls, 2003a). NRG1 is produced from the NRG1 gene located on the small arm of chromosome 8 (8p12-8p21) which spans approx. 1.4 megabases (Mei and Xiong, 2008). Being one of the largest genes in the mammalian genome, NRG1 comprises 21 exons and its transcription is regulated by at least nine alternative promoters (Steinthorsdottir et al., 2004). In combination with excessive splicing this results in the generation of at least 31 different NRG1 protein isoforms (Mei and Xiong, 2008). The first NRG1 isoforms were identified by several independent research groups and named according to the context of

their discovery: Neu differentiation factor (NDF) (Peles et al., 1992; Wen et al., 1992) or heregulin (HRG) (Holmes et al., 1992) as a ligand for the oncogene ErbB2/HER2/Neu, glial growth factor (GGF) (Goodearl et al., 1993; Marchionni et al., 1993) as a factor that induced proliferation of Schwann cells and acetylcholine receptor (AChR) inducing activity (ARIA) (Falls et al., 1993) or sensory motor neuron-derived factor (SMDF) (Ho et al., 1995) as a signal that enhanced the expression of acetylcholine receptors. It is now clear, however, that these names are not always indicating the main physiological function of the respective isoform as for example the physiologically relevant "glial growth factor" seems to be in fact SMDF rather than GGF (Falls, 2003b).

The formal terminology, classifies the NRG1 isoforms according to their very N-terminal sequence and divides them into six major groups (NRG1 type I-VI) (Falls, 2003b; Mei and Xiong, 2008) (Figure 5). The amino-terminal sequences of the type I, II, IV and V isoforms contain an immunoglobulin (Ig)-like domain and therefore are sometimes termed Ig-NRG1. This domain is thought to interact with the extracellular matrix of synapses thereby ensuring high local concentrations of NRG1 and sustained ErbB activation (Li and Loeb, 2001). In contrast, NRG1 type III isoforms share a cysteine-rich domain (CRD) near their N-terminus and are referred to as CRD-NRG1. As a part of the CRD forms an N-terminal transmembrane domain NRG1 type III isoforms are double pass membrane proteins and feature a unique hairpin-like topology with both the N- and the C-terminus in the cytosol (Wang et al., 2001) (Figure 5, 1.3.3.2.2 Figure 6).

Following their specific N-terminal sequences, all NRG1 isoforms contain an EGF-like domain in their extracellular part which is essential for the activation of ErbB receptors (Buonanno and Fischbach, 2001). While the N-terminal portion of the EGF-like domain is common to all isoforms, alternative splicing generates two different EGF C-termini (Figure 5). The two types of EGF-like domains, called α-type EGF and β-type EGF, therefore only differ in the sequence following the fifth conserved cysteine residue of the EGF-like domain (Holmes et al., 1992; Wen et al., 1994). Nevertheless, compared to the α-type the β-type EGF displays a significantly higher affinity towards ErbB receptors and is the predominant isoform in the brain (Meyer and Birchmeier, 1994; Wen et al., 1994).

In most NRG1 isoforms the EGF-like domain is followed by a short juxtamembrane linker sequence. This so called "stalk" region is highly variable and alternative splicing generates three different sequences named 1, 3 and 4 (Falls, 2003b). Stalks 1 and 4 separate the EGF-like domain from the C-terminal TMD and comprise 17 and 35 residues, respectively. In contrast, the stalk 3 is truncated and contains a stop codon before the TMD

resulting in the generation of soluble NRG1 isoforms that are secreted into the extracellular lumen. Finally, isoforms of NRG1 designated with 2 lack a stalk sequence and their EGF-like domain is directly connected to the TMD (Holmes et al., 1992; Wen et al., 1994) (Figure 5). Since most NRG1 isoforms are synthesized as transmembrane precursors they require shedding for full biological activity. Shedding occurs within the juxtamembrane region and the different stalk sequences not only influence the efficiency of this processing but may also determine which protease is able to cleave (Montero et al., 2000). After the juxtamembrane stalk, all membrane-bound NRG1 isoforms contain a common TMD that is followed by a C-terminal cytoplasmic tail. This intracellular domain consists of two parts: The first part is encoded by exons c1-c3 and is shared by all isoforms. The second part either comprises a short (b-type) or a long (a-type) sequence (Figure 5), with the latter being the predominant splice variant of the NRG1 isoforms in the nervous system (Falls, 2003a). At least two important functions of the TMD and the cytoplasmic tail of NRG1 are known: The TMD and part of the tail seem to contain an internal signal sequence and are crucial for NRG1 type I (and presumably type IV-VI) to enter the secretory pathway as its N-terminus lacks a classical signal sequence (Liu et al., 1998; Talmage, 2008). In addition, the TMD of NRG1 is cleaved by the γ-secretase and the liberated a-type ICD was shown to function as a transcription factor (1.3.3.3).

The terminology outlined above allows the specific designation of all NRG1 isoforms discovered so far. For example NRG1 III β1a refers to a type III NRG1 isoforms that contains a β-type EGF-like domain, a stalk region 1 and the long a-type cytosolic tail. Figure 5 provides a schematic overview of the NRG1 exons and their combinations through alternative splicing that give rise to the different isoforms. Not all combinations theoretically possible have been identified *in vivo* so far.
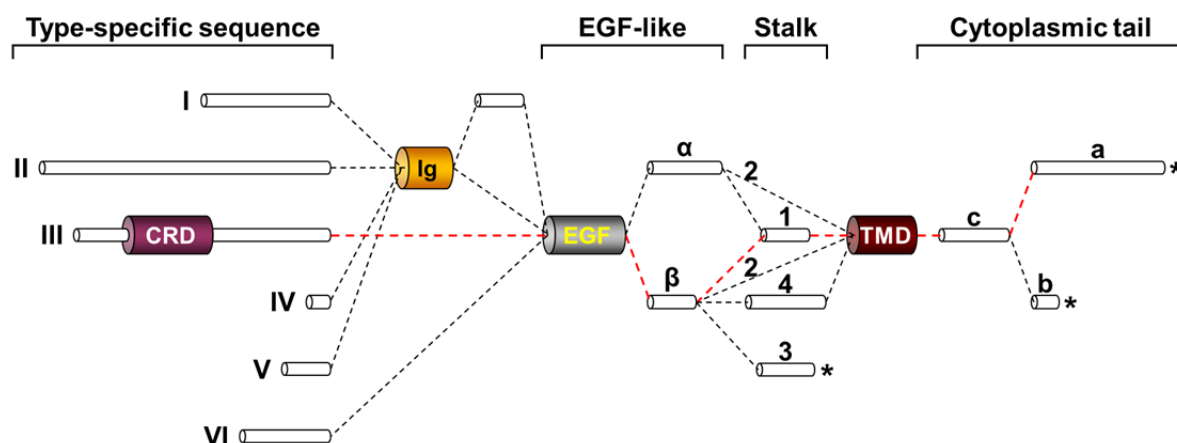
Figure 5. Overview of neuregulin-1 isoforms generated by differential promoter usage and alternative splicing. Six different N-terminal exons define the principle types of NRG1 (I-VI). Types I, II, IV and V contain an N-terminal Ig-like domain while type III instead includes a cysteine-rich domain (CRD) which forms a TMD. All isoforms share a common core EGF-like domain which may differ at its C-terminus (α or β). Different juxtamembrane sequences (stalks 1, 4; no stalk: 2) connect the ecto-domain to the TMD or terminate before (stalk 3) thereby generating soluble NRG1 isoforms. The TMD is followed by different intracellular domains (a- or b-type). The red line indicates the isoform NRG1 type III β1a which was used during this study. Based on scheme from (Falls, 2003a).

1.3.3 Proteolytic processing and signaling of NRG1

Although there are many different isoforms of NRG1, they all seem to convey their physiological functions through a common signaling paradigm: First, the activation of the membrane-bound precursor by proteolytic cleavage and second, the binding of the NRG1 EGF-like domain to ErbB receptors which subsequently are activated and mediate the further signaling.

1.3.3.1 ErbB receptors

The ErbB receptor family consists of four related receptor tyrosine kinases (Yarden and Sliwkowski, 2001): The EGF receptor ErbB1 (EGFR, HER1), ErbB2 (HER2, Neu) (Drebin et al., 1984; Schechter et al., 1984) for which no ligand is known, ErbB3 (HER3) (Kraus et al., 1989) which is catalytically inactive and ErbB4 (HER4) (Plowman et al., 1993). All ErbB receptors are single pass transmembrane proteins with an extracellular receptor domain and an intracellular tyrosine kinase domain. Binding of a ligand's EGF-like domain to the extra-cellular domain of ErbB induces receptor dimerization and subsequent activation of the intracellular kinase domain. This leads to the auto- and trans-phosphorylation of tyrosine residues at the C-terminus of the ErbB dimer which then serve as docking sites for different adaptor proteins and enzymes that mediate the intracellular downstream signaling (Bublil

and Yarden, 2007). In a process that seems to require endocytosis (Yang et al., 2005), ErbB receptors subsequently activate two major signaling cascades, the Ras/Raf/Erk1/2 and the PI3K/AKT pathway. Other intracellular cascades that are activated include for example the mTOR pathway as well as pathways regulated by the Ca^{2+} dependent protein kinase C (PKC) (Yarden and Sliwkowski, 2001; Zhang et al., 2007).

ErbB receptors differ in their affinity for NRG1 and in their requirement for dimerization (Buonanno and Fischbach, 2001). Despite serving as receptor for many growth factors, ErbB1 does not bind NRG1 and only participates in NRG1 signaling through hetero-dimerization with ErbB4. Likewise, ErbB2, which does not bind any known ligands, functions as NRG1 co-receptor by forming heterodimers with ligand-bound ErbB3 and ErbB4. Both ErbB3 and ErbB4 bind NRG1 but due to its inactive cytosolic kinase domain, ErbB3 critically depends on heterodimerization with either ErbB2 or ErbB4. In contrast, ErbB4 is the only autonomous ErbB receptor that may mediate NRG1 signaling as homodimer (Mei and Xiong, 2008).

The many cellular growth-responses elicited by ErbB receptor signaling include proliferation, differentiation, changes in motility and cell survival. As the different ErbB receptors have numerous functions in many cell types during both development and adulthood a comprehensive overview is beyond the scope of this introduction but may be found elsewhere (Yarden and Sliwkowski, 2001). In the following only the two aspects of ErbB receptor signaling most relevant for the present study will be introduced briefly.

1.3.3.1.1 ErbB4 receptor signaling in the CNS

ErbB4 is best characterized for its role in the CNS and is expressed in many of its parts (Carpenter, 2003). ErbB4 receptors play crucial roles during early brain development including the control of radial and tangential migration, axon guidance and migration of neuronal crest cells (Gassmann et al., 1995; Rio et al., 1997; Golding et al., 2000). Furthermore NRG1-ErbB4 signaling was shown to regulate the expression of neuronal AChR and $GABA_A$ (γ-aminobutyric acid) receptors and to influence the levels of synaptic glutamate receptors including NMDA (N-methyl-D-aspartic acid) and AMPA (2-amino-3-(3-hydroxy-5-methyl-isoxazol-4-yl)propanoic acid) receptors (Ozaki et al., 1997; Rieff et al., 1999; Liu et al., 2001; Li et al., 2007). Through this, ErbB4 signaling is involved in the maturation of synapses, the regulation of neuronal excitability and synaptic plasticity. It is for these many roles in neuronal development and plasticity that ErbB4 is implicated in the etiology of diseases such as epilepsy (Li et al., 2012; Tan et al., 2012) and schizophrenia (Mei and

Xiong, 2008). Indeed ErbB4 has been identified as a susceptibility gene for schizophrenia (Silberberg et al., 2006; Law et al., 2007; Walsh et al., 2008) and alterations in ErbB4-mediated signaling in mice lead to behavioral phenotypes considered rodent analogs of this neurodevelopmental disorder (Stefansson et al., 2002).

1.3.3.1.2 ErbB2/ErbB3 receptor signaling in the PNS

One of the most extensively studied functions of ErbB2 and ErbB3 is their role during myelination in the PNS (Newbern and Birchmeier, 2010). ErbB2 and ErbB3 expressed by glia cells and their precursors in the PNS are crucial during early Schwann cell development and mice with targeted mutations in these receptors exhibit an almost complete loss of Schwann cell progenitors (Riethmacher et al., 1997; Morris et al., 1999; Woldeyesus et al., 1999). In this regard, NRG1 signaling via ErbB2/3 seems to control not only differentiation and proliferation but also the axonal migration of Schwann cell precursors. After birth, the type (i.e. myelination of large caliber axon vs. formation of Remak bundle), time of onset and extent of myelination is determined by NRG1-ErbB2/3 signaling and targeted disruption of ErbB2 in Schwann cells causes hypomyelination (Garratt et al., 2000; Michailov et al., 2004; Chen et al., 2006) (1.3.4.1). Both receptors are also expressed during adulthood and therefore may be required in mature Schwann cells. However, while their ligand NRG1 is necessary for remyelination after injury (Fricker et al., 2011), the role of ErbB2/3 remains elusive as the loss of ErbB2 receptors had only minimal effects on this process (Atanasoski et al., 2006).

In summary, ErbB receptor-mediated cell-cell communication during development and adulthood controls numerous physiological functions. Growth factor signaling especially via ErbB1 and ErbB2 is also prominently involved in the development of cancer and hence both receptors are important drug targets (Zhang et al., 2007). Among many other functions, ErbB4 is crucial for neuronal development and plasticity and altered ErbB4 signaling seems to be implied in the etiology of schizophrenia (1.3.4.2.1). Lastly, together with NRG1, ErbB2 and ErbB3 receptors are key regulators of Schwann cell development and control myelination in the PNS (1.3.4.1.1).

1.3.3.2 Extracellular cleavage and forward signaling of NRG1

Although NRG1 isoforms are almost exclusively synthesized as transmembrane proteins, they were originally identified as factors in the supernatant of cancer cells that activate ErbB receptors on distant cells (Holmes et al., 1992; Peles et al., 1992). Such signaling requires the generation of a soluble, diffusible bioactive domain from the membrane-bound NRG1 and

indeed the ectodomains of almost all isoforms are detected as soluble peptides. Already upon their initial discovery it was therefore suggested that proteolytic processing may be responsible for the release of the EGF-like domain from the membrane (Holmes et al., 1992; Wen et al., 1992). It is now established that the membrane-bound forms of NRG1 are indeed precursor proteins that require proteolytic cleavage to gain full biological activity. Different proteases of the ADAM family and BACE1 have been shown to cleave NRG1 and the juxtamembrane region between the EGF-like domain and the TMD has been identified as the site where this shedding occurs (1.3.3.2.3).

Depending on the topology of the membrane-bound precursor, shedding in the stalk region either results in the generation of a soluble or a membrane-tethered EGF-like domain (Figure 6). This difference has important implications as it is thought to enable two principally different signaling modes of NRG1: paracrine and juxtacrine signaling (Falls, 2003a). Paracrine signaling refers to communication between cells that are not in direct contact with each other and such contact-independent signaling therefore requires soluble, diffusible signaling factors. In contrast, during juxtacrine signaling the ligand remains membrane-bound and receptor activation requires direct contact between the signal producing and signal receiving cell.

1.3.3.2.1 Paracrine signaling

NRG1 isoforms that feature a type I membrane topology (i.e. isoforms I, II, IV-VI) are believed to signal in a paracrine fashion. Shedding within the stalk region liberates their N-terminal extracellular part including the EGF-like domain into the extracellular environment (Figure 6). These soluble NRG1 peptides may then diffuse and act as paracrine signals activating ErbB receptors on distant target cells. Paracrine signaling by soluble NRG1 type I is crucial for a number of physiological processes including the development of the brain (Mei and Xiong, 2008) and heart (Meyer et al., 1997; Horiuchi et al., 2005), the formation and maintenance of neuromuscular synapses (Falls, 2003a) and muscle spindles (Hippenmeyer et al., 2002; Cheret et al., 2013).

1.3.3.2.2 Juxtacrine signaling

So far NRG1 type III is the only isoform that has been found to contain two TMDs and to feature a hairpin-like structure with both the N- and C-terminus in the cytosol (Wang et al., 2001). In contrast to other isoforms, shedding in its juxtamembrane region generates a membrane-bound N-terminal fragment that presents the EGF-like domain towards the extracellular environment (Figure 6). Due to its membrane anchor, the EGF-like domain of
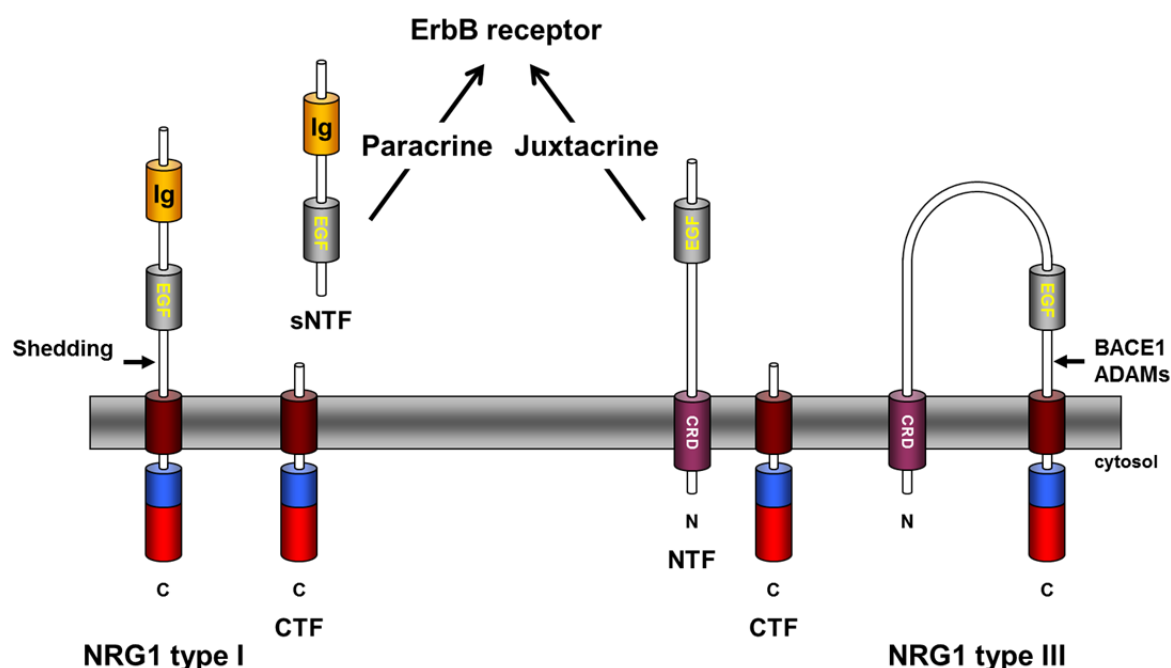
Figure 6. Different modes of forward signaling by neuregulin-1 after shedding. Shedding of NRG1 occurs in the juxtamembrane region close to the TMD and is mediated by BACE1 and members of the ADAM family of proteases. NRG1 isoforms I, II and IV-VI are single pass trans-membrane proteins and shedding releases their ectodomain (sNTF) into the luminal space where it acts as contact-independent (paracrine) signal and activates ErbB receptor on distant cells. Shedding of NRG1 type III which contains two TMDs generates a membrane-bound NTF that mediates contact-dependent (juxtacrine) signaling and activates receptor only on neighboring cells.

NRG1 type III only activates ErbB receptors on cells that are in direct contact and is therefore considered a juxtacrine signal (Falls, 2003a). Juxtacrine signaling between axonal NRG1 type III and ErbB2/3 receptors on Schwann cells is crucial for Schwann cell development and myelination in the PNS (1.3.4.1). Additionally, contact-dependent signaling by NRG1 type III via ErbB4 is implicated in the guidance of thalamocortical axons during brain development (Mei and Xiong, 2008). As ErbB-mediated NRG1 signaling seems to require endocytosis (Yang et al., 2005; Liu et al., 2007), an additional cleavage within the membrane-bound NRG1 type III NTF during or after juxtacrine receptor activation may be expected.

1.3.3.2.3 Proteases involved in the shedding of NRG1

The β-secretase BACE1 was identified as one of the most important physiological sheddase of NRG1 (Hu et al., 2006; Willem et al., 2006; Fleck et al., 2012). Full-length NRG1 accumulates in BACE1 KO mice (Hu et al., 2006; Willem et al., 2006) and in mice treated with a BACE1 inhibitor (Cheret et al., 2013) while the corresponding cleavage products are diminished. The physiological importance of BACE1-mediated NRG1 shedding is underlined

by the fact that ablation of BACE1 in mice causes prominent hypomyelination of peripheral nerves (Hu et al., 2006; Willem et al., 2006) and muscle spindle defects (Cheret et al., 2013). The cognitive and behavioral alterations displayed by these animals (1.1.3.2) may likewise be linked to the abolished processing of NRG1 by BACE1, but the mechanistic details still remain elusive. The BACE1 cleavage site in the stalk region of NRG1 has been mapped both *in vitro* (Hu et al., 2008) and in living cells (3.1.2) and unanimously was found to be located 10 residues upstream of the TMD (3.3 Figure 27).

Prior to BACE1, ADAM17 was the first protease shown to cleave NRG1 within the stalk region and to release the ectodomain of several NRG1 isoforms from the membrane (Montero et al., 2000). Interestingly, the efficiency of ADAM17-mediated shedding varies for different NRG1 isoforms and seems to depend in part on the length and type of the juxtacrine stalk region. ADAM17 cleavage of NRG1 is strongly enhanced upon treatment with PMA (phorbol 12-myristate 13-acetate) and ADAM17 was found to be responsible for the constitutive and regulated shedding of NRG1 isoforms $\beta1$ and $\beta2$ in mouse embryonic fibroblasts (Horiuchi et al., 2005). Based on the observation of a peripheral hypermyelination in conditional ADAM17 KO mice (La Marca et al., 2011), shedding of NRG1 type III by ADAM17 has recently been suggested to generate a biologically inactive NRG1 fragment that inhibits Schwann cell myelination and counteracts BACE1-cleaved NRG1 (1.3.4.1.5). In contrast to BACE1, ADAM17 seems to mediate a more heterogeneous shedding in the stalk region of NRG1 and several different cleavage sites 13 to 21 residues upstream of the TMD have been identified *in vitro* and in living cells (4.2 Figure 49).

Besides ADAM17, ADAM10 was identified as NRG1 sheddase but the physiological relevance of this cleavage is unclear. *In vitro*, ADAM10 cleaves NRG1 at a single site located 18 residues upstream of the TMD (Luo et al., 2011) but may additionally utilize a site nearby in living cells (3.1.2). Processing by ADAM10 generates signaling competent NRG1 type I and type III isoforms that activate ErbB receptors similar to the BACE1-cleaved fragments. Nevertheless, reduced or abolished ADAM10 activity does not result in impaired NRG1-dependent Schwann cell myelination *in vitro* or *in vivo* indicating no major role of ADAM10 as NRG1 sheddase in this context (Freese et al., 2009; Luo et al., 2011).

ADAM9 and ADAM19 have also been implicated in the shedding of NRG1. However, while some studies found ADAM19 to cleave NRG1, albeit only within the stalk region of β-type isoforms, (Shirakabe et al., 2001; Kurohara et al., 2004) this could not be confirmed by other groups (Zhou et al., 2004; Horiuchi et al., 2005). ADAM9 seems to cleave NRG1 not within the stalk region but N-terminal of the EGF-like domain and therefore does not release

a fragment capable of signaling (Shirakabe et al., 2001). No cleavage sites have been reported for either protease yet.

In summary, ectodomain shedding of the membrane-bound NRG1 precursor proteins appears to be critical for both paracrine and juxtacrine NRG1 signaling. In addition to its regulation by neuronal activity (Liu et al., 2011), the (regulated) activation of NRG1 through proteolytic cleavage thereby adds another level of control to the signaling of NRG1 linking it directly to the regulated expression and activity of different sheddases.

1.3.3.3 Intramembrane cleavage and reverse signaling of NRG1

Reverse signaling of NRG1 type III is initiated by binding of the ErbB4 receptor or its soluble ectodomain to the EGF-like domain of the NRG1 type III NTF (Bao et al., 2003) (Figure 7). This in turn induces γ-secretase-mediated intramembrane proteolysis of the corresponding CTF that results in the liberation of the NRG1 intracellular domain (NRG1-ICD) into the cytosol. Although the mechanistic details are still unclear, experimental evidence suggests that the NRG1 type III NTF and CTF remain physically associated during receptor binding and prior to intramembrane proteolysis. Besides stimulation by ErbB4 also neuronal depolarization was found to trigger liberation of the NRG1-ICD linking the regulation of reverse signaling by NRG1 type III to synaptic activity (Bao et al., 2003, 2004).

Once in the cytosol, the NRG1-ICD, which contains a nuclear localization sequence close to its N-terminus, translocates to the nucleus where it binds the zinc-finger transcription factor Eos (Figure 7). The NRG1-ICD-Eos complex then interacts with the Ilk1/2 site in the promoter of the postsynaptic density protein 95 (PSD-95) and induces upregulation of PSD-95 expression. Besides increasing the levels of PSD-95, signaling by the NRG1-ICD also represses the transcription of several regulators of apoptosis resulting in reduced neuronal cell death in an *in vitro* system (Bao et al., 2003, 2004). In addition, a recent study found the growth and branching of cortical dendrites to critically depend on the signaling of the NRG1-ICD and suggested the reverse signaling of NRG1 type III as a novel regulator of dendritic development independent of ErbB receptor kinase activity (Chen et al., 2010a).

Apart from its role as a regulator of transcription in the nucleus, the NRG1-ICD also seems to control cellular functions through activation of signaling cascades in the cytosol. Stimulation of neurons expressing NRG1 type III with ErbB4 induces NRG1-ICD-dependent PI3K signaling (Figure 7) and thereby leads to an increase of nicotinic acetylcholine receptors along the axonal surface. Interestingly, the increase in surface receptors was not

due to enhanced protein synthesis but instead resulted from a redistribution of the intracellular receptor pool (Hancock et al., 2008).

In comparison with the classical forward signaling, much less is yet known about the reverse signaling of NRG1 type III. Nevertheless the latter has emerged as an important regulator of synaptic maturation and plasticity and alterations in this signaling pathway are suggested to contribute to the development of abnormal neuroconnectivity observed in schizophrenia. This hypothesis is strongly supported by the presence of a schizophrenia-linked mutation within the TMD of NRG1 that impairs γ-secretase processing and subsequent signaling of the NRG1-ICD and causes aberrant development of cortical neurons (1.3.4.2.2).
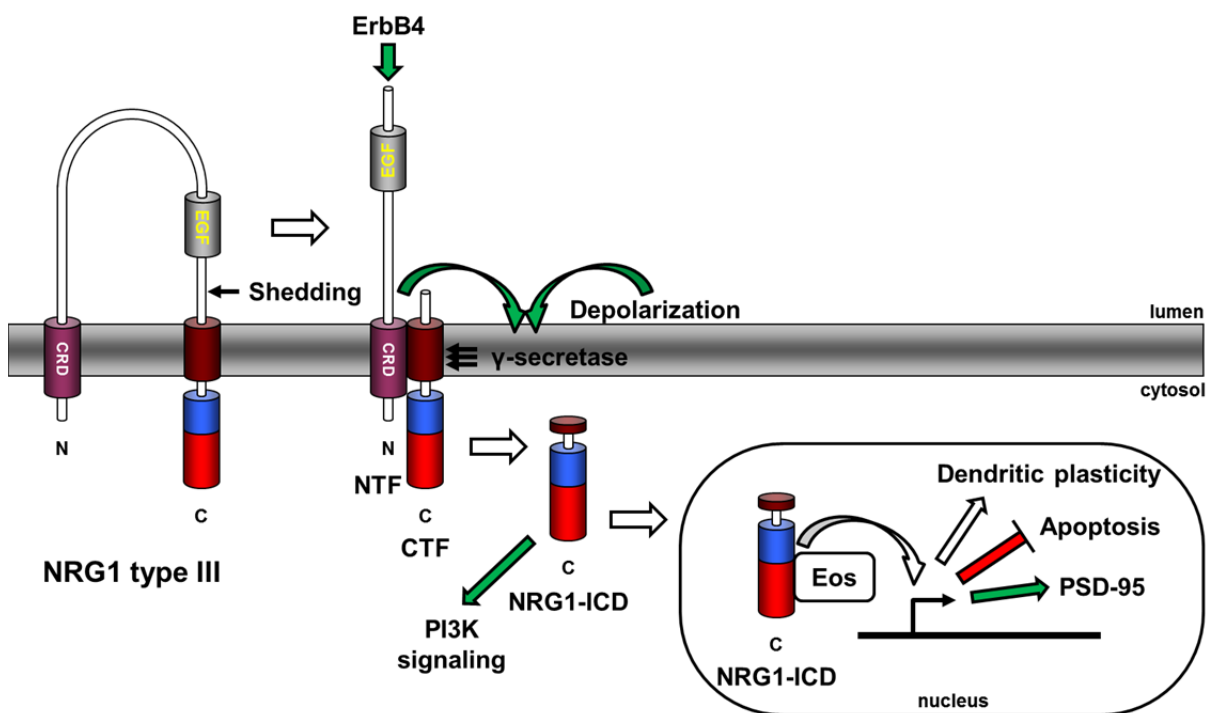
Figure 7. Reverse signaling by neuregulin-1 type III. Shedding of NRG1 type III generates a membrane-bound NTF and CTF. Neuronal depolarization or ligand binding to the NTF triggers intra-membrane proteolysis of the CTF by the γ-secretase which releases the NRG1-ICD from the membrane. The NRG1-ICD activates the PI3K signaling pathway in the cytosol but also translocates into the nucleus where it binds the transcription factor Eos. Together with Eos, the NRG1-ICD acts as transcriptional modulator of several genes involved in apoptosis and the development of dendrites.

1.3.4 Functions of NRG1 type III

Neuregulin-1 isoforms have many essential roles in the development and maintenance of the central and peripheral nervous system. They also mediate critical cell-cell communication in a number of other organs including the heart, the lung and the breasts. In addition to its physiological functions, neuregulin-1 signaling is also implicated in the pathogenesis of diseases including schizophrenia, cancer and multiple sclerosis. Due to this multitude of roles a comprehensive introduction into the functions of NRG1 cannot be given within the scope of this work. However a detailed overview of the biological importance of NRG1 in development, adulthood and disease may be found in a number of excellent reviews (Buonanno and Fischbach, 2001; Falls, 2003a, 2003b; Mei and Xiong, 2008). In the following only the aspects most relevant to this study will be introduced: the role of NRG1 type III during myelination in the PNS and the involvement of NRG1 in the pathogenesis of schizophrenia.

1.3.4.1 NRG1 type III controls myelination in the PNS

Many of the physiological functions of NRG1 were revealed through the study of mice in which all or specific isoforms of NRG1 were knocked out. Mice in which all isoforms of NRG1 are rendered non-functional (pan-NRG1 KO) die during embryogenesis at E10.5 due to defects in cardiac morphogenesis (Meyer and Birchmeier, 1995). These mice also display a severe reduction of cells descending from neural crest progenitors including Schwann cells and cranial sensory neurons (Meyer et al., 1997; Britsch et al., 1998). Interestingly, mice with all NRG1 isoforms inactivated except NRG1 type III (Ig-NRG1 KO) show a very similar phenotype but have a normal development of Schwann cell precursors (Meyer et al., 1997). Vice versa, NRG1 type III KO mice (CRD-NRG1 KO) do not suffer from defective cardiac morphogenesis but do display severely reduced numbers of Schwann cell precursors and furthermore lack functional neuromuscular synapses. Subsequent expression analysis revealed that NRG1 type III is particularly strongly expressed in sensory and motoneurons which are myelinated by Schwann cells. Together this suggested an important role of NRG1 type III in Schwann cell development and myelination in the PNS.

The majority of large axons in the mammalian nervous system is myelinated, i.e. they are surrounded by multiple layers of a lipid rich membrane, the myelin sheath (Figure 8). Myelination serves as electrical insulation and increases the speed at which nerve impulses are transmitted. At the same time the myelin sheath also supports the neurons with trophic factors and protects against axonal damage (Nave, 2010). Conversely, the axon provides

signals that regulate survival and differentiation of the myelinating cells. Myelination occurs during development when specialized glia cells, called oligodendrocytes in the CNS and Schwann cells in the PNS, wrap their membranes around axons multiple times. In contrast to the oligodendrocytes in the CNS which participate in the myelination of several different axons, myelinating Schwann cells establish a 1:1 contact with neurons and only myelinate one segment of a single axon (Baumann and Pham-Dinh, 2001). The thickness of the myelin sheath is determined by the size of the axon and directly correlates with its diameter. Consequently large axons are surrounded by a thick layer of myelin while smaller axons have thinner myelin sheaths. Small axons with diameters below 1 µm usually are not myelinated but instead, together with several other small caliber axons, are engulfed by non-myelinating Schwann cells to form a so called Remak bundle (Jessen and Mirsky, 2005; Birchmeier and Nave, 2008) (Figure 8).
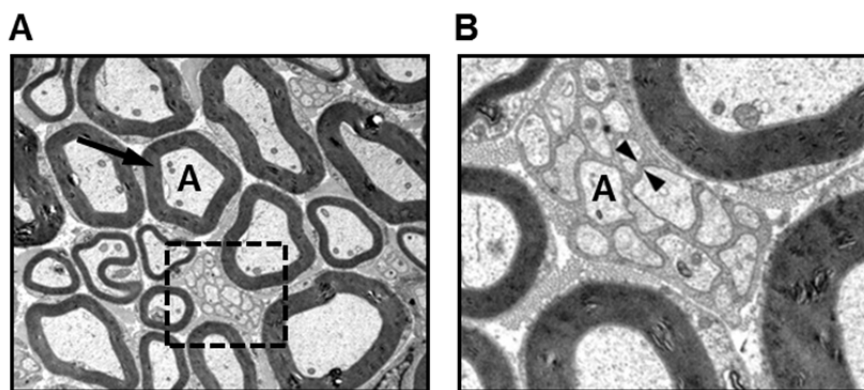
Figure 8. Myelination of axons in the peripheral nervous system. A) Electron microscopic image of a sciatic nerve section from mouse. Large caliber axons (marked with A) are surrounded by myelin sheaths (arrow) provided by myelinating Schwann cells. Smaller axons are sorted into Remak bundles (dashed box). **B)** Higher magnification of Remak bundle from A). Non-myelinating Schwann cells engulf several small caliber axons to form a Remak bundle. Within the bundle, axons (A) are separated from each other by the cytoplasm of the Schwann cell (arrowheads). Images taken from (Willem et al., 2006).

Three main transitions characterize the development from neural crest stem cells (NCSC) to mature Schwann cells. First neural crest stem cells differentiate into Schwann cell precursors (SCPs). In a second step these SCPs proliferate and become immature Schwann cells. Finally, mature Schwann cells are formed and myelination commences (Jessen and Mirsky, 2005) (Figure 9).
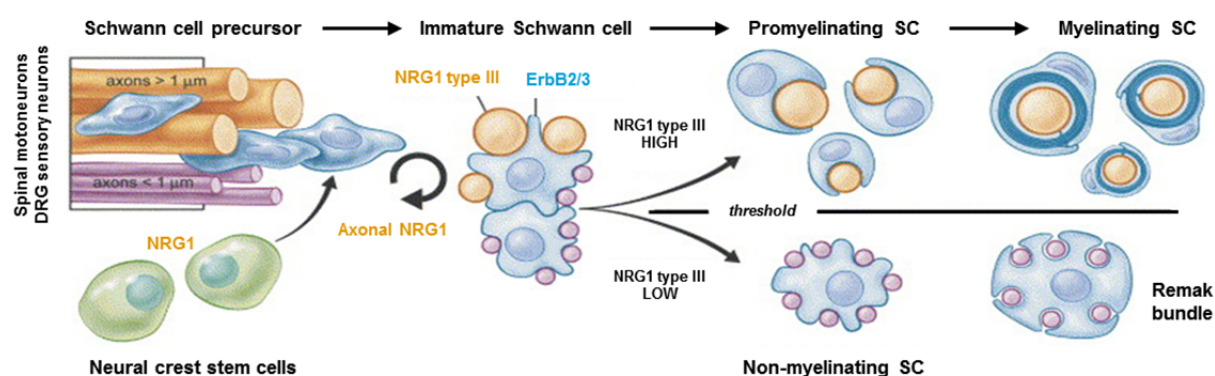
Figure 9. Control of Schwann cell development and myelination in the PNS by neuregulin-1. NRG1 promotes the migration of neural crest stem cells (NCSC) towards axons and their transition into Schwann cell precursor cells (SCPs). Axonal NRG1 type III is essential for the survival, proliferation and movement of the SCPs and also controls their differentiation into immature Schwann cells (SCs). Immature SCs associate with several axons and determine their size based on the level of NRG1 type III on their surface. Large axons with high NRG1 type III levels promote the transition of immature SCs into myelinating SCs and become surrounded by a myelin sheath. Lower levels of NRG1 type III on small axons lead to the formation of Remak bundles by non-myelinating SCs. Modified from (Nave and Salzer, 2006).

NRG1 type III, the main NRG1 isoform in the PNS, is highly expressed by neurons in the DRG and on the axons of motoneurons throughout Schwann cell development and myelination (Loeb et al., 1999; Michailov et al., 2004). Accordingly, signaling by axonal NRG1 type III through ErbB2/3 receptors on Schwann cells (which do not express ErbB4) has emerged as an important regulator of virtually all steps of Schwann cell development and myelination and carries out different functions at different developmental stages (1.3.4.1.1). It should be noted that although several studies implicated a similar role of NRG1 in the myelination of the CNS, a recent study clearly showed that myelination by oligodendrocytes is controlled in an NRG1-ErbB-independent way (Brinkmann et al., 2008).

1.3.4.1.1 Schwann cell development depends on NRG1-ErbB2/3 signaling

Very early during embryonal development, NRG1 inhibits neurogenesis of neural crest stem cells (NCSCs) and promotes their migration through the extracellular matrix towards the regions where peripheral ganglia form (Figure 9). The signals and mechanisms regulating the subsequent transition from NCSPs to Schwann cell precursors (SCPs) are still poorly understood but likewise seem to depend on NRG1-ErbB2/3 signaling (Jessen and Mirsky, 2005; Woodhoo and Sommer, 2008). The Schwann cell precursors then migrate along the developing nerve and establish a tight association with multiple axons (Figure 9). NRG1 type III was shown to be crucial in this context as in mice specifically lacking this isoform, SCPs initially populate peripheral nerve projections normally but then undergo cell death and are

absent in later stages (Wolpowitz et al., 2000). In addition to this role in survival and proliferation NRG1-ErbB2/3 signaling is essential for the directed migration of Schwann cell precursors. Inhibition of ErbB receptors or deletion of NRG1 type III in zebrafish caused SCPs to either stop their migration or deviate from their original path (Lyons et al., 2005; Perlin et al., 2011). Conversely, ectopic expression of NRG1 type III in neurons of both the CNS and the PNS directed SCPs to aberrantly migrate into the CNS, further corroborating the role of NRG1 type III as instructive signal in Schwann cell migration (Perlin et al., 2011). The strict axon-dependence of Schwann cell precursor survival and migration during these early phases of development probably serves as mechanism that adjusts the number of SCPs to the number of axons and facilitates correct spatial orientation (Jessen and Mirsky, 2005).

The second transition during Schwann cell development, the differentiation of SCPs into immature Schwann cells, occurs late in embryogenesis and is driven by NRG1 and canonical Notch signaling (Jessen and Mirsky, 2005; Woodhoo et al., 2009). Immature Schwann cells subsequently associate with groups of axons in nerves that already acquired their basic structure (Jessen and Mirsky, 2005) (Figure 9). A fundamental difference between SCPs and (immature) Schwann cells concerns the regulation of survival: While SCPs depend on axon-derived signals, (immature) Schwann cells survive axon-independently via autocrine stimulation by secreted growth factors. The switch to an autocrine support mechanism allows the Schwann cells to survive after axonal damage and to provide support during regrowth of peripheral nerves (Jessen and Mirsky, 2005).

1.3.4.1.2 NRG1 type III controls ensheathment fate and myelin thickness

Shortly before and after birth immature Schwann cells differentiate into either myelinating or non-myelinating Schwann cells and myelination commences (Figure 9). With the transition to mature Schwann cells, the role or NRG1 type III changes. During Schwann cell development, NRG1 signaling regulates differentiation, survival and proliferation of the precursors and serves to adjust the number of Schwann cells. In contrast, during the process of myelination, NRG1 signaling controls the ensheathment fate of axons (myelinated axons vs. Remak bundles), determines the final phenotype of Schwann cells (myelinating vs. non-myelinating) and regulates the thickness of the myelin sheaths (Nave and Salzer, 2006; Birchmeier and Nave, 2008).

The binary choice of whether a Schwann cell myelinates an axon or forms a Remak bundle is determined by the size of the respective axon. However, rather than the diameter,

the amount of NRG1 type III NTF on the axonal surface, being in fact a function of the diameter, is the key factor in this decision. Investigation of different nerves in mice revealed that the unmyelinated axons of sympathetic neurons express low levels of NRG1 type III while the strongly myelinated axons of DRG neurons express high levels (Taveggia et al., 2005; Nave and Salzer, 2006). In line, Schwann cells attach to neurons lacking NRG1 type III *in vitro* but subsequently fail to myelinate them. Conversely, ectopic expression of NRG1 type III in sympathetic neurons that physiologically are not myelinated induces their myelination (Taveggia et al., 2005). Together this demonstrates that a certain threshold level of NRG1 type III on axons is required to trigger Schwann cell myelination (Figure 9).

Besides determining the type of ensheathment, NRG1 type III also regulates the thickness of the myelin sheath, i.e. the number of times the Schwann cell wraps its membrane around the axon. This was demonstrated in mice with reduced levels of NRG1 type III (NRG1 type III +/-) which display abnormally thin myelin sheaths around peripheral axons (Michailov et al., 2004) (Figure 10). Importantly, this peripheral hypomyelination was not due to impaired development of precursor cells and Schwann cell numbers were unaffected. In line, transgenic mice with increased neuronal levels of NRG1 type III have markedly thicker myelin sheaths in the PNS (Michailov et al., 2004).

1.3.4.1.3 Signaling pathways in Schwann cells induced by NRG1

Myelination is a complex morphogenetic event that requires a significant increase in the size of the Schwann cell and the synthesis of large amounts of myelin. To this end myelin-specific genes are upregulated in Schwann cells prior to the onset of myelination and several intracellular signaling pathways have been shown to be involved in their regulation.

Activation of ErbB2/3 receptors on Schwann cells by axonal NRG1 type III triggers the recruitment of adaptor proteins and enzymes to the phosphorylated sites of the receptor (1.3.3.1). Among these, the phosphatidylinositol 3 kinase (PI3K) initiates one of the key signaling pathways implicated in the promotion of myelination. After its phosphorylation, PI3K activates the serine-threonine-specific kinase AKT (also known as protein kinase B, PKB) which then through a yet unknown mechanism induces transcription factors such as Oct-6, Krox-20 and Sox-10 (Taveggia et al., 2010). In contrast to PI3K-AKT signaling that promotes the transition of Schwann cells to the myelinating state, the extracellular signal-regulated kinase (Erk1/2) pathway (also known as MAP kinase pathway) was shown to inhibit this process. Activation of the Ras/Raf/Erk1/2 signaling cascade downstream of ErbB2/3 receptors blocks the expression of myelin genes and consequently suppresses Schwann cell

differentiation and myelination (Harrisingh et al., 2004; Ogata et al., 2004; Syed et al., 2010). Together this suggests that NRG1-ErbB2/3 signaling regulates myelination via a finely tuned balance between these two differentially activated pathways.

1.3.4.1.4 Juxtacrine and paracrine NRG1 signaling during myelination

Two findings suggest that Schwann cell myelination strictly depends on a juxtacrine NRG1 signal: First, soluble NRG1 fails to rescue myelination of neurons completely lacking NRG1 type III *in vitro* (Taveggia et al., 2005). Second, only overexpression of the type III isoform (thought to constitute a juxtacrine signal, 1.3.3.2.2), but not of the type I isoform of NRG1 increases peripheral myelination in mice (Michailov et al., 2004). However, the finding that soluble NRG1 promotes Schwann cell myelination of neurons that do not completely lack but instead express low levels of NRG1 type III has challenged this view. Application of soluble NRG1 type III (consisting of the N-terminal 296 residues including the EGF-like domain) to Schwann cell co-cultures of NRG1 type III +/- neurons enhanced myelination and rescued the hypomyelination phenotype observed otherwise (Syed et al., 2010). Similarly, sympathetic neurons which endogenously express very low amounts of NRG1 type III and therefore normally lack a myelin sheath became myelinated by Schwann cells after treatment with soluble NRG1 type III (Syed et al., 2010). The promyelinating effect of the paracrine NRG1 signal was found to be dose-dependent and involved activation of the PI3K-AKT cascade similarly to what is observed in Schwann cells after juxtacrine NRG1 signaling. Interestingly, higher doses of soluble NRG1 type III lead to the preferential activation of the Ras/Raf/Erk1/2 pathway and inhibited myelination (Syed et al., 2010). Together these observations suggest two distinct steps during Schwann cell myelination: An initial phase which includes radial sorting and initial ensheathment and depends on a juxtacrine NRG1 signal from the axon; and a second phase during which the promotion of myelination may be stimulated by a paracrine NRG1 signal.

1.3.4.1.5 BACE1 and ADAM17 control myelination through NRG1 type III processing

Neuregulin-1 type III requires proteolytic activation prior to signaling and the proteases mediating this cleavage are therefore expected to be involved in the regulation of Schwann cell myelination. BACE1 is strongly expressed in sensory and motor neurons of mice around birth and is considered the most important sheddase of NRG1 type III in the context of PNS myelination (Willem et al., 2006; Fleck et al., 2012). Consequently, genetic ablation of BACE1 in mice leads to the accumulation of unprocessed NRG1 type III and causes severe hypomyelination of peripheral nerves without disturbing Schwann cell development (Hu et al.,

2006; Willem et al., 2006) (Figure 10). The phenotype of BACE1 KO mice resembles the phenotype of conditional ErbB2 KO mice or mice heterozygous for NRG1 type III (Figure 10) and suggests that BACE1-mediated processing of NRG1 type III promotes myelination in the PNS. In agreement, expression of the BACE1 cleavage product NRG1 type III NTF in neurons of BACE1 KO mice suffices to rescue PNS hypomyelination (Velanac et al., 2012).

However, genetic deletion of BACE1 does not completely prevent the turnover of NRG1 type III as evidenced by low amounts of NRG1 type III cleavage products and the presence of residual albeit thin myelin sheaths in BACE1 KO mice. Moreover, neuronal overexpression of the uncleaved NRG1 type III full-length protein caused peripheral hyper-myelination in mice even in the complete absence of BACE1 (Velanac et al., 2012). This suggests that beside BACE1 also other, yet unidentified, neuronal proteases cleave NRG1 type III *in vivo* and promote Schwann cell myelination. Likely candidates for such compensating proteases are different members of the ADAM family of proteases that cleave NRG1 type III similarly to BACE1, including ADAM10 and ADAM19 (1.3.3.2.3).
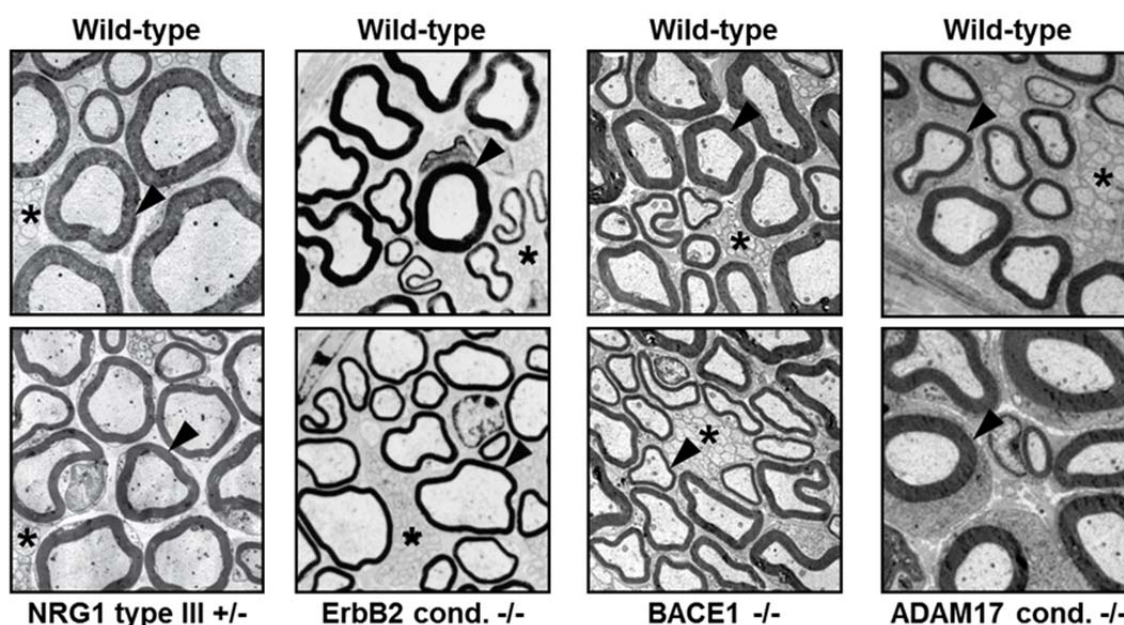
Figure 10. Myelination phenotypes in the PNS of mice with altered NRG1-ErbB signaling. Electron microscopic images of peripheral nerves from mice with reduced levels of NRG1 type III (NRG1 type III +/-), deficiency in ErbB2 receptors (ErbB2 cond. -/-) and deficiency in BACE1 and ADAM17 (BACE1 -/- and ADAM17 cond. -/-, respectively). A lack of ErbB2 receptors and of BACE1 leads to significantly thinner myelin sheaths around axons (arrowheads) resembling the phenotype of mice heterozygous for NRG1 type III. In contrast, thicker myelin sheaths are observed in mice lacking ADAM17. All animals except the ErbB2 KO also display defective bundling of small caliber axons into Remak fibers (asterisks; not shown for ADAM17 KO). Images from (Garratt et al., 2000; Taveggia et al., 2005; Willem et al., 2006; La Marca et al., 2011).

ADAM17 which also cleaves NRG1 type III has recently been proposed as a negative regulator of myelination. ADAM17 KO mice display increased myelin thickness in the PNS (Figure 10) and reduction of ADAM17 levels in neurons rescued the hypomyelination phenotype in NRG1 type III +/- mice (La Marca et al., 2011). The opposing effects of BACE1 and ADAM17 on myelination were suggested to arise from the different cleavage sites in the stalk region of NRG1 type III utilized by these enzymes (4.2 Figure 49, 4.7 Table 8). In line, ADAM17 processing *in vitro* was shown to generate an inactive NRG1 type III EGF-like domain unable to induce ErbB2/3 signaling in Schwann cells (La Marca et al., 2011). Collectively these findings suggest that BACE1 and ADAM17 regulate Schwann cell myelination in the PNS through differential shedding of NRG1 type III.

1.3.4.2 NRG1 and schizophrenia

Schizophrenia is a mental disease characterized by an abnormal perception of reality that often results in permanent disability (Corfas et al., 2004). The disease typically presents with both positive symptoms such as hallucinations, obsessive thoughts and delusions as well as with negative symptoms including apathy and social withdrawal. In addition patients also suffer from cognitive deficits (Buonanno, 2010). Schizophrenia usually manifests itself at the end of adolescence and during early adulthood and in total affects approx. 0.5-1.0% of the adult population. Most antipsychotic drugs used for the treatment of schizophrenic patients are antidopaminergic and mainly alleviate positive symptoms being only moderately effective against negative symptoms and cognitive dysfunction (Mei and Xiong, 2008). Given these limitations a more detailed understanding of the underlying genetic and molecular mechanisms of schizophrenia is desirable in order to develop more effective therapies.

1.3.4.2.1 NRG1-ErbB4 signaling in schizophrenia

Schizophrenia is thought to be caused by a combination of environmental and genetic factors of which the latter are estimated to be at least 50% (Tsuang et al., 2001). Multiple susceptibility genes have been identified, however, their low penetrance indicates that schizophrenia is a polygenic disease with only small contributing effects by different genes. The neuregulin-1 gene locus was found to be associated with an increased risk for schizophrenia in several different populations by genome wide analysis (Harrison and Weinberger, 2005). Similarly, certain variants of its main receptor in the CNS, ErbB4, also confer a higher risk (Mei and Xiong, 2008). Hence, NRG1 is viewed as one of the most important susceptibility genes for schizophrenia and altered NRG1-ErbB4 signaling was shown to be implicated in many pathways relevant to the etiology of the disease.

Schizophrenia is considered to be a neurodevelopmental disease with both alterations in the brain's structure and changes in the expression and signaling of neurotransmitters and their respective receptors. The structural alterations in the brains of schizophrenic patients which include enlarged ventricles and reductions in associative cortical areas are thought to be due to impaired neuronal migration and differentiation (Corfas et al., 2004). NRG1-ErbB4 signaling was shown to be crucial for these processes and it is plausible that disturbed NRG1 signaling during development could result in defective cortical connectivity leading to behavioral alterations. Likewise, NRG1 is involved in the regulation of neurotransmitter receptors in excitatory and inhibitory pathways, both of which are abnormal in schizophrenic patients (Buonanno, 2010). For example, decreased NRG1 signaling lead to the destabilization of postsynaptic AMPA receptors in hippocampal slices and caused the subsequent loss of NMDA currents and dendritic spines of excitatory neurons (Li et al., 2007). Furthermore, NRG1-ErbB4 signaling also modulates neurotransmitter release of inhibitory interneurons (Woo et al., 2007). Besides this acute effect on neurotransmission NRG1 and ErB4 also regulate the expression of neurotransmitter receptors (1.3.3.1.1) and hence are involved in the long-term plasticity of the brain. Consequently, mice with reduced NRG1 levels (NRG1 +/-) present with an altered transmission in both GABAergic and glutamatergic pathways and display behavioral abnormalities that can partially be reversed by treatment with antipsychotic drugs (Stefansson et al., 2002). Together this suggests that aberrant NRG1 signaling contributes to the pathogenesis of schizophrenia through an acute dysregulation of synaptic transmission and plasticity in an already abnormally developed brain.

1.3.4.2.2 NRG1 mutations in schizophrenia

Since the discovery of the first schizophrenia-associated single nucleotide polymorphisms (SNPs) in the NRG1 gene in families in Iceland (Stefansson et al., 2002) many follow-up studies have reported similar findings in multiple populations (Harrison and Weinberger, 2005). Most of the 80 SNPs identified so far cluster in non-coding intronic sequences in the 5' and 3' region of the NRG1 gene and therefore do not lead to mutations in the NRG1 protein that would change its processing or activity (Mei and Xiong, 2008). Instead, these SNPs are thought to affect splicing and expression of NRG1 and indeed altered mRNA levels of NRG1 isoforms have been detected in the prefrontal cortex and the hippocampus of schizophrenic patients (Hashimoto et al., 2003; Law et al., 2006). If these changes are also accompanied by altered protein levels remains unclear, however. Only very few

schizophrenia-associated SNPs actually generate a change in the amino acid sequence of the NRG1 protein and therefore could have direct functional consequences. One such mutation is caused by a SNP identified in families from Costa Rica and results in the substitution of a Valine (V) residue for a Leucine (L) (Walss-Bass et al., 2006). Interestingly, this V->L polymorphism is localized in the TMD region of NRG1 (3.6.2 Figure 46) and despite being a conservative mutation was shown to impair γ-secretase-mediated cleavage of the NRG1 CTF in cultured cells (Dejaegere et al., 2008). Consistently, the mutation severely reduces the generation of the NRG1-ICD and abolishes its nuclear signaling (Chen et al., 2010a) (1.3.3.3). This seems to have direct functional consequences as in contrast to wild-type NRG1 type III, the V->L mutant fails to rescue the dendritic length and branch point phenotype of NRG1 type III KO neurons (Chen et al., 2010a). In conclusion this raises the possibility that this schizophrenia-associated V->L polymorphism in NRG1 contributes to the disease pathology by disrupting the reverse signaling of NRG1 type III leading to deficits in the development of cortical dendrites and impaired neuronal connectivity. Together with the finding that reduced γ-secretase-mediated cleavage of NRG1 results in schizophrenia-like phenotypes in mice (Dejaegere et al., 2008) this calls for a closer investigation of the γ-secretase cleavage within the NRG1 TMD as well as of the mechanism by which sequence alteration influence this processing. Ultimately, the cleavage products of the intramembrane proteolysis of NRG1 could also serve as a marker for altered overall NRG1 processing in schizophrenia.

2 Aims of the study

The aim of this study was to investigate the proteolytic processing of NRG1 type III and the effects on its signaling. Two of the proteases involved in the turnover of NRG1 type III, BACE1 and γ-secretase, are also relevant to the etiology of Alzheimer's disease and are consequently major drug targets. It is therefore crucial to determine their specific roles in the processing and signaling of NRG1 type III in order to preclude side effects upon therapeutic inhibition of these enzymes.

NRG1 type III is an important neuronal growth factor regulating myelination in the peripheral nervous system. It is activated by ectodomain shedding which generates a membrane-retained N-terminal fragment containing its EGF-like domain that signals to Schwann cells and promotes myelination in a juxtacrine manner. With regard to myelination, BACE1, ADAM10 and ADAM17 have been shown to cleave NRG1 type III. In particular, cleavage by BACE1 was shown to be crucial for the promotion of myelination whereas in contrast ADAM17-mediated shedding was proposed to inactivate NRG1 type III thus acting inhibitory. This difference was attributed to slightly different cleavage positions of the proteases in the juxtamembrane region of NRG1 type III. However, a systematic characterization of the shedding sites in living cells has not been carried out so far and their effects on the activity of NRG1 type III remain controversial.

Therefore, in the first part of this study the precise shedding sites of BACE1, ADAM10 and ADAM17 were to be determined. Furthermore it was to be studied whether the processing of NRG1 type III allows for a paracrine signaling paradigm as has been proposed although evidence for the generation of a soluble signal has been missing. Finally, and with regard to the contradicting findings for BACE1- and ADAM17-mediated shedding, the effects of different cleavage sites on the ability of NRG1 type III to promote myelination were to be compared in a cell culture system as well as *in vivo*.

The goal of the second part of this work was the detailed characterization of the previously reported intramembrane proteolysis of the NRG1 type III C-terminal fragment by the γ-secretase. Interestingly, a mutation within the transmembrane domain may link this processing to the development of schizophrenia. Therefore, by identifying the respective cleavage products as well as the precise cleavage sites, NRG1 type III was to be established as an unambiguous γ-secretase substrate. Furthermore the processing sites were to be compared to the γ-secretase cleavage sites identified for other substrates and evaluated with regard to the position of the schizophrenia-associated mutation.

3   Results

3.1   BACE1, ADAM10 and ADAM17 are sheddases of NRG1 type III

Neuregulin-1 type III requires proteolytic processing (shedding) in its juxtamembrane region in order to induce myelination. BACE1 and ADAM17 have been shown to act as physiologically relevant sheddases of NRG1 type III but also shedding by ADAM10 has been demonstrated (Montero et al., 2000; Willem et al., 2006; La Marca et al., 2011; Luo et al., 2011). The exact cleavage positions, however, have only been investigated *in vitro* by digesting short recombinant peptides spanning the juxtamembrane region with purified proteases. Furthermore no systematic comparison of the cleavage sites of BACE1, ADAM10 and ADAM17 in NRG1 type III has been performed in living cells.

Investigation of the shedding sites in the juxtamembrane domain of NRG1 type III in living cells is complicated by the fact that also other regions of its ectodomain are subject to proteolytic processing. Wang et al. for example described cleavage of NRG1 type III close to its N-terminal cysteine-rich TMD. Therefore, to monitor the processing of NRG1 type III specifically in its juxtamembrane region and to exclude interferences by cleavages in other parts of the ectodomain, an N-terminally truncated construct was generated. NRG1ΔNT comprises the entire C-terminal region, the TMD, the juxtamembrane region as well as the EGF-like domain of NRG1 type III β1a but lacks its N-terminus. In this way, NRG1ΔNT constitutes a version of NRG1 type III that is exclusively subject to shedding in the juxtamembrane part of its ectodomain. A Flag tag immediately before the EGF-like domain allows isolation and subsequent mass spectrometric analysis of the domain after its release through shedding (Figure 11).

Upon expression in HEK293 cells, full-length NRG1ΔNT was detected in the cell lysate with antibodies against its C-terminus, as well as its EGF-like domain and the Flag tag. The diffuse western blot signal obtained with the C-terminal antibody is most likely due to the additional detection of the slightly smaller C-terminal fragment (CTF) that remains after shedding. However, due to its very similar size and its turnover by the γ-secretase this fragment is not easily detected and unambiguous identification of the CTF requires concomitant γ-secretase inhibition (Figure 13). The liberated soluble EGF-like domain (sEGF) was detected in the supernatant by an EGF antibody, demonstrating that NRG1ΔNT is subject to endogenous shedding in its juxtamembrane domain (Figure 11).
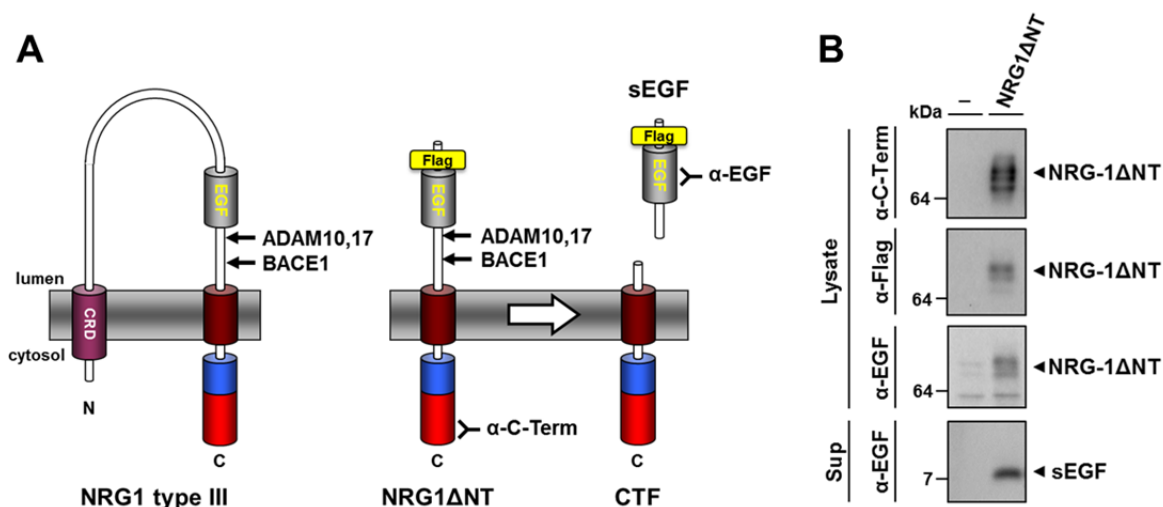
Figure 11. NRG1ΔNT is processed in its juxtamembrane region. A) Scheme depicting NRG1ΔNT. NRG1ΔNT represents an N-terminally truncated version of NRG1 type III and contains a Flag tag immediately upstream of the EGF-like domain that facilitates immunoprecipitation for MS analysis. Shedding by proteases like BACE1 and ADAMs generates a soluble EGF-like domain (sEGF), detectable with an EGF antibody. A C-terminal antibody detects NRG1ΔNT in the cell lysate. CRD = cysteine-rich domain. **B)** NRG1ΔNT is shed by endogenous proteases in HEK293 cells. Supernatants and lysates of cells expressing NRG1ΔNT were subjected to immunoblotting with the indicated antibodies. The sEGF domain released by shedding of NRG1ΔNT in its juxtamembrane region was directly detected in the supernatant.

3.1.1 BACE1, ADAM10 and ADAM17 cleave NRG1 type III in the juxtamembrane region

In the following NRG1ΔNT was used to investigate the processing of NRG1 type III by BACE1, ADAM10 and ADAM17 in living cells. Inhibition of endogenous BACE1 activity (by the BACE1 inhibitor IV) in cells expressing NRG1ΔNT decreased shedding of NRG1ΔNT significantly as demonstrated by reduced amounts of the soluble EGF-like domain in the supernatant (Figure 12). In line, concurrent accumulation of the full-length precursor protein was also detected, albeit to a much smaller extent. The smaller effect on the full-length protein is most likely due to the high concentration of NRG1ΔNT present in the cells. In contrast to the small amount of the liberated EGF-like domain which readily reflects decreased processing, the excess of uncleaved precursor protein causes the difference in processing upon BACE1 inhibition to be rather subtle (Figure 12).

Overexpression of BACE1 increased the release of sEGF to 400-500% of the control (Figure 12). This dramatic increase in cleavage was also accompanied by a strong reduction of the full-length precursor NRG1ΔNT in the cell lysate indicating that the juxtamembrane domain of NRG1 type III is highly sensitive to cleavage by BACE1.

Shedding of NRG1ΔNT in the juxtamembrane region generates a membrane-retained CTF lacking the EGF-like domain (Figure 11). This fragment is further processed by the γ-secretase (Bao et al., 2003) and was not observed in the experimental setup above. To confirm its generation, cells expressing NRG1ΔT and BACE1 were treated with the γ-secretase inhibitor DAPT. Upon inhibition by DAPT, the CTF accumulated and was observed as additional band on western blot, migrating below the full-length NRG1ΔNT (Figure 13).
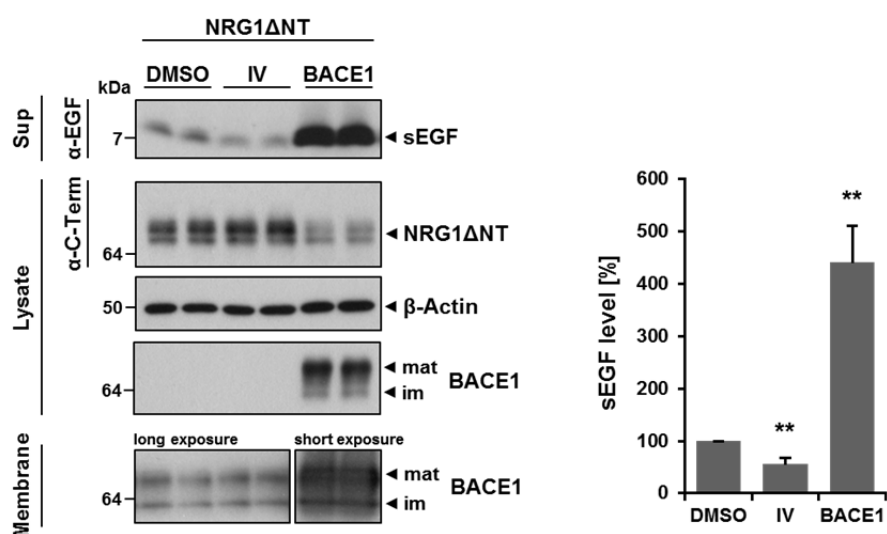
Figure 12. BACE1 is shedding NRG1ΔNT in the stalk region. Compared with control treated cells (DMSO) BACE1 activity in HEK293 cells expressing NRG1ΔNT was reduced by treatment with the specific BACE1 inhibitor IV (10 µM) or increased by coexpression of BACE1. Shedding of NRG1ΔNT was monitored by immunoblotting cell supernatants for sEGF. Expression of transfected and endogenous BACE1 was confirmed in lysates and isolated membranes, respectively. Note that endogenous BACE1 is only visible upon prolonged exposure of the western blot membrane. mat = mature, im = immature. Bar graph: Quantification of experiments (IV: n = 5, p<0.01; BACE1: n = 6, p<0.01).
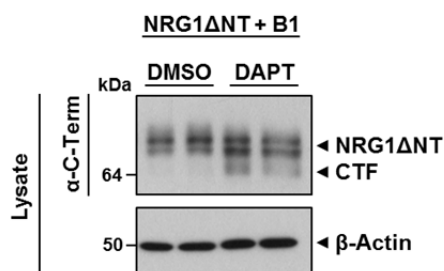
Figure 13. Shedding of NRG1ΔNT generates a CTF that is cleaved by the γ-secretase. HEK293 cells expressing NRG1ΔNT and BACE1 (B1) were treated with DMSO as control or the γ-secretase inhibitor DAPT (10 µM). Lysates were analyzed by western blotting.

Besides BACE1 proteases of the ADAMs family also cleave NRG1 type III in the juxtamembrane region (Montero et al., 2000; La Marca et al., 2011; Luo et al., 2011). To confirm that NRG1ΔNT similarly is subject to ADAM-mediated shedding, cells expressing the construct were treated with the broad-spectrum ADAM inhibitor GM6001 (Figure 14). This reduced shedding and liberation of the EGF-like domain into the supernatant by approx. 40%. Combined inhibition of both BACE1 and ADAMs abolished endogenous shedding almost completely and caused accumulation of the full-length precursor NRG1ΔNT to an extend that was detectable on western blot (Figure 14).

Finally it was tested whether the two ADAM proteases most prominently implicated in the shedding of NRG1 type III were able to process the truncated NRG1ΔNT. To this end, ADAM10 and ADAM17 were coexpressed with NRG1ΔNT and shedding was analyzed as before. Ectopic expression of ADAM10 and ADAM17 lead to enhanced shedding of NRG1ΔNT as evidenced by increased levels of the EGF-like domain detected in the supernatants (Figure 15).

Although ectopic expression of ADAM10 and ADAM17 increased shedding to approx. 140-150% of the endogenous level, this effect is small compared to the effect size observed for the overexpression of BACE1 (bar graphs in Figure 12, 15). This difference may indicate that BACE1 possesses a higher affinity to its shedding site in the juxtamembrane region of NRG1 type III compared to the ADAM proteases. However, as the exact amounts of catalytically active (mature) protease that resulted from ectopic expression were not determined, a quantitative statement regarding the affinity of BACE1, ADAM10 and ADAM17 towards NRG1 type III shedding is not possible.

The results above demonstrate that BACE1, ADAM10 and ADAM17 may act as NRG1 type III sheddases that cleave between its extracellular EGF-like domain and the C-terminal transmembrane domain.
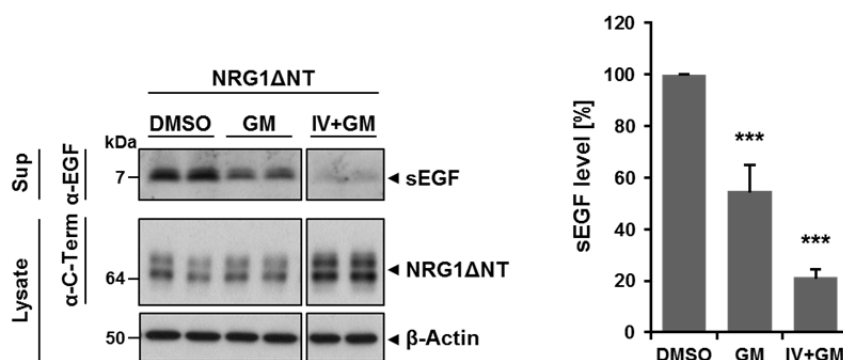
Figure 14. ADAM proteases contribute to the shedding of NRG1ΔNT. Processing of NRG1ΔNT by endogenous ADAM proteases in HEK293 cells was blocked by treatment with the broad-spectrum ADAM inhibitor GM6001 (GM, 25 μM). Combined treatment with GM and BACE1 inhibitor IV (25 μM and 10 μM, respectively) was used to block both ADAMs and BACE1 simultaneously and DMSO treatment served as control. Shedding was assessed by western blot analysis of the cell supernatants using an EGF antibody. Bar graph: Quantification of experiments (n = 5, p<0.001).
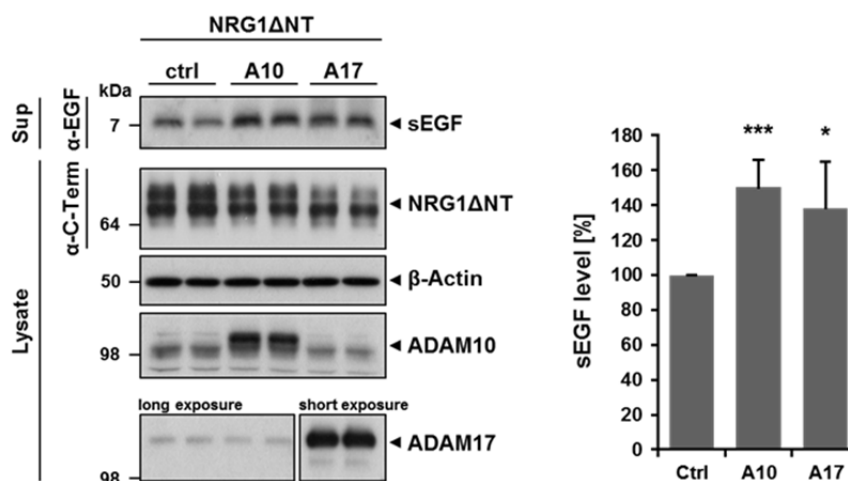
Figure 15. ADAM10 and ADAM17 shed NRG1ΔNT. ADAM10 (A10) and ADAM17 (A17) were coexpressed with NRG1ΔNT in HEK293 cells and supernatants were analyzed for soluble EGF-like domains by immunoblotting. Ectopic expression of ADAM10 and ADAM17 was confirmed in cell lysates. Note that endogenous ADAM17 is only detected upon prolonged exposure of the western blot membrane. Bar graph: Quantification of experiments (n = 6; A10: p<0.001; A17: p<0.05).

3.1.2 Shedding of NRG1 type III by BACE1, ADAM10 and ADAM17 occurs at close but distinct sites

Determination of the precise shedding sites within NRG1 type III requires identification of the very C-terminal residue of the liberated sEGF. Since the NRG1ΔNT construct possesses a defined N-terminus, this is possible once the mass of the liberated sEGF is known. For this purpose a combined immunoprecipitation mass spectrometry (IP-MS) approach was used.

NRG1ΔNT was expressed in HEK293 cells and the sEGF domain liberated into the supernatant by shedding was isolated using the N-terminal Flag tag for immunoprecipitation. Subsequently the molecular masses of the purified peptides were determined by MALDI-TOF mass spectrometry. Endogenous processing of NRG1ΔNT in HEK293 cells yields four prominent peptides that correspond to cleavages after A_{283}, F_{285}, Y_{286} and F_{293} in NRG1 type III (Figure 16, Table 1). To identify the site(s) after which BACE1-mediated cleavage occurs, the enzyme's activity was either reduced by treatment with a specific inhibitor or its cleavage was enhanced by overexpression. Inhibition of endogenous BACE1 in NRG1ΔNT expressing cells strongly diminished the abundance of the sEGF fragment detected in the supernatant at a mass of 7846.8 kDa (cleaved after F_{293}) in comparison to the other peptide species. Conversely, the liberation of this sEGF fragment was greatly increased upon overexpression of BACE1. In fact, overexpression of BACE1 caused preferential shedding of NRG1ΔNT at F_{293} to an extent that made detection of the other peptide species impossible (Figure 16). Together this identifies F_{293} as the shedding site of BACE1 in the juxtamembrane region of NRG1 type III β1a.

To assess which cleavage sites originate from shedding by members of the ADAMs family of proteases, cells expressing NRG1ΔNT were treated with the broad-spectrum ADAM inhibitor GM6001. Mass spectrometric analysis of the sEGF domains in the supernatant of these cells revealed the cleavages after A_{283}, F_{285} and Y_{286} to be strongly reduced compared to the cleavage at F_{293} (Figure 17, Table 1). For a semi-quantitative evaluation of this effect the signal intensity (area below the peak in the spectrum) of each ADAM-specific peak was normalized to the signal intensity of the BACE1-specific peak (F_{293}) and then compared to the control. This revealed broad-spectrum ADAM inhibition to reduce the cleavage after A_{283}, F_{285} and Y_{286} to 20-40% of the control (Table 2). GM6001 is an unselective inhibitor of ADAM and MMP proteases and therefore does not allow discrimination between ADAM10- and ADAM17-mediated shedding. For this purpose cells were treated with inhibitors that show a greater specificity and preferentially inhibit either ADAM10 (GI254023X) or ADAM17 (GL506-3). Treatment with GI254023X strongly reduced the generation of sEGF fragments terminating at Y_{286} to about 10% of the control (Figure 17, Table 2). Cleavage after F_{285} was mildly reduced (60% of control level), while cleavage after A_{283} was slightly increased (140%) compared to control conditions. In contrast, preferential inhibition of ADAM17 using GL506-3 did not change the abundance of sEGF cleaved after Y_{286} but strongly impaired cleavage after A_{283} (only 30% of control). As before, cleavage after F_{285} was mildly reduced to 60% of the levels in the supernatant of control treated cells.
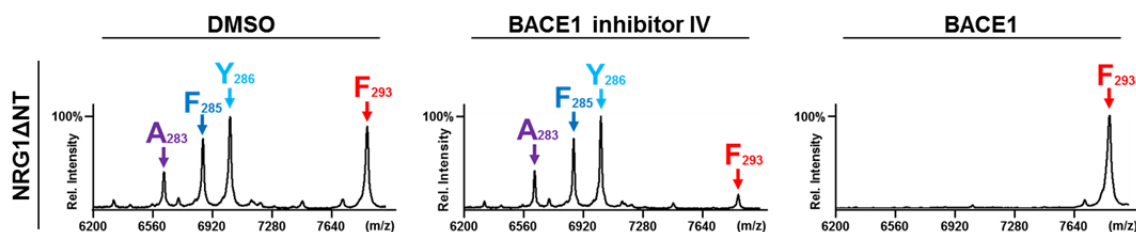
Figure 16. BACE1 cleaves NRG1 type III after F$_{293}$ in the juxtamembrane region. HEK293 cells expressing NRG1ΔNT were either treated with DMSO as control, with the BACE1 inhibitor IV (10 µM) or were cotransfected with BACE1 (Figure 12). Supernatants were immunoprecipitated using a Flag antibody and isolated sEGF peptides were analyzed by MALDI-TOF MS. The peptide corresponding to cleavage after F$_{293}$ (red arrows) is generated by BACE1 (Table 1). Note that with overexpression of BACE1, the other peaks are below the detection limit.
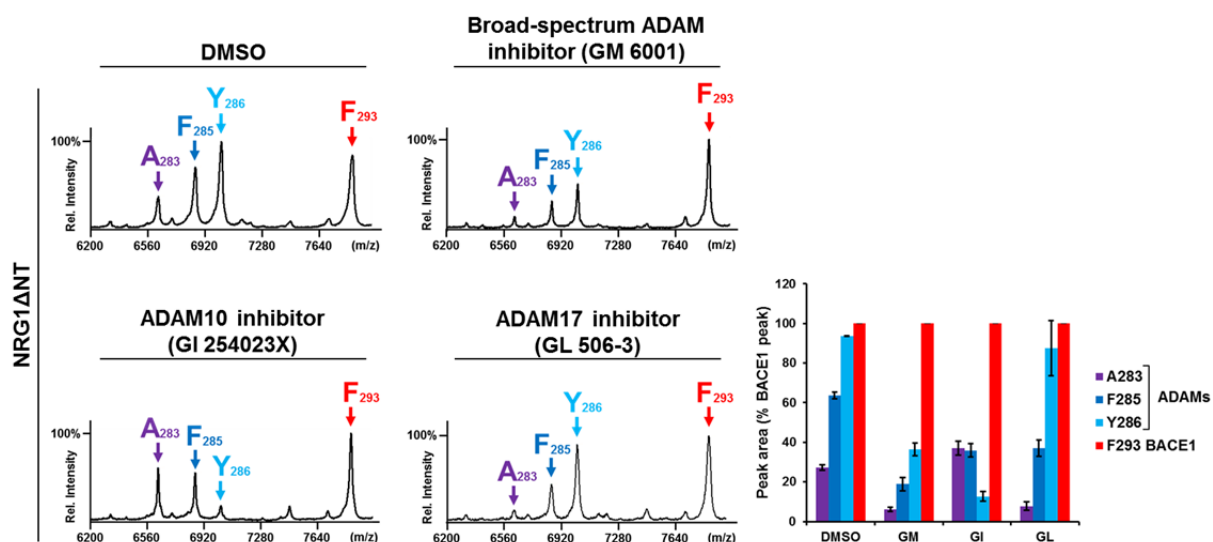
Figure 17. ADAM10 and ADAM17 shed NRG1 type III after A$_{283}$, F$_{285}$ and Y$_{286}$. After treatment with the indicated inhibitors (GM6001 (GM), 25 µM; GI254023X (GI) and GL506-3 (GL), 5 µM) or DMSO as control, supernatants of HEK293 cells expressing NRG1ΔNT were immunoprecipitated using Flag agarose beads and isolated sEGF peptides were analyzed by MALDI-TOF MS. Broad-spectrum ADAM inhibition revealed peptides terminating with A$_{283}$, F$_{285}$ and Y$_{286}$ (Table 1) to be generated by ADAMs. Selective inhibition of ADAM10 reduced cleavage after F$_{285}$ and Y$_{286}$ (blue and light blue arrows, respectively). ADAM17 inhibition decreased cleavage mainly after A$_{283}$ (purple arrows) but also after F$_{285}$. Red arrow: BACE1 cleavage after F$_{293}$. Bar graph: Representation of peak intensities normalized to the BACE1-specific peak (n = 3).

Residue	Cleavage by	Sequence	Mass [M+H]$^+$ (Da)	
			Calc.	Obs.
F$_{293}$	BACE1	SV*DYKDDDDK*IKCAEKEKTFCVNGGECFTVKDLSN PSRYLCKCPNEFTGDRCQNYVMASFYKHLGIEF	7845.9	7846.8
Y$_{286}$	ADAM10	SV*DYKDDDDK*IKCAEKEKTFCVNGGECFTVKDLSN PSRYLCKCPNEFTGDRCQNYVMASFY	7020.9	7020.6
F$_{285}$	ADAM10/17	SV*DYKDDDDK*IKCAEKEKTFCVNGGECFTVKDLSN PSRYLCKCPNEFTGDRCQNYVMASF	6857.7	6858.8
A$_{283}$	ADAM17	SV*DYKDDDDK*IKCAEKEKTFCVNGGECFTVKDLSN PSRYLCKCPNEFTGDRCQNYVMA	6623.5	6624.1

Table 1. List of peptides shed from NRG1ΔNT as identified by mass spectrometry. Peptide sequences with corresponding protease(s) are given and observed (Obs.) peptide masses are compared with calculated (Calc.) masses. Italic letters indicate the Flag tag, [M+H]$^+$ a singly charged peptide.

	A$_{283}$	F$_{285}$	Y$_{286}$
	x-fold change in cleavage vs. control		
Inhibitors			
GM (all ADAMs)	⬇ (0.2)	⬇ (0.3)	⬇ (0.4)
GI (ADAM10)	↑ (1.4)	↓ (0.6)	⬇ (0.1)
GL (ADAM17)	⬇ (0.3)	↓ (0.6)	→ (0.9)
Overexpression			
ADAM10	↑ (1.5)	⬆ (2.7)	⬆ (2.2)
ADAM17	⬆ (6.7)	⬆ (2.4)	→ (1.0)
Knockdown			
siADAM10	→ (1.0)	⬇ (0.3)	⬇ (0.1)
siADAM17	⬇ (0.3)	↓ (0.7)	→ (0.9)

Table 2. Semi-quantitative evaluation of MS data for ADAM10- and ADAM17-mediated shedding after A$_{283}$, F$_{285}$ and Y$_{286}$. Peak intensities (areas) of ADAM-specific peaks were normalized to the signal generated by BACE1 in each spectrum (Figure 17-19, n = 3). The normalized peak intensities were then compared with the respective controls. Changes of cleavage (fold) under different conditions (inhibition, overexpression, and knockdown of ADAM10 and ADAM17) are summarized as follows: increased: >1.6x (↑, big arrows), mildly increased: 1.5-1.2x (↑, small arrows), unchanged: 1.1-0.9x (→), mildly decreased: 0.8-0.5 (↓, small arrows) or decreased: 0.4x (↓, big arrows).

To further substantiate the results achieved by the pharmacological discrimination between ADAM10 and ADAM17, each protease was overexpressed in the presence of NRG1ΔNT (Figure 18). Ectopic expression of ADAM10 strongly increased shedding of NRG1ΔNT after F_{285} and Y_{286} (270% and 220% of control, respectively) but only moderately affected cleavage after A_{283} (150% of control). Conversely, cleavage after A_{283} was highly enhanced (670% of control) upon ADAM17 overexpression whereas shedding after Y_{286} was unaltered. Again, as with the ADAM17 inhibitor, the extent of cleavage alteration at F_{285} was determined to be in between (240% compared to control cells) (Figure 18, Table 2).
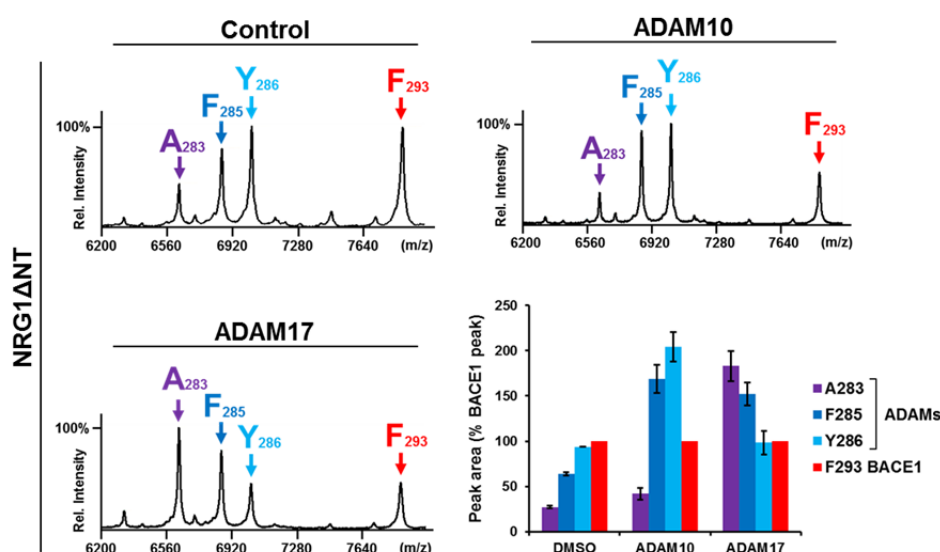
Figure 18. Overexpression of ADAM10 and ADAM17 confirms shedding sites in NRG1 type III. Supernatants of cells expressing NRG1ΔNT and ADAM10 or ADAM17 were analyzed as before (Figure 17). Ectopic ADAM10 expression enhanced cleavage after F_{285} and Y_{286} (blue and light blue arrows, respectively), while ADAM17 expression lead to increased cleavage after A_{283} (purple arrows) and after F_{285}. Red arrows: BACE1 cleavage after F_{293}. Bar graph: Representation of peak intensities normalized to the BACE1-specific peak (n = 3).

Overexpression of proteases harbors the risk of cleavage at sites that would not be used endogenously. Therefore in a third approach, RNA interference was used to knockdown endogenous ADAM10 and ADAM17 activity in HEK293 cells expressing NRG1ΔNT. As confirmed by western blot analysis of membrane preparations both the mature and the immature form of either protease were efficiently reduced by the respective siRNA pool (Figure 19). Mass spectrometric analysis of the sEGF fragments liberated into the supernatant by cells with transiently reduced ADAM10 showed shedding after Y_{286} to be decreased to 10% of the levels of cells treated with control siRNA (Figure 19, Table 2). Notably, cleavage after A_{283} was not changed. In contrast, transient knockdown of ADAM17 reduced shedding after A_{283} to 30% but did not affect cleavage after Y_{286}. In line with the observations made using inhibitors (Figure 17) and overexpression (Figure 18), knockdown of either protease affected cleavage after F_{285} to an intermediate extent (30% and 70% of control for ADAM10 and ADAM17 knockdown, respectively) (Figure 19, Table 2).
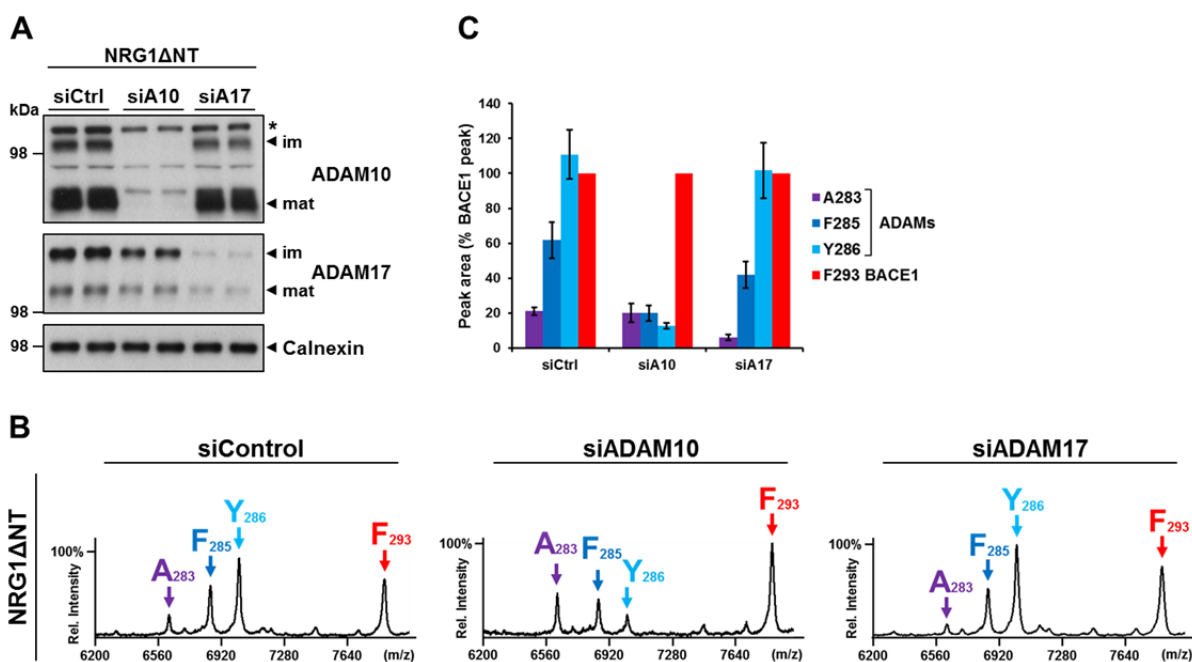
Figure 19. RNA interference confirms ADAM10 and ADAM17 shedding sites in NRG1 type III. HEK293 cells expressing NRG1ΔNT were transfected with siRNA (10 nM) against ADAM10 (siA10) or ADAM17 (siA17) and a non-targeting siRNA as a control (siCtrl). **A)** Western blot analysis of membrane preparations revealed efficient downregulation of both the immature (im) and mature (mat) form of ADAM10 and ADAM17. **B)** sEGF peptides were isolated from the supernatant by Flag tag immunoprecipitation and analyzed by MALDI-TOF MS. Reduced ADAM10 expression affected cleavage after F_{285} and Y_{286} (blue and light blue arrows, respectively). In contrast, downregulation of ADAM17 mainly reduced cleavage after A_{283} (purple arrows) but also after F_{285}. Red arrows: BACE1 cleavage after F_{293}. **C)** Bar graph representation of peak intensities normalized to the BACE1-specific peak (n = 3).

Together these data suggest a precise shedding site for BACE1 in the juxtamembrane region of NRG1 type III β1a and more heterogeneous sites for ADAM10 and ADAM17. BACE1 shedding was observed specifically after F_{293} and thus at a site located 10 residues N-terminal of the TMD. ADAM10-mediated cleavage mainly occurs after Y_{286}, while ADAM17 preferentially cleaves after A_{283}. However in addition, both proteases share F_{285} as a second and minor cleavage site. Compared to BACE1, ADAM10 and ADAM17 therefore mediate shedding of NRG1 type III more distant to the TMD at sites 7 and 10 residues upstream of the BACE1 shedding site (Figure 20).
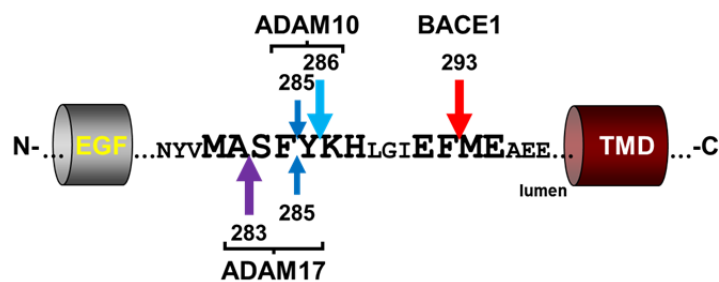
Figure 20. Schematic overview of the shedding sites identified in the juxtamembrane region of NRG1 type III. The cleavage sites of BACE1, ADAM10 and ADAM17 are shown. Longer arrows indicate the preferred cleavage sites of ADAM10 and ADAM17, respectively.

3.2   Processing of NRG1 type III generates soluble EGF-like domains

In contrast to all other NRG1 isoforms, shedding of NRG1 type III does not liberate the EGF-like domain but instead generates a membrane-bound NTF that tethers the EGF-like domain to the cell surface. NRG1 type III therefore is considered to signal in a juxtacrine fashion only (Falls, 2003b; Taveggia et al., 2005). Nevertheless an initial report described the liberation of the NRG1 type III ectodomain which would theoretically allow for paracrine signaling (Wang et al., 2001). The cleavage, however, was found to be very inefficient and the identity of the protease as well as the site of cleavage remained elusive. Recently, the model of strictly contact-dependent signaling was further challenged by the observation that soluble recombinant NRG1 type III NTF is able to signal *in vitro* (Syed et al., 2010). In order to gain insight into the processing of NRG1 type III, specifically of its NTF, full-length NRG1 type III containing an N-terminal V5 tag (V5-IIINRG1) was expressed in HEK293 cells. Figure 21 provides a schematic of V5-IIINRG1 and summarizes its processing as investigated below.
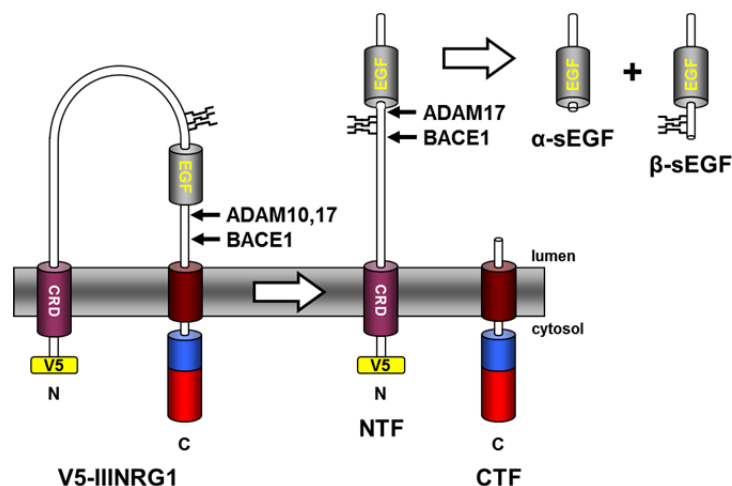
Figure 21. Scheme depicting V5 tagged NRG1 type III (V5-IIINRG1) and its processing. Shedding of V5-IIINRG1 generates a membrane-bound NTF containing the EGF-like domain and a CTF. Further processing by ADAM17 and BACE1 releases the EGF-like domain from the membrane (α- and β-sEGF, respectively). A site of O-linked glycosylation N-terminal of the EGF-like domain is indicated. The N-terminal V5 tag facilitates immunodetection of the NTF.

3.2.1 Cleavage by BACE1 and ADAM17 liberates the EGF-like domain of NRG1 type III

Western blot analysis of lysates from cells expressing V5-IIINRG1 revealed two prominent bands below the 148 KDa marker, indicating that full-length V5-IIINRG1 is subject to intensive posttranslational modifications such as glycosylation (Figure 22). Coexpression of BACE1, ADAM10 or ADAM17 increased shedding and lead to reduced amounts of the full-length protein. In line with the observations made with NRG1ΔNT (3.1.1), this effect was most pronounced for ectopic BACE1 expression. Similar to the observations above, increased shedding was not reflected by the accumulation of the CTF which is rapidly turned over by the γ-secretase. Compared to ADAM-mediated shedding, shedding by BACE1 occurs closer to the TMD of NRG1 type III and therefore generates a smaller CTF (Figure 20). This β-CTF was specifically detected upon overexpression of BACE1 and migrated slightly faster than the α-CTF resulting from ADAM10 and ADAM17 cleavage (Figure 22).

Enhanced shedding of V5-IIINRG1 should also lead to increased levels of the NTF containing the EGF-like domain. However, no such accumulation could be detected using antibodies against the V5 tag or the EGF-like domain. To the contrary, especially BACE1 and ADAM17 coexpression decreased the level of NTF indicating further processing of this fragment. Investigation of the supernatants revealed that both BACE1 and ADAM17 indeed liberate the EGF-like domain from V5-IIINRG1. Indicating different cleavage sites, the soluble EGF-like domain liberated by BACE1 (β-sEGF) has a higher molecular weight (detected above the 7 kDa marker) compared to the α-sEGF generated by ADAM17 (detected between the 4 and 7 kDa marker) (Figure 22). Endogenous proteases also liberated α- and β-sEGF but to a very small extent that was difficult to detect by western blot. Similarly low amounts of both fragments were detected with ADAM10 coexpression which therefore does not seem to liberate the EGF-like domain by a novel N-terminal cleavage.

NRG1 type III contains a serine/threonine-rich sequence immediately N-terminal of the EGF-like domain (Figure 26) that potentially is a site for O-linked glycosylation. Indicative of glycosylation and furthermore suggesting that it might contain the N-terminal serine/threonine-rich sequence, β-sEGF was observed as double band on western blot (Figure 22). To investigate this possibility, cells expressing V5-IIINRG1 were treated with benzyl-2-acetamido-2-deoxy-D-galactopyranoside (BG) a specific inhibitor of O-linked glycosylation (Alfalah et al., 1999). Incubation with BG abolished the higher-molecular weight band and caused β-sEGF to appear as single peptide (Figure 23). This demonstrates that a fraction of the β-sEGF liberated from NRG1 type III by BACE1 is O-glycosylated and

indicates that the respective cleavage site is located N-terminal of the serine/threonine-rich sequence.
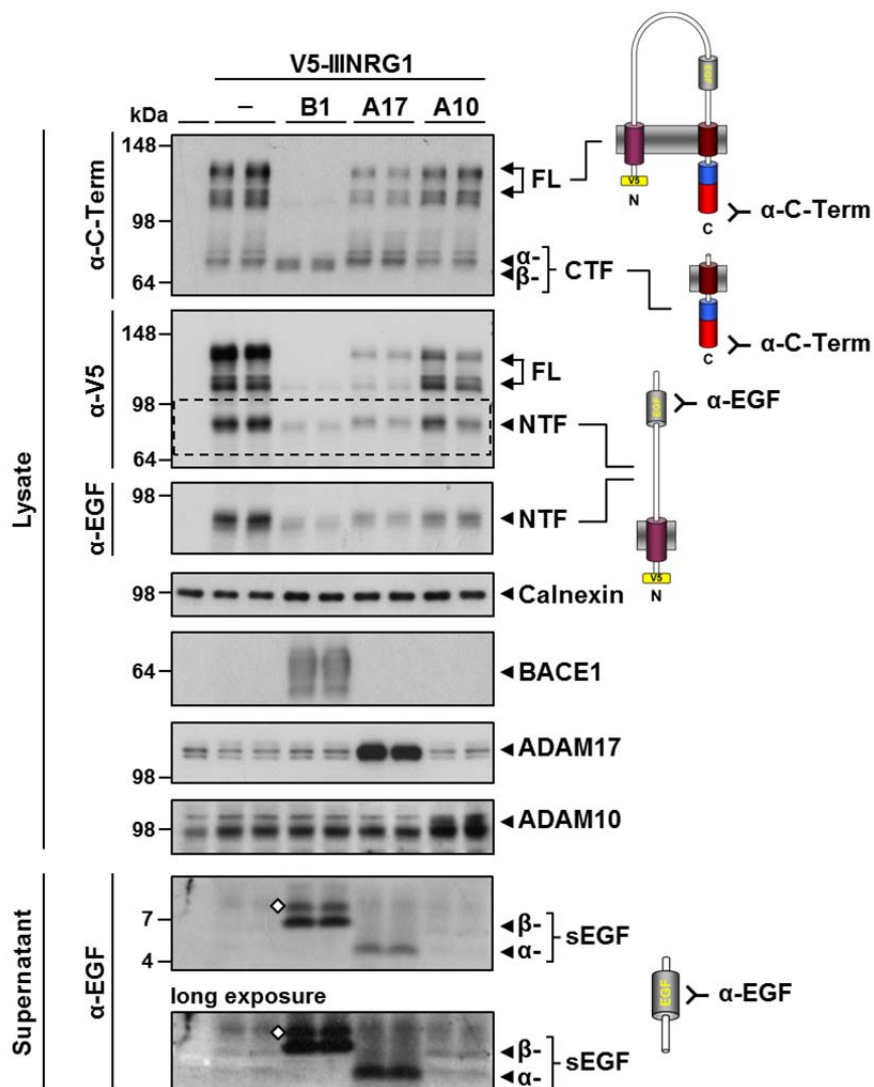
Figure 22. Processing of NRG1 type III generates a membrane-bound and a soluble EGF-like domain. Lysates of HEK293 cells expressing V5-IIINRG1 and BACE1 (B1), ADAM17 (A17) or ADAM10 (A10) were analyzed for membrane-tethered fragments by immunoblotting with the indicated antibodies. Note that the β-CTFs generated by BACE1 migrate slightly faster compared to the α-CTFs resulting from ADAM-mediated shedding. Reprobing of the membrane (dashed box) with an EGF antibody confirmed the NTF to contain the EGF-like domain. Expression of transfected proteases was controlled in the lysate. Soluble EGF-like domains of different sizes (α- and β-sEGF) were detected by western blot analysis of the supernatants. Diamonds denote posttranslational modifications.
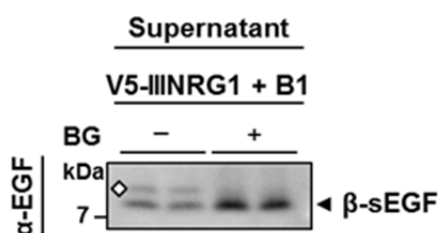
Figure 23. The β-sEGF liberated by BACE1 cleavage of NRG1 type III is O-glycosylated. O-linked glycosylation in HEK293 cells expressing V5-IIINRG1 and BACE1 was blocked by treatment with benzyl-2-acetamido-2-deoxy-α-D-galactopyranoside (BG, 4 mM). Supernatants were analyzed for β-sEGF by immunoblotting with an EGF antibody. The diamond denotes O-linked glycosylation.

3.2.2 BACE1 and ADAM17 cleave NRG1 type III at specific sites N-terminal of its EGF-like domain

In addition to shedding in the juxtamembrane region, liberation of the EGF-like domain requires cleavage of NRG1 type III N-terminal of that domain. To identify these novel cleavage sites, a combined IP-MS approach similar to the one described above was used (3.1.2). Mass spectrometric analysis of the liberated EGF-like domains requires their isolation from the cell culture supernatant. As there is no antibody available that is able to immuno-precipitate the EGF-like domain of NRG1 type III, an HA tag was inserted immediately C-terminal of the domain (V5-IIINRG1-HA) (Figure 25 A). Protein tags may, however, impair or alter normal proteolytic processing especially when located close to cleavage sites. To exclude this possibility the construct was expressed in HEK293 cells and proteolytic processing was analyzed as before (Figure 24). Compared to the untagged construct V5-IIINRG1, no difference in the generation of membrane-bound fragments from V5-IIINRG1-HA was observed (Figure 22, 24 A). However, the HA antibody readily detected the NTF comprising the EGF-like domain but did not recognize the full-length protein (not shown). This is most likely due to the different locations of the HA tag sequence. In the full-length protein the tag is located internally and therefore probably less efficiently recognized by the antibody. In contrast, shedding causes the tag sequence to be exposed at the C-terminus of the NTF thereby allowing a more efficient detection.

Analysis of supernatants from cells expressing V5-IIINRG1-HA and BACE1 or ADAM17 revealed generation of HA tagged β- and α-sEGF in a very similar fashion compared to V5-IIINRG1 (Figure 22, 24 B). Due to the additional HA sequence, both fragments were detected at slightly higher molecular weights. Unlike for the untagged construct however, a second western blot band that migrated above the α-sEGF was noted.
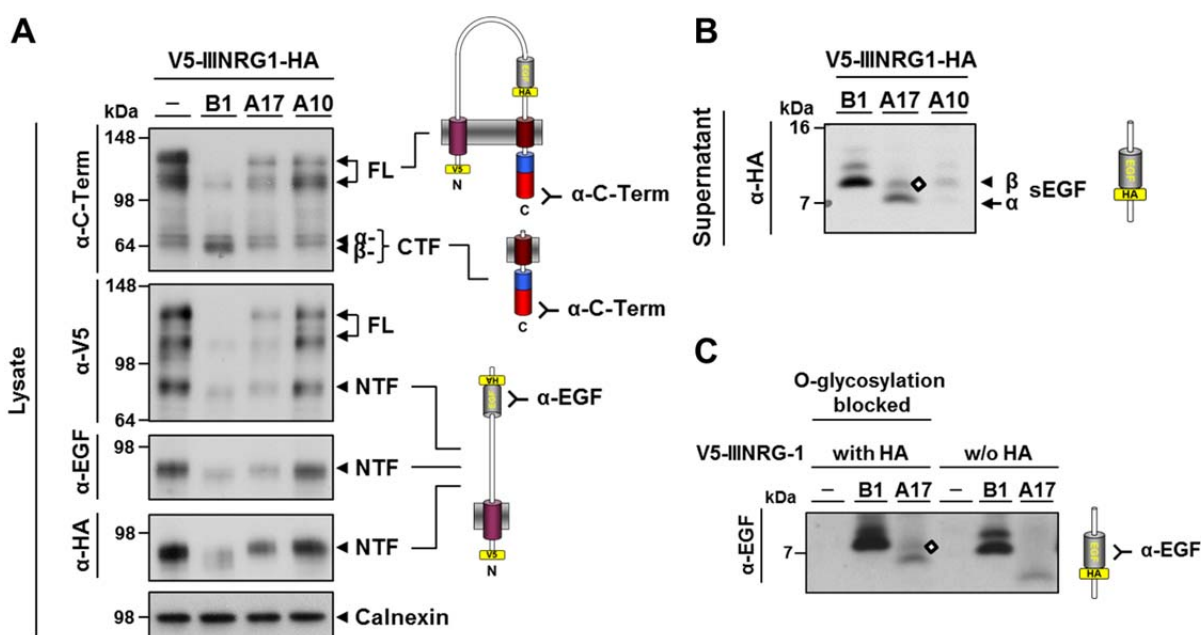
Figure 24. An HA tag C-terminal of the EGF-like domain does not impair processing of NRG1 type III. A) The processing of V5-IIINRG1-HA generates an NTF and CTF similar to V5-IIINRG1 (Figure 22). V5-IIINRG1-HA was expressed in HEK293 cells with BACE1 (B1), ADAM17 (A17) or ADAM 10 (A10). Membrane-bound fragments were detected in the cell lysates by immunoblotting with the indicated antibodies. No difference in processing was observed compared to a construct lacking the HA tag (Figure 22). **B)** V5-IIINRG1-HA is processed to release α- and β-sEGF. Supernatants from A) were analyzed for the liberation of the EGF-like domain. An additional band (marked by a diamond) was observed for the HA tagged α-sEGF (compare to untagged α-sEGF in Figure 22). **C)** The additional western blot band of HA tagged α-sEGF is not due to glycosylation. sEGF domains were detected in supernatants from cells expressing V5-IIINRG1 with or without an HA tag. While blocking O-glycosylation (BG, 4 mM, Figure 23) did not abolish the additional band (indicated by a diamond) for α-sEGF, removal of the HA tag did.

Generation of this band cannot be prevented by BG treatment (Figure 24 C) and is only detected upon expression of the HA tagged construct. It therefore does not represent O-linked glycosylation as observed for β-sEGF but seems to be caused solely by the tag during western blot detection. However, as the shedding sites observed for V5-IIINRG1-HA are the same sites identified with the NRGΔNT construct (which does not contain the HA sequence), the tag does not seem to interfere with normal processing of NRG1 type III (3.1.2 Table 1, Table 3).

To determine the exact cleavage site(s) responsible for the liberation of the EGF-like domain, supernatants of cells expressing V5-IIINRG1-HA (Figure 24, 25 A) were immuno-precipitated using HA agarose. Subsequent mass spectrometric analysis of the isolated peptides showed that processing of V5-IIINRG1-HA by endogenous proteases in HEK293 cells results in the generation of a soluble EGF-like domain of 8558.9 kDa (Figure 25 B,

Table 3). This molecular weight corresponds to an EGF-like domain comprising 68 residues, liberated from the full-length protein by cleavages N-terminal (after L_{217}) and C-terminal (after F_{285}) of the domain. Cleavage after F_{285} is the result of shedding in the juxtamembrane domain and was found to be mediated by ADAMs (Figure 20). The N-terminal cleavage site between L_{217} and Q_{218}, however, has not been observed before. Proteolysis at this novel site which is located 16 residues N-terminal of the EGF-like domain (Figure 26) liberates a sEGF containing the serine/threonine-rich sequence upstream of that domain and therefore may be mediated by BACE1 (Figure 22, 23). Consistent with this, inhibition of endogenous BACE1 activity (BACE1 inhibitor IV) abolished the generation of the sEGF demonstrating that ADAM activity is not responsible for the cleavage after L_{217} (Figure 25 B). Further supporting cleavage by BACE1, the sequence immediately upstream of the novel cleavage site (ETNL|QTAP) bears striking resemblance to that of the Swedish mutation of APP (EVNL|DAEF) (Mullan et al., 1992) (4.2 Figure 48) which is known to dramatically increase BACE1 affinity (Citron et al., 1992, 1995; Cai et al., 1993). Finally, coexpression of BACE1 strongly increased cleavage after L_{217} and released a sEGF fragment of 76 residues (β-$sEGF_{76}$), comprising Q_{218} as N-terminal and F_{293} as C-terminal residue (Figure 25 B, Table 3). In case of BACE1 overexpression, shedding of the full-length precursor is no longer mediated by endogenous ADAMs after F_{285} but exclusively by BACE1 after F_{293} which explains the slightly larger size of β-$sEGF_{76}$ (9548.1 kDa) compared to β-$sEGF_{68}$ (8558.9 kDa) (Table 3). In contrast to western blot analysis which detected both, glycosylated and non-glycosylated β-sEGF (Figure 22) only a single non-glycosylated β-sEGF species was identified by mass spectrometry (Figure 25 B). This is explained by the fact that the parameters used here for MS analysis do not allow detection of glycosylated peptides and therefore only the fraction of non-glycosylated β-sEGF (lower band on western blot in Figure 22) was measured.

Next, the α-sEGF liberated from V5-IIINRG1-HA by ADAM17 (Figure 24) was investigated by means of mass spectrometry. ADAM17 was found to generate soluble EGF-like domains ranging from residue L_{235} to A_{283} (α-$sEGF_{49}$, 6642.2 kDa) or F_{285} (α-$sEGF_{51}$, 6786.1 kDa), respectively (Figure 25 C, Table 3). These fragments are derived from cleavage at a novel site after H_{234} which is located immediately N-terminal of the EGF-like domain (Figure 26). ADAM17 cleavage at this site liberates an EGF-like domain that does not contain the serine/threonine-rich stretch and explains why, unlike the β-sEGF, α-sEGF is not subject to O-linked glycosylation (Figure 22, 26). The positions of the two novel cleavage sites N-terminal of the EGF-like domain, L_{217} for BACE1 and H_{234} for ADAM17, which are

separated by 17 amino acid residues, are also the reason for the marked size difference observed for α-sEGF and β-sEGF, respectively (Figure 22).

In contrast to the homogenous shedding by BACE1 (after F_{293}), ADAM17-mediated shedding in the juxtamembrane region of NRG1 type III was found to be heterogeneous and to occur at both A_{283} and F_{285} (Figure 20). This explains the detection of two distinct α-sEGF species, α-sEGF$_{49}$ and α-sEGF$_{51}$, with identical N- but different C-termini. Furthermore this demonstrates that both the truncated NRG1ΔNT and the full-length V5-IIINRG1-HA construct are shed in a similar manner. As detected by western blot, coexpression of ADAM10 did not result in the liberation of sEGF peptides above the level caused by endogenous proteases (Figure 22). Consistently, the mass spectra derived from supernatants of cells expressing both V5-IIINRG1-HA and ADAM10 did not differ from the spectra of cells expressing only the construct but not the protease (Figure 25 B, C). This demonstrates that ADAM10 is not able to liberate the EGF-like domain on its own but depends on BACE1 or ADAM17 for the N-terminal cleavage.

Overall the mass spectrometric analysis confirms that both BACE1 and ADAM17 are able to liberate the EGF-like domain of NRG1 type III by a dual cleavage. The different sizes of the respective soluble EGF-like domains are caused by the distinct N-terminal cleavage sites identified for BACE1 and ADAM17, respectively. Table 3 provides an overview of the different soluble EGF-like domains that were detected, including their sequences and the calculated and observed masses. The relative positions of the identified cleavage sites are depicted in Figure 26.
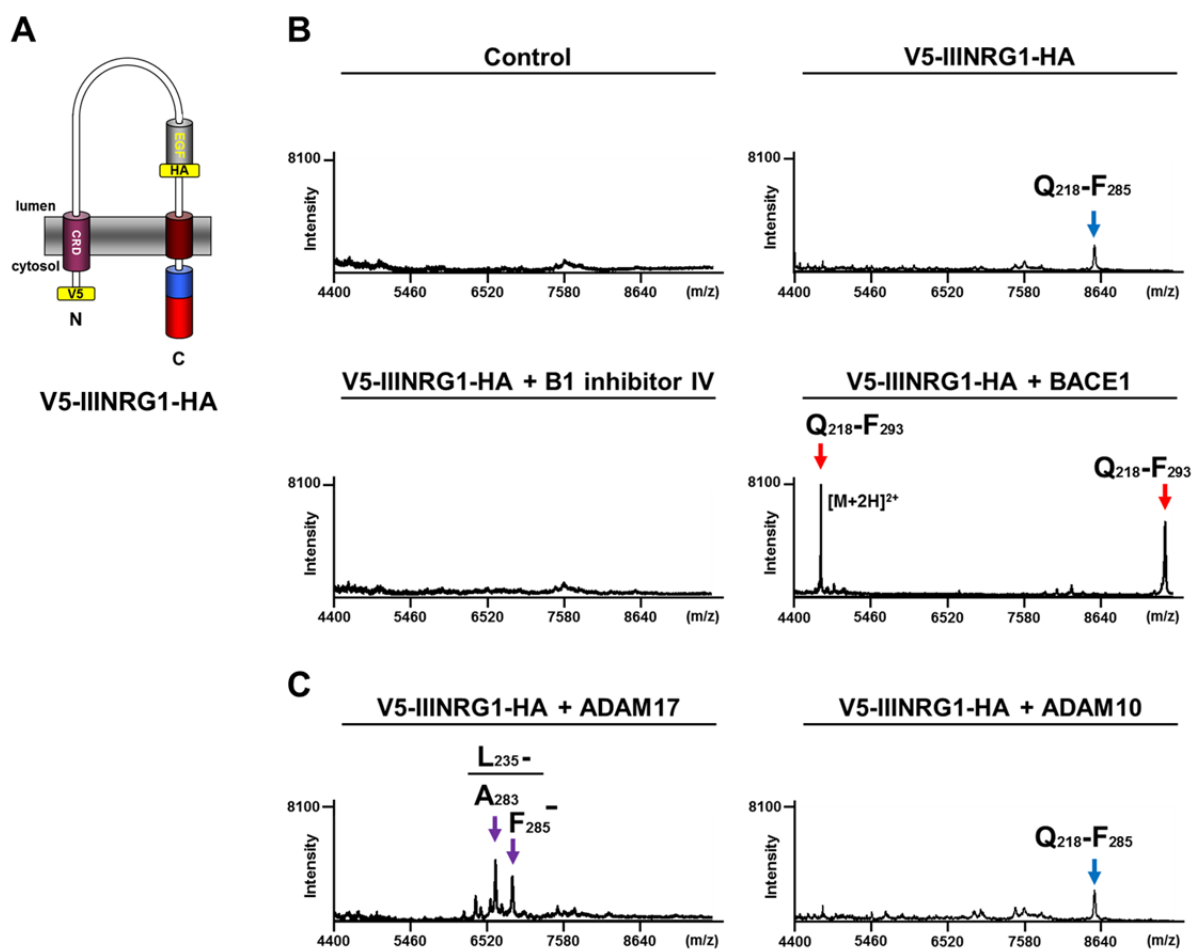
Figure 25. Novel cleavages before Q$_{218}$ by BACE1 and before L$_{235}$ by ADAM17 liberate the EGF-like domain of NRG1 type III. A) Graphical depiction of V5-IIINRG1-HA. An HA tag was inserted immediately after the EGF-like domain of NRG1 type III to allow immunoprecipitation. **B)** BACE1 cleaves NRG1 type III after L$_{217}$ and releases β-sEGF. V5-IIINRG1-HA was expressed in HEK293 cells (Figure 24) and BACE1 activity was repressed by inhibition (B1 inhibitor IV, 10 µM) or enhanced by overexpression. Peptides were isolated from supernatants by HA tag immunoprecipitation and subsequently analyzed by MALDI-TOF MS. As determined by their molecular weights (Table 3), a β-sEGF comprising residues Q$_{218}$-F$_{285}$ (blue arrow) was liberated by endogenous BACE1 levels, while enhanced BACE1 cleavage liberated residues Q$_{218}$-F$_{293}$ (red arrows). [M+2H]$^{2+}$ indicates a doubly charged peptide. **C)** ADAM17 but not ADAM10 liberates α-sEGF from NRG1 type III by a novel cleavage before L$_{235}$. Supernatants of cells expressing V5-IIINRG1-HA and ADAM17 or ADAM10 were analyzed as in B). ADAM17 cleavage between H$_{234}$ and L$_{235}$ released α-sEGF peptides L$_{235}$-A$_{283}$ and L$_{235}$-F$_{285}$ (purple arrows) (Table 3). In contrast, ADAM 10 coexpression yielded a soluble fragment with a BACE1-cleaved N-terminus and an ADAM-cleaved C-terminus (Q$_{218}$-F$_{285}$, blue arrow).

Peptide	N- / C-terminal cleavage	Residues	Sequence	Mass [M+H]$^+$ (Da)	
				Calc.	Obs.
β-sEGF76	BACE1 / BACE1	Q_{218}-F_{293}	QTAPKLSTSTSTTGTSHLIK-EGF-NYV*YPYDVPD*YAMASFYKHLGIEF	9548.8 (4775.4)*	9548.1 (4772.9)*
β-sEGF68	BACE1 / ADAM10	Q_{218}-F_{285}	QTAPKLSTSTSTTGTSHLIK-EGF-NYV*YPYDVPD*YAMASF	8560.7	8558.9
α-sEGF51	ADAM17 / ADAM17	L_{235}-F_{285}	LIK-EGF-NYV*YPYDVPD*YAMASF	6873.9	6876.1
α-sEGF49	ADAM17 / ADAM17	L_{235}-A_{283}	LIK-EGF-NYV*YPYDVPD*YAMA	6639.6	6642.1

Table 3. Overview of α- and β-sEGF peptides liberated from NRG1 type III as identified by mass spectrometry. Peptide names include the number of residues comprised by each sEGF (excluding the HA tag). Corresponding proteases and peptide sequences (without residues of the EGF-like domain) are given and observed masses (Obs.) are compared with calculated (Calc.) masses. Italic letters indicate the HA tag, [M+H]$^+$ a singly charged and the asterisk a doubly charged peptide.
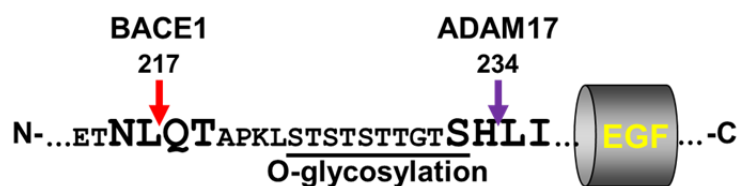
Figure 26. Graphic representation of the novel BACE1 and ADAM17 cleavage sites N-terminal of the EGF-like domain. Cleavage sites are indicated and the numbers of the residues after which cleavage occurs are given. The serine/threonine-rich sequence which is subject to O-linked glycosylation is underlined.

3.3 Neoepitope-specific antibodies detect BACE1-cleaved NRG1 type III fragments

To investigate processing of NRG1 type III in greater detail and to facilitate detection of untagged and endogenous protein for example in primary neurons, suitable antibodies were required. However, only very few commercially available antibodies detect NRG1 type III and none are specific for processed fragments. Therefore monoclonal antibodies specific to the identified cleavage sites in NRG1 type III were produced.

Two monoclonal antibodies were raised against the neoepitopes arising from BACE1-mediated shedding in the juxtamembrane region: Antibody 10E8 against the epitope immediately C-terminal of the BACE1 shedding site, i.e. the N-terminus of the β-CTF (M_{294}EAEE…) and antibody 4F10 against the sequence directly upstream of this site (…$GIEF_{293}$). An additional antibody 7E6 was raised against the residues (Q_{218}TAPK…) after the novel N-terminal BACE1 cleavage site. In combination, these antibodies allow detection and identification of β-sEGF by both its N- and C-terminal residues. Figure 27 provides an overview of the epitopes and NRG1 type III fragments that are recognized by the generated antibodies.
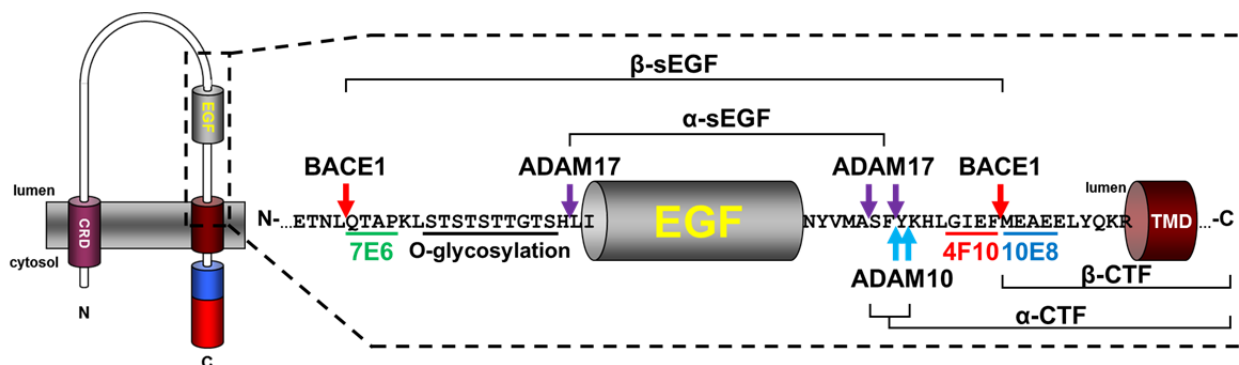
Figure 27. Schematic overview of NRG1 type III cleavage sites and fragments recognized by novel antibodies. Cleavage sites of respective proteases are marked by arrows and α- and β-sEGF as well as α- and β-CTF are indicated. Epitopes recognized by the novel antibodies and the site of glycosylation are shown.

Lysates (Figure 28, 29) and supernatants (Figure 30) from cells expressing untagged NRG1 type III were used to assess the specificity of the novel antibodies. Similar to the EGF antibody, 4F10 detected a NRG1 type III NTF of approx. 80 kDa in the cell lysates (Figure 28). Due to the liberation of the EGF-like domain, total amounts of the NTF, as recognized by the antibody against the EGF-like domain, are strongly reduced upon overexpression of BACE1. Demonstrating its specificity towards the BACE1-cleaved C-terminus of the NTF, however, 4F10 yielded the strongest signal under this condition (Figure 28, lanes 4 and 5). This indicates that of the small amount of NTF still present under this condition (weak signal with the EGF antibody), the majority is generated by BACE1-mediated shedding (strong 4F10 signal). In contrast, the high amount of total NTFs (strong EGF antibody signal) present under endogenous protease levels mainly results from ADAM- and not BACE1-mediated shedding (weak 4F10 signal). Its specificity for the BACE1-cleaved NTF also explains why enhanced shedding by overexpression of ADAM10 and ADAM17 was not detected by the 4F10 antibody.
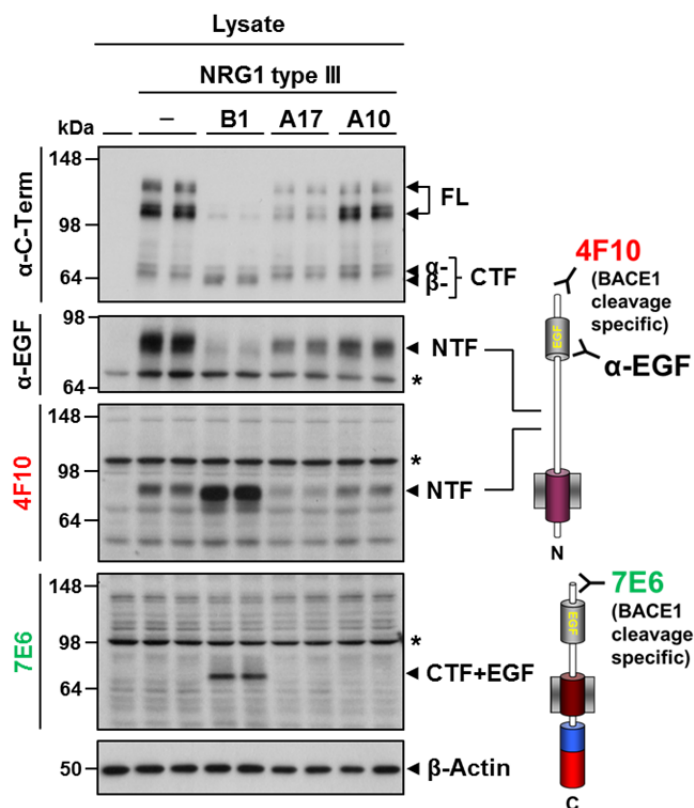
Figure 28. Novel antibodies 4F10 and 7E6 detect BACE1-cleaved membrane-bound NRG1 type III fragments. Lysates of HEK293 cells expressing untagged NRG1 type III and BACE1 (B1), ADAM17 (A17) or ADAM10 (A10) were used for western blot analysis with the indicated antibodies. Membrane-bound fragments resulting from BACE1-mediated cleavage were specifically detected with the neo-epitope specific antibodies 4F10 and 7E6.

Cleavage of NRG1 type III at the novel sites N-terminal of the EGF-like domain without subsequent shedding in the juxtamembrane region would yield a CTF containing the EGF-like domain (CTF+EGF, scheme in Figure 28). Although this fragment was never observed with antibodies against the C-terminus or the EGF-like domain of NRG1 type III, the 7E6 antibody detected a CTF+EGF of approx. 70 kDa when BACE1 was overexpressed (Figure 28). Its size which is larger than the size of the CTF alone (approx. 64 kDa) is in line with the size observed for NRG1ΔNT (3.1 Figure 11) that represents an artificial, Flag tagged version of the CTF+EGF fragment. The presence of the CTF+EGF in the lysate indicates that at least in cells with a high level of BACE1 activity, N-terminal cleavage precedes shedding in a fraction of NRG1 type III. Compared to the NTF, however, the CTF+EGF seems to be present in rather small amounts. Most likely this low abundance is the reason for the fragment not being detected by antibodies other than the 7E6 antibody which is specific (and sufficiently sensitive) for the N-terminus of the CTF+EGF.

Finally the antibody 10E8 which was raised against the N-terminus of the β-CTF was checked for its specificity. In the presence of comparable amounts of total CTFs (C-terminal antibody, Figure 29), the 10E8 antibody yielded a strong western blot signal at approx. 64 kDa only in case of BACE1 but not ADAM10 or ADAM17 overexpression. This demonstrates that 10E8 is specific for the BACE1-cleaved β-CTF and indicates that under endogenous protease levels in HEK293 cells, a large portion of the CTFs are in fact α-CTF, generated by ADAM-mediated shedding. This is in line with the data obtained by mass spectrometry (Figure 25) which also found endogenous shedding of NRG1 type III to mainly occur at the ADAM site.

As an additional confirmation of their BACE1 neoepitope specificity, none of the three antibodies, 7E6, 4F10 and 10E8 recognized the full-length NRG1 type III protein in cell lysates (Figure 28, 29).
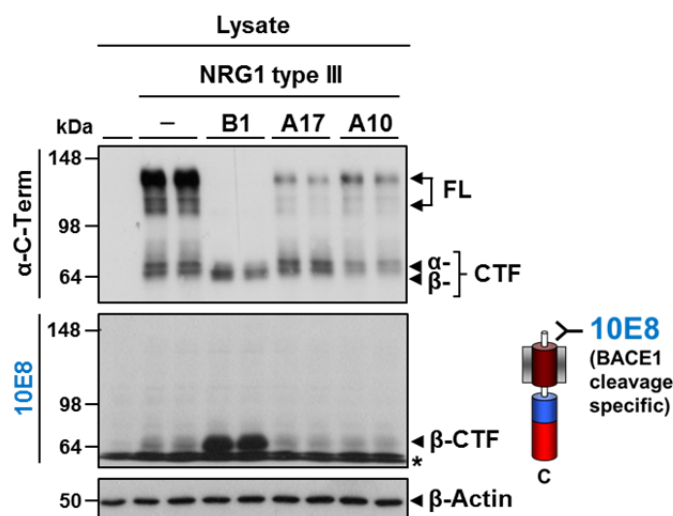
Figure 29. The novel antibody 10E8 specifically detects the NRG1 type III β-CTF generated by BACE1 shedding. HEK293 cells expressing untagged NRG1 type III and BACE1 (B1), ADAM17 (A17) or ADAM10 (A10) were lysed and analyzed by immunoblotting with the indicated antibodies. β-CTFs resulting from BACE1-mediated shedding were recognized specifically by the 10E8 antibody.

Supernatants of cells expressing NRG1 type III and BACE1, ADAM17 or ADAM10 were then used to examine the ability of the newly generated antibodies to recognize β-sEGF. Both, the 7E6 and the 4F10 antibody detected the N- and C-terminus of β-sEGF$_{76}$ released from cells overexpressing BACE1, respectively (Figure 30). Similar to the commercial EGF antibody (3.2.1 Figure 22) both antibodies also detected the O-glycosylated fraction of β-sEGF$_{76}$ (Figure 30, marked by a diamond).

Previously, MS analysis had revealed that in contrast to BACE1 overexpression, endogenous proteases in HEK293 cells liberate small amounts of β-sEGF$_{68}$ (not β-sEGF$_{76}$) through N-terminal BACE1 cleavage and C-terminal ADAM-mediated shedding (3.2.2 Figure 25, Table 3). Accordingly, the β-sEGF$_{68}$ fragment may only be recognized at its N-terminus (BACE1-cleaved) by the 7E6 antibody but not at its C-terminus (ADAM-cleaved) by 4F10. Consistent with that is the detection of low amounts of β-sEGF$_{68}$ with the 7E6 but not the 4F10 antibody in supernatants of cells expressing NRG1 type III only (Figure 30, lanes 2 and 3, long exposure). In line, ectopic expression of ADAM10 further enhanced shedding and lead to slightly increased levels of β-sEGF$_{68}$ as detected by the 7E6 antibody (Figure 30, lanes 8 and 9, long exposure) in the supernatant. ADAM17 is capable of liberating the NRG1 type III EGF-like domain independent of BACE1 cleavage (3.2.1). Consequently, the α-sEGF as generated by ADAM17 does not contain the BACE1-cleaved epitopes and thus cannot be recognized by antibodies 7E6 and 4F10. Confirming these considerations and in line with the MS data, overexpression of ADAM17 prevented the release of the EGF-like domain through

an N-terminal BACE1 cleavage and no 7E6 and 4F10 signals were observed (Figure 30, lanes 6 and 7, long exposure).
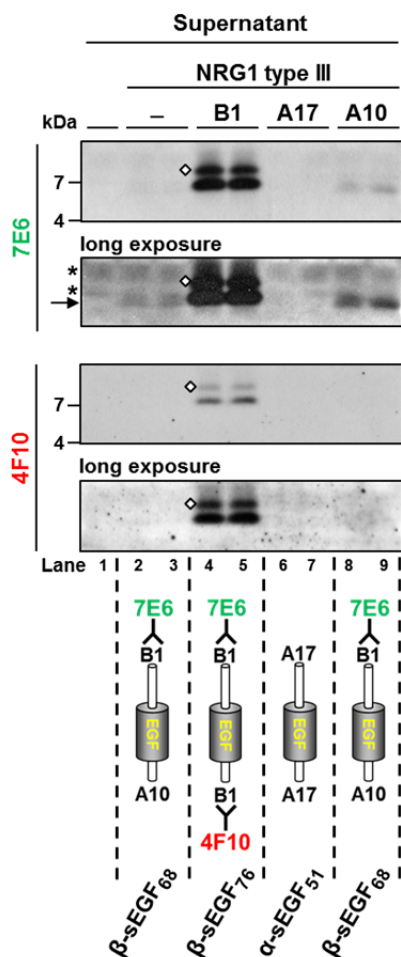
Figure 30. The novel antibodies 7E6 and 4F10 recognize the β-sEGF liberated from NRG1 type III by BACE1 cleavage. Supernatants of HEK293 cells expressing NRG1 type III and BACE1 (B1) ADAM17 (A17) or ADAM10 (A10) were analyzed by western blot using the 7E6 antibody to detect the N-terminus and the 4F10 antibody to detect the C-terminus of β-sEGF. Both antibodies detected glycosylated (diamonds) and non-glycosylated β-sEGF$_{76}$ liberated by a dual BACE1 cleavage. β-sEGF$_{68}$ is generated by endogenous processing or cleavage by overexpressed ADAM10 (3.2.2 Figure 25, Table 3) and is liberated by N-terminal BACE1 cleavage (7E6 signal in lanes 2 and 3 and lanes 8 and 9, indicated by an arrow) but not C-terminal BACE1 shedding (no 4F10 signal in lanes 2 and 3 and lanes 8 and 9). ADAM17 liberates α-sEGF (3.2.2 Figure 25, Table 3) which is not recognized by BACE1 cleavage-specific antibodies. Asterisks indicate unspecific background bands. The scheme below depicts the detected fragments and the proteases responsible for their liberation.

In summary, the novel neoepitope-specific antibodies allowed the detection of both soluble and membrane-bound NRG1 type III fragments. At all times, the abundance of the fragments detected by 7E6, 4F10 and 10E8 was increased by enhanced BACE1 expression. In contrast, expression of ADAM10 and ADAM17 had no effect or, in case of ADAM17-mediated α-sEGF generation, abolished the release of fragments detectable by these antibodies. This demonstrates that the novel antibodies are indeed specific for their respective neoepitopes resulting from BACE1 cleavage and do not recognize ADAM-cleaved sites. Furthermore, in the context of ectopic expression of NRG1 type III in stable cell lines, the antibodies proofed to be sensitive enough to allow detection without the need of prior enrichment by immunoprecipitation. Nevertheless, 7E6, 4F10 and 10E8 are also suitable as capture antibody during immunoprecipitation (3.4 Figure 32, 3.6.1 Figure 41). Overall, using the novel antibodies for western blot analysis confirmed the identified BACE1 cleavage sites in NRG1 type III independent of the IP-MS approach.

3.4 Primary neurons process NRG1 type III to release α- and β-sEGF

The use of stable cell lines and ectopic expression of the substrate (and the proteases) were the means of choice to identify cleavage sites in NRG1 type III and to generate site-specific antibodies. Ultimately however, the aim is to investigate the processing and cleavage of NRG1 type III endogenously, i.e. in cells that naturally express NRG1 type III. Neurons of the peripheral nervous system (PNS), especially dorsal root ganglion (DRG) cells express and process NRG1 type III endogenously (Michailov et al., 2004; Willem et al., 2006). However, the culture of DRGs is time consuming and it is difficult to obtain sufficient amounts of cell material for a systematic biochemical investigation. To still be able to study the processing of NRG1 type III by endogenous proteases in primary neuronal cells, the construct V5-IIINRG1-HA was expressed in hippocampal neurons using lentiviral transduction. Lentiviral delivery ensures protein levels high enough to be detected by means of biochemistry and the HA tag of V5-IIINRG1-HA allows the efficient isolation of the soluble ADAM-cleaved EGF-like domain from the supernatant that is not recognized by the novel antibodies 4F10 and 7E6.

Western blot analysis of lysates from hippocampal neurons expressing V5-IIINRG1-HA revealed neuronal shedding to generate a NRG1 type III CTF and NTF, the latter containing the EGF-like domain (Figure 31). Inhibition of BACE1-mediated shedding (by treatment with the specific BACE1 inhibitor IV) reduced overall shedding as indicated by the

accumulation of the full-length protein and reduced levels of CTF. β-CTFs resulting from BACE1 shedding were specifically detected with the 10E8 antibody. Upon inhibition of BACE1, the 10E8 signal was completely abolished, demonstrating the high degree of BACE1 inhibition. The remaining CTFs (as detected with the C-terminal antibody) most likely resulted from shedding by ADAMs, supporting the idea that under physiological conditions both BACE1 and ADAMs contribute to NRG1 type III shedding. Indeed, concomitant inhibition of both BACE1 and ADAM activity (by IV and GM6001) further reduced shedding. The residual turnover of NRG1 type III under this condition is probably due to incomplete ADAM inhibition by the inhibitor GM6001.

To identify BACE1-cleaved NTFs among the total NTFs, a membrane previously incubated with an EGF antibody was reprobed with the 4F10 antibody (Figure 31). This confirmed that endogenous shedding of NRG1 type III indeed generates a membrane-bound EGF-like domain comprising the identified BACE1 shedding site as C-terminus. Production of this BACE1-cleaved NTF that is supposed to be the signaling active fragment in the context of myelination (Taveggia et al., 2005; Willem et al., 2006) was consequently abolished upon BACE1 inhibition (Figure 31). As the remaining NTFs arose from ADAM-mediated processing and therefore terminated at the ADAM cleavage sites they were not recognized by 4F10.
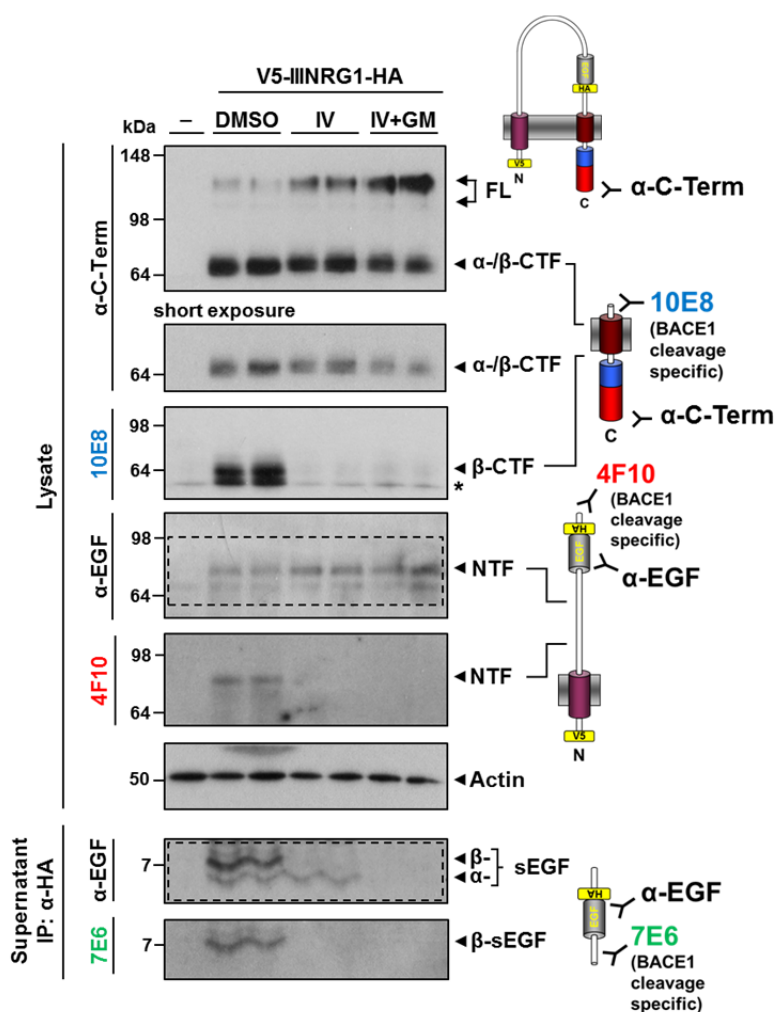
Figure 31. Processing of NRG1 type III in primary neurons generates a membrane-tethered and a soluble EGF-like domain. V5-IIINRG1-HA was expressed in hippocampal neurons using lentiviral transduction and cells were treated with inhibitors of BACE1 and ADAM proteases (BACE1 inhibitor IV, 5 µM; ADAM inhibitor GM6001, 25 µM). Cell lysates were analyzed for membrane-bound fragments by immunoblotting with the indicated antibodies. Of the total amounts of NTFs and CTFs generated by shedding, BACE1-cleaved fragments were specifically detected with the antibodies 4F10 and 10E8. Soluble EGF-like domains were isolated from the conditioned supernatant using the HA tag for immunoprecipitation. Dashed boxes indicate membranes reprobed with the antibodies shown directly below. The asterisk indicates unspecific background bands.

In HEK293 cells expressing high levels of BACE1, a CTF containing the EGF-like domain was observed (3.3 CTF+EGF in Figure 28). This fragment that represents an EGF-like domain tethered to the membrane by the C-terminus of NRG1 type III results from a single BACE1 cleavage after L_{216} (N-terminal of the EGF-like domain) without subsequent shedding. Although not described before, such a CTF+EGF could potentially also represent a signaling active fragment of NRG1 type III that binds and activates ErbB receptors in a juxtacrine manner. To check for its generation in primary neurons, lysates of hippocampal

neurons expressing V5-IIINRG1-HA were analyzed using the antibody 7E6 for immuno-detection. However, no CTF+EGF could be detected in these cells (data not shown). The presence of detectable amounts of CTF+EGF therefore seems to be limited to cells expressing extremely high levels of BACE1 which allow a fraction of NRG1 type III to be cleaved N-terminal of the EGF-like domain without subsequent shedding. Together these results support the concept that, physiologically, the EGF-like domain of NRG1 type III is indeed anchored to the membrane via its NTF.

As observed with non-neuronal cells before (3.2.1 Figure 22), also primary hippocampal neurons released the EGF-like domain of V5-IIINRG1-HA into the supernatant (Figure 31). However, due to the smaller cell number, probably lower expression level of the substrate as well as the fact that no proteases were expressed ectopically, detection of the sEGF fragments required immunoprecipitation beforehand. Using an EGF antibody for western blot detection two sEGF fragments corresponding to α- and β-sEGF, respectively, were observed above and below the 7 kDa marker (Figure 31). Inhibition of BACE1 activity selectively prevented generation of the slightly larger β-sEGF, whereas the smaller α-sEGF was abolished only upon ADAM inhibition. To further confirm the identity of the observed fragments, the membrane was reprobed with the 7E6 antibody. This antibody, being specific for the BACE1 cleavage site N-terminal of the EGF-like domain only detected the larger β-sEGF (Figure 31) demonstrating that also in neurons the β-sEGF is liberated by cleavage at the novel BACE1 site.

To further confirm processing of NRG1 type III at the identified sites, immuno-precipitations from supernatants of hippocampal neurons expressing V5-IIINRG1-HA (Figure 31) were performed using the BACE1 cleavage site-specific antibodies 4F10 and 7E6. In contrast to the antibody against the HA tag (Figure 32, upper panel), both 4F10 and 7E6 only isolated the larger β-sEGF but not the smaller α-EGF (Figure 32). Inhibition of BACE1 abolished precipitation of β-sEGF by either antibody, thereby confirming that this fragment is generated through a dual BACE1 cleavage at the identified sites.

Together these results demonstrate that processing of NRG1 type III by endogenous BACE1 and ADAM proteases in primary neurons occurs at the identified cleavage sites and results in the release of the EGF-like domain as β- and α-sEGF.
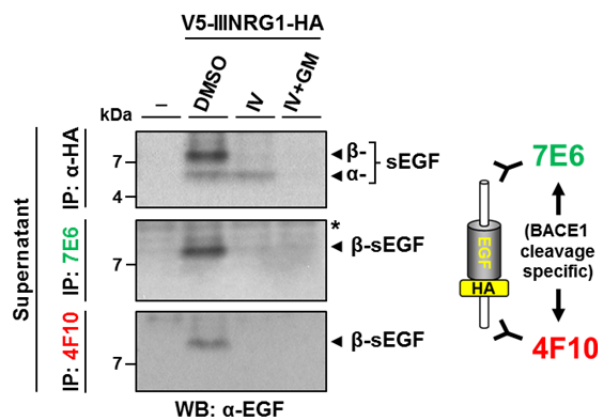
Figure 32. A dual BACE1 cleavage liberates β-sEGF from NRG1 type III in neurons. Supernatants of neurons expressing V5-IIINRG1-HA (Figure 31) were immunoprecipitated with the indicated antibodies against the HA tag or the BACE1 cleavage sites. Isolated peptides were detected on western blot using an EGF antibody. The asterisk indicates unspecific background bands.

3.5 The EGF-like domains released from NRG1 type III constitute a paracrine signal that promotes myelination

Myelination in the PNS depends on the juxtacrine activation of Schwann cells by NRG1 type III signaling from adjacent axons. Mechanistically it is thought that the neuronal NRG1 type III NTF anchors the EGF-like domain to the axonal surface thereby allowing only contact-dependent activation of ErbB receptors on the surface of Schwann cells (Wang et al., 2001; Birchmeier and Nave, 2008). In this context NRG1 type III has been shown to stimulate ErbB2/3 receptors, which, upon autophosphorylation, then activate the downstream PI3 kinase signaling pathway. In the further course of the PI3K pathway the downstream effector kinase AKT becomes phosphorylated and finally proliferation of Schwann cells and induction of myelination is initiated (Newbern and Birchmeier, 2010). Soluble NRG1 type III failed to rescue myelination in co-cultures of NRG1 type III^{-/-} neurons and Schwann cells, suggesting that NRG1 type III induces and promotes myelination only in a strictly contact-dependent manner (Taveggia et al., 2005). In contrast, such soluble NRG1 type III peptides recently were found to restore myelination of neurons with heterozygous levels of NRG1 type III (Syed et al., 2010). This effect was concentration-dependent and indicates that if not the induction, at least the promotion of myelination may be controlled by soluble NRG1 type III in a paracrine manner.

3.5.1 α- and β-sEGF activate ErbB3 receptors and initiate signaling required for myelination

The above mentioned studies relied on the addition of soluble recombinant NRG1 type III peptides as paracrine signal. In contrast, the liberation of the EGF-like domain as α- and β-sEGF by ADAM17- and BACE1-mediated processing of NRG1 type III (3.2) constitutes a cellular source of such soluble EGF-like domains. To investigate whether indeed these sEGF domains could act as a paracrine signal, their ability to activate and signal through ErbB3 receptors was assessed.

To this end, the sequences of α- and β-sEGF (containing an HA tag after the EGF-like domain) were cloned into a vector that allows their secretion and a furin cleavage site was inserted directly upstream of their respective N-termini. Furin cleavage facilitates removal of the leader peptide and simultaneously generates the N-terminus identified for α- and β-sEGF, respectively. Furthermore, both constructs terminate with the residues resulting from BACE1 or ADAM17 cleavage and therefore are synthesized as soluble peptides that are secreted independently of shedding (Figure 33 A).

Western blot analysis of conditioned supernatants from CHO wt cells expressing α- and β-sEGF revealed robust secretion of both peptides (Figure 33 B). The presence of a diffuse band at higher molecular weight indicated O-linked glycosylation of a fraction of β-sEGF and was abolished in cells deficient in O-glycosylation (Figure 35 A, B). To further confirm the integrity of α- and β-sEGF, the peptides were immunoprecipitated using the HA tag and analyzed by MALDI-TOF MS (Figure 33 C). As deduced from the observed molecular weight both peptides comprised the expected sequence and were intact without additional undesired cleavages within the EGF-like domain (Table 4).

Nevertheless, mass spectrometric analysis revealed that a fraction of α-sEGF was truncated by one residue at the C-terminus while simultaneously the N-terminus comprised one additional residue (Figure 33 C, Table 4). The heterogeneous N-terminus could be the result of an imprecise furin cleavage but the reason for this is not known. In contrast, C-terminal truncations of peptides are observed regularly (3.6.2) and are most likely due to the activity of exopeptidases. Unlike α-sEGF, β-sEGF was observed as a homogenous peptide. Due to the high amount of material available for MS analysis, the partial O-glycosylation of β-sEGF could be detected as multiple poorly separated peaks at higher molecular weight (Figure 33 C).
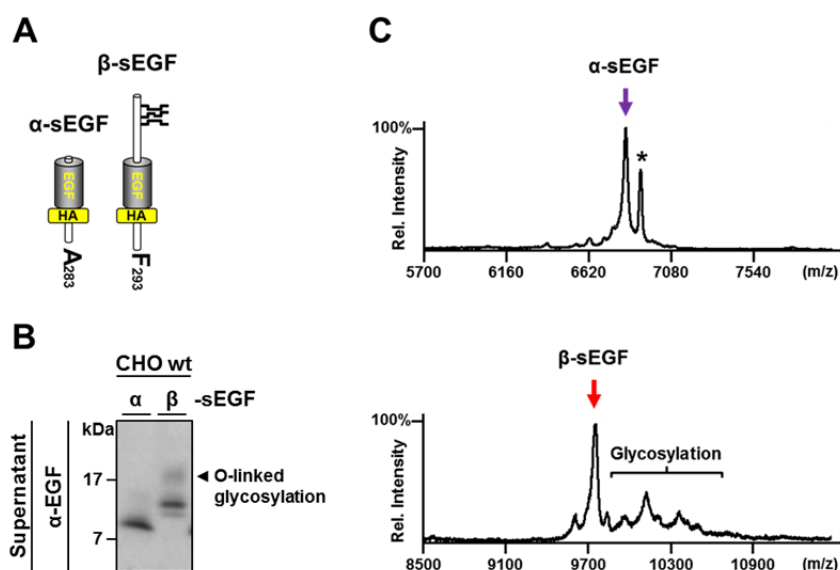
Figure 33. CHO wild-type cells produce secreted versions of α- and β-sEGF. A) Schematic depiction of the secreted α- and β-sEGF constructs. Both constructs are expressed using a secretion vector, comprise an HA tag after the EGF-like domain and the respective N- and C-termini identified before (3.3 Figure 27). O-glycosylation is indicated for β-sEGF. **B)** sEGF domains are secreted into the supernatant by CHO wild-type cells. Supernatants of CHO cells expressing α- and β-sEGF were analyzed by immunoblotting with an EGF antibody. A diffuse band at higher molecular weight indicates glycosylation of β-sEGF. **C)** Mass spectrometric analysis reveals secretion of intact α- and β-sEGF domains. sEGF domains of B) were isolated by HA immunoprecipitation and analyzed by MALDI-TOF MS. A minor fraction of α-sEGF was found to contain an additional residue at the N-terminus while lacking a residue at the C-terminus (indicated by an asterisk) (Table 4). Glycosylation of β-sEGF caused multiple peaks at higher m/z ratios.

Peptide	C-terminus	Sequence	Mass [M+H]$^+$ (Da)	
			Calc.	Obs.
α-sEGF	A283	SVLIKCAEKEKTFCVNGGECFTVKDLSNPSRYLCKCP NEFTGDRCQNYV*YPYDVPD*YAMA	6825.8	6828.0
α-sEGF*	M282	RSVLIKCAEKEKTFCVNGGECFTVKDLSNPSRYLCK CPNEFTGDRCQNYV*YPYDVPD*YAM	6910.9	6911.1
β-sEGF	F293	SVQTAPKLSTSTSTTGTSHLIKCAEKEKTFCVNGGEC FTVKDLSNPSRYLCKCPNEFTGDRCQNYV*YPYDVPD* *Y*AMASFYKHLGIEF	9735.0	9741.5

Table 4. Overview of α- and β-sEGF peptides secreted by CHO wt cells as identified by MALDI-TOF MS. Peptide sequences and respective C-terminal residues are given and observed (Obs.) peptide masses are compared with calculated (Calc.) masses. The asterisk denotes a minor α-sEGF peptide with altered N- and C-termini (Figure 33). Italic letters indicate the HA tag, [M+H]$^+$ a singly charged peptide.

In a next step, the ability of α- and β-sEGF to activate ErbB3 receptors and initiate PI3K downstream signaling in a paracrine fashion was assessed. Therefore, MCF-7 cells which express ErbB3 receptors and allow monitoring of NRG1 signaling via ErbB3 (Luo et al., 2011) were incubated with conditioned medium containing equal amounts of α- and β-sEGF (Figure 34 A) or with supernatants from cells expressing a control vector. As positive control, MCF-7 cells were stimulated with a recombinant NRG1 EGF-like domain (0.5 nM). Both α- and β-sEGF lead to ErbB3 activation and initiation of the PI3K downstream signaling in MCF-7 cells as evidenced by increased levels of phosphorylated ErbB3 and AKT in the lysate (Figure 34 B). Quantification and comparison of the ratios of phosphorylated and total levels of ErbB3 and AKT revealed that α- and β-sEGF activated receptor and signaling to a very similar degree. Although there was a trend towards a slightly stronger activation by α-sEGF this was not significant, indicating that α- and β-sEGF do not substantially differ in their ability to activate and signal through ErbB3 receptors (Figure 34 C).

Apart from their size and N- and C-terminal residues, the fact that β-sEGF but not α-sEGF may be O-glycosylated is a key difference between these signaling peptides. Glycosylation can affect interactions between proteins (e.g. between ligand and receptor) and therefore the O-linked glycosylation of β-sEGF could alter its ability to stimulate ErbB3 receptors. To investigate this possibility α- and β-sEGF were expressed in CHO ldlD cells (Kingsley et al., 1986) that are deficient in O-linked glycosylation. Both constructs were secreted as before but as indicated by the absence of a diffuse western blot band at higher molecular weight, β-sEGF lacked O-glycosylation (Figure 35 A). The absence of glycosylation was confirmed by mass spectrometric analysis as in contrast to the β-sEGF from CHO wt cells no additional peaks at higher molecular weight were observed (Figure 33 C, 35 B).

Similar to stimulation with glycosylated β-sEGF before, stimulation of MCF-7 cells with non-glycosylated β-sEGF activated ErbB3 and AKT to the same extent as stimulation with α-sEGF (Figure 35 C). This demonstrates that O-linked glycosylation of β-sEGF does not significantly change its capacity to activate ErbB3 receptors and subsequent AKT signaling in MCF-7 cells.
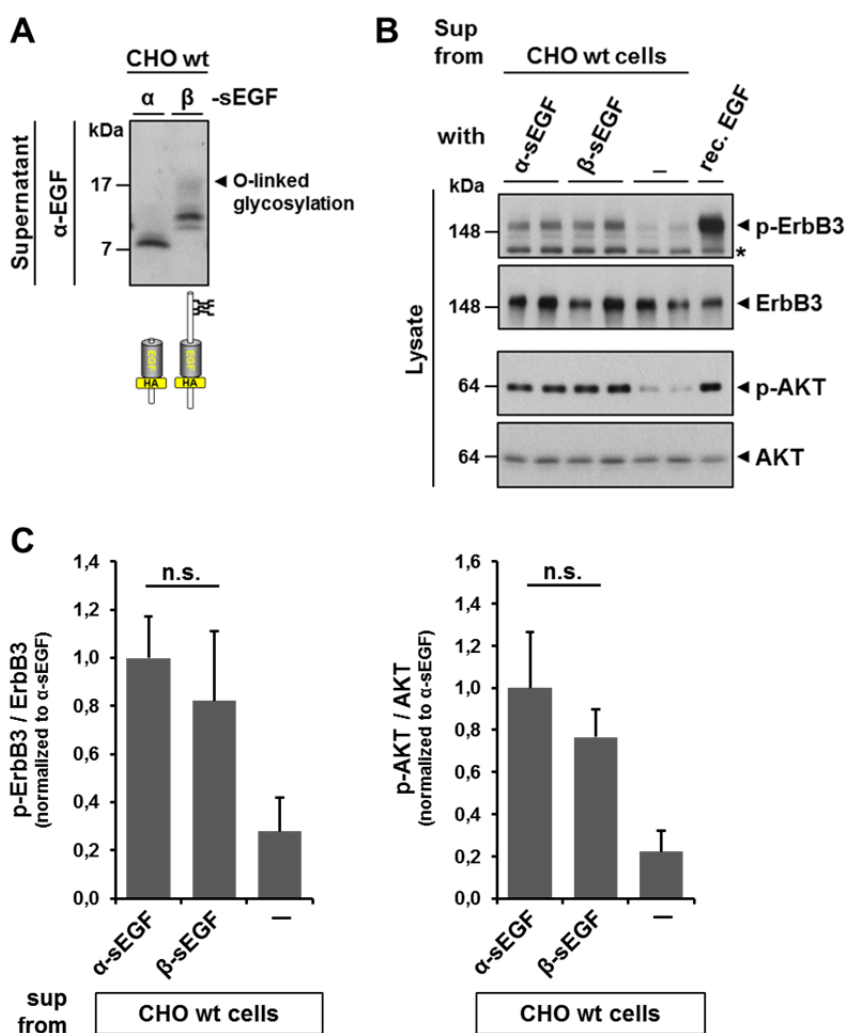
Figure 34. α- and β-sEGF stimulate ErbB3 receptors and activate PI3K signaling in MCF-7 cells.
A) Preparation of conditioned supernatants. Media of CHO wt cells expressing α- and β-sEGF were analyzed by immunoblotting and the levels of α- and β-sEGF were adjusted by dilution with medium from control cells. **B)** Stimulation of ErbB3 and AKT phosphorylation in MCF-7 cells by α- and β-sEGF. Supernatants from A) were used to incubate MCF-7 cells. Medium from cells expressing an empty vector was used as negative and treatment with a recombinant NRG1 EGF-like domain (0.5 nM) as positive control. Cell lysates were analyzed for (phosphorylated) ErbB3 and AKT by western blotting. The asterisk indicates an unspecific band. **C)** Quantification of phosphorylated protein/total protein ratio (normalized to α-sEGF; n = 3; n.s., not significant).
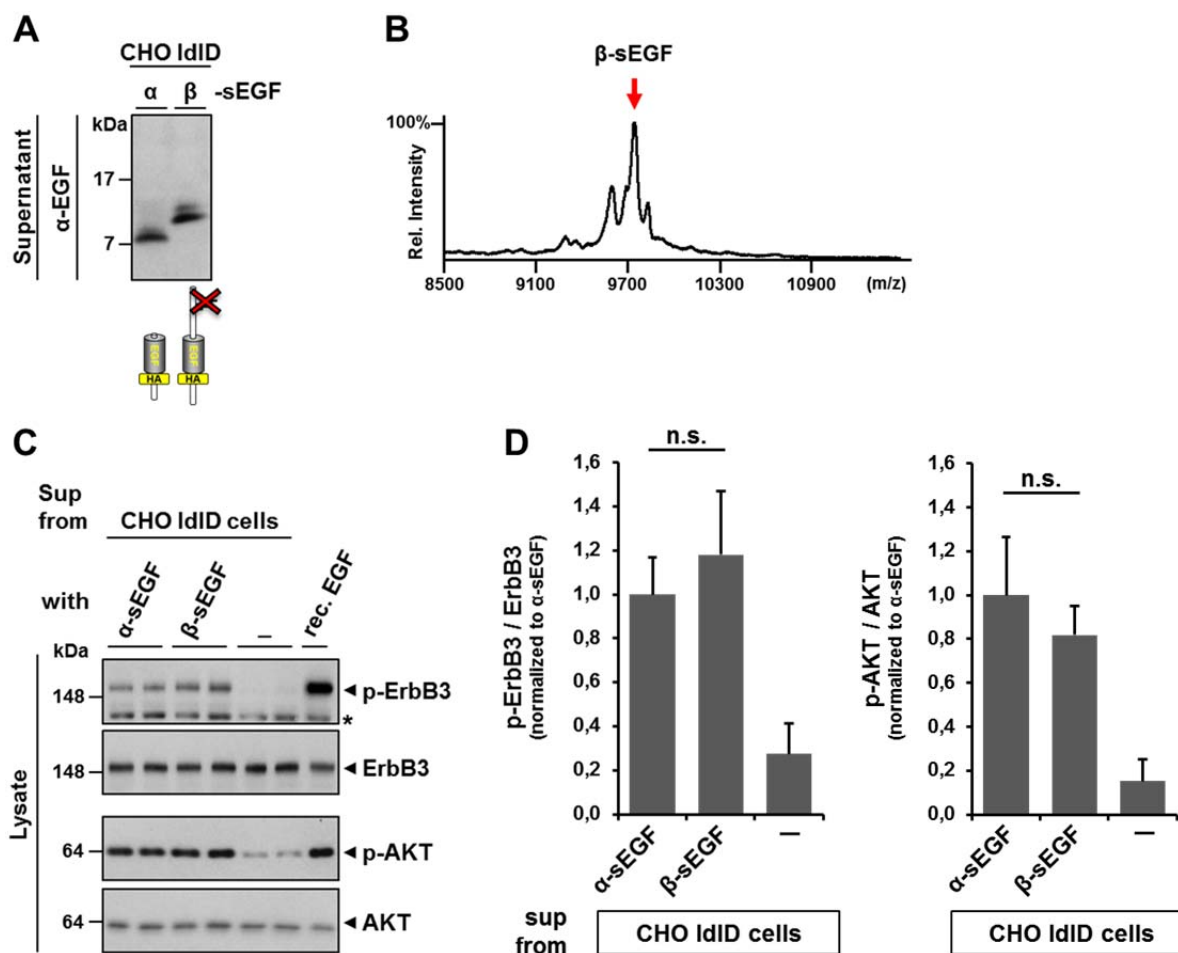
Figure 35. O-glycosylation of β-sEGF does not affect its ability to activate ErbB3 receptors and AKT in MCF-7 cells. A) Secretion of non-glycosylated sEGF peptides by CHO ldlD cells. α- and β-sEGF were expressed in CHO ldlD cells deficient in O-glycosylation, supernatants were analyzed by immunoblotting and levels of α- and β-sEGF were adjusted by dilution with medium from control cells. **B)** Mass spectrometric analysis of β-sEGF confirms absence of glycosylation. β-sEGF was isolated from supernatants of A) by HA immunoprecipitation and analyzed by MALDI-TOF MS. No peaks at higher m/z ratios were observed (Figure 33 C). **C)** α-sEGF and non-glycosylated β-sEGF stimulate ErbB3 and AKT phosphorylation to a similar extent. MCF-7 cells were incubated with supernatants from A) or medium of cells expressing an empty vector as control. Treatment with a recombinant NRG1 EGF-like domain (0.5 nM) served as positive control. Cell lysates were analyzed for (phosphorylated) ErbB3 and AKT by western blotting. The asterisk indicates an unspecific band. **D)** Quantification of phosphorylated protein/total protein ratio (normalized to α-sEGF; n = 3; n.s., not significant).

A paracrine signaling mode of NRG1 type III in the context of PNS myelination requires the release of soluble EGF-like domains that activate Schwann cells. In a first step it was shown that α- and β-sEGF as released from NRG1 type III by ADAM17 and BACE1 are able to stimulate ErbB3 receptors on MCF-7 cells in a paracrine manner. As MCF-7 cells express ErbB3 receptor endogenously they allow the investigation of sEGF induced signaling without the need to overexpress the receptor which could lead to artificially enhanced sensitivity

towards its ligand. However, MCF-7 cells are stable cancer cells and paracrine activation of ErbB3 signaling by α- and β-sEGF in these cells does not automatically translate to a similar effect in Schwann cells.

To investigate whether α- and β-sEGF were also able to induce the signaling required for myelination in cells that more closely resemble the physiological target cells, purified rat primary Schwann cells were used. Incubation of these cells with medium containing equal amounts of α- and β-sEGF resulted in significantly elevated levels of phosphorylated ErbB3 and AKT (Figure 36). In line with previous observations, α- and β-sEGF again caused very similar activation of receptor and downstream signaling. Finally, purified rat primary Schwann cells were stimulated with α-sEGF and non-glycosylated β-sEGF derived from O-glycosylation deficient CHO ldlD cells. The abolished glycosylation did not change the ability of β-sEGF to activate ErbB3 signaling (Figure 36), thereby confirming the results obtained with MCF-7 cells.
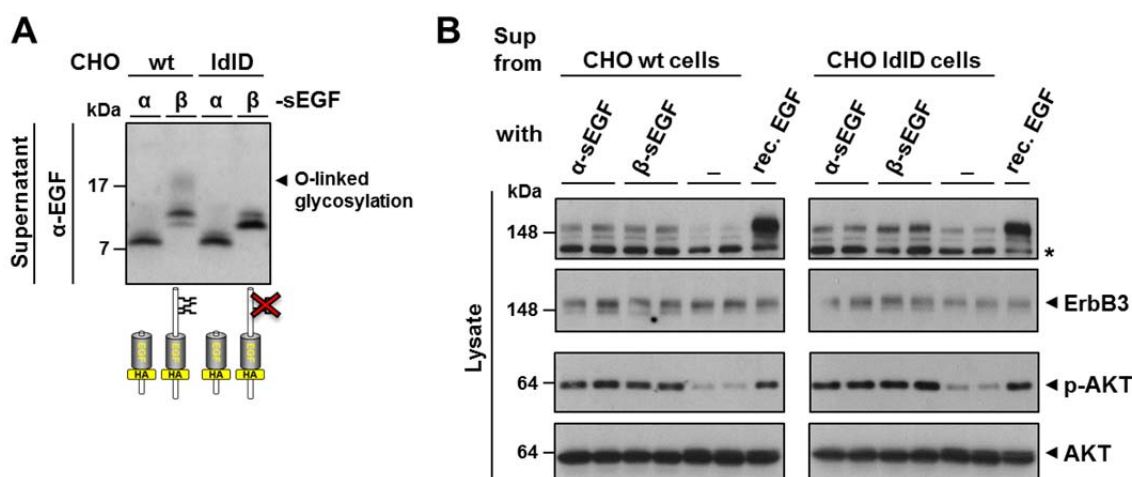
Figure 36. α-sEGF and β-sEGF stimulate ErbB3 receptors and AKT signaling in primary Schwann cells similarly and independent of glycosylation. A) Preparation of supernatants containing equal amounts of α-sEGF, glycosylated and non-glycosylated β-sEGF. sEGF constructs were expressed in wt and O-glycosylation deficient (ldlD) CHO cells. Conditioned media were analyzed by western blot and levels of α- and β-sEGF were adjusted by dilution with medium from control cells. O-glycosylated β-sEGF migrated as an additional, diffuse band of higher molecular weight which is abolished in CHO ldlD cells. **B)** Primary Schwann cells were incubated with media from A) or from cells expressing an empty vector as control. Incubation with a recombinant NRG1 EGF-like domain (0.5 nM) served as positive control. Cell lysates were analyzed for (phosphorylated) ErbB3 and AKT by western blotting. The asterisk indicates an unspecific band.

Overall the results above demonstrate that both ADAM17 and BACE1 liberate a functionally active EGF-like domain from NRG1 type III. Both α- and β-sEGF exert NRG1 type III signaling in a paracrine manner and activate the signaling pathway required for myelination in primary Schwann cells. Although these two EGF-like domains differ in size and terminal residues, their ability to stimulate ErbB3 receptor signaling was found to be identical. Likewise, the O-linked glycosylation of β-sEGF was found to have no effect on receptor activation.

3.5.2 C-terminal cleavage of sEGF by ADAM17 does not abolish signaling through ErbB3 receptors

The finding that α- and β-sEGF similarly activate Schwann cells (3.5.1) suggests that both ADAM17- and BACE1-mediated processing of NRG1 type III promotes myelination. This is in conflict with observations made by other researchers (La Marca et al., 2011) who demonstrated an inhibitory effect of ADAM17-processed NRG1 type III on PNS myelination. Specifically these researcher emphasized the importance of the very C-terminal residues of the NRG1 type III EGF-like domain for its biological activity. In this regard it was shown that a recombinant EGF-like domain cleaved by BACE1 after F_{293} induced ErbB3 signaling in Schwann cells, whereas an EGF-like domain cleaved by ADAM17 after G_{290} did not. Consequently, shedding of NRG1 type III by ADAM17 was proposed to inactivate the EGF-like domain (La Marca et al., 2011).

The observed discrepancies regarding the signaling of ADAM17-derived EGF-like domains may be due to the different cleavage sites identified for ADAM17: Using recombinant peptides in an *in vitro* digest, the ADAM17 cleavage site was mapped to G_{290} (La Marca et al., 2011) as opposed to A_{283} which was the site identified in the cellular setup used in this work (3.1.2).

In a next step it was therefore investigated whether indeed the different C-terminal residues are responsible for the different biological activities of BACE1- and ADAM17-cleaved NRG1 type III EGF-like domains. To this end, a construct named β-sEGF-G was generated which is identical to β-sEGF-F (as derived from BACE1 cleavage) but terminates at G_{290} thereby mimicking the ADAM17-cleaved C-terminus as observed by others (La Marca et al., 2011) (Figure 37 A). To compare the effect of the different C-terminal residues on the activity of the EGF-like domain, conditioned media containing similar amounts of β-sEGF-F and β-sEGF-G were used to stimulate MCF-7 and purified primary Schwann cells as described before (3.5.1). Treatment with β-sEGF-F and β-sEGF-G induced similar

phosphorylation of ErbB3 receptors and AKT kinases in MCF-7 cells (Figure 37 B). In contrast to the expected inhibitory effect of the ADAM17-generated C-terminus, β-sEGF-G showed a slight trend towards increased ErbB3 activation. However, this trend was found to be non-significant upon quantification (Figure 37 C). Confirming these results, incubation with β-sEGF-F and β-sEGF-G also elicited similar activation of receptor and downstream signaling in primary Schwann cells (Figure 38).
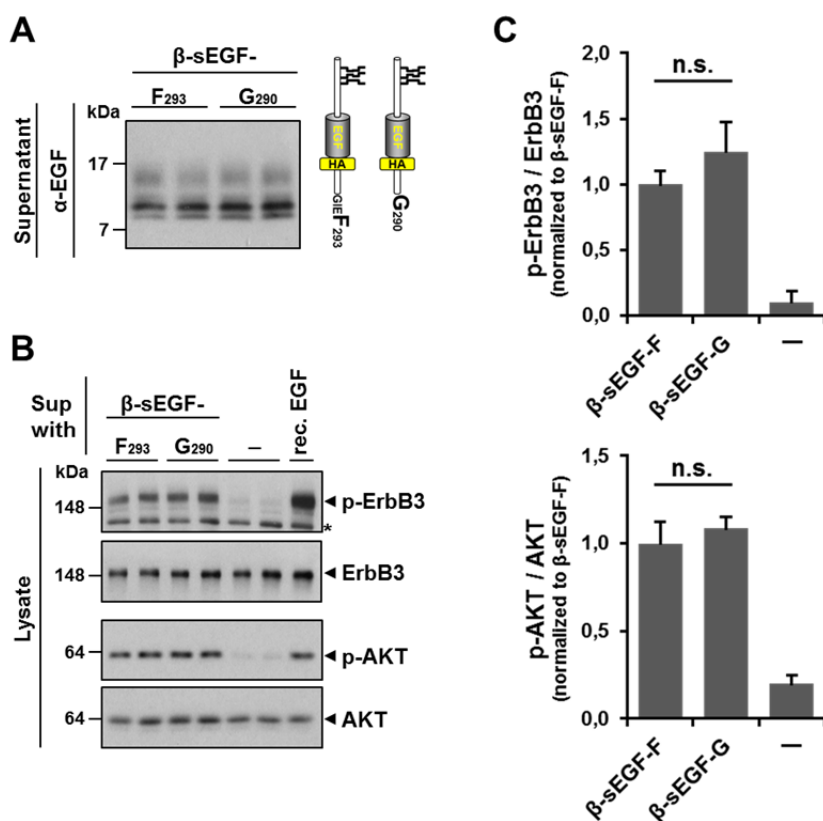
Figure 37. Shedding by BACE1 and ADAM17 generates β-sEGF domains that similarly activate ErbB receptors and downstream signaling in MCF-7 cells. A) Preparation of supernatants containing β-sEGF-F and the truncated β-sEGF-G. The constructs have identical N-termini but comprise C-terminal residues resulting from BACE1- or ADAM17-mediated shedding (F_{293}, BACE1 cleavage; G_{290}, ADAM17 cleavage) as observed by (La Marca et al., 2011). Conditioned supernatants from CHO wt cells expressing either construct were collected and analyzed by western blot. **B)** β-sEGF-F and β-sEGF-G stimulate ErbB3 and AKT phosphorylation in MCF-7 cells. Supernatants of A) or medium from cells expressing an empty vector were used to incubate MCF-7 cells. Treatment with a recombinant NRG1 EGF-like domain (0.5 nM) served as positive control. Cell lysates were analyzed for (phosphorylated) ErbB3 and AKT levels by immunoblotting. The asterisk indicates an unspecific band. **C)** Quantification of phosphorylated protein/total protein ratio (normalized to β-sEGF-F; n = 3; n.s., not significant).
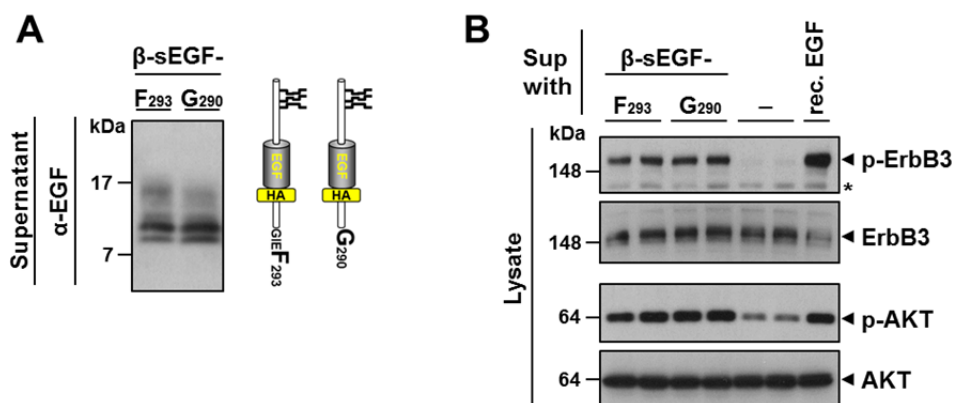
Figure 38. β-sEGF derived from BACE1- or ADAM17-mediated shedding similarly activates primary Schwann cells. A) Preparation of supernatants containing β-sEGF-F and β-sEGF-G. Constructs were expressed in CHO wt cells and conditioned media were analyzed for equal levels by western blot. **B)** Stimulation of primary Schwann cells with β-sEGF-F and β-sEGF-G. Schwann cells were incubated with media from A) and from cells expressing an empty vector. A recombinant NRG1 EGF-like domain (0.5 nM) was used as positive control. After cell lysis the levels of (phosphorylated) ErbB3 and AKT were determined by immunoblotting.

Together with the observations made for α-sEGF above (3.5.1) this indicates that shedding of NRG1 type III at either A_{283} or G_{290} does not render the EGF-like domain inactive. Instead, these sEGF domains which are possibly generated by ADAM17 are biologically active and signal through ErbB3 receptors on Schwann cells in a manner indistinguishable from the BACE1-cleaved β-sEGF. This result also suggests that small differences in the C-terminal residues of the EGF-like domain, as resulting from shedding at different sites in the juxtamembrane region, do not overly affect its activity.

3.5.3 β-sEGF is a paracrine signal *in vivo* and rescues hypomyelination in a BACE1 KO zebrafish

The previous experiments established α- and β-sEGF as paracrine NRG1 type III signals *in vitro*. Using the activation of ErbB3 receptor and downstream signaling as readout it was shown that both ADAM17- and BACE1-derived sEGF activates Schwann cells in cell culture. However, this does not necessarily hold true for the activation of Schwann cells *in vivo*. Moreover, it is unclear whether the activation of Schwann cells by α- and β-sEGF would indeed initiate the entire cellular program required for subsequent myelination of neighboring axons by these cells in a living organism. To address these questions and to investigate the signaling potential of the NRG1 type III derived sEGF domains *in vivo*, a homozygous mutant BACE1 (bace1 -/-) zebrafish was used (van Bebber et al., 2013). In addition to the BACE1 mutation, these fish express GFP under the control of the claudin k promoter which therefore specifically labels Schwann cells and oligodendrocytes and facilitates the visualization of myelination *in vivo* (Münzel et al., 2012) (Figure 39 A).

Compared to the wild-type, the lack of BACE1-mediated NRG1 type III signaling in bace1-/- zebrafish leads to severely reduced Schwann myelination. This is evident at 3 days postfertilization (3 dpf) from the absence of myelin around the axons of the lateral line organ (Figure 39). In contrast to the strongly impaired myelination in the PNS, myelination of Mauthner axons by oligodendrocytes in the CNS is not affected (Figure 39). This selective hypomyelination in the PNS of bace1-/- zebrafish is consistent with the reduced myelination observed in BACE1 KO mice and supports the distinct roles of BACE1-mediated NRG1 type III signaling in the PNS and CNS (Willem et al., 2006; Brinkmann et al., 2008).

To determine whether β-sEGF indeed acts as a paracrine NRG1 type III signal promoting myelination *in vivo* and therefore could compensate the lack of BACE1-processed NRG1 type III, *in vitro* transcribed β-sEGF mRNA was injected into bace1-/- zebrafish oocytes. At 3 dpf, myelination of lateral line axons in bace1-/- zebrafish injected with β-sEGF was assessed using immunofluorescence microscopy and compared to control injected fish (Figure 39). In a total of 5 independent clutches that were used for injections, expression of β-sEGF lead to a partial rescue of PNS hypomyelination in 24 out of 63 bace1-/- zebrafish. In contrast, none of the 189 control fish (11 independent clutches) showed rescued myelination of the lateral line axons (Table 5).
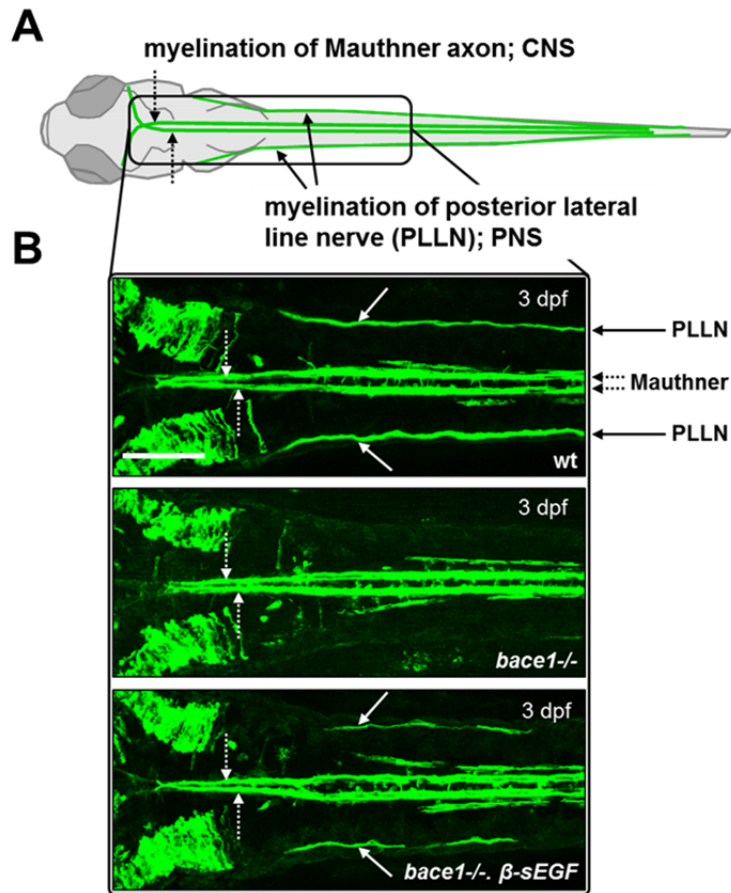
Figure 39. β-sEGF liberated from NRG1 type III by a dual BACE1 cleavage promotes PNS myelination *in vivo*. A) The claudin k:GFP zebrafish line allows visualization of myelination *in vivo*. Schematic dorsal view of a claudin k:GFP zebrafish larvae (3 dpf) with GFP-labeled myelin around Mauthner axons (CNS, dotted arrows) and lateral line axons (PNS, arrows). **B)** β-sEGF rescues myelination in the PNS of bace1-/- zebrafish. Shown are dorsal views of wt (top), uninjected bace1-/- (middle) and β-sEGF mRNA injected bace1-/- (bottom) zebrafish larvae (3 dpf). Middle: Myelination of the lateral line axons in the PNS of bace1-/- zebrafish is severely reduced to absent (compare arrows in other panels). In contrast, myelination of Mauthner axons (dotted lines) in the CNS is not affected. Bottom: Injection of β-sEGF mRNA partially rescues hypomyelination in the PNS of bace1-/- zebrafish. Scale bar, 100 μm.

3.5.4 An ADAM17-cleaved C-terminus does not abolish the signaling activity of sEGF *in vivo*.

The results obtained from the experiments *in vitro* (3.5.2) suggest no significant difference in the paracrine signaling activity of sEGF domains derived from BACE1- or ADAM17-mediated processing of NRG1 type III. In contrast, shedding by ADAM17 was shown to inhibit myelination *in vivo*, supposedly by generating an inactive membrane-tethered EGF-like domain (La Marca et al., 2011).

Therefore in a next step the bace1 -/- zebrafish model was used to test *in vivo*, whether a C-terminus generated by ADAM17 would abolish the ability of sEGF to promote myelination as a paracrine signal. To allow comparison with the BACE1-cleaved β-sEGF, two constructs were generated that are identical to β-sEGF but mimic ADAM17 shedding after either G_{290} (β-sEGF-G, La Marca et al., 2011) or A_{283} (β-sEGF-A, this work).

Three different clutches of bace1-/- zebrafish eggs were injected with the constructs and analyzed for myelination at 3 dpf. Similar to the rescue observed with β-sEGF, both β-sEGF-G and β-sEGF-A partially rescued hypomyelination in 12 out of 49 and 27 out of 72 bace1-/- zebrafish (Table 5). Since the expression levels of the different constructs after mRNA injection were not quantified the extent of the rescue effects cannot be compared in a quantitative fashion. Nevertheless, the fact that both β-sEGF-G and β-sEGF-A rescued hypo-myelination indicates that sEGF domains act as paracrine promyelinating signals *in vivo*, independently of their C-termini being generated by BACE1- or ADAM17-mediated shedding.

Construct	# of rescued mutants	# of clutches
β-sEGF (β-sEGF-F_{293})	24/63	5
β-sEGF-G_{290}	12/49	3
β-sEGF-A_{283}	24/72	3
Control (uninjected)	0/189	11

Table 5. β-sEGF domains derived from BACE1- and ADAM17-mediated shedding promote myelination *in vivo*. Summary of rescue experiments in bace1-/- zebrafish. Number of bace1-/- zebrafish with partial rescue out of the total number of zebrafish analyzed is shown. In addition to β-sEGF (Figure 39) also β-sEGF constructs with truncated C-termini (β-sEGF-G_{290} and β-sEGF-A_{283}, see 3.5.2 for details) were assessed for their myelination promoting potential in bace1-/- zebrafish. Regardless of their very C-terminal residues, all constructs partially rescued the hypomyelination phenotype.

3.6 NRG1 type III is a substrate for regulated intramembrane proteolysis by the γ-secretase

Shedding of NRG1 type III results in the generation of membrane-bound NTFs and CTFs (3.2). Both fragments are transmembrane proteins and as such could be subject to processing by intramembrane cleaving proteases (1.2.2). The members of the SPP/SPPL family of proteases were shown to mediate intramembrane proteolysis of proteins with type II topology and are therefore candidate proteases for the cleavage of the type II oriented NRG1 type III NTF. Similarly, the CTF, possessing a type I topology, is a putative substrate for the γ-secretase complex which exclusively cleaves transmembrane proteins of this orientation (Fluhrer et al., 2009). So far nothing is known about intramembrane processing of the NRG1 type III NTF. In contrast, it has indeed been demonstrated that the CTF is turned over by the γ-secretase and that this processing liberates the ICD of NRG1 type III into the cytosol (Bao et al., 2003). However, the respective cleavage sites within the TMD of NRG1 type III remain unknown. Likewise it is not known whether γ-secretase cleavage also liberates the N-terminal part of the CTF from the membrane.

3.6.1 Processing of NRG1 type III by the γ-secretase releases a NRG1 β-peptide

Besides liberating the substrate's ICD into the cytosol, intramembrane cleavage by the γ-secretase also generates short, soluble fragments that are secreted into the luminal space (1.1.2 Figure 2). The N-terminus of such fragments is generated by cleavage during the preceding shedding step and fragments shed by BACE1 at the β-site are therefore called β-peptides (e.g. amyloid β-peptide, Aβ or notch β-peptide, Nβ). In analogy to the Aβ peptides generated during APP processing, intramembrane proteolysis of the BACE1-cleaved NRG1 type III CTF hence is expected to release NRG1 β-peptides (NRG1-β) (Figure 40).
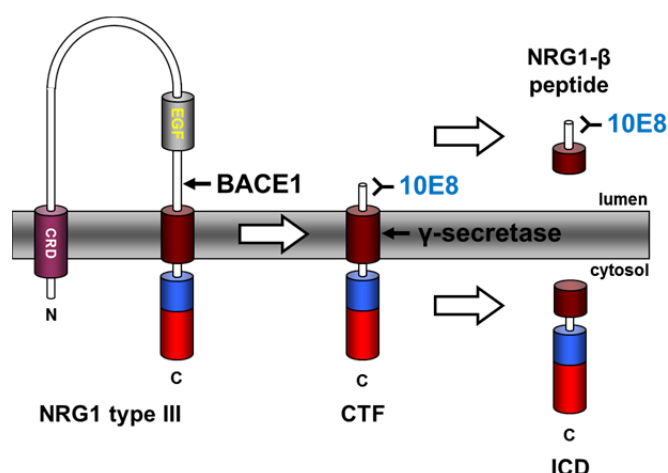
Figure 40. Scheme illustrating the generation of NRG1 β-peptides from NRG1 type III. Shedding of NRG1 type III by BACE1 produces a CTF that is further processed by the γ-secretase complex. This releases the ICD into the cytosol and liberates a NRG1 β-peptide. Both the BACE1-cleaved CTF and the β-peptide are recognized by the BACE1 cleavage site-specific antibody 10E8.

The monoclonal antibody 10E8 selectively recognizes the N-terminus of the BACE1-generated NRG1 type III β-CTF and therefore was used to identify such NRG1 β-peptides (3.3 Figure 27, Figure 40). In a first step, NRG1 type III was transiently expressed with or without BACE1 in HEK293 cells and lysates and supernatants were analyzed for β-CTFs and secreted NRG1 β-peptides, respectively. Western blot detection with an antibody against the C-terminus confirmed increased turnover of NRG1 type III upon BACE1 coexpression (Figure 41). Simultaneously, this lead to increased amounts of BACE1-cleaved β-CTFs, as detected by the 10E8 antibody. In line, immunoprecipitation with 10E8 revealed low amounts of NRG1-β in the supernatant from cells with endogenous BACE1 expression but strongly increased amounts upon enhanced BACE1 expression. Treatment with the γ-secretase inhibitor DAPT prevented the generation of the NRG1 β-peptides and caused accumulation of the CTFs in the cell lysate (Figure 41, left panel). This demonstrates that the identified β-peptides were indeed generated in a γ-secretase-dependent manner. In addition to pharmacological inhibition, a catalytically inactive γ-secretase mutant PS1 D385N (PS1DN) was used to confirm the generation of NRG1-β by γ-secretase-mediated intramembrane cleavage. Similar to DAPT treatment the inactive γ-secretase mutant abolished turnover of the NRG1 type III CTF and secretion of the NRG1 β-peptide (Figure 41, right panel).
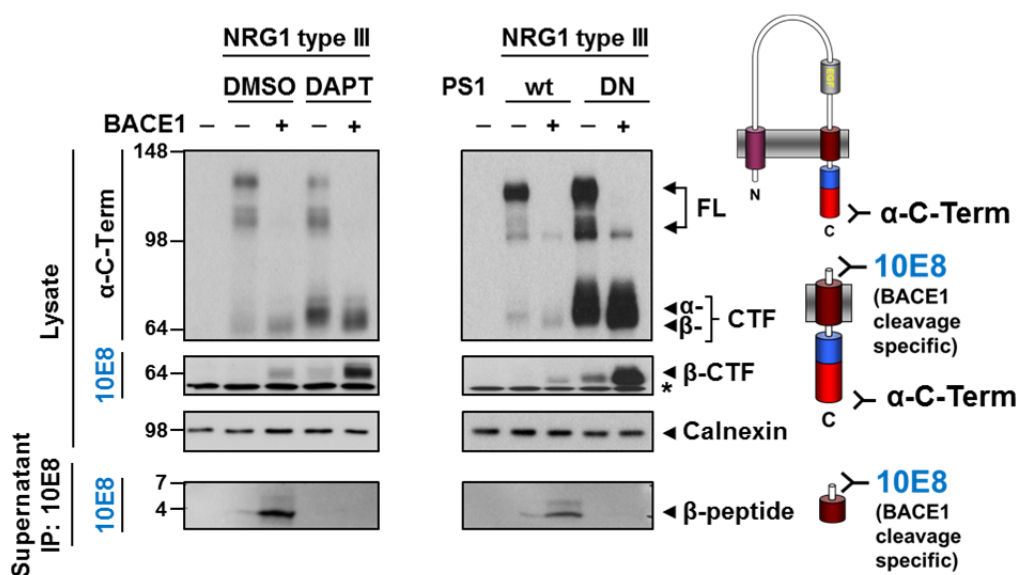
Figure 41. γ-Secretase-dependent generation and release of a NRG1 β-peptide from NRG1 type III. Wild-type HEK293 cells (left panel) or cells stably expressing either wild-type PS1 (PS1wt) or the dominant-negative PS1 D385N mutant (PS1DN) (right panel) were transfected with NRG1 type III and additionally with or without BACE1 to increase shedding. The specific inhibitor DAPT (5 μM) was used to inhibit γ-secretase in wild-type cells. Cell lysates were analyzed by immunoblotting with the indicated antibodies. β-peptides were isolated from conditioned supernatants by immunoprecipitation with the BACE1 cleavage site-specific 10E8 antibody prior to western blot detection. The asterisk denotes an unspecific band.

While the BACE1 shedding site constitutes the N-terminus of the NRG1 β-peptide, its C-terminus is defined by the site at which the γ-secretase cleaves the NRG1 type III β-CTF within the membrane. To determine the precise cleavage site(s), also referred to as the γ-site (1.1.3.3), NRG1-β was immunoprecipitated from the supernatants of cells expressing NRG1 type III as before and then subjected to mass spectrometric analysis.

Of note, the NRG1 β-peptide requires reduction prior to its analysis by MS. In its unreduced state the β-peptide contains an additional cysteine residue which seems to be linked to C_{311} (the only cysteine of the β-peptide) via a disulfide bridge. This cysteinylation adds 119 Da to the actual mass of the β-peptide and is removed by DTT treatment (Figure 42). Spontaneous cysteinylation of unpaired cysteine residues has been reported before (Gadgil et al., 2006) and in case of the NRG1 β-peptide may result from the reaction with free cysteine contained in the cell culture medium.
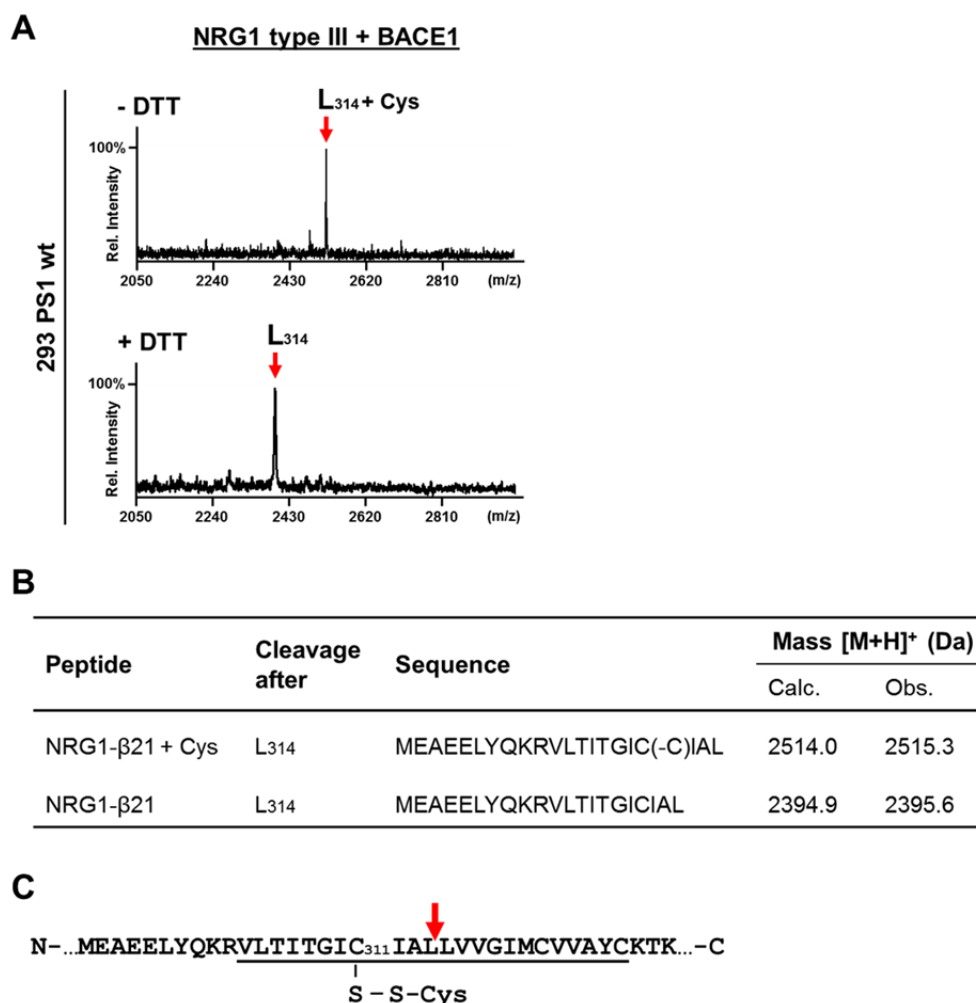
Figure 42. The NRG1 β-peptide is subject to cysteinylation. A) Unreduced NRG1 β-peptides contain an additional cysteine residue. NRG1 β-peptides were isolated from the supernatant of HEK293 PS1wt cells expressing NRG1 type III and BACE1. Without reduction (-DTT) MS analysis revealed a mass shift of +119 Da for the β-peptide. Reduction prior to analysis (+DTT) abolishes cysteineylation. **B)** Comparison of the cysteinylated and non-cysteinylated NRG1 β-peptide. The additional cysteine residue is indicated in the sequence and observed masses (Obs.) are compared with calculated (Calc.) masses. [M+H]$^+$ indicates a singly charged peptide. **C)** Scheme depicting the position of the cysteinylation within the NRG1 β-peptide. The TMD of NRG1 type III is underlined and the γ-secretase cleavage site (as identified in Figure 43) is shown (arrow). Cysteinylation of the residue C_{311} is indicated.

Mass spectrometric analysis identified a peptide with a molecular mass of 2395.1 kDa which corresponds to a γ-secretase cleavage site between L_{314} and L_{315} in the TMD of NRG1 type III (Figure 42, 43). Accordingly, the NRG1 β-peptide liberated by cleavage at this site comprises 21 residues (NRG1-β21) (Table 6). Enhanced shedding upon overexpression of BACE1 increased generation of this peptide and revealed additional but minor cleavage products (Figure 43, Table 6). These are most likely caused by the heterogeneous nature of

the γ-secretase cleavage within the membrane and are in line with similar observations that have been made for other substrates such as APP and notch (Gu et al., 2001; Okochi et al., 2002). Analysis of supernatants from cells treated with DAPT or expressing a catalytically inactive γ-secretase mutant (PS1DN) revealed no signals confirming again the γ-secretase dependence of β-peptide secretion (Figure 43). The position of the γ-secretase cleavage site in the TMD of NRG1 type III is depicted in 3.6.2 Figure 46.

In summary these data confirm the β-CTF of NRG1 type III as substrate for the γ-secretase complex. Furthermore they identify L_{314} as the main γ-cleavage site within the C-terminal transmembrane domain of NRG1 type III. Processing at this site releases a NRG1 β-peptide from the membrane that may be detected with the novel 10E8 antibody.
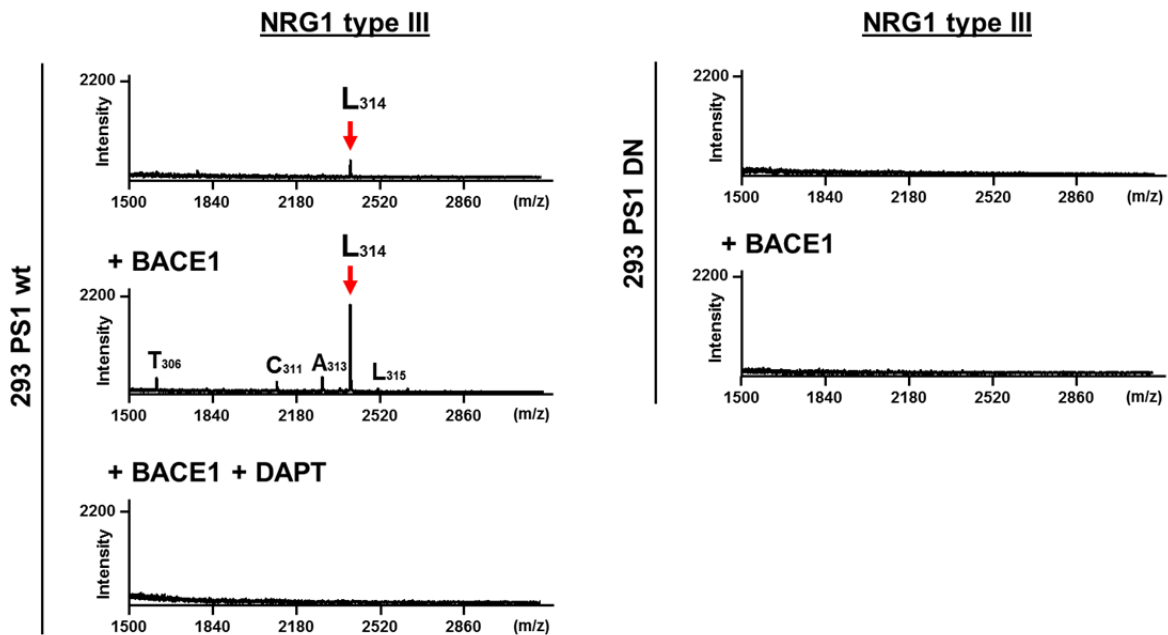
Figure 43. γ-Secretase cleavage after L_{314} in the TMD of NRG1 type III liberates the NRG1 β-peptide. NRG1 type III was expressed in HEK293 cells stably expressing wild-type PS1 (PS1wt, left panels) or the inactive mutant D385N (PS1DN, right panels). After immunoprecipitation of the supernatants with the 10E8 antibody, isolated peptides were analyzed by MALDI-TOF MS. γ-Secretase cleavage yielded a peptide of 2395.1 Da corresponding to cleavage of NRG1 type III after L_{314} (Table 6). Enhanced shedding by coexpression of BACE1 strongly increased the abundance of this peptide and additional but minor peptides were detected. Inhibition of the γ-secretase with DAPT (5 μM) or expression of the inactive mutant prevented generation of the β-peptide.

	Peptide	Cleavage after	Sequence	Mass [M+H]$^+$ (Da)	
				Calc.	Obs.
Major peptide	NRG1-β21	L$_{314}$	MEAEELYQKRVLTITGICIAL	2394.9	2395.1
Minor peptides	NRG1-β12	T$_{306}$	MEAEELYQKRVLTIT	1609.9	1610.6
	NRG1-β18	C$_{311}$	MEAEELYQKRVLTITGIC	2097.5	2097.1
	NRG1-β20	A$_{313}$	MEAEELYQKRVLTITGICIA	2281.7	2282.2
	NRG1-β22	L$_{315}$	MEAEELYQKRVLTITGICIALL	2508.0	2508.7

Table 6. List of β-peptides liberated from NRG1 type III by γ-secretase cleavage. Peptide names include the number of residues comprised by each peptide. The C-terminal residues and the peptide sequences are given and observed masses (Obs.) are compared with calculated (Calc.) masses. [M+H]$^+$ indicates a singly charged peptide.

3.6.2 γ-Secretase cleavage at the ε-site liberates the ICD of NRG1 type III

As revealed by investigation of the processing of APP and notch, γ-secretase mediates multiple cleavages within the TMD of its substrates. In addition to the γ-cleavages, which define the C-terminus of the secreted peptides, additional intramembrane cleavages occur (summarized for APP in Steiner et al., 2008; for notch, in Schroeter et al., 1998; Okochi et al., 2002). The most C-terminal of these occurs close to the cytoplasmic border of the membrane at the so called ε-site (1.1.3.3). It liberates the ICD of the substrate into the cytosol and is thought to be the earliest cleavage mediated by the γ-secretase. Although γ-secretase-dependent generation of a NRG1 ICD has been shown (Bao et al., 2003), the ε-cleavage site responsible for its liberation is not known.

ICDs are rapidly turned over within the cytosol and are difficult to detect (Edbauer et al., 2002). Therefore, a well characterized cell-free γ-secretase assay (Fukumori et al., 2006) was used to generate NRG1 ICDs for subsequent mass spectrometric analysis. To this end the construct FNRGΔC-HA was designed to comprise an N-terminal Flag tag followed by a short extracellular part, the TMD, a short intracellular part as well as a C-terminal HA tag (Figure 44 A). C-terminal degradation of FNRGΔC-HA (most likely by an exopeptidase) which was originally observed (not shown) was blocked by insertion of two proline residues directly after the HA tag at the C-terminus of the construct. Truncation of the intracellular domain of NRG1 type III was necessary since this domain (approx. 64 kDa) is too large to

allow MALDI-TOF MS analysis. Facilitating its use in the *in vitro* assay, the short extracellular domain of FNRGΔC-HA allows γ-secretase cleavage without prior shedding.

In a first step, the γ-secretase assay was performed using membranes from cells expressing wild-type γ-secretase (PS1wt) and FNRGΔC-HA. Western blot analysis of the soluble assay fraction revealed de-novo generation of NRG1 ICD(ΔC), while the corresponding membrane-bound NTF was detected in the insoluble fraction (Figure 44 B). Inhibition of the γ-secretase with the specific inhibitor L-685,458 or incubation at 4°C abolished the generation of both fragments. Likewise, performing the assay with membranes of cells expressing an inactive γ-secretase (PS1DN) did not result in the generation of the NRG1 ICD(ΔC) (or the NTF) but in the accumulation of uncleaved FNRGΔC-HA (Figure 44 B). This confirms that the NRG1 ICD(ΔC) is indeed generated by a γ-secretase-mediated cleavage.
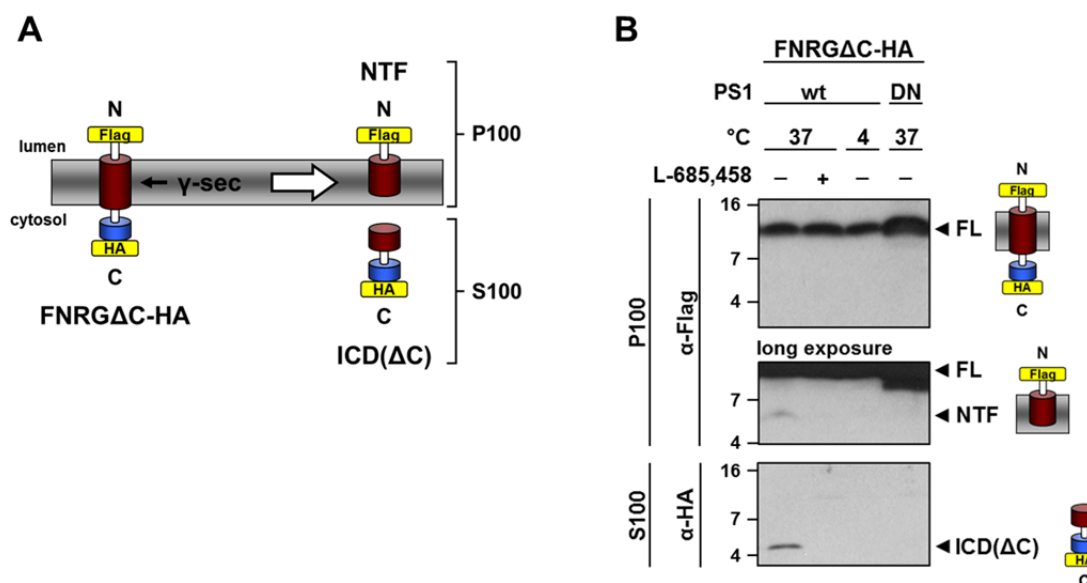
Figure 44. γ-Secretase cleavage generates the NRG1 type III ICD in a cell-free assay. A) Schematic depiction of the cell-free γ-secretase assay. Membranes containing the truncated construct FNRGΔC-HA are incubated and processing by the γ-secretase generates a soluble HA tagged ICD(ΔC) and a Flag tagged NTF. After ultracentrifugation, the ICD(ΔC) is present in the soluble fraction (S100) while the insoluble NTF remains in the pellet (P100). **B)** The cell-free γ-secretase assay generates a NRG1 type III ICD. FNRGΔC-HA was expressed in cells stably expressing either wild-type PS1 (wt) or a dominant-negative PS1 mutant (DN) and isolated cell membranes were used for the *in vitro* assay at indicated temperatures. As control, the inhibitor L-685,458 (1 µM) was used to block γ-secretase activity. After the assay, the insoluble (P100) and soluble (S100) assay fractions were separated and analyzed by immunoblotting with the indicated antibodies.

To identify the ε-cleavage site within the TMD of NRG1 type III, ICD(ΔC) fragments were isolated from the soluble assay fraction using the HA tag. Free cysteine residues were blocked by alkylation and peptides were analyzed by MALDI-TOF MS. A major peptide of 3030.4 Da was detected which corresponds to an ε-cleavage site between C_{321} and V_{322} (residue are numbered according to the full-length NRG1 type III) (Figure 45, Table 7). Additional peptides generated by cleavages after V_{322} and A_{324} were observed but their abundance was very low. These minor cleavages most likely arise from heterogeneous γ-secretase cleavage at the ε-site (also observed for APP, Fukumori et al., 2006) or are the result of N-terminal truncations by an exopeptidase. No peptides were detected when the *in vitro* assay was performed in the presence of a γ-secretase inhibitor, at 4°C or when a PS1 loss-of-function mutation (PS1DN) was expressed (Figure 45).
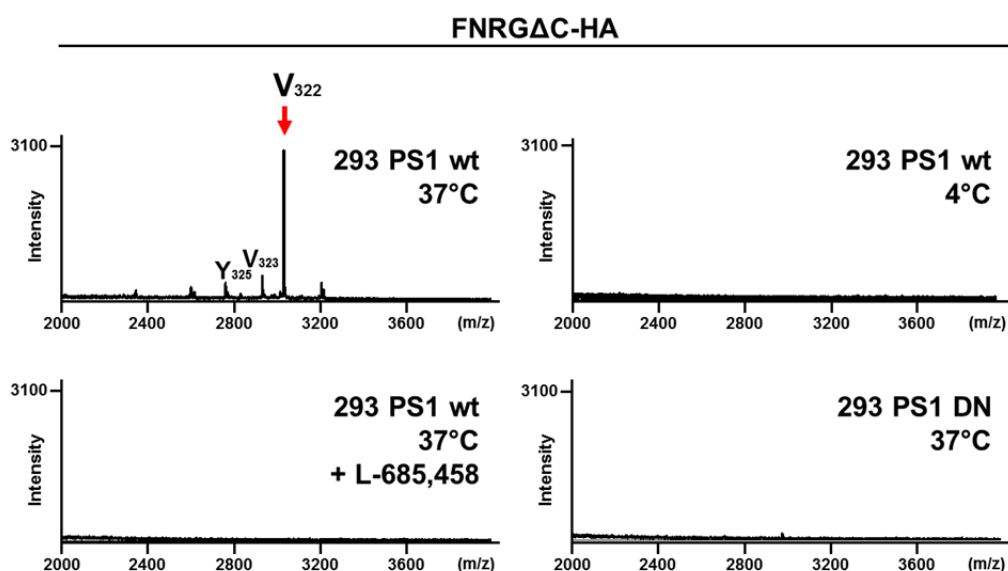
Figure 45. The NRG1 ICD is released by γ-secretase cleavage N-terminal of V_{322} at the ε-site in the TMD of NRG1 type III. Membranes of cells expressing FNRGΔC-HA and wild-type (PS1wt) or an inactive (PS1DN) γ-secretase were used for the *in vitro* γ-secretase assay at indicated temperatures. The inhibitor L-685,458 (1 µM) was added to block γ-secretase activity. The soluble assay fractions were immunoprecipitated with HA agarose and isolated ICDs were analyzed by MALDI-TOF MS. Processing at the ε-site by the γ-secretase released a major peptide of 3030.4 Da corresponding to cleavage between C_{321} and V_{322} (residue numbers according to the full-length NRG1 type III) (Table 7).

	Peptide	Cleavage after	Sequence	Mass [M+H]$^+$ (Da)*	
				Calc.	Obs.
Major peptide	NRG1 ICD-V$_{322}$	C$_{321}$	V^{322}VAYCKTKKQRQKGG*YPYDVPDY*APP	3030.5	3030.4
Minor peptides	NRG1 ICD-V$_{323}$	V$_{322}$	V^{323}AYCKTKKQRQKGG*YPYDVPDY*APP	2931.3	2930.8
	NRG1 ICD-Y$_{325}$	A$_{324}$	Y^{325}CKTKKQRQKGG*YPYDVPDY*APP	2761.1	2761.5

Table 7. List of ICD peptides liberated from FNRGΔC-HA by the γ-secretase. Peptide names include the N-terminal residue of each ICD according to the residue numbers of the full-length NRG1 type III. The peptide sequences are given and observed masses (Obs.) are compared with calculated (Calc.) masses. Note that two proline residues were added to the C-terminus of FNRGΔC-HA to prevent degradation. Asterisk: Due to alkylation with IAA prior to MS analysis the mass of each peptide is increased by 58.0 Da per cysteine residue. Italic letters indicate the HA tag, [M+H]$^+$ a singly charged peptide.

Together these data demonstrate that the BACE1-cleaved NRG1 type III β-CTF is a substrate for intramembrane proteolysis by the γ-secretase. In analogy to other substrates like APP or notch, γ-secretase mediates a dual cleavage within the C-terminal TMD of NRG1 type III at a central γ- and a C-terminal ε-cleavage site (Figure 46). While cleavage at the γ-site occurs after L$_{314}$ and releases a NRG1 β-peptide into the lumen, the ε-cleavage takes place after C$_{321}$ and liberates the ICD into the cytosol. Interestingly, cleavage at the ε-site localizes precisely to a position where a valine to leucine substitution is associated with an increased susceptibility to schizophrenia (Walss-Bass et al., 2006) (1.3.4.2.2).
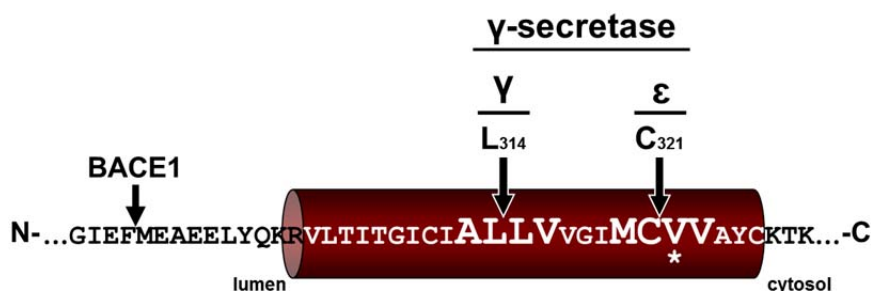
Figure 46. Schematic overview of the γ-secretase cleavage sites within the TMD of NRG1 type III. The positions of the γ- and the ε-cleavage sites are indicated and the numbers of the residues after which cleavage occurs are given. The BACE1 shedding site is depicted for orientation. The asterisk marks the position at which a valine to leucine substitution is associated with an increased risk of schizophrenia.

4 Discussion

The growth factor NRG1 type III is a key regulator of myelination in the PNS and controls both the development of Schwann cells as well as the process of ensheathment (Nave and Salzer, 2006; Birchmeier and Nave, 2008) (1.3.4.1). Besides the coordinated temporal expression of NRG1 type III on neurons and its receptor ErbB2/3 on glia cells, proteolytic processing of NRG1 type III has emerged as an important control mechanism in this context (Hu et al., 2006; Willem et al., 2006; Taveggia et al., 2010; La Marca et al., 2011; Fleck et al., 2012) (1.3.4.1.5). Shedding of neuronal NRG1 type III by BACE1 (and possibly ADAM10 and other proteases) generates a membrane-bound NRG1 type III NTF which activates ErbB2/3 receptors on adjacent Schwann cells in a juxtacrine manner and promotes ensheathment and myelination (Taveggia et al., 2005; Hu et al., 2006; Willem et al., 2006; Velanac et al., 2012). In contrast to the cleavage by BACE1, processing by ADAM17 was found to render NRG1 type III inactive and to inhibit Schwann cell myelination (La Marca et al., 2011). The opposing effects of BACE1- and ADAM17-mediated shedding were suggested to be due to the different shedding sites of these proteases in the stalk region of NRG1 type III. Despite their proposed importance, the shedding sites in NRG1 type III have only been determined *in vitro* so far. Furthermore evidence suggests that in contrast to previous assumptions myelination in the PNS does not entirely depend on juxtacrine signaling by NRG1 type III but may also be promoted by a soluble, paracrine signal (Syed et al., 2010). However, the mechanism that would liberate such a soluble EGF-like domain from NRG1 type III remained elusive.

In the present study the proteolytic processing of NRG1 type III was investigated in detail and it was found that the EGF-like domain of NRG1 type III is liberated. Furthermore, the capacity of the liberated EGF-like domain to promote myelination in a paracrine manner was characterized *in vitro* and *in vivo*.

In addition to ectodomain cleavage, NRG1 type III is a known substrate for intra-membrane proteolysis of its CTF by the γ-secretase (Bao et al., 2003). This processing generates an NRG1-ICD whose nuclear signaling is involved in the maturation of cortical neurons and seems to be impaired by a schizophrenia-linked mutation within the TMD (Bao et al., 2004; Dejaegere et al., 2008; Chen et al., 2010a) (1.3.4.2.2). The current study provides an initial characterization of the γ-secretase cleavage in the C-terminal TMD of NRG1 type III and identifies a small soluble β-peptide that is released into the extracellular space upon this processing.

4.1 NRG1 type III is shed by BACE1, ADAM10 and ADAM17

Almost all isoforms of NRG1 are synthesized as transmembrane proteins but were discovered as soluble growth factors (1.3.2) (Figure 47). Immediately upon their discovery it was therefore suggested that proteolytic processing liberates the NRG1 ectodomain from the membrane and that such a cleavage would occur in the stalk region between the EGF-like domain and the TMD (Holmes et al., 1992; Wen et al., 1992). Soon after, several processing sites in the juxtamembrane regions of the α2, β1, β2 and β4 NRG1 isoforms isolated from CHO cells were identified using Edman degradation in combination with mass spectrometry (Lu et al., 1995b).
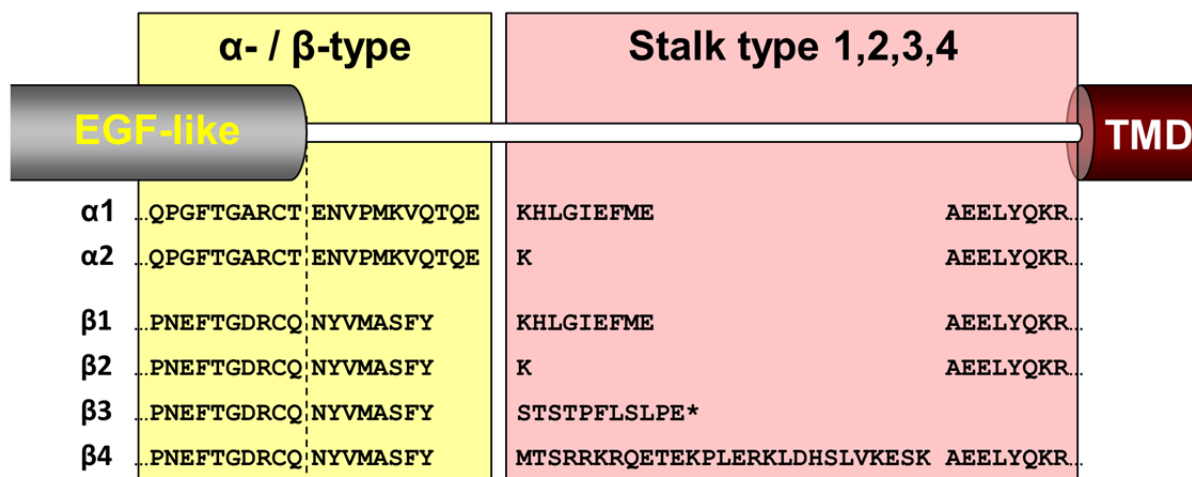
Figure 47. Comparison of juxtamembrane sequences from different NRG1 isoforms. The amino acid sequences of NRG1 isoforms containing the α- or β-type EGF-like domain in combination with different stalk types are shown. The dashed line indicates the end of the core sequence of the EGF-like domain and the asterisk denotes a stop codon. The sequences were assembled from the UniProtKB database (accession number P43322) and from (Wen et al., 1994; Lu et al., 1995b).

Of all the proteases implicated in the processing of NRG1 type III within its stalk region (1.3.3.2.3), BACE1 is the least controversial. The juxtamembrane region of the NRG1 isoform β1 was shown to be cleaved by BACE1 in different (primary) cells (Willem et al., 2006; Velanac et al., 2012; Cheret et al., 2013) and recombinant peptides of the β1 stalk are readily processed by purified BACE1 *in vitro* ((Hu et al., 2008), own observation). In line, the absence of BACE1 leads to increased levels of full-length NRG1 type III and reduced amounts of the corresponding CTF and NTF *in vivo* (Hu et al., 2006; Willem et al., 2006). Furthermore a robust phenotype is associated with the lack of BACE1-mediated shedding of NRG1 type III as the ablation of BACE1 in both mice and zebrafish leads to severe

myelination defects in the PNS (Hu et al., 2006; Willem et al., 2006; van Bebber et al., 2013). Together this leaves little doubt that BACE1 is indeed a physiologically relevant sheddase of NRG1 type III.

Chronologically, ADAM17 was the first sheddase reported for NRG1. One study found ADAM17 in CHO cells to efficiently cleave the isoforms β4 and to a lesser extent α2, while the β2 stalk was relatively resistant to processing (Montero et al., 2000). Although this indicates an important role of the length of the linker region for ADAM17-mediated shedding, the authors also suspected additional, yet unknown parameters within that region to determine the cleavage efficiency. In addition, ADAM17 was reported to constitute the inducible protease activity that mediates enhanced NRG1 shedding after PMA treatment (Montero et al., 2000). Despite the finding that the β2 isoform is only poorly processed by ADAM17, another study found this protease to be responsible for the constitutive cleavage of NRG1 isoforms β1 and β2 in mouse embryonic fibroblasts (Horiuchi et al., 2005). In support of this, knockdown of ADAM17 in HEK293 cells transfected with the β1 isoform of NRG1 type I significantly reduced its shedding (Luo et al., 2011). Experimental evidence for the ability of ADAM17 to cleave within the stalk sequence of the NRG1 isoform β1 in a cell-free system is contradicting. While one study observed ADAM17-mediated cleavage of a recombinant peptide (comprising the entire EGF-like domain until the TMD) within the stalk region (La Marca et al., 2011), another study using a shorter peptide (spanning only the stalk region) failed to do so (Luo et al., 2011). Likewise, *in vitro* cleavage assays conducted in the course of the present study also failed to detect ADAM17 cleavage of recombinant NRG1 peptides (not shown).

No physiological function for ADAM10-mediated shedding of NRG1 type III is known as of yet. Mice expressing a dominant-negative mutant of ADAM10 do not display an NRG1 type III related phenotype in the PNS (Freese et al., 2009) and knockdown of ADAM10 in co-cultures of Schwann cells and DRGs does not result in altered myelination (Luo et al., 2011). However, on the level of processing the data are controversial: siRNA-mediated reduction of ADAM10 in HEK293 cells transfected with the β1 isoform of NRG1 strongly reduced shedding (Luo et al., 2011) but this was not observed for endogenous α2 and β2 NRG1 isoforms in U373 cells (Freese et al., 2009). Likewise no altered shedding of these isoforms was detected in mice expressing high levels or an inactive mutant of ADAM10. The contradicting results particularly for the isoforms β1 and β2 are startling because both isoforms contain the sequence to which the cleavage site of ADAM10 was mapped (Luo et

al., 2011) and only differ in eight residues. Therefore reduced ADAM10 levels should affect their shedding similarly (Figure 47, 4.2 Figure 49).

In the present study a truncated version of NRG1 β1a type III was used to investigate shedding by BACE1, ADAM10 and ADAM17 in living cells. The stalk region β1 of NRG1 type III was readily cleaved by cellular levels of BACE1 and ADAMs as evidenced by decreased shedding upon inhibition with BACE1 and ADAM inhibitors. Furthermore, knockdown of ADAM10 and ADAM17 differentially affected the shedding sites confirming the contribution of endogenous ADAM10 and ADAM17 to the shedding of NRG1 type III in stable cell lines. Consistently, overexpression of the three proteases increased shedding, an effect that was most pronounced for BACE1.

The higher cleavage efficiency of BACE1 compared to the ADAMs could be due to a higher affinity of BACE1 towards its shedding site in the juxtamembrane sequence. However, it could also result from BACE1 being more efficiently overexpressed in HEK293 cells than ADAM10 or ADAM17 which are often retained in the immature and inactive form after transfection. The exact amounts of catalytically active (mature) proteases were not determined and quantifying the affinity of BACE1, ADAM10 and ADAM17 towards their shedding sites would require an *in vitro* assay. Hence, the setup used in this study is not suitable to determine the precise extent to which each protease contributes to the shedding of NRG1 type III or to determine which is the most relevant physiologically. Such an investigation furthermore would require endogenous BACE1, ADAM10 and ADAM17 activity but optimally also endogenous NRG1 type III substrate preferably in primary cells. Also, as cell types differ in the expression of specific enzymes, different proteases may be the principal and physiological relevant sheddases of NRG1 type III in different cell types. In order to determine the latter in primary cells, a carefully controlled RNAi-mediated knock-down approach or the use of conditional knockout animals would be required. While this has not yet been done systematically, the analysis of BACE1 KO mice indicates that at least during early development in the context of myelination, BACE1 is the main physiological sheddase of NRG1 type III in neurons of the PNS (Hu et al., 2006; Willem et al., 2006).

4.2 The sheddases BACE1, ADAM10 and ADAM17 cleave NRG1 type III at distinct sites

Besides the identity of the NRG1 type III sheddase, the positions of the respective cleavage sites which determine the C-terminus of the bioactive NRG1 type III NTF have recently attracted considerable attention. This is because compared to the shedding sites of BACE1 and ADAM10, the site utilized by ADAM17 has been proposed to have an opposing effect on the signaling capability of NRG1 type III (La Marca et al., 2011) (1.3.4.1.5). During this study, the precise shedding sites of BACE1, ADAM10 and ADAM17 were determined under cellular conditions using an N-terminally truncated construct of NRG1 type III and a combined IP-MS approach. BACE1 was found to cleave the β1 stalk of NRG1 type III after F_{293} at a site located ten residues upstream of the TMD which confirms previous results obtained in *in vitro* cleavage systems ((Hu et al., 2008), own observations).

As of yet no clear consensus sequence for BACE1 processing sites could be determined (Stockley and O'Neill, 2008). However, comparison of the reported cleavage sites in known BACE1 substrates indicates that BACE1 has a preference for bulky and hydrophobic residues like leucine and phenylalanine at the P1 position (Stockley and O'Neill, 2008) (Figure 48). The shedding site of BACE1 in the β1 stalk of NRG1 type III features a phenylalanine at this position and also contains residues at P3 (I_{291}), P2 (E_{293}), P4' (E_{297}) and P5' (E_{298}) which are present in other substrates as well (Figure 48). Interestingly, NRG3 comprises a juxtamembrane sequence highly homologous to the NRG1 β1 isoform and therefore most likely is also cleaved by BACE1 at the same position (Figure 48) ((Hu et al., 2008), own observations). In summary, considering the primary sequence, it is conceivable that the identified cleavage site in the β1 stalk of NRG1 type III indeed constitutes a high-affinity shedding site for BACE1. Of note, the juxtamembrane sequences of the other membrane-bound NRG1 isoforms β2 and β4 do not contain similar or comparable sites (4.2 Figure 47) and therefore may not be subject to BACE1-mediated shedding. The β2 isoform has recently been shown to be insensitive to BACE1 cleavage *in vitro* (Cheret et al., 2013) but a comprehensive and systematic investigation of the shedding of different stalk isoforms has not been published as of yet and overall the physiological relevance of the different stalks in the NRG1 protein isoforms is unclear.
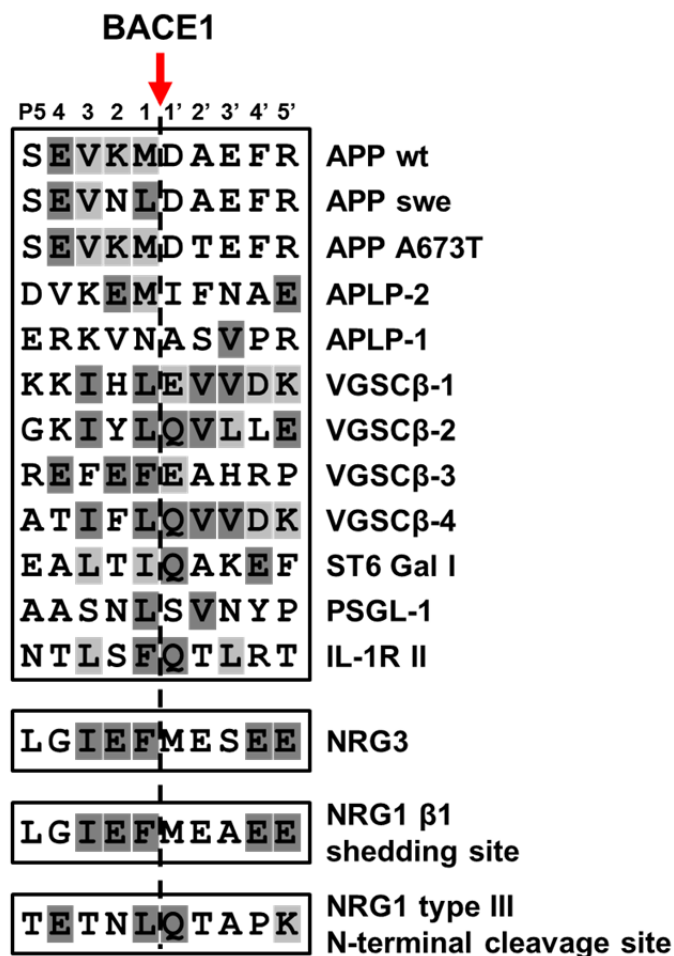
Figure 48. Alignment of cleavage site sequences of different BACE1 substrates. The amino acid sequences surrounding the BACE1 cleavage site (from the N-terminal P5 to the C-terminal P5' position) in different substrates are given. The alingment is colored according to the BLOSUM62 score and was modified from (Stockley and O'Neill, 2008).

In contrast to BACE1, the shedding sites of ADAM10 and ADAM17 within the stalk of NRG1 seem to be heterogeneous (Lu et al., 1995b; La Marca et al., 2011) (Figure 49). Initial investigations of the juxtamembrane processing of different NRG1 stalk isoforms indicated ADAM cleavage sites in a region of approx. four to eight residues downstream of the EGF-like domain (Lu et al., 1995b; Montero et al., 2000) (Figure 49). The respective region features the sequence NYMASFY which is contained in all β isoforms of NRG1, regardless of their stalk (1,2,3 or 4) or their N-terminal sequence (types I-VI) (1.3.2 Figure 5, 4.1 Figure 47). One study showed that shedding of NRG1 β1, β2 and β4 (the latter two not containing the BACE1 cleavage site) in CHO cells occurs mainly after NYVMA but also after NYVM and NYVMASF (Lu et al., 1995b). While this report could not assign specific cellular protease(s) to the different cleavages, *in vitro* assays with recombinant proteases were later used to

propose specific cleavage sites for ADAM10 and ADAM17 respectively (La Marca et al., 2011; Luo et al., 2011) (Figure 49). During the present study, selective inhibitors, RNAi and overexpression were employed to identify the ADAM10 and ADAM17 shedding sites in the β-isoform of NRG1 in HEK293 cells.

This revealed that ADAM17 cleaves mainly after A_{283} and to a minor extent after F_{285} (numbers according to the NRG1 β1a type III isoform) in the NYVMASFY sequence (Figure 49). These sites are identical with the shedding positions reported in CHO cells (Lu et al., 1995b) and therefore suggest that in fact ADAM17 is responsible for the observed cleavage of NRG1 in these cells. Similar to the heterogeneous cleavage pattern observed in living cells, recombinant ADAM17 also processed a NRG1 peptide at two distinct sites *in vitro* (La Marca et al., 2011), namely after Y_{286} and G_{290}. The residue Y_{286} still lies within the NYVMASFY sequence that is present in all NRG1 β isoforms and indeed seems to be the site of ADAM-mediated shedding. However, cleavage close to or after this residue was assigned to ADAM10 rather than ADAM17 in both living cells and *in vitro* ((Luo et al., 2011), this study) (Figure 49). By contrast, the second cleavage site G_{290} is positioned downstream of the NYVMASFY sequence, close to the BACE1 site F_{293} and cleavage after G_{290} has not been reported by other groups. Of note, another study used a similar assay but could not observe any ADAM17 cleavage within the recombinant NRG1 peptide (Luo et al., 2011).

While the controversial findings *in vitro* cannot readily be explained, the differences between the ADAM17 cleavage sites identified in living cells and *in vitro* may be due to the different experimental setups. Unlike under cellular conditions where ADAM17 and its substrate NRG1 are present as transmembrane proteins on the cell surface, these proteins are diffusible reaction partners in the *in vitro* setup. Firstly, this could prevent both the enzyme and the substrate from adopting their native confirmation but secondly could also alter their correct spatial orientation during proteolysis. It is conceivable that these artificial conditions potentially allow cleavage at sites that are not used under cellular conditions. With regard to possible artificial cleavages *in vitro* it is interesting to note that cleavage by ADAM17 in this system was reported to inactivate the NRG1 EGF-like domain and to abolish its signaling via ErbB3 receptors (La Marca et al., 2011). Such inactivation could be caused by undetected additional proteolytic cleavages inside the EGF-like domain which would explain the observed differences in signaling. It is therefore important to carefully monitor all cleavage events and to detect not only some but all resulting peptide fragments by mass spectrometry.

Discussion

ADAM10-mediated shedding of NRG1 type III in HEK293 cells was found to occur mainly after Y_{286} but cleavage was also detected after F_{285}. Both residues are within the NYVMASFY sequence of NRG1 β isoforms and in close vicinity of the sites of ADAM17-mediated proteolysis (Figure 49). Confirming the results from HEK293 cells, cleavage after F_{285} was also observed in CHO cells (Lu et al., 1995b) and likewise was assigned to ADAM10 *in vitro* (Luo et al., 2011). In contrast, the adjacent Y_{286} has not been previously reported as ADAM10 shedding site (Figure 49). While the conflicting results derived from cell-based and *in vitro* systems may be explained by the different reaction conditions, there is currently no definite explanation for the inconsistencies of the cellular setups. A possible explanation could be that Y_{286} in fact is the initial cleavage site of ADAM10 under cellular conditions and that the peptides ending with F_{285} arise from further processing of the initial fragments by an exopeptidase which cleaves off Y_{286} independent of ADAM10. Such an exopeptidase-processed fragment would accumulate in the supernatant of cells expressing the NRG1 construct over time and a shortened collection period might therefore possibly facilitate the identification of the genuine ADAM10 cleavage site (a similar phenomenon was described for the ADAM10 cleavage of APP (Kuhn et al., 2010)).

A long-standing argument concerns the question of a specific cleavage site motif that determines cleavage by either ADAM10 or ADAM17 as amino acid exchanges at ADAM cleavage sites often do not abolish or alter cleavage of the substrate (Sisodia, 1992; Caescu et al., 2009). Together with the fact that multiple proteins may be cleaved by different ADAMs (Gall et al., 2009) this lead to the perception that ADAMs in general lack a specific cleavage site sequence (Janes et al., 2005) or cleave their substrates in a specific distance to the plasma membrane (Sisodia, 1992).

In addition to the investigation of cleavage sites in natural substrates, peptide libraries were used to deduce the amino acid preferences of ADAM10 and ADAM17 around cleavage sites but it was not possible to identify specific sequences (Caescu et al., 2009). Overall, the cleavage site sequence requirements of ADAM10 and ADAM17 seem to be fairly similar to one another. Based on peptide screening, both proteases prefer alanine and serine residues at two positions upstream (P2 position) and an alanine residues immediately before (P1 position) the cleavage site. The only major difference was found for the P1' position immediately downstream of the cleaved peptide bond. Here, ADAM17 prefers small, hydrophobic residues, with valine being found most frequently. In contrast, ADAM10 favors larger residues, most frequently leucine, but also aromatic residues like tyrosine (Caescu et al., 2009). However, comparison of cleavage sites in natural substrates reveals great

diversity in cleavage sequences and to date it is not possible to predict the cleavage sites of ADAM10 or ADAM17 in novel substrates.

Cleavage after A_{283} as identified during the present study fits well with the substrate sequence preference of ADAM17 (Figure 49) which favors alanine residues at P1 and valine residues at P3. Additionally, ADAM17 cleaves several substrates which possess serine residues immediately C-terminal to the cleavage site as is the case in the NRG1 stalk (Caescu et al., 2009) (Figure 49). Despite lacking an alanine at P1, also the minor cleavage site after F_{285} assigned to ADAM17 features residues preferred by this enzyme at the P3, P2 and P2' positions. The same cleavage site was also found to be utilized by ADAM10 in this study and *in vitro* (Luo et al., 2011) and it fits this enzyme's requirement equally well.
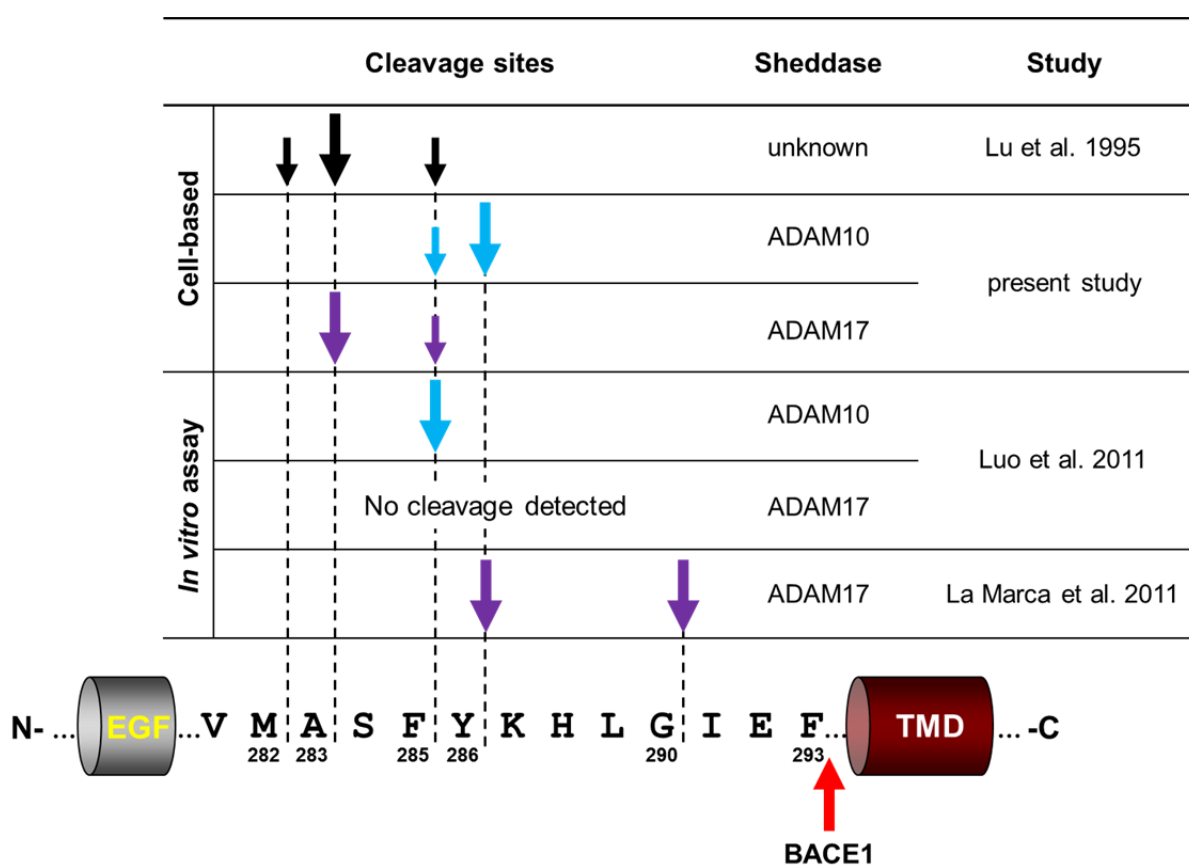
Figure 49. Overview of the shedding sites in the juxtamembrane region of the NRG1 β1 isoform reported for ADAM10 and ADAM17. The cleavage positions of ADAM10 and ADAM17 as identified by different studies in cell-based or *in vitro* cleavage systems are indicated by arrows. Large arrows denote major, small arrows minor cleavage sites. Numbering of the amino acid residues is based on the NRG1 β1a type III isoform and the BACE1 cleavage site is given for orientation. The data are taken from the present study and (Lu et al., 1995b; La Marca et al., 2011; Luo et al., 2011).

Discussion

In contrast, Y_{286} which was observed as the main ADAM10 shedding site in the present work is not surrounded by any residues that are preferred by ADAM10 in peptide library screenings (Caescu et al., 2009) (Figure 49). It is noteworthy, however, that betacellulin is also cleaved by ADAM10 after a phenylalanine and tyrosine residue (Caescu et al., 2009) indicating that these still allow shedding. The finding of close and, in case of F_{285}, even identical shedding sites for ADAM10 and ADAM17 within the NRG1 β isoform may be explained by the fact that these enzymes share fairly similar cleavage site requirements and are able to cleave some substrates at the same peptide bond (e.g. APP at the α-site (Caescu et al., 2009)). In contrast to the BACE1 shedding site which is only present in isoforms with the stalk 1, the ADAM shedding sites are present in all isoforms of NRG1 with a β-type EGF-like domain. It could therefore be speculated that ADAM10 or ADAM17 represent the main sheddases of NRG1 isoforms lacking the stalk region 1, however, this has not been investigated yet.

In summary, when compared to the shedding site of BACE1, the exact positions of ADAM-mediated shedding in the β isoforms of NRG1 remain somewhat controversial. Nonetheless there is now substantial evidence that both ADAM10 and ADAM17 cleave at close sites within the MASFY sequence located immediately C-terminal of the β-type EGF-like domain and 17-21 residues upstream of the TMD of NRG1. Consequently, shedding of NRG1 at the α-site occurs in greater distance to the cell membrane than shedding at the β-site (only ten residues upstream of the TMD) and hence represents an inversion of the situation found for the shedding of APP (1.1.2 Figure 2, Figure 49).

In addition to the shedding in stable cells, the processing of NRG1 type III was also investigated in primary hippocampal neurons. Using inhibitors and novel neoepitope-specific antibodies against the identified cleavage site, endogenous BACE1 was found to similarly shed NRG1 type III after F_{293} in neurons. Due to the heterogeneity of their shedding, currently no ADAM cleavage site-specific antibodies are available and therefore the identified shedding sites of ADAM10 and ADAM17 could not be confirmed by this approach. Nevertheless, treatment with inhibitors revealed that under endogenous protease levels both BACE1 and ADAMs contribute to the shedding of ectopically expressed NRG1 type III in neurons. Although it was not possible to quantify their relative contributions this suggests that in the absence of BACE1, the reduced shedding of NRG1 type III may at least be partially compensated by ADAMs and vice versa. If this holds true *in vivo*, such compensatory shedding by ADAMs could explain the residual myelination observed in BACE1 KO mice (Hu et al., 2006; Willem et al., 2006; Velanac et al., 2012).

Although no systematical analysis regarding the identity of a compensating protease has been published as of yet, the findings reported by others (Horiuchi et al., 2005; Luo et al., 2011) and in the present work (3.5) suggest both ADAM10 and ADAM17 as possible candidates. In contrast, the reported inactivation of NRG1 type III by ADAM17-mediated cleavage (La Marca et al., 2011) would exclude this protease from such a role and instead implies that ADAM17 activity actually exacerbates the hypomyelination observed in BACE1 KO mice. Given the limitations of the latter study (discussed in 4.2, 4.7), however, inactivation of NRG1 type III by ADAM17 remains controversial and the observed effects on myelination in ADAM17 KO mice could be independent of NRG1 type III proteolysis (4.7).

4.3 BACE1 and ADAM17 cleave NRG1 type III at novel N-terminal sites

In addition to the shedding that takes place C-terminal of the EGF-like domain of NRG1 type III, this study discovered novel proteolytic cleavage sites N-terminal of that domain. Proteolytic processing of NRG1 type III at these sites liberates the EGF-like domain from the membrane-anchored NTF and generates soluble EGF-like domains (sEGF) of different sizes. Using mass spectrometry and site-specific antibodies, BACE1 was found to cleave NRG1 type III after L_{217} liberating the larger β-sEGF while ADAM17, through cleavage after H_{234}, generates the smaller α-sEGF. The novel BACE1 cleavage site upstream of the EGF-like domain strongly resembles the β-site in APP with the Swedish mutation (APPswe) (Mullan et al., 1992) which comprises the residues NL instead of KM directly before the cleaved peptide bond (4.2 Figure 48). BACE1 displays a dramatically enhanced affinity to the mutant cleavage site in APPswe leading to increased Aβ production and subsequently early-onset AD (Citron et al., 1992, 1995; Cai et al., 1993). In addition, the novel BACE1 site in NRG1 type III features a glutamine at P1' a residue which is similarly present at this position in several other BACE1 substrates (4.2 Figure 48). Based on the sequence it is therefore likely that BACE1 indeed has a high affinity towards the identified cleavage site and may also efficiently cleave NRG1 type III after L_{217} *in vivo*.

A recent study reported that a substitution of alanine by threonine at the P2' position of the β-site in APP (A673T) reduces BACE1 cleavage and conveys protection against AD (Jonsson et al., 2012) (4.2 Figure 48). Of note, the novel BACE1 cleavage site in NRG1 type III also contains a threonine residue at P2' which therefore could have an inhibitory effect on BACE1-mediated cleavage (4.2 Figure 48). It remains to be seen whether the substitution of

the respective threonine by an alanine residue in NRG1 type III would indeed allow an even more efficient cleavage by BACE1 and would promote the generation of β-sEGF.

In contrast to BACE1 which cleaves NRG1 type III 19 residues upstream of its bioactive domain, ADAM17-mediated processing takes place after H_{234} located within the sequence GTSHLIKC directly at the border of the EGF-like domain (3.3 Figure 27). Except for the two residues SH directly before the cleaved peptide bond, the identified site is exclusively surrounded by residues known to be favored by ADAM17 (Caescu et al., 2009), indicating that it might indeed be a genuine cleavage site.

Further support for the identified BACE1 and ADAM17 cleavage sites comes from the different glycosylation observed for α- and β-sEGF, respectively. BACE1 cleaves NRG1 type III upstream of a serine/threonine-rich stretch and consequently includes this site of potential O-linked glycosylation into β-sEGF. By contrast, α-sEGF does not contain this site because ADAM17 cleavage occurs downstream of the S/T sequence (3.3 Figure 27). In agreement, only β-sEGF but not α-sEGF was found to be subject to O-linked glycosylation.

The finding that ADAM10 in contrast to ADAM17 is not able to cleave within the GTSHLIKC sequence may be explained by the fact that most residues surrounding the cleavage site after H_{234} are not well tolerated by ADAM10. Consequently, enhanced expression of ADAM10 in HEK293 cells did not increase the amount of soluble α-sEGF but rather caused the generation of $\beta\text{-sEGF}_{68}$ which is N-terminally cleaved by BACE1 but terminates at the ADAM10 shedding site (3.2.2 Table 3). In conclusion, ADAM10 seems not capable of liberating the EGF-like domain of NRG1 type III on its own but depends on either BACE1 or ADAM17 for the N-terminal processing.

Mass spectrometric analysis of the soluble EGF-like domains liberated from the full-length NRG1 type III in principle confirmed the shedding sites determined previously with the truncated construct NRG1ΔNT. However it also revealed a minor inconsistency regarding the contribution of BACE1 and ADAM10 to the shedding in HEK293 cells. According to the MS analysis shedding of the truncated construct occurred to an almost similar extent after F_{293} and Y_{286} and was mediated by endogenous BACE1 and ADAM10, respectively (3.1.2 Figure 16-19). In contrast, the $\beta\text{-sEGF}_{68}$ generated from the full-length NRG1 type III by endogenous levels of these proteases exclusively terminated after F_{285}, the minor shedding site of ADAM10 in the truncated construct NRG1ΔNT (3.2.2 Figure 25). No β-sEGF species with a C-terminus resulting from BACE1- or ADAM10-mediated shedding after F_{293} or Y_{286} could be detected and overexpression of BACE1 was required to shift shedding to the BACE1 site F_{293} and to generate $\beta\text{-sEGF}_{76}$. In agreement, the site-specific antibody 4F10 did

not detect any sEGF species resulting from endogenous BACE1-mediated shedding of full-length NRG1 type III but did so only after overexpression of BACE1. At the same time, however, membrane-bound NRG1 NTFs resulting from BACE1 shedding were clearly detected in the cell lysates by the 4F10 antibody demonstrating that shedding by BACE1 did in fact occur.

Several different reasons could account for these conflicting observations. First and foremost both approaches, the identification of shedding sites using the truncated construct NRG1ΔNT as well as the confirmation of the latter sites in the full-length NRG1 type III construct by means of western blotting and mass spectrometry are not quantitative. It is therefore not possible to determine the absolute extent of BACE1- and ADAM10-mediated shedding of the two constructs and to compare the results quantitatively. Furthermore the different topologies of the truncated (N_{out}/C_{in}) and the full-length (N_{in}/C_{in}) constructs could impact on the shedding by BACE1 and ADAM10. This would of course also implicate that NRG1 type I (N_{out}/C_{in}) and NRG1 type III (N_{in}/C_{in}) are subject to differential shedding by these proteases which has not been reported yet. Given that in the absence of its descending counterpart β-$sEGF_{76}$ (C-terminus F_{293}) in the supernatant, the BACE1-shed precursor NRG1 NTF (C-terminus F_{293}) was still found in the lysate, the most likely explanation for the observed discrepancy is that after BACE1 shedding and prior to its release from the membrane via N-terminal cleavage, the C-terminus of the EGF-like domain was further truncated until F_{285}, possibly by ADAM10-mediated cleavages. Under endogenous protease levels in HEK293 cells this truncation of the NRG1 NTF seems to occur to a large extent as no β-$sEGF_{76}$ fragments with BACE1-shed C-termini were detected. This could be due to the relatively low levels of BACE1 in HEK293 cells because enhanced BACE1 expression caused a robust generation of β-$sEGF_{76}$. Similarly, the higher protein levels of BACE1 in hippocampal neurons clearly lead to the generation of β-$sEGF_{76}$. In contrast to the full-length NRG1 type III, the ectodomain of the truncated NRG1ΔNT is immediately released from the membrane upon initial shedding. Its C-terminus therefore is not available as substrate for subsequent truncations by membrane-bound proteases such as ADAM10 and the liberated domains contain C-termini reflecting the initial shedding by both BACE1 and ADAM10.

Although the outlined hypothesis remains unverified it constitutes a plausible explanation for the observed discrepancies in the shedding pattern of type I and type III oriented NRG1 proteins in cell culture.

4.4 Sequential order of C-terminal shedding and N-terminal cleavage

The model described above assumes a sequential order of a primary shedding that generates a membrane-bound NTF and a subsequent N-terminal cleavage releasing the EGF-like domain from said NTF. The order of the proteolytic processing has implications on the mode of juxtacrine signaling by NRG1 type III (Figure 50). A primary shedding event leads to the EGF-like domain being anchored to the membrane via the NTF which currently is the widely assumed juxtacrine signal (1.3.3.2) (Figure 50 A). By contrast, if the N-terminal processing were to precede shedding, a CTF comprising the EGF-like domain (CTF+EGF) would remain (Figure 50 B). Compared to the NTF such a CTF+EGF fragment presents the EGF-like domain towards the luminal space in a reverse orientation.

It is important to note that the order of cleavage has not been determined yet and cannot be deduced from the experiments presented in this study. A respective investigation would require an elaborate pulse-chase setup and furthermore depend on antibodies to the EGF-like domain and the N- and C-terminus of NRG1 type III that are suitable for IP. The available western blot data, however, show that under endogenous protease levels in both stable and primary cells the processing of NRG1 type III leads to the accumulation of an NTF that contains the EGF-like domain. By contrast, the CTF+EGF was only observed in BACE1 overexpressing HEK293 using the 7E6 antibody against the N-terminal BACE1 cleavage site. The antibody against the NRG1 type III C-terminus was not sensitive enough to detect this fragment indicating that it is present in rather small amounts and its generation depends on high levels of BACE1.

Although the actual order of cleavage cannot be ascertained, together with the data from the literature (Taveggia et al., 2005; Velanac et al., 2012) this supports the model in which the juxtacrine signaling of NRG1 type III is exerted by the EGF-like domain contained in the NTF generated by shedding (Figure 50 A).
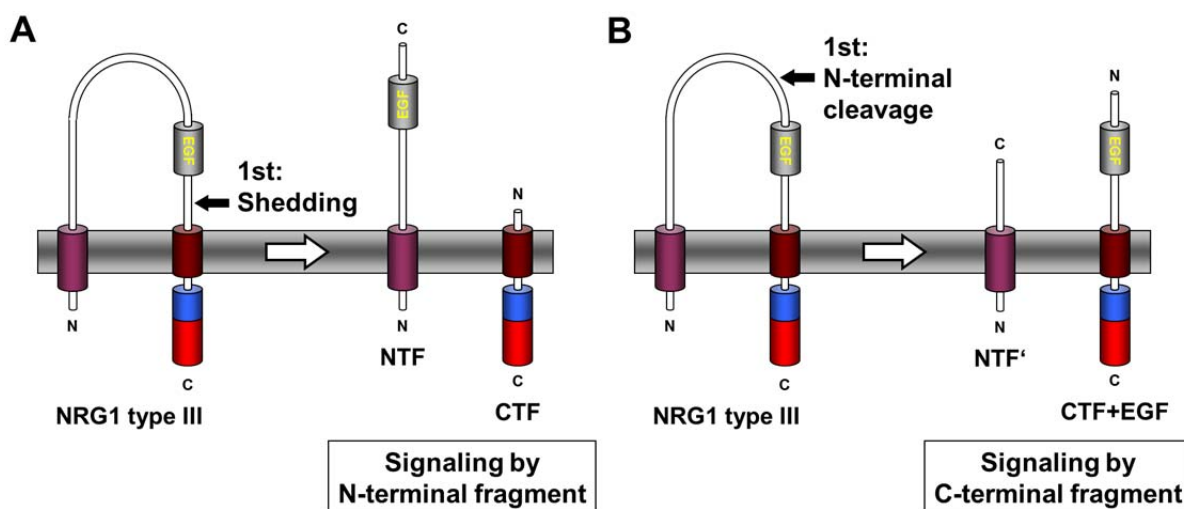
Figure 50. Scheme depicting the presentation of the EGF-like domain during juxtacrine signaling of NRG1 type III according to the order of cleavage events. A), **B)** Depending on the order of shedding and N-terminal cleavage, the bioactive EGF-like domain is anchored to the membrane by the NTF or the CTF of NRG1 type III. Note that the actual sequential order of the cleavage events is currently unknown.

4.5 Generation of soluble NRG1 type III EGF-like domains in neurons

Analysis with the neoepitope-specific antibodies 7E6 and 4F10 (3.3 Figure 27) revealed that, similar to HEK293 cells with enhanced BACE1 expression, neurons transduced with NRG1 type III generate β-sEGF$_{76}$ by a dual BACE1 cleavage at the identified shedding and N-terminal sites. The lack of antibodies prevented a similar confirmation of the N-terminal ADAM17 cleavage site in NRG1 type III but the ADAM-dependent generation of a smaller α-sEGF not detectable with either of the BACE1 neoepitope-specific antibodies strongly suggests the utilization of this site in neurons as well. However, as of now the release of α-sEGF by another protease besides ADAM17 via cleavage at a site distinct from the BACE1 site cannot be ruled out completely.

The unambiguous identification of the protease(s) that in addition to BACE1 process NRG1 type III in neuronal cells would either require knockdown of the candidate proteases or the use of neurons derived from respective knockout animals. In this regard it would also be desirable to ascertain the cleavage sites in NRG1 type III and the sequences of the sEGF peptides using neuronal supernatants for mass spectrometric analysis. However, due to the relatively low expression of the substrate in neurons and the lower cell number compared to HEK293 cells it was not possible to obtain enough material for the IP-MS approach so far.

Discussion

In order to assess the physiological importance of the novel N-terminal cleavages it will be necessary to investigate the processing of endogenous NRG1 type III, ideally *in vivo.* However, several technical limitations have prevented such an analysis to date. Acquiring sufficient amounts of material for western blot or mass spectrometry has proven to be one of the major obstacles in this regard. Lysates of mouse brains as well as of isolated sciatic nerves did yield western blot signals with the antibody to the C-terminus of NRG1 (not shown). However, as this antibody recognizes the NRG1 a-type C-terminal tail it is not specific for the type III isoform. Consequently, while the full-length NRG1 type III may be identified on western blot by its larger molecular weight, it is not possible to distinguish the CTFs of different isoforms. Likewise, the BACE1 cleavage site-specific antibody 4F10 detected NTFs in the analyzed lysates (not shown) but their size strongly indicates that they arise from the shedding of NRG3 instead of NRG1. This is explained by the fact that NRG3 is strongly expressed in the nervous system and harbors a juxtamembrane sequence identical to the sequence upstream of the BACE1 site in the NRG1 stalk (4.2 Figure 48). Therefore, like NRG1, NRG3 will likely be shed by BACE1 as well and its NTF comprising the identical C-terminal residues will be recognized by the 4F10 antibody.

In addition, neither analysis with the 10E8 nor with the 7E6 antibody yielded specific signals from mouse brain homogenates. This is particularly puzzling in the case of 10E8 which recognizes the BACE1-cleaved NRG1 β-CTF. Provided that the BACE1 cleavage site was mapped correctly, shedding of any transmembrane isoform of NRG1 β1 (type I-VI) by BACE1 should result in a β-CTF detectable by this antibody. The reason for the failure of the 10E8 antibody to detect endogenous β-CTFs on western blot is currently not known. Possible explanations include the rapid turnover of this fragment by the γ-secretase resulting in a very low abundance under steady-state conditions. Support for this explanation comes from experiments in cell culture which showed that inhibition of the γ-secretase by DAPT results in strong 10E8 signals. Moreover IP experiments with the 10E8 antibody indicate that its affinity towards its epitope is only moderate (not shown). As the C-terminal antibody does detect NRG1 CTFs (sum of α- and β-CTFs) this could mean that the 10E8 antibody is just not sensitive enough. Alternatively, the inability of the 10E8 antibody to detect endogenous NRG1 β-CTFs could be due to an N-terminal truncation of this fragment after BACE1 shedding. Such a truncation, possibly mediated by an exopeptidase, would result in the removal of the residues recognized by the 10E8 antibody and could explain the absence of 10E8 western blot signals in the presence of signals for the CTF by the C-terminal antibody.

Analysis of cultured cortical and hippocampal neurons for processing of endogenous NRG1 type III yielded similar results: Detection of full-length NRG1 and CTFs was possible with the C-terminal antibody but the NTF detected with 4F10 most likely arose from shedding of NRG3 (not shown). This illustrates another major obstacle for the analysis of endogenous NRG1 type III: As of yet, no antibody specific for the type III isoform is available which renders its identification difficult and causes the need to work with N-terminal tags. Although cultured DRG neurons are described to express high levels of NRG1 type III (Taveggia et al., 2005) western blot analysis of lysates and supernatants of these cells likewise did not yield specific signals with the novel neoepitope antibodies (not shown). In all cases described above also performing IPs of the respective fragments prior to western blot analysis did not lead to improved detection. The lack of antibodies for immunofluorescence (IF) constitutes another limitation regarding the analysis of endogenous NRG1 type III and its processed fragments. Both commercial as well as home-made antibodies against NRG1 type III were found not to be suitable for the detection of the endogenous protein by means of immunofluorescence microscopy (not shown).

Taken together, although its existence is likely and ectopically expressed NRG1 NTF compensates for the lack of NRG1 type III *in vivo* (Velanac et al., 2012) it is so far not possible to unambiguously demonstrate the existence of endogenous NRG1 type III NTF by means of WB, MS or microscopic analysis. Likewise it is currently not possible to detect soluble EGF-like domains generated by the processing of endogenous NRG1 type III. The development of sensitive antibodies specific for the N-terminal sequence of the type III NRG1 isoform and its processed fragments will be crucial in order to successfully address this issue.

4.6 Activity of soluble NRG1 type III EGF-like domains

The experimental evidence provided in the present study shows that the soluble EGF-like domains liberated from NRG1 type III constitute a paracrine promyelinating signal that induces ErbB3 receptor phosphorylation and subsequent AKT downstream signaling in MCF-7 cells and primary Schwann cells. Activation of the PI3K/AKT pathway in response to NRG1 type III triggers the transcription of several myelin genes and is a key event in the transition of Schwann cells into the myelinating state (1.3.4.1.3). Importantly, the findings of the present work are in agreement with another study that found soluble NRG1 type III peptides to stimulate Schwann cells in a paracrine manner and to promote myelination in Schwann

cell-DRG co-cultures (Syed et al., 2010). The authors of this study used recombinant peptides consisting of the entire N-terminus of NRG1 type III and the EGF-like domain terminating with the stalk isoform 3 before the TMD. Similar to the result presented here, treatment of primary Schwann cells with the recombinant soluble NRG1 peptides caused robust phosphorylation of ErbB2 and ErbB3 receptors as well as activation of AKT. In addition to the promyelinating PI3K/AKT pathway the authors also investigated the activation of the Ras/Raf/Erk1/2 cascade in response to soluble NRG1 type III. The latter pathway which is known to inhibit myelination was not activated by low doses of the soluble NRG1 type III peptides that already sufficed to activate the PI3K pathway. However, higher doses of the soluble peptides induced the Ras/Raf/Erk1/2 pathway and lead to an inhibition of myelination in Schwann cell-DRG co-cultures (Syed et al., 2010). A similar differential activation of the two pathways was observed for a peptide that comprised only the EGF-like domain and the stalk region of NRG1. Although the precise mechanism is currently elusive this suggests that stimulation of ErbB receptors on Schwann cells by the EGF-like domain of NRG1 leads to a dose-dependent activation of opposing intracellular signaling cascades that either promote or inhibit myelination (1.3.4.1.3).

It is currently unknown whether sufficiently high concentrations of the α- and β-sEGF peptides investigated in this study would also activate the inhibitory Erk1/2 signaling. As no recombinant peptides of these fragments are available, no experiments concerning such dose-dependent effects were conducted. However, the finding that different recombinant versions of the NRG1 EGF-like domain (EGF-like domain only, EGF-like domain with N-terminus of NRG1 type III) caused activation of AKT and Erk1/2 at low and high concentrations respectively (Syed et al., 2010), renders a similar effect of α- and β-sEGF highly likely.

The vast majority of mature NRG1 isoforms are highly glycosylated (carbohydrate content approx. 40%) and contain both N- and O-linked carbohydrates (Burgess et al., 1995; Lu et al., 1995a, 1995b; Cabedo et al., 2004). At least 11 serine and threonine residues were identified as potential sites of O-linked glycosylation, most of which are located immediately upstream of the EGF-like domain in the serine/threonine-rich linker region of NRG1. The overall glycosylation pattern seems to be similar for all NRG1 isoforms (Lu et al., 1995a) and several of the putative O-glycosylation sites are present N-terminal of the EGF-like domain in NRG1 type III. In contrast to the smaller α-sEGF, the larger β-sEGF as liberated from NRG1 type III by BACE1, contains this serine/threonine-rich sequence and was found to be subject to O-linked glycosylation. The soluble ectodomains of NRG1 isoforms containing an Ig-like

domain are known to bind to components of the extracellular matrix, an interaction which serves to locally increase their concentration and modulates their ability to activate ErbB receptors (Li and Loeb, 2001). As protein-bound carbohydrates could potentially participate in receptor interactions, the effect of O-linked glycosylation on the activity of β-sEGF was investigated. When compared to α-sEGF which is not subject to glycosylation, the glycosylated and non-glycosylated form of β-sEGF displayed similar activation of both ErbB3 receptors and AKT signaling in MCF-7 and primary Schwann cells. Thus O-linked glycosylation at the N-terminus of β-sEGF does not significantly alter its ability to activate and signal through ErbB3 receptors.

It is, however, important to note that the β-sEGF used in the present study consisted of both glycosylated and non-glycosylated species. Additionally, owing to the nature of detection and readout (western blot quantification) no truly quantitative comparison can be made. Together this implies the risk that a rather subtle effect of glycosylation on the activity of β-sEGF may have remained undetected. Still, the results are in line with previous findings of a similar stimulatory effect of both glycosylated and non-glycosylated forms of NRG1 on the growth of NIH3T3 cells (Lu et al., 1995a). Likewise, glycosylation has no effect on the principal structure of the NRG1 ectodomain and the EGF-like domain because no difference in the secondary and tertiary folding features were observed for glycosylated and non-glycosylated NRG1 (Lu et al., 1995a). In addition to O-linked glycosylation at least two sites of N-linked glycosylation located near the N-terminus of NRG1 type III were reported (Lu et al., 1995a). However, neither α- nor β-sEGF was found to be N-glycosylated (not shown) and it is therefore unlikely that such glycosylation would influence the activity of the soluble EGF-like domain.

4.7 Similar activities of ADAM17- and BACE1-cleaved soluble EGF-like domains

The experiments conducted in the course of this study indicate similar biological activities of α- and β-sEGF with regard to paracrine activation of ErbB receptors. Furthermore, β-sEGF peptides with C-termini mimicking either BACE1- or ADAM17-mediated shedding similarly were able to rescue hypomyelination in a BACE1 KO zebrafish model *in vivo*. Although no major difference seems to exist between these soluble peptides it is possible that, due to the nature of the readout (western blot quantification), more subtle differences in their activities remained undetected.

Discussion

Nevertheless, the finding that BACE1 and ADAM17 generate active EGF-like domains from NRG1 type III is in sharp contrast with a recent study that claimed an inhibitory effect of ADAM17-processed NRG1 type III on myelination in the PNS (La Marca et al., 2011). Specifically this study claimed that the hypermyelination observed in the PNS of ADAM17 KO mice is due to the NTF resulting from ADAM17-mediated shedding after Y_{286} and G_{290} in the juxtamembrane region of NRG1 type III. According to the model proposed by this report, shedding by ADAM17 inactivates the EGF-like domain and generates an NRG1 type III NTF that is unable to activate ErbB receptors on Schwann cells in a juxtacrine fashion (suppl. Figure 9 in (La Marca et al., 2011)). Consequently, while ablation of BACE1 leads to much less active NRG1 type III NTFs and results in hypomyelination, knockout of ADAM17 reduces the amount of inactive NRG1 type III fragments and causes increased myelination. In agreement, a recombinant NRG1 type III peptide digested with BACE1 *in vitro* induced AKT signaling when applied to Schwann cells while in contrast after digestion with ADAM17 no AKT phosphorylation was observed. Moreover, a NRG1 type III NTF terminating at H_{288} (between the ADAM17 cleavage sites identified by the authors) failed to rescue myelination when expressed in a Schwann cell-DRG co-culture of NRG1 type III KO neurons (La Marca et al., 2011).

The reasons for the observed discrepancies regarding the impact of the very C-terminal residues of the EGF-like domain on its activity are currently unclear. However, there are several aspects that are worth noting: Possible reasons that could account for the different shedding sites identified for ADAM17 in NRG1 type III have already been discussed above (4.2). Interestingly, a systematic comparison of the activities of different NRG1 fragments reported so far reveals only a minor overall effect of the C-terminal residues on the ability of the EGF-like domain to induce signaling (Table 8). Regardless of the identity of the sheddase mediating the cleavage, NRG1 EGF-like domains terminating at M_{282}, A_{283}, S_{284}, F_{285}, G_{290} and F_{293} (numbers according to the NRG1 β1a type III isoform) were found to stimulate receptor phosphorylation (and AKT signaling) in a paracrine fashion *in vitro* by different independent studies (Table 8). With regard to juxtacrine signaling the membrane-anchored NRG1 type III NTFs ending with F_{285} and F_{293} equally activated ErbB3 receptors and AKT *in vitro*. Additionally, the NRG1 EGF-like domains terminating with A_{283}, G_{290} and F_{293} were found to be active paracrine signals *in vivo* during this study (3.5.4).

Taken together, none of the investigated C-terminal residues of the EGF-like domain of NRG1 abolished its signaling activity. In fact, inactivation of the EGF-like domain due to shedding at specific sites within the stalk region of NRG1 type III was only reported once (La

Marca et al., 2011) and may be due to additional albeit undetected cleavages within the EGF-like domain itself (4.2). Even if not complete, such additional cleavages during the *in vitro* digest would significantly reduce the amount of functional EGF-like domains and could easily account for the observed inability of the assay solution to activate AKT signaling in Schwann cells. The reason for the failure of the NRG1 type III NTF terminating after H_{288} to rescue myelination of NRG1 type III KO neurons *in vitro* (La Marca et al., 2011) is currently unclear. However, a final evaluation of this observation is not possible as it was not controlled whether BACE1-cleaved NRG1 type III NTF (described to be active) was able to rescue the hypomyelination phenotype in that particular experimental paradigm.

C-terminus EGF-like domain	Test - System (readout)		Result	Study
...M_{282} ...MA_{283} ...MAS_{284} ...$MASF_{285}$	paracrine	*in vitro* (pY of surface receptor)	active	Lu et al. 1995
...MA_{283} ...$MASFYKHLG_{290}$ ...$MASFYKHLGIEF_{293}$	paracrine	*in vitro* (p-ErbB3, p-AKT) *in vivo* (myelination)	active	present study
...$MASFY_{286}$ ...$MASFYKHLG_{290}$ ...$MASFYKHLGIEF_{293}$	paracrine	*in vitro* (p-AKT)	inactive inactive active	La Marca et al. 2011
...$MASFYKH_{288}$	juxtacrine	*in vitro* (myelination)	inactive	
...$MASF_{285}$ ...$MASFYKHLGIEF_{293}$	juxtacrine	*in vitro* (p-ErbB3, p-AKT)	active	Luo et al. 2011

Table 8. Comparison of reported activities of NRG1 β1 EGF-like domains comprising different C-termini. The different C-terminal amino acid sequences of the EGF-like domains generated by shedding are given. The experimental setup and read-out parameter(s) used by the respective study are indicated. Numbering of the amino acid residues is based on the NRG1 β1a type III isoform. The data are taken from the present study and (Lu et al., 1995b; La Marca et al., 2011; Luo et al., 2011).

Discussion

Depending on which cleavage site was determined, the sites of BACE1 and ADAM17-mediated shedding are separated by minimal three or maximal 11 residues (4.2 Figure 49). The close vicinity specifically of the ADAM17 site after G_{290} to the BACE1 site after F_{293} renders inactivation of the EGF-like domain due to a reduced length of the C-terminus unlikely. All the more as EGF-like domains containing shorter C-termini were found to be active (Table 8) and reduced length (truncation beyond F_{285}) even correlated with slightly increased ErbB3 activation *in vitro* (not shown). Truncation of residues important for the biological activity of the EGF-like domain due to ADAM17-mediated shedding also seems unlikely as all cleavage sites reported so far are outside the core of the EGF-like domain (4.1 Figure 47, 4.2 Figure 49). Specifically the sites identified as "inhibitory", Y_{286} and G_{290}, are located nine and 13 residues downstream of the 6th cysteine residue critical for the EGF-like domain's structure and function.

In addition to altered NRG1 type III signaling, the observed inhibitory effect of ADAM17 on PNS myelination could also be mediated by changes in the proteolysis of substrates other than NRG1 type III. A prime candidate for such a substrate outside the NRG1 type III signaling pathway is notch. Although canonical notch signaling promotes the development of SCPs to mature Schwann cells, its non-canonical signaling inhibits myelination (Woodhoo et al., 2009). Increased levels of NICD in Schwann cells block the upregulation of positive regulators of myelination such as Krox20 and delay the onset of myelination *in vivo*. In agreement, inactivation of notch promotes myelination and leads to significantly thicker myelin sheaths around nerves in mice. Moreover, in the adult, increased notch signaling contributes to demyelination after nerve injury (Woodhoo et al., 2009). Overall notch therefore seems to be a negative regulator of myelination and reduced proteolysis and subsequent signaling by the NICD is expected to result in hypermyelination of the PNS.

The question whether the shedding of notch is mainly mediated by ADAM17 is still controversial. On the one hand, only ADAM10 but not ADAM17 KO mice display a classical notch phenotype (1.1.3.1). On the other hand, ADAM17 was identified as main notch sheddase in several cell lines *in vitro* (Brou et al., 2000). In general the extent to which each protease participates in the proteolysis of notch seems to be strongly context-dependent (Bozkulak and Weinmaster, 2009). It is therefore conceivable that the ablation of ADAM17 contributes to reduced notch signaling and consequently results in increased myelination in ADAM17 KO mice in a manner independent of NRG1 type III. While it is tempting to attribute the myelination phenotype of ADAM17 KO mice to such altered notch signaling, it must be

noted that hypermyelination in these mice was found to be neuron-autonomous and NICD levels in Schwann cells were reportedly unaltered (La Marca et al., 2011).

Another ADAM17 substrate important in the process of myelination is the p75 neurotrophin receptor (p75^NTR) expressed by both neurons and Schwann cells (Weskamp et al., 2004; La Marca et al., 2011). Signaling of the nerve growth factor (NGF) and the brain derived neurotrophic factor (BDNF) through p75^NTR is a positive regulator of myelination and its inhibition results in thinner myelin sheaths *in vivo* (Cosgaya et al., 2002; Buser et al., 2009). Importantly, shedding of the p75^NTR receptor is impaired in Schwann cells of ADAM17 KO mice (La Marca et al., 2011) and consequently the increased level of p75^NTR could be responsible for the observed hypermyelination. Besides p75^NTR, neurotrophin signaling in the context of myelination is mediated through Trk receptors (Cosgaya et al., 2002) which also are among the substrates of ADAM17 (Reiss and Saftig, 2009). Independent of NRG1 type III, altered processing of Trk receptors could therefore also be involved in the abnormal myelination observed in ADAM17 KO mice although this has not been investigated yet.

In summary, given that besides NRG1 type III several other substrates of ADAM17 are important regulators of myelination it seems likely that their altered processing contributes to the reported hypermyelination in ADAM17 KO mice. Especially considering the discussed discrepancies in the shedding of NRG1 type III and its effect on myelination it seems advisable to much more closely investigate the role of these other substrates in the context of hypermyelination upon ablation of ADAM17. Eventually this may lead to alternative models that are less dependent on the processing of NRG1 type III and thereby resolve some of the current discrepancies.

4.8 Partial rescue of myelination in a BACE1 KO zebrafish by β-sEGF and its C-terminally truncated variants

The finding that β-sEGF itself and β-sEGF variants with C-termini corresponding to ADAM17-mediated shedding similarly rescue the myelination in a BACE1 deficient zebrafish model strongly argues for a promyelinating effect of both BACE1- and ADAM17-cleaved NRG1 type III. In addition this demonstrates that the EGF-like domain liberated from NRG1 type III by a dual proteolytic cleavage constitutes an active soluble signal that promotes myelination in a paracrine manner *in vivo*.

It is evident that none of the investigated β-sEGF peptides completely rescued the hypomyelination of the BACE1 KO zebrafish larvae (3.5.4 Table 5). The only partial rescue is

mainly caused by two complementary mechanisms inherent to the experimental setup: Firstly, the mRNA encoding the β-sEGF peptides is injected into a single cell during very early zebrafish larvae development. As the larvae develops, the initial amount of mRNA per cell decreases upon every cell division leading to a dilution effect that results in a progressively lower expression of the ectopic protein in individual cells with time. Secondly, the degradation of the injected mRNA by cellular enzymes also contributes to the reduced expression of the ectopic protein over time. Together these mechanisms account for the fact that the extent of the rescue observed in this experimental setup inversely correlates with the time between injection and analysis. In case of the rescue of myelination in the BACE1 KO zebrafish, analysis was performed rather late, at three days post fertilization. At this point in time the β-sEGF was no longer detectable in the lysates of the injected fish by western blot analysis (not shown) indicating a low expression of the peptide. The fact that in spite of its low abundance β-sEGF still lead to a marked rescue of the hypomyelination in BACE1 KO zebrafish indicates that this peptide is a potent promyelinating paracrine signal.

The global expression of a growth signal such as the NRG1 EGF-like domain harbors the risk of toxic side effects. Toxicity affecting normal development of the zebrafish larvae was indeed observed upon initial injections of β-sEGF mRNA. To avoid such toxic effects, the amount of injected mRNA was carefully titrated down to a level that still allowed the partial rescue of the hypomyelination phenotype but at the same time did not interfere with normal development of the larvae. It is furthermore known that neuronal overexpression of NRG1 type III in both the CNS and PNS of zebrafish causes Schwann cells to bypass their natural boundaries and aberrantly migrate into the CNS (Perlin et al., 2011). However, the *in vivo* rescue experiments of the present study were designed to assess the ability of the soluble NRG1 EGF-like domain to promote myelination in the PNS. Its ability as an instructive signal for the directed migration of Schwann cells was not investigated and the readout which is based on the immunofluorescent labeling of myelin is not suited for the detection of single Schwann cells in the BACE1 KO zebrafish larvae. Therefore, although the universal presence of β-sEGF in the injected larvae renders misguidance of migrating Schwann cells highly likely, it remains unknown whether similar to the NRG1 type III full-length protein also the soluble EGF-like domain causes migration of Schwann cells into the CNS. If indeed upon β-sEGF expression Schwann cells entered the CNS of the larvae they did so without substantially participating in myelination as no overt changes in the myelination of central nerves were detected.

In contrast to the *in vitro* experiments where the extent of ErbB3 and AKT phosphorylation served as readout, the effect of β-sEGF on myelination in the BACE1 KO zebrafish was not rated by its extent but only by its occurrence, i.e. a larvae was either judged to be (partially) rescued or not. This method of analysis precludes any quantitative comparison of the different β-sEGF peptides that were tested. However, it allows the statement that the different C-terminal residues resulting from shedding by BACE1 or ADAM17 do not abolish the biological activity of the EGF-like domain with regard to paracrine ErbB3 activation. Therefore, according to the results of this study, the length of the sEGF C-terminus does not affect the domain's ability to signal through ErbB3 receptors and to promote myelination *in vitro* or *in vivo*.

Similar to the C-termini, the different N-termini of α- and β-sEGF did not significantly alter ErbB3 activation in cell culture. However, whether like β-sEGF, also α-sEGF is able to promote myelination *in vivo* remains unknown as only EGF-like domains containing a BACE1-cleaved N-terminus (i.e. β-sEGF peptides with different C-termini) were investigated in the BACE1 KO zebrafish model. The reason for this lies in the generally much lower secretion of α-sEGF compared to β-sEGF, a phenomenon that was first observed in HEK293 cells (not shown). It is currently not known why transfection with similar amounts of α- and β-sEGF constructs results in the secretion of much less α-sEGF than β-sEGF peptides into the supernatant of cultured cells. However it is likely that a difference in secretion efficiency rather than expression causes this phenomenon as equal levels of the peptides were detected in cell lysates (not shown). Unfortunately, the mechanism and determinants of such differential secretion remain elusive so far. The difficulties in achieving a high level of secretion for α-sEGF in the cell culture system in combination with the requirement of an initial as high as possible secretion in the BACE1 KO zebrafish model lead to the decision to focus on the analysis of β-sEGF peptides only. Another reason for the selection of the different β-sEGF peptides over α-sEGF was that only the C-terminal residues of the EGF-like domain were reported to affect the signaling of NRG1 type III while the prior cell culture experiments indicated no such effect of the N-terminus.

4.9 Physiological importance of the soluble NRG1 type III EGF-like domains

It is important to note that the results obtained in the zebrafish model do not establish paracrine signaling by NRG1 type III via its soluble EGF-like domain as the sole or most important regulator of myelination under physiological conditions. It has already been convincingly shown that the membrane-tethered NRG1 type III NTF is able to signal through ErbB3 receptors on Schwann cells and to promote myelination in a juxtacrine manner (Taveggia et al., 2005). Moreover, the inability of soluble NRG1 EGF-like domains to rescue myelination of neurons completely devoid of NRG1 type III (NRG1 type III -/-) argues for an essential role of juxtacrine signaling by membrane-retained NRG1 type III (Taveggia et al., 2005; Syed et al., 2010). On the other hand it has become apparent that different species of soluble NRG1 EGF-like domains are able to strongly enhance myelination of neurons with reduced levels of NRG1 type III (NRG1 type III +/-) and even lead to the ensheathment of physiologically non-myelinated axons (Syed et al., 2010). In contrast to the previous reports, the current study provides evidence that such soluble EGF-like domains are indeed generated from the full-length precursor NRG1 type III under cellular conditions. A model that tries to reconcile these findings proposes a first phase during which the initiation and onset of myelination is dependent on the juxtacrine signaling of NRG1 type III, while in a second phase the promotion of myelination may be mediated by paracrine signals (Syed et al., 2010) (4.10 Figure 51). The rescue of myelination in the BACE1 KO zebrafish by β-sEGF is in accordance with this model which also implies that *in vivo* another protease partially compensates for the loss of BACE1-mediated shedding and provides enough membrane-bound NRG1 type III NTF for the (juxtacrine) initiation of myelination. In the later phase, however, the relative low abundance of this juxtacrine signal is not sufficient to sustain the promotion of myelination resulting in a global hypomyelination of the PNS (van Bebber et al., 2013). The ectopically expressed β-sEGF would therefore not initiate but only promote the already ongoing process of myelination. Since so far mainly established on the basis of *in vitro* data, definite proof of this two-phase model *in vivo* would require similar experiments in NRG1 type III KO animals which have not been reported yet.

Another question that currently remains unresolved regards the overall physiological importance of paracrine NRG1 type III signaling for the process of myelination in the PNS. The paracrine promotion of Schwann cell myelination in the BACE1 KO zebrafish model by ectopically expressed β-sEGF does not necessarily translate into the physiological context.

Morevoer, the applied experimental approach does not allow for an estimation of the extent to which paracrine and juxtacrine signaling contribute to myelination, respectively. Clarification of the question whether paracrine signaling is crucial for peripheral myelination under physiological conditions would require the expression of an N-terminally uncleavable NRG1 type III protein in a knock-in animal. Unimpaired PNS myelination in this setup would then indicate that, physiologically, juxtacrine signaling of NRG1 type III is not only required but also sufficient for normal myelination. By contrast, reduced myelination would suggest a requirement of the N-terminal cleavage in NRG1 type III and the liberation of the EGF-like domain, however, could also be due to other, unknown shortcomings of the experimental paradigm. Unfortunately so far it has not been possible to engineer an NRG1 type III NTF that is no longer subject to proteolysis. Attempts to abolish cleavage at the N-terminal cleavage sites by altering their sequences using site-directed mutagenesis were not successful (not shown) which is in agreement with the ability of BACE1 and especially ADAM17 to cleave within a very diverse set of cleavage site sequences. Furthermore experimental evidence suggests the existence of additional, yet so far unidentified proteolytic cleavage sites located closer to the N-terminal TMD of the NRG1 type III NTF (Wang et al., 2001). Cleavage at such sites would liberate a large portion of the ectodomain including the EGF-like domain of NRG1 type III which in turn could again act as a paracrine signal. Generation of a membrane-bound NRG1 type III EGF-like domain that cannot be released from the membrane by proteolysis and represents a truly exclusive juxtacrine signal therefore would probably require the use of an artificial membrane anchor like for example the GPI anchor. The highly artificial features of such a construct, however, would counteract the attempt to experimentally mimic physiological myelination. Given these technical obstacles it therefore seems currently impractical to determine the exact contribution of juxtacrine and paracrine signaling to myelination *in vivo.*

4.10 Hypothetical model of NRG1 type III-regulated myelination in the PNS

Since several aspects are controversial or even entirely unclear, a model describing the regulation of myelination in the PNS by NRG1 type III signaling must remain speculative. Nevertheless it is possible to combine the available experimental data into a hypothetical model in which the α- and β-NTF generated through shedding of NRG1 type III by ADAM17 and BACE1 represent juxtacrine signals on the surface of neurons (Figure 51). Contact-dependent interaction of the β-NTF with ErbB receptors of Schwann cells in close vicinity causes receptor auto-phosphorylation and downstream signaling leading to the initiation of myelination. During this initial phase of myelination the myelinating Schwann cells strictly depend on the presence of a membrane-tethered NRG1 EGF-like domain on the neuronal surface. The strict requirement of a juxtacrine signal during onset of myelination may be explained by the need of a reliable spatial cue for the Schwann cells in order to correctly orient themselves towards the axon. Following the initiation, the growth of the myelin sheath during the second phase of myelination may then also be further promoted by the membrane-bound β-NTF. While the results of this study imply a similar role for α-NTF, others have reported that the α-NTF resulting from ADAM17-mediated shedding of NRG1 type III has an inhibitory effect on both onset and promotion of myelination (La Marca et al., 2011) (Figure 51). Thus, by competing with BACE1 for the shedding of NRG1 type III and the generation of an active NTF, ADAM17 would act as a regulatory brake on myelination in the peripheral nervous system.

In addition to shedding and through further cleavages N-terminal of the EGF-like domain of NRG1 type III, ADAM17 and BACE1 generate α- and β-sEGF, respectively. Although these soluble EGF-like domains comprise different N- and C-terminal residues and also differ in their glycosylation, both similarly activate ErbB receptors on Schwann cells and promote myelination as paracrine signals.
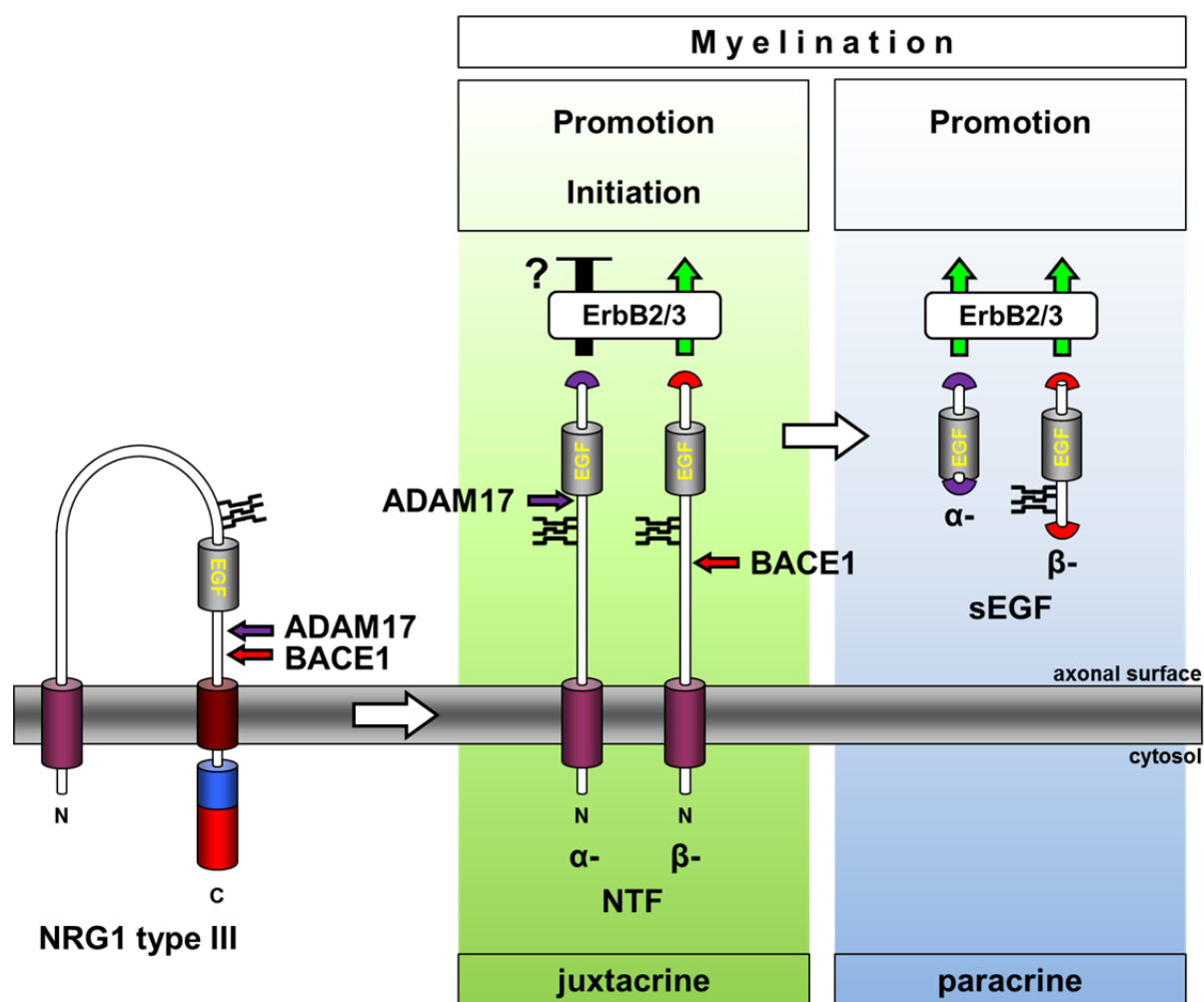
Figure 51. Hypothetical model of NRG1 type III signaling during myelination in the PNS. Shedding by ADAM17 and BACE1 generates α- and β-NTF, respectively. β-NTF acts as juxtacrine signal, stimulates ErbB receptors on neighboring Schwann cells and initiates myelination. The role of ADAM17-cleaved α-NTF is controversial but it was suggested that it is unable to activate Schwann cells and therefore inhibits myelination. Further cleavages of the α- and β-NTF by ADAM17 and BACE1 generate α- and β-sEGF that both promote myelination through ErbB receptor activation in a paracrine fashion. While the initial phase of myelination depends on juxtacrine signaling, the subsequent promotion of myelin growth is mediated by both, juxtacrine and paracrine signaling.

According to this model the two key differences between juxtacrine and paracrine signaling of NRG1 type III are: Only juxtacrine signaling by the NTF is able to mediate both, onset and further promotion of myelination. In contrast, the paracrine signaling of the soluble EGF-like domain can solely promote but not initiate this process. However, while the ADAM17-generated juxtacrine signal α-NTF reportedly inhibits myelination (La Marca et al., 2011), the analogous α-sEGF resulting from further ADAM17 cleavage acts as a promyelinating signal (this study). Although backed by reported experimental data, this difference between α-NTF and α-sEGF remains one of the less plausible aspects of the proposed model.

It must also be noted that evidence for this model *in vivo* is scarce. As the N-terminal cleavages by BACE1 and ADAM17 have only been observed *in vitro* so far it remains possible that the soluble EGF-like domains are not generated during physiological myelination but exclusive juxtacrine signaling of NRG1 type III is sufficient. In this regard, detection of α-sEGF or β-sEGF peptides *in vivo* would be needed to demonstrate the necessity of paracrine signaling by NRG1 type III. It is also possible that physiologically the cleavages N-terminal of the EGF-like domain do not occur before but only after binding of the domain to ErbB receptors. In this scenario, signaling by NRG1 type III would be entirely contact-dependent whereas the identified additional cleavages would merely serve to release the bound EGF-like domain from its membrane anchor after receptor binding and would allow internalization of the receptor by the Schwann cell. Proof for this model would require the detection of liberated EGF-like domains bound to ErbB receptors *in vivo* or abolished signaling upon the expression of an uncleavable NRG1 type III construct.

4.11 Intramembrane cleavage of NRG1 type III by the γ-secretase

4.11.1 γ-Secretase mediates a dual cleavage within the TMD of NRG1

The CTF generated by the shedding of NRG1 type III represents a type I transmembrane protein and is a substrate for the γ-secretase complex (Figure 52). Indeed, intramembrane cleavage of the NRG1 type III CTF by the γ-secretase has been observed by different groups (Bao et al., 2003; Dejaegere et al., 2008) and the resulting NRG1-ICD has been implicated as a transcriptional regulator of different (synaptic) proteins, in dendritic development and in the activation of the PI3K signaling pathway (1.3.3.3). The identification of a schizophrenia-associated mutation in the TMD of NRG1 (Walss-Bass et al., 2006) which seems to inhibit processing by the γ-secretase (Dejaegere et al., 2008) has additionally spiked interest in the intramembrane processing of the NRG1 CTF and its functional implications regarding neuronal development and the occurrence of schizophrenia-like symptoms in mice (Stefansson et al., 2002; O'Tuathaigh et al., 2006; Boucher et al., 2007; Karl et al., 2007; Chen et al., 2010b; Duffy et al., 2010). The actual sites of γ-secretase cleavage within the NRG1 TMD, however, have remained elusive so far as has the mechanism by which the schizophrenia-linked V->L mutation impairs this cleavage. Importantly, since the NRG1 gene only contains a single exon encoding for a TMD, all membrane-bound isoforms of NRG1 share the same TMD sequence and are similarly processed by the γ-secretase complex.

Consequently, mutations within the TMD should in principle affect the turnover of the CTFs of all NRG1 isoforms in a similar manner.

Based on the investigation of multiple substrates, the cleavage mechanism of the γ-secretase suggests at least two distinct cleavage sites or regions within the TMD of NRG1 (1.1.3.3): An initial ε-like cleavage close to the cytosolic border which liberates the NRG1-ICD and a subsequent γ-like cleavage in the middle of the TMD. The latter cleavage should lead to the liberation of the CTF's N-terminus and, in analogy to the processing of APP, to the generation of a soluble fragment called NRG1 β-peptide or NRG1 p3-like peptide depending on whether the preceding shedding was mediated by BACE1 or ADAMs, respectively (Figure 52). However, the large size of the cytosolic domain of NRG1 and the lack of suitable antibodies for its immunoprecipitation render the mass spectrometry-based identification of the NRG1-ICD and the respective ε-like cleavage site challenging. Detection of the NRG1 β-peptide and determination of the γ-like cleavages likewise depend on the availability of suitable antibodies.
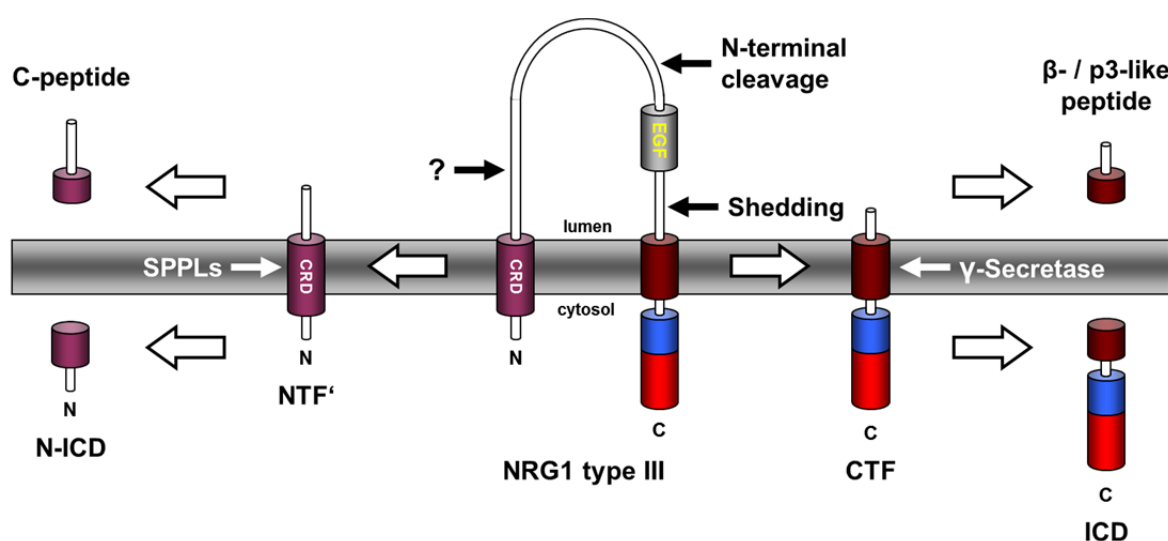
Figure 52. Scheme depicting the proposed dual regulated intramembrane proteolysis of NRG1 type III. Shedding and N-terminal cleavage generates two membrane-bound fragments: The CTF is processed by the γ-secretase complex and a small NRG1 β-peptide or p3-like peptide (depending on whether BACE1 or an ADAM mediated the shedding) is released into the lumen. Simultaneously the C-terminal tail is liberated from the membrane as ICD. After the release of the EGF-like domain and possibly further processing by another as of yet unidentified protease (indicated by "?"), a short N-terminal fragment (NTF') remains in the membrane. This NTF' is a potential substrate for intramembrane proteolysis by SPPLs which would result in the liberation of a luminal C-peptide and an intracellular N-ICD.

Discussion

The current study used a C-terminally truncated, HA tagged NRG1 construct in a cell-free *in vitro* assay, as well as the novel antibody 10E8 to overcome these difficulties. This approach lead to the identification of the ε-like cleavage site after C_{321} and the γ-like cleavage site after L_{314} in the TMD of NRG1, respectively (3.6.2 Figure 46).

No consensus recognition sequence of the γ-secretase has been found to date. Instead, different features of the TMD and the intracellular part of the CTF (Hemming et al., 2008) as well as the length of the remaining extracellular sequence (Struhl and Adachi, 2000) seem to determine whether cleavage by the γ-secretase occurs. However, comparison of the ε-like cleavage sites identified in known γ-secretase substrates indicates a preference for valine at the P1' position and cleavage between two and four residues upstream of the C-terminal membrane border (Figure 53). The identified ε-like cleavage site between C_{321} and V_{322} is located five residues upstream of the membrane border and fits well with these observations. In addition to the main cleavage after C_{321} minor ε-like cleavage sites were determined between V_{322} and V_{323} and A_{324} and Y_{325} and thus more closely to the cytosolic membrane surface. Such additional but minor ε-like cleavage sites are also observed for other γ-secretase substrates (indicated for APP in Figure 53). However, since the sequential order of the ε-like cleavages in NRG1 is not known, it is also possible that these cleavages result from an exopeptidase activity that truncates the ICD subsequent to its initial generation after C_{321}.

Compared to the ε-like site, there is an even greater heterogeneity in the position of the γ-like cleavage site within the TMD of different γ-secretase substrates (Figure 53). In addition, besides a main γ-like site located in the middle of the TMD, almost always several minor cleavage sites are found ranging from the middle to nearly the N-terminal border of the TMD. In APP for example the main γ-like cleavage that gives rise to the Aβ40 peptide occurs 12 residues away from both ends of the TMD (1.1.3.3 Figure 3, Figure 53). However, the γ-secretase mediates multiple additional cleavages at positions around this site in APP that generate Aβ peptides of different length (Wang et al., 1996). Comparison of known γ-secretase substrates reveals that the main γ-like site is usually located in a region between 11 and 15 residues upstream of the cytosolic and between eight and 12 residues downstream of the luminal membrane border, respectively (Figure 53). APLP2 seems to constitute an exception from this observation as its main γ-like site was found to be very close (six residues) to the N-terminus of the TMD. However, due to uncertainties in the prediction of the exact length of its TMD it is possible that the γ-like site is in fact located 11 residues away from the N-terminal TMD border (Hogl et al., 2011).
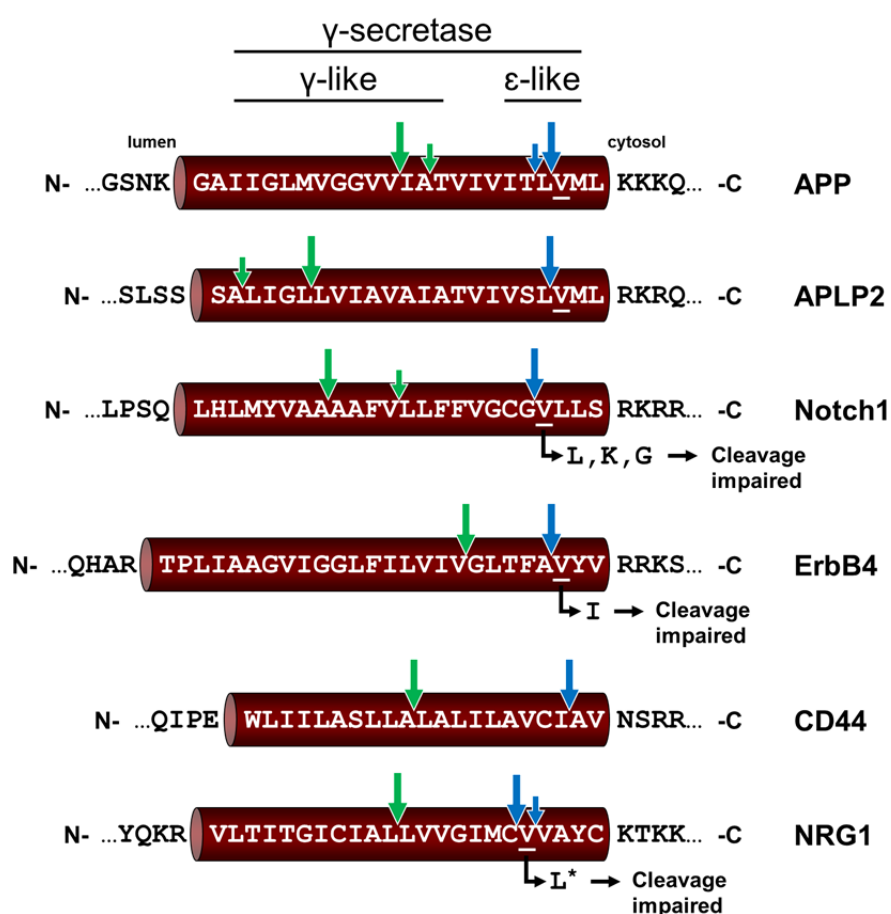
Figure 53. Comparison of identified cleavage sites in the TMD of different γ-secretase substrates. The sequences of the substrates' TMDs are shown and the γ-like (green) and ε-like (blue) cleavage sites are indicated (arrows). Smaller arrows denote the most prominent minor cleavage sites while the multiple less prominent sites were omitted for clarity. The valine residue present at the P1' position of the ε-like cleavage site in most of the substrates is underlined. Artificial mutations at this position that lead to impaired ε-like cleavage in Notch1 and ErbB4 are indicated. The asterisk denotes a schizophrenia-associated mutation in the TMD of NRG1 that also impairs this cleavage. Data from (Fortini, 2002) and the following studies were used for figure assembly: APP (Gu et al., 2001; Sastre et al., 2001), APLP2 (Gu et al., 2001; Hogl et al., 2011), Notch1 (Schroeter et al., 1998; Huppert et al., 2000; Okochi et al., 2002, 2006), ErbB4 (Ni et al., 2001; Lee et al., 2002; Vidal et al., 2005), CD44 (Okamoto et al., 2001; Lammich et al., 2002), NRG1 (Walss-Bass et al., 2006; Dejaegere et al., 2008) and this study.

The main γ-secretase cleavage site identified in NRG1 (between L_{314} and L_{315}) is 11 and 12 residues away from the luminal and cytosolic end of the TMD, respectively, and thus in very good agreement with the observations made for other substrates. Of note, a similar γ-like cleavage between two leucine residues was reported for APLP2 (Hogl et al., 2011) and γ-cleavages with a leucine residue at the P1' position were also found in the TMD of Notch1 (Okochi et al., 2002) and CD44 (Lammich et al., 2002). The additional minor γ-secretase cleavage sites identified in NRG1 (3.6.1 Table 6) cluster around the main site after L_{314} with

the exception of the site after T_{306} which is located only three residues downstream of the luminal membrane interface. Again it is not known whether this reflects genuine cleavage by the γ-secretase or results from the truncation of a longer peptide by an exopeptidase. Alternatively this cleavage may also be caused by the overexpressed BACE1 protease which was previously shown to truncate Aβ peptides after their initial generation (Fluhrer et al., 2003).

A minor caveat to the present investigation is the exclusive use of *in vitro* systems for the determination of the γ-secretase cleavage sites. However, difficulties in the detection of the NRG1 β-peptide and ICD have so far rendered the confirmation of the identified sites in primary cells or *in vivo* impossible. Nevertheless, the employed *in vitro* assays have long been established and faithfully reproduce processing by the γ-secretase (Pinnix et al., 2001; Fukumori et al., 2006). Together with the fact that the identified γ-secretase cleavage sites in the TMD of NRG1 are in good agreement with the sites found in other substrates it is highly likely that they indeed represent genuine γ-secretase cleavage positions that are also used *in vivo*.

4.11.2 Liberation of a β-peptide from the NRG1 type III CTF by the γ-secretase

Cleavage of the NRG1 type III β-CTF by the γ-secretase generates a NRG1 β-peptide that is released from the membrane into the luminal space (4.11.1 Figure 52). Depending on the exact position at which the cleavage occurs, β-peptides ranging from 12 to 22 residues in length are liberated with NRG1-β21 being by far the most prominent species. Despite this heterogeneity, the NRG1 β-peptides appear as a single band on western blot, with an additional but very weak band migrating slightly above (3.6.1 Figure 41). As of yet it is unclear whether this additional band represents a β-peptide of bigger size. However, the finding that also a synthetic recombinant peptide appears as double band on western blot (not shown) argues against this assumption. Alternatively, the hydrophobic nature of the NRG1 β-peptides could cause residual structures in a fraction of the peptides even under the denaturing conditions of the SDS-PAGE that would result in a different migration behavior. Comparison of the hydropathy indices (Kyte and Doolittle, 1982) of different Aβ peptides with the NRG1-β21 peptide indicates that the latter is indeed highly hydrophobic (Table 9). Although comprising only half as many residues, NRG1-β21 is approx. 2.8 times more hydrophobic in nature compared to Aβ42 and still twice as hydrophobic as Aβ42 containing the arctic FAD mutation (E22G) which enhances the hydrophobicity of the Aβ peptide and causes increased aggregation (Nilsberth et al., 2001).

Further support for the likeliness of NRG1 β-peptides to form aggregates comes from the high Zagg value (Tartaglia and Vendruscolo, 2008) calculated for the NRG1-β21 peptide (Table 9). The Zagg value predicts the aggregation propensity of an unfolded peptide and indicates that compared to Aβ42, NRG1-β21 has an even higher tendency to aggregate. Indeed, upon western blot detection both recombinant and NRG1 β-peptides isolated from the supernatant of cells cause a signal at the 16 kDa marker (not shown) indicative of aggregation. Whether these aggregates are already formed within the cell or upon secretion and whether their formation is of any physiological significance is currently unknown. Alternatively they could also constitute an artifact arising during sample preparation prior to electrophoresis.

Peptide	Sequence	Hydropathy index	Aggregation propensity (Z_{agg})
NRG1-β21	MEAEELYQKRVLTITGICIAL	0.55	1.79 ± 0.3
Aβ38	DAEFRHDSGYEVHHQKLVFFAEDVGSNKGAIIGLMVGG	-0.16	0.85 ± 0.1
Aβ40	DAEFRHDSGYEVHHQKLVFFAEDVGSNKGAIIGLMVGG VV	0.06	0.94 ± 0.1
Aβ42	DAEFRHDSGYEVHHQKLVFFAEDVGSNKGAIIGLMVGG VVIA	0.20	0.98 ± 0.1
Aβ42 (E22G)	DAEFRHDSGYEVHHQKLVFFAGDVGSNKGAIIGLMVGG VVIA	0.28	1.12 ± 0.1

Table 9. Predicted hydrophobicities and aggregation propensities of the NRG1 β-peptide and different Aβ species. The amino acid sequences of the different peptides are shown and the hydropathy index as well as the Zagg value is listed for each peptide. A higher number indicates an increased hydrophobicity and a higher tendency to aggregate, respectively. The hydropathy index was calculated according to (Kyte and Doolittle, 1982) and the aggregation propensity was predicted using the zyggregator tool (Tartaglia and Vendruscolo, 2008). Further details are given in (5.2.6).

In contrast to the concomitantly produced ICDs, much less is known about the physiological functions of β-peptides. In fact, with the exception of Aβ, none of the β-peptides have been investigated in detail and their properties and cellular importance remain completely elusive. Thus they could potentially represent anything from a signaling molecule to a pure byproduct generated during the removal of membrane proteins by intramembrane proteolysis.

Most familial AD-associated mutations in PS1 alter the cleavage precision of the γ-secretase at the γ-like site and cause an increase in the generation of Aβ42 (Selkoe, 2001).

Discussion

Similarly, several FAD PS1 mutations shift the ratio of the notch β-peptides Nβ21 and Nβ25 towards the longer species (Okochi et al., 2002). It is tempting to speculate that such a change in cleavage precision which might reflect an impaired processivity of the mutant γ-secretase is a common phenomenon of FAD PS1 mutations and therefore applies to all γ-secretase substrates including NRG1. Comparing the ratios of the NRG1 β-peptides generated by cells harboring different PS1 FAD mutations with the respective profiles of Aβ and Nβ could help determining if the underlying mechanism is indeed of general nature.

In addition to mutations in PS1, several FAD mutations in APP close to the γ-like site but also around the ε-like site cause an increase in the production of the longer Aβ42 (Selkoe, 2001; Cruts et al., 2012). Given that the schizophrenia-associated mutation in the TMD of NRG1 is located at the ε-like site it will be interesting to examine if this mutation similarly affects the profile or amount of the secreted NRG1 β-peptides. If this is the case, such alterations could in theory be used as biomarker for the presence of the schizophrenia-associated mutation or for changes in the turnover of NRG1 in general. However, it is currently unknown whether like Aβ also NRG1 β-peptides are present in blood and CSF in concentrations sufficient for the detection by ELISA (enzyme-linked immunosorbent assay), MS or WB analysis. In order to be able to distinguish between the different NRG1 β-peptide species such detection would also depend on antibodies specific towards the respective C-termini of these peptides which are currently not available. Moreover, although the antibody 10E8 is specific for the N-terminus of the NRG1 β-peptide generated by BACE1-mediated shedding and hence should recognize β-peptides generated by the γ-secretase from all NRG1 isoforms, detection of endogenous NRG1 β-peptides has not been possible so far. The reasons for this are currently unclear but could include the removal of the β-peptide's neoepitope by exopeptidases. Furthermore, the successful detection of β-peptides in the supernatants of primary hippocampal neurons transduced with NRG1 type III (not shown) indicates that endogenously the concentration of these peptides is rather low and not sufficient to be detected by the 10E8 antibody. In this regard it will be interesting to investigate whether NRG1 β-peptides are detectable in mice during embryonic and early postnatal development when both BACE1 and its substrate NRG1 are highly expressed (Meyer et al., 1997; Willem et al., 2006).

Another interesting, yet completely open question concerns the existence of a NRG1 peptide analogous to the p3 peptide of APP (Lichtenthaler et al., 2011) (1.1.2). Such a NRG1 p3-like peptide should particularly be generated in cells with low BACE1 expression in which ADAM10 or ADAM17 constitutes the main sheddase of NRG1. Cleavage of the NRG1 α-CTF

by the γ-secretase should then release p3-like peptides featuring the ADAM cleavage sites as N-termini. Again, the generation of antibodies specific to these neoepitopes or against regions downstream of the ADAM or BACE1 cleavage sites will be necessary to identify such peptides.

In summary this study adds NRG1 to the growing list of γ-secretase substrates for which the precise γ-like cleavage sites have been identified. Comparison of the cleavage sites of different substrates offers the exciting possibility to better understand the mechanism of γ-secretase-mediated processing, its sequence requirements and also allows to investigate if the observed parameters can be generalized. Due to its secretion and hence its assumed presence in blood and CSF, the NRG1 β-peptide has the potential to serve as biomarker for altered γ-secretase processing for example due to PS1 mutations. Furthermore, it could also be used as readout for abnormal cleavage of NRG1 in the context of schizophrenia-associated mutations in NRG1. Except for the V->L mutation in the TMD, most of these mutations are non-coding (1.3.4.2.2) and therefore will most likely not change the proteolytic processing of NRG1 by the γ-secretase. However, the β-peptide could still be an indicator of decreased or elevated NRG1 levels due to disease-linked mutations in general and independent of the specific isoform. All of this will of course depend on the generation of specific antibodies and the establishment of sensitive methods like ELISAs to reliably determine the level of NRG1 β-peptides.

4.11.3 Generation of a NRG1-ICD by the γ-secretase

A significant body of evidence implicates altered signaling by NRG1 in the aetiology of schizophrenia (Mei and Xiong, 2008) (1.3.4.2). Indeed, many schizophrenia-linked SNPs are present in the NRG1 gene, mostly in non-coding regions towards the 5' and 3' end (Mei and Xiong, 2008). These mutations are expected to either change the splicing of NRG1 or affect its level of expression and several studies have reported altered NRG1 mRNA levels in the brain of schizophrenic patients (Hashimoto et al., 2003; Law et al., 2006) (1.3.4.2.2). In addition to the hypothesis that aberrant NRG1 forward signaling through ErbB4 receptors is causative for or contributes to the pathology of schizophrenia (1.3.4.2.1), recently an alternative mechanism relying on the reverse signaling pathway of NRG1 (1.3.3.3) has been proposed. This alternative model is mainly based on two observations: Firstly, the ICD of NRG1 generated through γ-secretase processing was found to act as a transcriptional regulator of synaptic proteins and also affects the levels of AMPA receptors (Bao et al., 2003, 2004; Hancock et al., 2008). Secondly, a schizophrenia-associated SNP was identified in the

Discussion

TMD of NRG1 that leads to a valine to leucine exchange and impairs cleavage by the γ-secretase (Walss-Bass et al., 2006; Dejaegere et al., 2008). Together with the finding that reduced γ-secretase cleavage of NRG1 leads to a schizophrenia-like phenotype in mice (Dejaegere et al., 2008) and the observation that the V->L mutation impairs dendritic development of neurons *in vitro* (Chen et al., 2010a), this is taken as indication that reduced generation of the NRG1-ICD contributes to the pathogenesis of schizophrenia.

Interestingly, as determined by the present study, the V->L mutation is indeed located exactly at the ε-like γ-secretase cleavage site in the TMD of NRG1 (4.11.1 Figure 53). Provided that the mechanism of γ-secretase processing as identified for APP, i.e. initial cleavage at the ε-like site and subsequent cleavage at the γ-like site, also applies to other substrates, this could therefore in fact explain the impaired turnover and subsequent accumulation of the NRG1 CTF harboring this very mutation. Although the exchange of a valine for a leucine is of very conservative nature and only adds one additional CH_2 group to the original residue, such subtle changes at the P1' position have been shown to impair the ε-like cleavage of other γ-secretase substrates before. For instance, substitution of the valine residue at P1' of the ε-like site in Notch1 with leucine, lysine or glycine strongly impaired γ-secretase cleavage and reduced the generation and subsequent signaling of the NICD in cell culture (Schroeter et al., 1998; Huppert et al., 2000) (4.11.1 Figure 53). Further supporting a critical role of this valine residue at P1' for an efficient γ-secretase cleavage, mice homozygous for the V->G mutation in Notch1 die at E10.5 and display alterations resembling the Notch1 KO phenotype (Huppert et al., 2000). Impaired γ-secretase-mediated processing due to a conservative mutation at the P1' position of the ε-like site has likewise been reported for ErbB4. Here, substitution of the valine residue by an isoleucine also diminished γ-secretase cleavage and almost completely abolished generation of the ErbB4 ICD (Vidal et al., 2005) (4.11.1 Figure 53). Importantly, the mutations mentioned above did not alter the expression levels of the Notch1 and ErbB4 holoproteins, their shedding or the abilities of the respective ICDs to regulate the transcription of their target genes. This indicates that the observed effects are indeed solely due to impaired γ-secretase processing and stresses the critical importance of the residue at P1' of the ε-like cleavage site for the efficient generation of ICDs.

The ε-like cleavage site in APP is also localized immediately upstream of a valine residue (Sastre et al., 2001) (4.11.1 Figure 53). However, in contrast to Notch1 and ErbB4 this residue seems to be of minor importance for an efficient ε-like cleavage and liberation of the ICD from APP. Deleting the residues around this site or exchanging them for alanine

residues only modestly affected the overall Aβ generation and cleavage precision of the γ-secretase (Murphy et al., 1999). Similarly, although decreasing the generation of Aβ42, substitution of the valine residue at the P1' position of the ε-like cleavage site for a phenylalanine did not alter the overall Aβ level (Lichtenthaler et al., 1999). Finally and in direct contrast to Notch1, mutation of this valine to a glycine did not impair the generation of AICD suggesting that the ε-like cleavage in APP is not dependent on a valine at the P1' position (Sastre et al., 2001). The effects of more conservative mutations, to isoleucine or leucine as in Notch1 and ErbB4, have not been investigated yet but it is unlikely that such mutations would yield different results.

In summary, the importance of the specific residues surrounding the ε-like site for efficient γ-secretase cleavage seems to strongly vary from substrate to substrate. This is in agreement with the observation that the γ-secretase has only loose primary sequence requirements and that efficient processing depends on a broad range of factors such as length and structure of both the ectodomain and the TMD of the respective substrate. Nevertheless the presence of the schizophrenia-associated V->L mutation directly after the ε-like site in NRG1, together with the fact that such V->L mutations at the same position impair γ-secretase cleavage of other substrates, support the idea that reduced NRG1-ICD generation indeed contributes to the pathogenesis of schizophrenia.

It must be noted, however, that the observed reduction in γ-secretase cleavage of the NRG1 V->L mutant is much smaller compared to the effects reported for the respective mutation in ErbB4 and Notch1 (two-fold compared to at least nine-fold) (Schroeter et al., 1998; Huppert et al., 2000; Vidal et al., 2005; Dejaegere et al., 2008). Moreover, there are currently no data available that confirm the effect of this mutation *in vivo* and directly connect it to the occurrence of schizophrenia-like behavior. So far the importance of the intra-membrane cleavage of NRG1 in the context of altered behavior and memory has been limited to the study of mice heterozygous for a deletion of the whole TMD of NRG1 (NRG1 TM HET mice) (Stefansson et al., 2002; O'Tuathaigh et al., 2006; Duffy et al., 2010). Aside from the fact that the obtained results remain in part controversial (Karl et al., 2011), the NRG1 TM HET mice do not primarily model the consequences of reduced NRG1-ICD generation due to a mutated TMD. Rather, these animals represent a heterozygous knockout of all membrane-bound NRG1 isoforms. Accordingly, mice homozygous for the NRG1 TMD deletion genotype die in utero and phenocopy Ig-NRG1 KO animals (Stefansson et al., 2002). It is therefore debatable if these mice represent a suitable model to investigate the effect of reduced NRG1 intramembrane cleavage and ICD generation in the context of

schizophrenia-like symptoms. Unequivocally linking the V->L NRG1 mutant to such a phenotype *in vivo* will require the generation of a knock-in mouse and its careful investigation with regard to impaired γ-secretase cleavage of NRG1, reduced NRG1-ICD signaling and accompanying behavioral alterations indicative of schizophrenia-like symptoms. In order to evaluate the potential of the NRG1 β-peptide as a biomarker for impaired γ-secretase processing of NRG1 (4.11.2) it will furthermore be necessary to determine whether the V->L exchange after the ε-like site also affects cleavage at the γ-like site and whether this only alters the amount or also the profile of the secreted β-peptides.

Taken together, NRG1 is now one of the few γ-secretase substrates for which both the γ-like and ε-like cleavage sites have been identified. The identification of the ε-like site in particular enables the generation of antibodies specific for the N-terminus of the NRG1-ICD. Such neoepitope antibodies may be used to detect this signaling molecule endogenously within the cell and the nucleus, thereby abolishing the need to work with tagged ICD constructs. Certainly this will assist in the further investigation of the NRG1-ICD's role regarding intracellular signaling, transcriptional regulation and neuronal development. The finding that NRG1, like Notch1 and ErbB4, is cleaved by the γ-secretase directly N-terminal of a valine residue at the ε-like site supports the hypothesis that this residue may indeed be important for efficient ICD generation. It could also explain the impaired turnover of the NRG1 V->L mutant CTF, although further research is clearly needed to unequivocally determine the precise effect of this mutation on the generation of the NRG1 β-peptide and ICD as well as the ensuing cellular consequences.

4.12 Outlook

4.12.1 Ectodomain processing and forward signaling of NRG1 type III

It is now well established that BACE1 regulates myelination in the PNS through the cleavage of NRG1 type III. Although many aspects regarding the mechanism of Schwann cell myelination have been elucidated, several open questions remain. For instance, different lines of evidence suggest that in addition to the juxtacrine signaling of axonal NRG1 type III a paracrine signaling pathway exists that promotes myelination. However, the physiological significance of this novel pathway is unclear and so far no soluble EGF-like domains of NRG1 type III have been detected *in vivo.* Likewise, provided that only juxtacrine signaling occurs, it is unclear how ErbB receptor internalization and deactivation would be facilitated

without another cleavage event that liberates the EGF-like domain from the membrane. In order to address these questions *in vivo* the generation of sensitive antibodies that specifically detect the type III isoform of NRG1 will be crucial. Similarly, further investigation of the identified ADAM cleavage sites as well as the chronological order of cleavage depends on the availability of site-specific antibodies that are able to immunoprecipitate the cleaved NRG1 type III fragments. Future analyses of NRG1 type III signaling *in vivo* will also require the use of KO animals. With regard to the role of the soluble EGF-like domain for example, overexpression of α- and β-sEGF fragments in a NRG1 type III KO zebrafish could shed light onto its ability not only to promote but also to initiate myelination in the PNS. The use of KO animal models will also be required to investigate the compensatory proteolytic mechanisms that are responsible for the residual myelination in BACE1 KO mice. In this perspective it is urgent to much closer investigate the role of ADAM17 in the processing of NRG1 type III and in the regulation of myelination in general. Given the controversy in the literature, the confirmation of the hypermyelination phenotype of ADAM17 KO mice by independent groups is strongly needed. Furthermore, analysis of BACE1/ADAM17 and BACE1/ADAM10 double KO animals would certainly help elucidating the contributions of these different enzymes to myelination *in vivo*. Although technically challenging, the generation and analysis of such double or even triple conditional KO animals will likely be key to the identification of the compensating protease.

Another open question reaching beyond the scope of the present study concerns the differential regulation of NRG1 type I and type III signaling within a single neuron: By mechanisms that are still largely unclear axonal NRG1 type III facilitates Schwann cell myelination, while NRG1 type I controls the formation of muscle spindles at the axon terminal of proprioceptive sensory neurons (Birchmeier and Nave, 2008). It has been argued that the different modes of signaling by type I (exclusively paracrine) and type III (only juxtacrine) mediate these distinct functions but the finding of paracrine NRG1 type III signaling raises doubts as to the validity of this concept. Instead, differential temporal expression or spatial localization could be responsible for the distinct functions of NRG1 type I and type III, respectively, but this has not been investigated so far.

4.12.2 Intramembrane proteolysis and reverse signaling of NRG1 type III

The processing of the NRG1 type III ectodomain generates two fragments that remain membrane-bound after the liberation of the EGF-like domain: a CTF with a large intracellular tail and a short N-terminal fragment (NTF', not to be confused with the NTF that still contains

the EGF-like domain) (4.11.1 Figure 52). It is now well established that the CTF undergoes intramembrane cleavage by the γ-secretase complex and both the γ-like and the ε-like cleavage sites have been identified.

There is also good evidence that the ICD generated through this processing serves as intracellular signal and has physiological significance with regard to transcriptional regulation and neuronal development. The presence of a mutation which impairs γ-secretase cleavage at the ε-like site and which is linked to an increased risk of schizophrenia furthermore implies a function of the NRG1-ICD relevant to the pathogenesis of this disease. However, aside from these descriptive and correlative findings, many mechanistic details remain elusive. For example it is unclear how exactly the binding of the EGF-like domain, which is presented by the NRG1 type III NTF to ErbB receptors, stimulates γ-secretase processing of the CTF. Likewise it is unknown whether only the type III or also other isoforms of NRG1 mediate this kind of reverse signaling and if this is of any physiological relevance. More detailed analyses and the detection and investigation of NRG1-ICD signaling *in vivo* will be required to address these points. The generation of sensitive and cleavage site-specific antibodies will be crucial for this endeavor.

Another aspect that requires further investigation concerns the mechanism by which the NRG1 CTF is processed by the γ-secretase. Although the concept of initial ε-like cleavage and subsequent γ-like cleavage seems universal, this has not been proven for any other substrate besides APP. It would therefore be interesting to analyze the γ-secretase processing of NRG1 with regard to intermediate cleavage sites by means of mass spectrometry as was done for APP (Takami et al., 2009). Similarly, the mechanism by which the schizophrenia-associated V->L mutation impairs γ-secretase cleavage must be evaluated much more carefully. So far, only an accumulation of the mutant NRG1 CTF has been observed (Dejaegere et al., 2008). However, does the leucine residue only impair the ε-like cleavage and the generation of the ICD, while the γ-like cleavage remains unaffected? Or are the two cleavages coupled and the V->L substitution subsequently also leads to a reduced β-peptide generation? Finally, does this mutation, or FAD mutations in PS1, alter the cleavage precision of the γ-secretase within the TMD of NRG1? Answering these questions will require careful measurement of the β-peptide levels by WB or ELISA and mass spectrometric determination and subsequent comparison of the ratios between the different NRG1 β-peptide species.

The detection of endogenous NRG1 β-peptides (and ICDs) constitutes another challenge that must be met in future studies. Most likely this will require the use of (primary)

cells that highly express both NRG1 and BACE1 and furthermore will depend on the availability of antibodies that are more sensitive than the 10E8 antibody used in this study. Alternatively it might be necessary to generate antibodies against internal sequences of the β-peptide or, in case ADAMs are the main sheddases, to focus on the detection of the NRG1 p3-like peptide. The ability to detect fragments resulting from γ-secretase processing of endogenous NRG1 will also be crucial in order to establish the physiological relevance of the schizophrenia-linked V->L mutation. Convincingly the latter can only be achieved by carefully analyzing a V->L knock-in mouse for altered NRG1 CTF turnover and phenotypes considered rodent analogs of schizophrenic symptoms.

Finally, until now, the cellular fate of the NRG1 type III NTF' which is generated through the liberation of the EGF-like domain and possibly another shedding event remains completely unknown. The fact that the NTF' is a type II transmembrane protein suggests that it could be a substrate for intramembrane processing by SPPL proteases (4.11.1 Figure 52). As only a few substrates for these proteases have been identified so far it will be interesting to investigate if the N-terminal TMD of NRG1 type III is indeed cleaved by SPPLs and whether this occurs in a manner comparable to other substrates like TNFα. If in fact both TMDs were subject to intramembrane proteolysis this would identify NRG1 type III as the first reported protein to undergo dual RIP by both the γ-secretase and members of the SPPL family, respectively (4.11.1 Figure 52).

4.12.3 NRG1 type III and Alzheimer's disease therapy

Taken together, the proteolysis of NRG1 type III by both γ-secretase and BACE1 is of physiological significance. However, many of the reported phenotypes resulting from abolished or altered NRG1 type III signaling may be due to deficits during development and much less is known about the consequences in adult organisms. Given that the γ-secretase and BACE1 are prime targets for a potential AD therapy it will be crucial to investigate the consequences of altered NRG1 type III signaling due to chronic treatment with γ-secretase or BACE1 inhibitors during adulthood. Such investigations will require the long-term treatment of animal models with γ-secretase and BACE1 inhibitors and the generation of conditional BACE1 KO animals. The phenotypes observed upon impaired proteolysis of NRG1 type III during adulthood may likely differ from the phenotypes so far reported using conventional KO mice. However, they constitute the potential unwanted side effects of an AD therapy based on the chronic inhibition of γ-secretase and BACE1 and therefore should be taken very seriously.

5   Material and methods

5.1   Material

5.1.1   Laboratory equipment and chemicals

All experiments were performed using standard laboratory equipment. Chemicals were purchased from Merck, Roth and Sigma with analytical grade p.a. unless otherwise stated. The composition of solutions and buffers is stated above the respective method.

5.1.2   Primer

Whenever possible oligonucleotide primers were designed according to the following parameters which were assessed using the CLC Main Workbench 6.6 software (CLC bio): The length of the primers was chosen to be at least 18 bp and, in case of overhanging ends, primers contained at least 15 bp complementary to the template. Primers were designed to have a GC content of 40-60% and similar melting temperatures (Tm between 55 and 80°C). A maximum of four similar consecutive bases was allowed, 3' ends were chosen to contain two or three G's or C's and care was taken to avoid 3' complementarity. The primers for site-directed mutagenesis (5.2.1.2) were designed following the manufacturer's instructions. Finally, the absence of prominent internal secondary structures (such as hairpins) was confirmed and primers were ordered at Sigma or Thermo Scientific. Table 10 provides the names, numbers and sequences of the oligonucleotide primers used during this study.

Table 10

Name	Number	Sequence
NRG VL --> wt_for	p4	GGTCGGCATCATGTGTGTGGTGGCCTACTGC
NRG VL --> wt_rev	p5	GCAGTAGGCCACCACACACATGATGCCGACC
NRGconFurRes_For	p6	CGCGGCCCAGCGGGCCAGGCGCTCCGTAGATTACAAGG
NRGconFurRes_Rev	p7	CCTTGTAATCTACGGAGCGCCTGGCCCGCTGGGCCGCG
AscI.NRG1FlagEGF.F	p8	AGGCGCGCCGTAGATTACAAGGATGACGACGATAAGATAA AGTGTGCGGAGAAGGAGAAAACTTTCTGT

Table 10

Name	Number	Sequence
NRG1.Xhol.R	p9	TCCTCGAGCACGGCCGCCCATGTGA
NRG1TM.Flag.Hindlll.F	p11	TACGAAGCTTGGATTACAAGGATGACGACGATAAGATCATGATGGAAGCGGAGGAACTCTACCAGAAGAGGGTGCTG
FNRGdEdC_HA_Xhol_R	p12	CCTCCTCGAGTTAAGCGTAATCTGGAACATCGTATGGGTAGCCGCCAAGACTCTGCCGAAGCCGATCATGAAGTTTC
0013a0014a_A-G_sense	p13aF	CCAGGCGCGCCGTACGAAAGCTTGATTACAAGGATGACG
0013a0014a_A-G_antisense	p13aR	CGTCATCCTTGTAATCAAGCTTTCGTACGGCGCGCCTGG
NrgHindEGFHA.R	p14	CCGATCATGAAGCTTCTGCCGCTGCTTCTTGG
Nrg_MCS_Hind_F	p15	GCTAGTTAAGCTTGGTACCGAGCTCGGATCCACTAGTC
I +lllNRG_EGF.R	p18	CTCCTTCTCCGCACACTTTATGAGATGGCTGGTCC
I+lllNRG_EGF.F	p19	GGACCAGCCATCTCATAAAGTGTGCGGAGAAGGAG
EcoRl-M-V5.For	p25	GTGGAATTCACCGCCATGGGTAAGCCTATCCCTAACC
V5-ElYSPDM.R	p26	CATGTCTGGGGAATAAATCTCCGTAGAATCGAGACC
ElYSPDM.F	p27	GAGATTTATTCCCCAGACATGTCTGAGGTAGC
lllNRG-BstEll.R	p28	GCATGGTCACCTTGTACTGTAACATGAGC
NrgEGF_F	p29	GCGGAGAAGGAGAAAACTTTCTGTGTGAATGGGGG
Nrg_Bgl_FlagEGF F	p30	CGGGAGATCTCCCGATCCCC
NrgEGF.R	p31	GGCAACGATCACCAGTAAACTCATTTGGGC
SDM 0018aPP.F	p32	CCAGATTACGCTCCTCCTTAACTCGAGGAGGGCC
SDM 0018aPP.R	p33	GGCCCTCCTCGAGTTAAGGAGGAGCGTAATCTGG
Sfil_LIKCNrg.F	p36	GCGGCCCAGCGGGCCAGGCGCTCCGTACTCATAAAGTGCGCGGAGAAGGAG
Xhol_STOPAMA.R	p37	CGATCCTCGAGTCATTAGGCCATAGCGTAATCTGGAACATCGTATGG
Sfil_QTAPNrg.F	p38	GCGGCCCAGCGGGCCAGGCGCTCCGTACAAACTGCTCCTAAACTTTCCAC
Xhol_STOPFEIGL.R	p39	CGATCCTCGAGTCATTAAAATTCAATCCCAAGATGCTTGTAGAAGCTGG
SDM_del_0058.For	p51	GCTTCTACAAGCATCTTGGGTAATGACTCGAGGAGGGCC
SDM_del_0058.Rev	p52	GGCCCTCCTCGAGTCATTACCCAAGATGCTTGTAGAAGC

Name	Number	Sequence
SDM_del0060.For	p55	GTTCCAGATTACGCTATGGCCTAATGACTCGAGGAGGGC C
SDM_del0060.Rev	p56	GGCCCTCCTCGAGTCATTAGGCCATAGCGTAATCTGGAAC
NheI_V5IIINRG1.For	p57	GATCGCTAGCACCATGGGTAAGCCTATCCCTAAC
IIINRG1STOP_EcoRI.Rev	p58	GATCGAATTCTCATTATACAGCAATAGGGTCTTGGTTAG

Table 10. List of oligonucleotide primers. For each primer the name, the internal number (pXX) and the nucleotide sequence is given.

5.1.3 Plasmids

The vectors and constructs used in the present study are listed in Table 11 which also details their construction. The NRG1 isoform designated NRG1 type III corresponds to the isoform NRG1 type III β1a (GenBank: AF194438.1) from rattus norvegicus. This sequence was used throughout the entire study. The NRG1 isoform designated NRG1 type I corresponds to the NRG1 type I β1a (EMBL-Bank: AY995221) from rattus norvegicus.

Table 11

Name	Number	Expressed cDNA	Vector backbone	Cloning	**Ref./ Provider
pSecTag2A	pl23	Mammalian protein expression vector			Invitrogen
pcDNA4/ Myc-HisA	pl20	Mammalian protein expression vector			Invitrogen
psPAX2		2nd generation lentiviral packaging plasmid			Dr. D. Edbauer
pVSVg		Lentiviral envelope vector			Dr. D. Edbauer
AD149 FhSynW2 Δzeo	pl36	Lentiviral expression vector with human synapsin promoter			Dr. D. Edbauer
GFP (lentivirus)		GFP	AD149 FhSynW2- Δzeo		Dr. D. Edbauer

Table 11

Name	Number	Expressed cDNA	Vector backbone	Cloning	**Ref./ Provider
BACE1	e1	Human BACE1	pcDNA4/ Myc-HisA		Capell et al., 2000
ADAM10	e3	Bovine ADAM10	pcDNA3.1/ Hygro(-)		Wild-Bode et al., 2006
ADAM17	e2	Human ADAM17	pDC406		Black et al., 1997
NRG1 type III	0003	NRG1 type III with HA tag after the EGF-like domain	pcDNA4/ Myc-HisA		Dr. M. Willem
V5-IIINRG1	0045a	NRG1 type III with N-terminal V5 tag	pcDNA4/ Myc-HisA	Insert: Cloned from 0046 via EcoRI, BstEII; ligated into 0045	This study
V5-IIINRG1-HA	0046	NRG1 type III with N-terminal V5 tag and HA tag after the EGF-like domain	pcDNA4/ Myc-HisA	Insert: Fusion of PCR1: p25+p26, template MV01 and PCR2: p27+p28, template 0003; ligated into 0003 via BstEII, EcoRI	This study
	MV01	Flag tagged N-terminus of NRG1 type III (2-114) with C-terminal Flag tag	pcDNA3.1/ Hygro(-)		M. Voss
V5-IIINRG1-HA (lentivirus)	0061	NRG1 type III with N-terminal V5 tag and HA tag after the EGF-like domain	AD149 FhSynW2-Δzeo	Insert: PCR with p57+p58, template 0046; ligated into pl36 via NheI, EcoRI	This study
NRG1ΔNT	0047	N-terminally truncated NRG1 type III (236-700) with N-terminal Flag tag	pSecTag 2A*	Insert: Fusion of PCR1: p29+p14, template 0045 and PCR2: p30+p31, template 0040a; ligated into 0040a via BglII, HindIII	This study
	0045	NRG1 type III w/o tag	pcDNA4/ Myc-HisA	Insert: Fusion of PCR1: p15+p18, template 0003 and PCR2: p14+19, template 0001; ligated into 0003 via 2x HindIII	This study
	0001	NRG1 type I with N-terminal HA tag	pSecTag2A		Dr. M. Willem

Table 11

Name	Number	Expressed cDNA	Vector backbone	Cloning	**Ref./ Provider
	0040a	N-terminally truncated NRG1 type IIII (236-700) with N-terminal Flag tag and HA tag after the EGF-like domain	pSecTag 2A*	Site-directed mutagenesis: p6+p7, template 0040	This study
	0040	N-terminally truncated NRG1 type III (236-700) with N-terminal Flag tag and HA tag after the EGF-like domain	pSecTag2A	Insert: Cloned from 0009 via AscI, HindIII; ligated into 0013	This study
	0009	N- and C-terminally truncated NRG1 type III (236-358) with N-terminal Flag tag and HA tag after the EGF-like domain	pSecTag2A	Insert: PCR with p8+p9, template 0005; ligated into pl23 via AscI, XhoI	This study
	0005	N- and C-terminally truncated NRG1 type III (234-358) with N-terminal HA tag and HA tag after the EGF-like domain	pSecTag2A		Dr. M. Willem
	0013	N-terminally truncated NRG1 type III (294-700) with N-terminal Flag tag	pSecTag2A	Insert: Cloned from 0007 via 2xHindIII; ligated into 0001	This study
	0007	N- and C-terminally truncated NRG1 type III (294-358) with N-terminal Flag tag	pSecTag2A		Dr. M. Willem
FNRGΔC-HA	0018b	N- and C-terminally truncated NRG1 type III (294-334) with N-terminal Flag and C-terminal HA tag followed by PP	pSecTag2A	Site-directed mutagenesis: p4+p5, template 0018a	This study

Name	Number	Expressed cDNA	Vector backbone	Cloning	**Ref./Provider
	0018a	N- and C-terminally truncated NRG1 type III (294-343) with N-terminal Flag and C-terminal HA tag followed by PP	pSecTag2A	Site-directed mutagenesis: p32+p33, template 0018	This study
	0018	N- and C-terminally truncated NRG1 type III (294-343) with N-terminal Flag and C-terminal HA tag	pSecTag2A	Insert: PCR with p11+p12, template 0013a; ligated into pl23 via HindlII, Xhol	This study
	0013a	N-terminally truncated NRG1 type III (294-700), lacking an internal HindlII site, with N-terminal Flag and C-terminal HA tag	pSecTag2A	Site-directed mutagenesis: p13aF+p13aR, template 0013	This study
α-sEGF (α-sEGF-A283)	0051	N- and C-terminally ADAM17-cleaved, HA tagged soluble EGF-like domain (235-283)	pSecTag 2A*	Insert: PCR with p36+p37, template 0003; ligated into 0047 via Sfil, Xhol	This study
β-sEGF (β-sEGF-F293)	0052	N- and C-terminally BACE1-cleaved, HA tagged soluble EGF-like domain (218-293)	pSecTag 2A*	Insert: PCR with p38+p39, template 0003; ligated into 0047 via Sfil, Xhol	This study
β-sEGF-G290	0058	N-terminally BACE1-cleaved, HA tagged soluble EGF-like domain terminating at G290 (218-290)	pSecTag 2A*	Site-directed mutagenesis: p51+p52, template 0052	This study
β-sEGF-A283	0060	N-terminally BACE1-cleaved, C-terminally ADAM17-cleaved, HA tagged soluble EGF-like domain (218-283)	pSecTag 2A*	Site-directed mutagenesis: p55+p56, template 0052	This study

Table 11. Overview of plasmids and constructs. The list provides each construct's name and number as well as details of its construction. The numbering of the amino acid residues in the description of the cDNA is based on the NRG1 β1a type III isoform and the primers are given with their respective numbers (pXX, 5.1.2 Table 10). The constructs designated only with a number but not with a name were not used in the experiments described in the result section but represent intermediate steps during cloning. Most of them were, however, used in other (pilot) experiments not detailed in this

work. *The suboptimal furin cleavage site RAVRSL after the secretion signal sequence in pSecTag2A was optimized to RARRSV. **Affiliations: Dr. D. Edbauer, German Center for Neurodegenerative Diseases, DZNE, Munich; Dr. M. Willem & M. Voss, Adolf-Butenandt-Institute, Biochemistry, Ludwig-Maximilians-University, Munich.

5.1.4 Inhibitors

Table 12 lists the inhibitors used during this work. All compounds were dissolved in DMSO and stored as specified by the provider. Cells were treated at the indicated concentrations for 12-24 h under standard cell culture conditions (5.2.2.1).

Table 12

Name	Full name	Drug target/ application	Conc.	Ref./ Provider
DAPT/ LY-374973	LY-374973, N-[N-(3,5-Difluorophenacetyl)-L-alanyl]-S-phenylglycine t-butyl ester	γ-secretase inhibitor	10 μM	Boehringer-Ingelheim
MerckA/ γ-Secretase Inhibitor X/ L-685,458	L-685,458, {1S-Benzyl-4R-[1-(1S-carbamoyl-2-phenethyl-carbamoyl)-1S-3-methylbutyl-carbamoyl]-2R-hydroxy-5-phenylpentyl}carbamic Acid tert-butyl Ester	γ-secretase inhibitor	1 μM (for *in vitro* assay only)	Calbiochem
C3/ β-secretase inhibitor IV/ MerckIV	N-[(1S,2R)-3-(cyclopropylamino)-2-hydroxy-1-(phenylmethyl)propyl]-5-[methyl(methylsulfonyl)amino]-N'-[(1R)-1-phenylethyl]-1,3-Benzenedicarboxamide	β-secretase inhibitor	5-10 μM	Axon Medchem, Merck
GM6001/ Galardin/ Ilomastat	N-[(2R)-2-(hydroxamido-carbonylmethyl)-4-methyl-pentanoyl]-L-tryptophan methylamide	Broad-spectrum inhibitor of matrix metallo-proteinases and ADAMs	25 μM	Enzo Life Sciences
GI/ GI254023X	(2R)-N-[(1S)-2,2-Dimethyl-1-[(methylamino)carbonyl]-propyl]-2-[(1S)-1-[formyl-(hydroxy)amino]ethyl]-5-phenylpentanamide	ADAM10 inhibitor (100-fold selectivity over ADAM17)	5 μM	Dr. B. Schmidt*

continues on the following page

Name	Full name	Drug target/ application	Conc.	Ref./ Provider
GL/ GL 506–3		ADAM17 inhibitor (ADAM inhibitor with preference for ADAM17 over ADAM10)	5 µM	Galderma
BG/ BADGP	Benzyl-2-acetamido-2-deoxy-D-galactopyranoside	O-GlcNAc (OGT) trans-ferase inhibitor, blocks incorporation of glucos-amine into O-glycans	4 mM	Merck

Table 12. List of inhibitors. The inhibitors used in this study are listed with their abbreviated or brand name as well as with the full name of the compound (if known). Each inhibitor's target and the concentration used for treatment is given. *Affiliation: Dr. B. Schmidt, Technical University of Darmstadt.

5.1.5 Cell lines

The different continuous cell lines used in this study were cultivated as described in 5.2.2.1 and are listed below (Table 13).

Table 13

Name	Description	Resistance	Culture medium
HEK293T	Human embryonic kidney (HEK) cells (ATTC CRL-1573)	None	Standard medium: DMEM high glucose + GlutaMAX, 10% FCS, 1% P/S
HEK293 PS1 wt	HEK293 cells stably expressing human PS1 (Steiner et al., 1998)	Zeocin	Selection medium: DMEM high glucose + GlutaMAX, 10% FCS, 1% P/S, 200 µg/ml zeocin
HEK293 PS1 DN	HEK293 cells stably expressing human PS1 D385N (Steiner et al., 2001)	Zeocin	Selection medium: DMEM high glucose + GlutaMAX, 10% FCS, 1% P/S, 200 µg/ml zeocin
CHO wt	Chinese hamster ovary (CHO) cells, CHO-K1 (ATCC CCL-61)	None	Medium with NEAA: DMEM high glucose + GlutaMAX, 10% FCS, 1% P/S, non-essential amino acids

Name	Description	Resistance	Culture medium
CHO ldlD	Chinese hamster ovary (CHO) cells lacking LDL receptor activity and deficient in UDP-galactose and UDP-N-acetylgalactosamine (GalNAc) 4-epimerase (Kingsley et al., 1986)	None	Medium with NEAA: DMEM high glucose + GlutaMAX, 10% FCS, 1% P/S, non-essential amino acids
MCF-7	Human mammary gland cells (ATCC HTB-22)	None	Standard medium: DMEM high glucose + GlutaMAX, 10% FCS, 1% P/S

Table 13. List of continuous wild-type and transgenic cell lines. The overview provides the name, a brief description, the resistance gene as well as the culture medium of each cell line. Where applicable, the American Type Culture Collection (ATCC) number of the cell line or a reference is given. A more detailed description of the culture media can be found below (5.2.2.1).

5.1.6 Antibodies

The following monoclonal and neoepitope-specific antibodies were generated in collaboration with Dr. Elisabeth Kremmer (Institute of Molecular Immunology, Helmholtz Center, Munich) by immunization with the respective peptides: 4F10, rat, SFYKHLGIEF; 10E8: mouse, MEAEELYQKR; 7E6: mouse, QTAPKLSTS. All primary antibodies as well as antibody coated agarose beads used in this study are provided in Table 14. The secondary antibodies used for immunodetection are listed in Table 15.

Table 14

Antibody	Antigen	Type	Dilution	Supplier
4F10	Neoepitope N-terminal of BACE1 cleavage site (F293) in NRG1 type III	Rat, monoclonal, hybridoma supernatant	WB: 1:40 IP: 10-40 µl/ml	Dr. M. Willem, Dr. E. Kremmer*
7E6	Neoepitope C-terminal of BACE1 cleavage site (L217) in NRG1 type III	Mouse, monoclonal, hybridoma supernatant	WB: 1:40 IP: 10-40 µl/ml	Dr. M. Willem, Dr. E. Kremmer*
10E8	Neoepitope C-terminal of BACE1 cleavage site (F293) in NRG1 type III	Mouse, monoclonal, hybridoma supernatant	WB: 1:40 IP: 10-40 µl/ml	Dr. M. Willem, Dr. E. Kremmer*
β-actin (A5316)	β-actin	Mouse, monoclonal, purified	WB: 1:5000	Sigma

continues on the following page

Antibody	Antigen	Type	Dilution	Supplier
ADAM10 (422751)	ADAM10 (aa 735-749)	Rabbit, polyclonal, purified	WB: 1:4000	Calbiochem
ADAM17 (ab39162)	ADAM17 (aa 807-823)	Rabbit, polyclonal, purified	WB: 1:2000	Abcam
Akt (pan) (C67E7)	Akt (C-terminus)	Rabbit, monoclonal, purified	WB: 1:3000	Cell Signaling
Phospho-Akt (Ser473) (D9E) XP	Phospho-Akt (Ser473)	Rabbit, monoclonal, purified	WB: 1:2000	Cell Signaling
BACE1 (AB5940)	BACE1 (C-terminus)	Rabbit, polyclonal, purified	WB: 1:1000	Millipore
Calnexin	Calnexin (N-terminus)	Rabbit, polyclonal, purified	WB: 1:5000	Enzo Life Sciences
Heregulin/NDF/GGF Neuregulin Ab-2 (lot: 276P1002l)	NRG EGF-like domain	Rabbit, polyclonal, purified	WB: 1:2000	Thermo Scientific
ErbB3 (C-17) sc-285	ErbB3 (C-terminus)	Rabbit, polyclonal, purified	WB: 1:1000	Santa Cruz
Phospho-ErbB3 (Tyr1328) sc-135654	Phospho-ErbB3 (Tyr1328)	Rabbit, polyclonal, purified	WB: 1:1000	Santa Cruz
Anti-Flag F7425	Flag tag	Rabbit, polyclonal, purified	WB: 1:5000	Sigma
Anti-Flag M2 Affinity Gel	Flag tag	Mouse, monoclonal, purified, agarose conjugated	IP: 15-30 µl/sample	Sigma
Anti-HA-HRP (3F10)	HA tag	Rat, monoclonal, purified, HRP conjugated	WB: 1:2000	Roche
Anti-HA Agarose Conjugate HA-7	HA tag	Mouse, monoclonal, purified, agarose conjugated	IP: 15-30 µl/sample	Sigma
NRG1 α/β 1/2 (C-20) sc-348 G1808	NRG1 C-terminus	Rabbit, polyclonal, purified	WB: 1:10000	Santa Cruz
Anti-V5	V5 tag	Mouse, monoclonal, purified	WB: 1:5000	Life Technology

Table 14. List of primary and agarose conjugated antibodies used in this study. For each antibody the name, the antigen and the type are given. The dilution used for western blotting or immunoprecipitation is indicated. *Affiliations: Dr. M. Willem, Adolf-Butenandt-Institute, Biochemistry, Ludwig-Maximilians-University, Munich; Dr. E. Kremmer, Institute of Molecular Immunology, Helmholtz Center, Munich.

Antibody	Antigen	Type	Dilution	Supplier
Anti-rabbit IgG HRP (W401B)	Rabbit IgG (H+L)	Goat, polyclonal, purified, HRP conjugated	WB: 1:10000	Promega
Anti-mouse IgG HRP (W402B)	Mouse IgG (H+L)	Goat, polyclonal, purified, HRP conjugated	WB: 1:10000	Promega
Anti-rat IgG HRP (SC2006)	Rat IgG (H+L)	Goat, polyclonal, purified, HRP conjugated	WB: 1:4000	Santa Cruz

Table 15. List of secondary antibodies. Each antibody is listed with its name, epitope and type. Additionally the dilution used for immunodetection is indicated.

5.2 Methods

5.2.1 Molecular biology and recombinant DNA techniques

5.2.1.1 Polymerase chain reaction (PCR)

Polymerase chain reactions were performed using the primers and cDNA plasmids described in 5.1.2 & 5.1.3 and typically set up as follows.

10 µl	Pwo-buffer (10x, PeqLab)
1 µl	dNTP-Mix (10 mM, Roche)
1 µl	forward primer (100 pmo/µl)
1 µl	reverse primer (100 pmo/µll)
20 ng	template DNA
1 µl	Pwo-DNA-Polymerase (1 U/µl, PeqLab)
Ad 100 µl	ddH$_2$O

All PCR reactions were prepared on ice and performed in a pre-heated thermocycler ("hot-start") using the following program.

	Cycles	Temperature	Duration
Initial denaturation	1	95°C	5 min
Amplification	30		
Denaturation		95°C	30 sec
Annealing		55°C	30 sec
Extension		72°C	250 bp/min
Final extension	1	72°C	10 min
Storage	1	4°C	ever

If necessary, the annealing temperature was adjusted to the melting temperature of the primers (usually starting 5°C below the respective Tm). The PCR product was purified by subjecting the entire PCR sample to agarose gel electrophoresis and gel extraction as described below (5.2.1.5).

5.2.1.2 Site-directed mutagenesis (SDM)

In order to introduce specific mutations and to delete or insert multiple amino acids into a cDNA construct, the QuickChange Site-Directed mutagenesis protocol (Agilent) was used. The site-directed mutagenesis primers were designed following the manufacturer's suggestions and are listed in 5.1.2 Table 10. A typical site-directed mutagenesis PCR reaction was set up as follows.

5 µl	Cloned Pfu reaction buffer (10x, Agilent)
50 ng	template DNA
1.3 µl	forward primer (10 pmol/µl)
1.3 µl	reverse primer (10 pmol/µl)
1 µl	dNTP-Mix (10 mM, Roche)
1 µl	PfuTurbo Polymerase (2.5 U/µl, Agilent)
Ad 50 µl	ddH$_2$O

All PCR reactions were prepared on ice and performed in a pre-heated thermocycler ("hot-start") using the following program.

	Cycles	Temperature	Duration
Initial denaturation	1	95°C	30 sec
Amplification	12-18*		
Denaturation		95°C	30 sec
Annealing		55°C	1 min
Extension		68°C	500 bp/min
Final extension	1	68°C	10 min
Storage	1	4°C	ever

*Point mutations: 12 cycles; single amino acid exchange: 16 cycles; multiple amino acid deletions or insertions: 18 cycles

Following the PCR 1 µl of Dpn I restriction enzyme (20 U/µl, NEB) was directly added to the reaction and the sample was mixed and incubated at 37°C for 1.5 h in order to digest the parental (non-mutated) cDNA. Afterwards 1 µl of the digest was used to transform chemically competent E.coli DH5α as described in 5.2.1.8 with the exception that only 50 µl of competent bacteria per sample were used. After incubation on an LB agar plate containing

the appropriate antibiotic for selection, six single clones were picked and their DNA was isolated using the NucleoSpin Plasmid kit (Macherey-Nagel) ("Miniprep", 5.2.1.9). The presence of the desired mutation was confirmed by sequencing (5.2.1.10).

5.2.1.3 Enzymatic restriction of DNA

All restriction enzymes, reaction buffers and additives were obtained from Fermentas, Roche or New England Biolabs (NEB) and were used according to the manufacturer's instructions. For analytical purposes 10 µl of a small-scale plasmid preparation ("Miniprep", 5.2.1.9) and for preparative restrictions (for subsequent ligations) 17 µl of a cleaned up PCR product (5.2.1.5) or 1 µl (≈ 1 µg DNA) of a large-scale plasmid preparation ("Maxiprep", 5.2.1.9) were incubated with 1-5 U of the respective enzyme(s) in the appropriate reaction buffer. Restrictions were performed in a final volume of 20 µl for at least 2 h at the temperature specified by the enzyme's manufacturer.

5.2.1.4 Dephosphorylation of DNA

To prevent re-ligation of the linearized DNA plasmid (especially when restriction was performed with a single enzyme) the terminal phosphate at the 5' end was removed through treatment with alkaline phosphatase. 3 µl of 10x rAPid reaction buffer and 1 U of rAPid alkaline phosphatase (1 U/µl, both Roche) were directly added to a preparative restriction sample (20 µl, 5.2.1.3) which was then adjusted to a total volume of 50 µl with ddH$_2$O. Dephosphorylation was performed for 1 h at 37°C and the DNA was purified via gel electrophoresis and gel extraction afterwards (5.2.1.5).

5.2.1.5 Agarose gel electrophoresis and gel extraction of DNA

TAE buffer	40 mM Tris/HCl pH 8.0, 20 mM NaAcetat, 2 mM EDTA in ddH$_2$O, pH 8.0
DNA loading buffer 10x	100 mM Tris pH 9.0, 10 mM EDTA, 50% glycerol, 0.5% Orange G in ddH$_2$O, pH 9.0

DNA was separated and analyzed using agarose gel electrophoresis with 0.8-2.0% agarose gels (depending on the size of the DNA fragment). Agarose was dissolved in TAE buffer by heating and supplemented with 0.3 µg/ml ethidium bromide prior to casting of the gel. The DNA samples were mixed with loading buffer and electrophoresis was performed in TAE buffer at a constant voltage of 120 V using the 100 bp or 1 Kb DNA Ladder (both Invitrogen) as standard. After electrophoresis the DNA was visualized under UV light and, if required, separated DNA fragments were cut from the agarose gel and subsequently purified using the

Nucleo Spin Extract II kit (Macherey-Nagel). Purification was done according to the manufacturer's instructions with the following modifications: 400 µl of the buffer NT were used to dissolve the agarose slice without determining its weight and the DNA was eluted with 80 µl ddH$_2$O.

5.2.1.6 Ligation

After purification via agarose gel electrophoresis DNA fragments were ligated into linearized, dephosphorylated vectors using the T4 DNA ligase (5 U/µl, Thermo Scientific). Without determining the DNA concentrations, 2 µl of the vector and 8 µl of the insert as eluted after agarose gel extraction (5.2.1.5) were incubated with 5 U T4 DNA ligase in a final volume of 20 µl containing the T4 DNA ligase buffer (Thermo Scientific). Ligations were performed for at least 2 h at RT and 5 µl of the ligation sample were used to transform competent E.coli (5.2.1.8).

5.2.1.7 Preparation of competent bacteria

Transformation buffer	50 mM CaCl$_2$, 10 mM PIPES, pH 6.6, 15% glycerol in ddH$_2$O, sterile filtered
LB medium	1% Bacto Tryptone, 0.5% yeast extract (both Becton Dickinson), 17.25 mM NaCl in ddH$_2$O, pH 7.0, autoclaved at 1.2 bar, 120°C for 20 min

Chemically competent Escherichia coli (E.coli) DH5α cells were prepared using a modified calcium chloride method. 3 ml of LB medium were inoculated with E.coli and incubated (2-3 h, 37°C, agitation) until an optical density of OD$_{600}$ = 0.2 was reached. Subsequently this pre-culture was used to inoculate 200 ml of LB medium which were again incubated to an OD$_{600}$ of 0.2. Afterwards the bacterial culture was divided into 50 ml aliquots and chilled on ice for 10'. From now on all subsequent steps were performed at 4°C. The bacteria were collected by centrifugation (10', 2000 g at 4°C) and each pellet was resuspended in 25 ml of ice-cold transformation buffer. The suspensions were incubated on ice for 20', centrifuged again (10', 2000 g at 4°C) and finally each pellet was resuspended in 2.5 ml ice-cold transformation buffer. The bacteria were divided into 100 µl aliquots and then immediately frozen in liquid nitrogen and stored at -80°C until use.

5.2.1.8 Transformation of bacteria

LB medium	1% Bacto Tryptone, 0.5% yeast extract (both Becton Dickinson), 17.25 mM NaCl in ddH$_2$O, pH 7.0, autoclaved at 1.2 bar, 120°C for 20 min
LB$_{AMP}$ medium	LB medium supplemented with ampicillin (100 µg/ml, Roth)
LB agar plates	LB medium supplemented with agar (15 g/l, Becton Dickinson), autoclaved at 1.2 bar, 120°C for 20 min. If desired, ampicillin was added after cooling.

An aliquot (100 µl) of chemically competent E.coli DH5α (5.2.1.7) was thawed on ice and 5 µl of a standard ligation (5.2.1.6) or 20-50 ng plasmid were added. The suspension was mixed gently, incubated on ice for 20' and then heat shocked for 30'' at 42°C. After chilling on ice for 2', 500 µl LB medium (w/o AMP) were added and the bacteria were incubated for 30' (37°C with agitation). 50 µl and 300 µl of the suspension were spread onto pre-warmed LB$_{AMP}$ agar plates using glass beads and the plates were incubated o/n at 37°C. Clones were selected by picking single, separated colonies from the plates and 3 ml of LB$_{AMP}$ medium were inoculated for subsequent isolation of DNA (5.2.1.9). Positive clones were identified by analytical digest (5.2.1.3) and sequencing (5.2.1.10).

5.2.1.9 Plasmid DNA preparation

LB$_{AMP}$ medium	LB medium (5.2.1.8) supplemented with ampicillin (100 µg/ml, Roth)

Small scale, analytical plasmid preparation ("Miniprep")

For analytical purposes small amounts of plasmid DNA were purified from transformed bacteria using the NucleoSpin Plasmid kit (Macherey-Nagel). The respective E.coli clone was grown in 3 ml of LB$_{AMP}$ medium o/n (37°C with agitation) and 1.5 ml of the suspension were used for DNA isolation following the manufacturer's instructions. Plasmid DNA was eluted twice (with 2x 25 µl of buffer AE after 3' incubation at RT) and was used for analytical restriction digest (10 µl) or sequencing (30 µl).

Large scale, preparative plasmid preparation ("Maxiprep")

To obtain plasmid DNA amounts sufficient for further cloning or transfection of eukaryotic cells, the NucleoBond Xtra Maxi EF plasmid purification kit (Macherey-Nagel) was used. 300 ml of LB$_{AMP}$ medium were inoculated with 10 µl of an E.coli culture remaining from a previous small scale plasmid preparation or directly with a clone picked from a selection plate. After o/n incubation (37°C with agitation) the bacteria were harvested by centrifugation (15', 6000

g at 4°C) and plasmid DNA was isolated according to the manufacturer's instructions. The DNA was dissolved in 400 µl of endotoxin-free H_2O (provided with the kit) by incubation o/n at 4°C and the concentration and purity were determined by UV spectrophotometry using a NanoPhotometer (Implen). The DNA concentration was usually adjusted to 1.0-1.5 µg/µl and aliquots were kept at 4°C and -20°C for short-term and long-term storage, respectively.

5.2.1.10 Sequencing of DNA

DNA sequencing reactions were performed by GATC Biotech AG using Sanger sequencing on the 3730xl DNA analyzer (Applied Biosystems). The sequencing data were analyzed with the CLC Main Workbench 6.6 software (CLC bio).

5.2.2 Cell culture methods

5.2.2.1 Cultivation of continuous cell lines

PBS	140 mM NaCl, 10 mM Na_2HPO_4, 1.75 mM KH_2PO_4, 2.7 mM KCl in ddH_2O, pH 7.4, autoclaved at 1.2 bar, 120°C for 20 min
Trypsin-EDTA	0.05% Trypsin, 0.53 mM EDTA-4Na (Gibco)
Penicillin/Streptomycin	5000 U/ml penicillin, 5 mg/ml streptomycin (100x, Gibco)
Standard medium	Dulbecco's modified Eagle's medium (DMEM) high glucose + GlutaMAX (Gibco) supplemented with 10% fetal calf serum (Sigma) and 1% penicillin/streptomycin
Selection media	Standard medium supplemented with 200 µg/ml zeocin (Gibco)
Medium with NEAA	Standard medium supplemented with non-essential amino acids (NEAA) solution (100x, Gibco)

Stable cell lines (5.1.5 Table 13) were cultured in the appropriate medium using a standard incubator set to 37°C, 5% CO_2 and 95% relative humidity. For passaging and propagation, cells were washed once with PBS and incubated with trypsin solution until the cell layer detached from the culture dish. Cells were collected in standard medium, pelleted by centrifugation (5', 1000 g at RT) and resuspended in fresh medium. The cell suspension was then transferred to new culture dishes (containing appropriate medium) to achieve the desired dilution.

5.2.2.2 Cryopreservation of cell lines

Freezing medium   Fetal calf serum (Gibco) supplemented with 10% DMSO (Sigma)

Cells were collected from a 10 cm culture dish grown to 90% confluency as described above (5.2.2.1). The cell pellet was carefully resuspended in 1.5 ml of freezing medium and two times 0.75 ml of the suspension were transferred into micro cryotubes (Sarstedt). Cells were frozen at -80°C using an isopropanol cryo 1°C freezing container (Nalgene) and stored in vapor phase nitrogen.

Cells were thawed by placing the cryotube in a water bath (37°C) and then immediately diluted in 10 ml of culture medium. After centrifugation (5', 1000 g at RT), the cells were resuspended in standard culture medium (5.2.2.1) and transferred to a culture dish. If required, medium was supplemented with antibiotics as soon as cell growth was apparent.

5.2.2.3 Primary Schwann cell culture

Trypsin solution   2.5% trypsin in dH_2O (both Gibco)

Collagenase solution   1.0% collagenase (Worthington) in dH_2O (Gibco)

D-medium   Dulbecco's modified Eagle's medium (DMEM) high glucose, supplemented with 10% fetal bovine serum, 1% penicillin/strepto-mycin and 2 mM glutamine (all Gibco)

Poly-L-lysine solution   1.0% poly-L-lysine hydrobromide (Sigma) in dH_2O (Gibco)

Ara-C   Cytosine-β-arabino furanoside hydrochloride (Ara-C, Sigma) in dH_2O, sterile filtered

Forskolin   2 mM forskolin (Sigma) in 100% EtOH

Primary Schwann cells were provided by Dr. Alessio Colombo and Dr. Stefan F. Lichtenthaler (German Center for Neurodegenerative Diseases, DZNE, Munich) and were prepared as described previously (Einheber et al., 1997). Briefly, sciatic nerves were isolated from Sprague-Dawley rats (postembryonic day 3) and collected in ice-cold Leibovitz's L-15 medium (Gibco). After centrifugation (3', 100 g at 4°C), the supernatant was decanted and 8 ml of pre-warmed L-15 medium as well as 1 ml of pre-warmed collagenase and trypsin solution were added to the isolated nerves. The sample was mixed gently, incubated for 30' at 37°C and then spun for 10' (800 g at RT). The pellet was washed twice with 10 ml of D-medium and cells were dissociated mechanically by careful pipetting. Approx. $4x10^5$ cells were seeded into 6 cm culture dishes coated with poly-L-lysine and cultured in D-medium

using a standard incubator set to 37°C, 5% CO_2 and 95% relative humidity. On the following day the cells were washed twice with HBBS (Gibco) and incubated for two days with D-medium containing 10 µM Ara-C to eliminate proliferating cells. After two washes with HBBS the Schwann cells were recovered for two days in D-medium and on day 6 fibroblasts were eliminated using complement-mediated cellular cytotoxicity. To this end the cells were washed once with HBBS and once with D-medium containing 20 mM HEPES (Gibco) and then incubated for 10' to 15' with D-medium containing 20 mM HEPES and 40 µl of α-Thy1.1 antibody (Serotec). Subsequently 400 µl of complement rabbit serum (Calbiochem) were added and the cells were again incubated for 30' to 40'. Afterwards the Schwann cells were cultured in D-medium containing 2 µM forskolin and 10 µg/ml pituitary extract (Sigma) to allow proliferation. The medium was replaced every other day and proliferation was stopped one day before the experiment.

5.2.2.4 Primary neuron culture

Poly-D-lysine solution	1.5% poly-D-lysine hydrobromide (Sigma) in 0.1 M borate buffer
Borate buffer	40 mM boric acid, 10 mM $Na_2B_4O_7$ in ddH_2O, pH 8.5, autoclaved at 1.2 bar, 120°C for 20 min
HBSS	140 mM NaCl, 5.4 mM KCl, 0.25 mM Na_2HPO_4, 5.6 mM glucose, 0.44 mM KH_2PO_4, 1.3 mM $CaCl_2$, 1 mM $MgSO_4$, 4.2 mM $NaHCO_3$ in ddH_2O, autoclaved at 1.2 bar, 120°C for 20 min
Trypsin solution	0.08% trypsin (Gibco) in HBSS
Neuronal medium	Neurobasal medium with 2% B27 supplement, 1% penicillin/streptomycin and 2 mM L-glutamine (all Gibco)

Primary hippocampal neurons were provided by Benjamin Schwenk and Dr. Dieter Edbauer (German Center for Neurodegenerative Diseases, DZNE, Munich) and were prepared as described previously (Edbauer et al., 2010). Briefly, hippocampi were isolated from embryonic day 18 Sprague-Dawley rat embryos, washed four times with ice-cold HBSS and incubated in trypsin solution for 15' at 37°C. Afterwards hippocampi were washed again four times with pre-warmed HBSS and neurons were dissociated mechanically by careful pipetting. Approx. $1x10^6$ neurons/well were seeded in 6 well culture plates coated with poly-D-lysine and equilibrated with neuronal medium. Hippocampal neurons were cultivated using a standard incubator set to 37°C, 5% CO_2 and 95% relative humidity.

5.2.2.5 Transient transfection

Cells were grown to a confluency of approx. 70-90% in the absence of antibiotics. Liposome-mediated transient transfections were done using Lipofectamine2000 (LFA, Invitrogen) following the manufacturer's instructions but the amount of DNA and volume of LFA was adjusted (Table 16). Both DNA and LFA were separately diluted in OptiMEM + GlutaMAX (Gibco) and incubated for 5' at RT. Afterwards the solutions were combined, incubated again for 20' at RT and then added dropwise to the cells. The medium was changed after 12-24 h and the cells were used to condition supernatant and/or were lysed within the following 12 to 60 h.

Culture vessel	Volume of culture medium	cDNA diluted in OptiMEM	Lipofectamine2000 diluted in OptiMEM
6 cm	6 ml	2 µg in 0.2 ml	5 µl in 0.2 ml
10 cm	10 ml	8 µg in 0.5 ml	20 µl in 0.5 ml

Table 16. Amount of cDNA and volumes of medium, Lipofectamine2000 and OptiMEM for transient transfections.

5.2.2.6 Production of lentivirus

OptiMEM+FCS	OptiMEM + GlutaMAX (Gibco) supplemented with 10% FCS (Sigma)
Packaging medium	Dulbecco's modified Eagle's medium (DMEM) high glucose + GlutaMAX (Gibco) supplemented with 10% FCS (Sigma), 1% penicillin/streptomycin, non-essential amino acids (both Gibco) and 1.3% BSA (Sigma)

Production of lentiviral particles was done in cooperation with Benjamin Schwenk and Dr. Dieter Edbauer (German Center for Neurodegenerative Diseases, DZNE, Munich) using a modified third-generation packaging system (Tiscornia et al., 2006). Three different vectors, namely a lentiviral expression construct, psPAX2 and pVSVg (5.1.3 Table 11) were combined to produce VSVg pseudotyped lentiviral particles. HEK293FT cells of a low passage number which had never reached confluency were used as packaging cell line and 5.5×10^6 cells were plated per 10 cm culture dish 24 h prior to transfection. For each virus three 10 cm dishes were transfected using Lipofectamine2000 (Invitrogen) following the manufacturer's instruction. The transfection mixture was prepared by diluting 108 µl of LFA in 4.5 ml of OptiMEM + GlutaMAX (Gibco) and, after 5' of incubation at RT, combining this

solution with 4.5 ml of OptiMEM containing the lentiviral plasmids (Table 17). After mixing, the solution was again incubated at RT for 20' during which the HEK293FT cell medium was replaced by 5 ml of OptiMEM+FCS. Finally, 3 ml of the transfection mix were added dropwise to each plate and the cells were incubated for 24 h. Afterwards the medium was aspirated and 10 ml of packaging medium were added to the cells which then were incubated for another 24 h. After collection, the conditioned medium was centrifuged (10', 600 g at RT) and passed through a sterile PES membrane filter (pore size: 0.45 µm, VWR International). The lentiviral particles were isolated by ultracentrifugation (2 h, 112500 g at 4°C) and the virus pellet was resuspended in 160 µl neurobasal medium (Gibco). Aliquots of the virus were stored at -80°C until usage.

Plasmid	Amount of DNA
Lentiviral vector	18.6 µg
psPAX2	11.0 µg
pVSVg	6.4 µg

Table 17. Amount of plasmids for the production of lentivirus.

5.2.2.7 Lentiviral transduction

Neuronal medium   Neurobasal medium with 2% B27 supplement, 1% penicillin/strepto-
                                mycin and 2 mM L-glutamine (all Gibco)

Lentiviral transduction of primary neuronal cells was done in cooperation with Benjamin Schwenk and Dr. Dieter Edbauer (German Center for Neurodegenerative Diseases, DZNE, Munich). Primary hippocampal neurons were cultivated in 6 well plates (approx. 1×10^6 cells/well, 2.5 ml neuronal medium) and transduced after five to six days in culture. Prior to transduction 1 ml of medium was removed from each well and kept in the incubator. The desired amount of lentivirus (2-5 µl/well) was added to the cells which were then incubated for 8 h. Afterwards the medium was aspirated and replaced by 1 ml of the previously withdrawn medium mixed with 1 ml of fresh neuronal medium. Neurons were allowed to recover for 48 h before the medium was removed and 1.5 ml of fresh neuronal medium (containing inhibitors) were added and conditioned for 12-24 h.

5.2.2.8   Inhibitor treatment and conditioning of supernatant

Medium   Standard medium (5.2.2.1)

For inhibitor treatment the cell culture medium was replaced with fresh, pre-warmed medium supplemented with inhibitors of the appropriate concentration (5.1.4 Table 12) or DMSO as control. Cells in 10 cm culture dishes were incubated with 6.5 ml medium and 2.5 ml and 1.5 ml medium were used for cells in 6 cm dishes and 6 well plates, respectively. Treatment was usually initiated when cells reached a confluency of 90-100% or 12-24 h after transfection and lasted for 8-24 h. Afterwards conditioned medium and cells were collected (5.2.2.10) and analyzed as described (5.2.3).

5.2.2.9   RNA interference experiments

ADAM10 & control siRNA   siGENOME siRNA, human ADAM10; control: siGENOME Non-Targeting siRNA Pool #1; used at 10 nM (both Thermo Scientific)

ADAM17 & control siRNA   On-TARGETplus SMARTpool ADAM17, human ADAM17; control: ON-TARGETplus Non-Targeting pool; used at 15 nM (both Dharmacon)

Medium without antibiotics   Standard medium (5.2.2.1) without penicillin/streptomycin

Poly-L-lysine solution   0.1 mg/ml poly-L-lysine hydrobromide in PBS (5.2.2.1)

RNAi experiments in HEK293 cells were carried out in 10 cm culture dishes using reverse transfection with Lipofectamine2000 (Invitrogen). The siRNA and 45 µl of Lipofectamine2000 were each diluted in 750 µl Optimem + GlutaMAX (Gibco) and incubated for 5' at RT. Afterwards the solutions were combined and incubated for another 20' at RT. 5 ml of standard medium without antibiotics were transferred to a 10 cm dish coated with poly-L-lysine and the transfection mix was added. HEK293 cells from a 90-100% confluent 10 cm dish were then split 1:3.5 or 1:4.5 into the prepared dish and incubated for 24 h after which 5 ml of fresh medium (no antibiotics) were added. If necessary, cDNA was transfected 45-50 h after the reverse transfection following the protocol described before (5.2.2.5), except only 5 µg of DNA and 13 µl of Lipofectamine2000 were used. Prior to transfection the medium was replaced by 10 ml of fresh medium (no antibiotics) and the cells were incubated for 24 h after transfection. For conditioning, the medium was exchanged again and conditioned supernatant and cells were collected after another 20-24 h.

5.2.2.10 Collection of conditioned supernatant and cell harvest

PBS   140 mM NaCl, 10 mM Na_2HPO_4, 1.75 mM KH_2PO_4, 2.7 mM KCl in ddH_2O, pH 7.4, autoclaved at 1.2 bar, 120°C for 20 min

For the collection of supernatant and cells, culture vessels were put on ice and the medium was aspirated and immediately supplemented with Protease Inhibitor Cocktail (Sigma). Remaining cells and debris were removed by centrifugation (10', 5500 g at 4°C) and the medium was either analyzed immediately or stored at -20°C. The cell monolayer was washed once with ice-cold PBS and cells were collected in no more than 1 ml of PBS (depending on the size of the culture vessel) using a cell scraper. The suspension was transferred to a plastic tube, cells were pelleted by centrifugation (5', 1000 g at 4°C) and either lysed immediately or stored at -80°C until further analysis.

5.2.3 Protein biochemistry

5.2.3.1 Preparation of total cell lysate

Lysis buffer   20 mM sodium citrate pH 6.4, 1 mM EDTA, 1% Triton X-100 in ddH_2O, supplemented with Protease Inhibitor Cocktail (Sigma)

To prepare total lysates, cell pellets obtained from 10 cm dishes were resuspended in 0.8-1.2 ml of lysis buffer and 500-800 µl and 100-300 µl of lysis buffer were used for pellets from 6 cm dishes and 6 well plates, respectively. The cell suspension was incubated for 30' at 4°C (with agitation) to ensure complete lysis. Nuclei and undissolved cell debris were removed by centrifugation (15', 10000 g at 4°C). The lysate was analyzed immediately or stored at -80°C.

5.2.3.2 Measurement of protein concentration

The protein concentration of lysates was determined using the Uptima BC Assay Protein Quantitation kit (Interchim). The assay was performed in a 96 well plate following the manufacturer's instruction and typically 2-5 µl of lysate were used. Serial dilutions (0.2-2.0 µg/µl) of bovine serum albumin (BSA, provided with the kit) served as standard and after incubation (30' at 37°C) absorbance was measured at 562 nm using an ELISA reader (PowerWave XS, BioTek).

5.2.3.3 Preparation of cell membranes

Hypotonic buffer	10 mM Tris pH 7.4, 1 mM EDTA, 1 mM EGTA in ddH$_2$O, supplemented with Protease Inhibitor Cocktail (Sigma)
Laemmli sample buffer (4x)	0.25 M Tris pH 6.8, 8% SDS, 40% glycerol, 1% DTT, bromphenol blue in ddH$_2$O

For the detection of endogenous BACE1, ADAM10 and ADAM17 in HEK293 cells, cell membrane fractions were prepared. Cells from a 10 cm dish were resuspended in 1.2 ml hypotonic buffer, incubated on ice for 10' and disrupted by passing the suspension through a needle (gauge 23, 0.6 mm, 1 ml syringe) for 10 times. Intact cells, nuclei, large organelles and cytoskeleton compounds were removed by centrifugation (15', 1000 g at 4°C) and the post nuclear supernatant was spun again (30', 17000 g at 4°C) to pellet membranes. The membrane pellet was resuspended in 100-140 µl of 4x laemmli sample buffer for 5' at 95°C (with agitation) and 5-10 µl were used for SDS-PAGE and immunoblot analysis (5.2.3.5 & 5.2.3.6).

5.2.3.4 Immunoprecipitation (IP) for western blot analysis

STEN buffer	50 mM Tris pH 7.6, 150 mM NaCl, 2 mM EDTA, 0.2% NP-40 in ddH$_2$O
Laemmli sample buffer (4x)	0.25 M Tris pH 6.8, 8% SDS, 40% glycerol, 1% DTT, bromphenol blue in ddH$_2$O

Prior to IP, the conditioned supernatant was pre-cleared with 2-5 µl/ml (at least 20 µl) of Protein G Sepharose (PGS 4 Fast Flow, GE Healthcare) for at least 1 h at 4°C (overhead rotation). The PGS was pelleted by centrifugation (5', 2000 g at 4°C) and the cleared supernatant was transferred to fresh tubes. An appropriate amount of the respective antibody (5.1.6 Table 14) was added and the sample was incubated o/n at 4°C (overhead rotation). Usually 10-20 µl/ml of non-purified antibody solution (hybridoma supernatant) were added while purified antibodies were used at a concentration of 1 µg/ml. After antibody binding, 25-50 µl of PGS were added, incubated for at least 3 h at 4°C (overhead rotation) and subsequently collected by centrifugation (5', 2000 g at 4°C). In case the antibody was provided as agarose bead conjugate, 15-30 µl of the suspension were added to the cleared supernatant, similarly incubated o/n and also collected by centrifugation. The beads were washed 1x with 1 ml STEN buffer and 1x with 1 ml ddH$_2$O (collected each time by centrifugation: 5', 1000 g at 4°C) and the remaining liquid was thoroughly removed using a syringe (1 ml) equipped with a gauge 27 needle (0.4 mm). Washed beads were either stored at -20°C or eluted immediately. For elution the beads were resuspended in 35 µl 4x laemmli

sample buffer and incubated for 5' at 95°C. After centrifugation (5', 17000 g at RT) the supernatant was analyzed by SDS-PAGE and immunoblotting (5.2.3.5 & 5.2.3.6).

5.2.3.5 SDS Polyacrylamide gel electrophoresis (SDS-PAGE)

Stacking gel buffer	0.5 M Tris, 0.4% SDS in ddH$_2$O, pH 6.8
Separating gel buffer	1.5 M Tris, 0.4% SDS in ddH$_2$O, pH 8.8
Acrylamide	40% Acrylamide-bismethylenacrylamide (37.5:1, Serva)
Laemmli sample buffer (4x)	0.25 M Tris pH 6.8, 8% SDS, 40% glycerol, 1% DTT, bromphenol blue in ddH$_2$O
Tris-glycine buffer	25 mM Tris, 190 mM glycine, 0.1% SDS in ddH$_2$O
Tris-tricine buffer	100 mM Tris, 100 mM Tricine, 0.1% SDS in ddH$_2$O

Proteins were separated under denaturing conditions using discontinuous SDS-PAGE. Polyacrylamide gels (LxWxD 7.0 cm x 8.3 cm x 1.5 mm) were cast using the Mini-PROTEAN system (BIORAD) and consisted of a stacking gel (4% acrylamide) and a separating gel (8-14% acrylamide, depending on the size of the protein to be separated). The preparation of an 8% polyacrylamide gel is exemplified in Table 18. Prior to loading, laemmli sample buffer was added to the protein solutions and the samples were heated to 95°C for 5'. After cooling, equal amounts of protein were loaded into the wells of the gel and 10 µl of the SeeBlue Plus2 Prestained Standard (Invitrogen) served as molecular weight standard. Electrophoresis was performed in Tris-glycine buffer using the Mini-PROTEAN system (BIORAD) and applying 50 V before and 120 V after the proteins migrated into the separation gel. Small proteins (> 10 kDa) were separated with precast gradient Tricine Protein Gels (10-20%, 1 mm, Novex) in Tris-tricine buffer using the XCell SureLock Mini-Cell system (Novex).

	Separating gel (8%)	Stacking gel (4%)
ddH$_2$O	4.4 ml	3.25 ml
Stacking gel buffer	-	1.25 ml
Separating gel buffer	2.0 ml	-
Acrylamide	1.6 ml	0.5 ml
TEMED	15 µl	15 µl
APS	15 µl	15 µl

Table 18. Composition of a separating (8%) and stacking (4%) gel for SDS-PAGE. Volumes of the ingredients are indicated for one mini-gel of 1.5 mm thickness.

5.2.3.6 Western blotting and immunodetection

Transfer buffer	25 mM Tris, 190 mM glycine in ddH$_2$O
PBS	140 mM NaCl, 10 mM Na$_2$HPO$_4$, 1.75 mM KH$_2$PO$_4$, 2.7 mM KCl in ddH$_2$O, pH 7.4, autoclaved at 1.2 bar, 120°C for 20 min
I-Block solution	0.2% Tropix I-Block (Applied Biosystems), 0.1% Tween20 in PBS
TBS-T buffer	140 mM NaCl, 2.68 mM KCl, 24.76 mM Tris, 0.3% Triton X-100 in ddH$_2$O, pH 7.6

After separation by SDS-PAGE proteins were transferred onto membranes using the tank/wet Mini Trans-Blot cell system (BIORAD). Polyvinylidene fluoride membranes (PVDF, 0.45 µm, Immobilon-P Transfer Membrane, Millipore) were used for proteins separated with handcast gels (8-14% acrylamide) and were activated beforehand with isopropanol followed by three washes with dH$_2$O. Proteins from precast gradient gels (10-20% acrylamide) were transferred onto nitrocellulose membranes (0.45 µm, Protran BA 85, GE Healthcare) and membranes of both types were equilibrated in transfer buffer for 5' prior to blotting. Western blotting was performed in transfer buffer at a constant current of 400 mA for 1 h using the Mini Trans-Blot cell system (BIORAD). Upon completion of the transfer and prior to blocking, proteins transferred to nitrocellulose membranes were additionally denatured by boiling the membrane in PBS for 5'. After cooling to RT the nitrocellulose membranes, as well as the PVDF membranes, were blocked in I-Block solution for 1 h at RT or o/n at 4°C (with agitation).

Transferred proteins were detected and identified using immunodetection and enhanced chemiluminescence (ECL). To this end, blocked membranes were incubated with primary antibodies (5.1.6 Table 14) diluted in I-Block solution o/n at 4°C (with agitation). After removal of the antibody solution the membranes were washed three times in TBS-T buffer (10' each, at RT, with agitation) and subsequently incubated with a horseradish peroxidase (HRP) coupled secondary antibody (5.1.6 Table 15) specific for the species of the primary detection antibody. Secondary antibodies were diluted in I-Block solution as well and membranes were incubated for 1 h at RT (with agitation), again followed by three washes in TBS-T (as before). For ECL detection, the membranes were incubated in 2 ml of HRP substrate (ECL, GE Healtchcare or ECL Plus, Thermo Scientific) for 1' at RT and signals were captured with X-ray films (Super RX Medical X-Ray, Fujifilm) which subsequently were developed using an automated film developer (CAWOMAT 2000 IR, CAWO). Alternatively, western blot signals were acquired with the Luminescent Image Analyzer LAS-4000 (Fujifilm). Densitometric quantification of western blot signals was done using the Multi Gauge software v3.0 (Fujifilm).

5.2.3.7 Stripping of gels

Stripping buffer	62.5 mM Tris pH 6.7, 2% SDS, 100 mM β-mercaptoethanol in ddH$_2$O
TBS-T buffer	140 mM NaCl, 2.68 mM KCl, 24.76 mM Tris, 0.3% Triton X-100 in ddH$_2$O, pH 7.6
I-Block solution	0.2% Tropix I-Block (Applied Biosystems), 0.1% Tween20 in PBS

To remove previous antibodies and to allow for redecoration with different antibodies, membranes were incubated in stripping buffer for up to 1 h at 50°C (with agitation). Afterwards the membranes were washed three times with TBS-T (10' each, at RT, with agitation) and were blocked again with I-Block solution for at least 1 h at RT.

5.2.3.8 Preparation of sEGF domains and phosphorylation assay

RIPA-PP buffer	20 mM Tris pH 7.4, 150 mM NaCl, 1 mM EGTA, 1 mM EDTA, 1% NP-40, 0.5% Na-desoxycholat, 0.05% Triton X-100 in ddH$_2$O supplemented before use with 10 mM NaF, 1 mM Na-orthovanadate, Phosphatase Inhibitor Cocktail (PhosSTOP, Roche) and Protease Inhibitor Cocktail (Sigma)
PBS	140 mM NaCl, 10 mM Na$_2$HPO$_4$, 1.75 mM KH$_2$PO$_4$, 2.7 mM KCl in ddH$_2$O, pH 7.4, autoclaved at 1.2 bar, 120°C for 20 min

Constructs encoding soluble EGF-like domains (sEGF) (5.1.3 Table 11) were transfected into CHO wt and CHO ldlD cells (5.1.4 Table 13) seeded in 10 cm culture dishes as described before (5.2.2.5). 8 h after transfection the medium was aspirated and 8 ml of fresh medium were added and conditioned for 24 h. The collected supernatants were cleared of cell debris by centrifugation (5', 1000 g at RT) and the initial concentrations of the soluble EGF-like domains were determined by immunodetection. Afterwards, medium of control cells was used to adjust and equalize the sEGF concentrations by dilution. Equal levels were controlled by immunodetection again and adjusted supernatants were either used immediately for stimulation or stored at -20°C.

MCF-7 or primary Schwann cells to be used for the phosphorylation assay were seeded in 6 well culture plates or 6 cm dishes and stimulated upon reaching a confluency of approx. 60-80%. In case of Schwann cells, proliferation was stopped one day prior to the phosphorylation assay. For stimulation, the culture medium was removed, 1.5-2.5 ml of medium containing the adjusted sEGF domains were added carefully and the cells were incubated for 30'. Incubation with 0.5 nM recombinant EGF-like domain (NRG1-β1, 396-HB/CF, R&D Systems) served as positive control and medium of cells expressing an empty vector was used as negative control. Afterwards the culture vessels were placed on ice, the cells were washed once with ice-cold PBS and 200-300 µl of RIPA-PP buffer were distributed onto the cell layer. After 5' of incubation on ice, the cells were collected into sample tubes using a cell scraper and the suspension was further incubated on ice for 15' to ensure complete lysis. Insoluble cell debris was removed by centrifugation (30', 17000 g at 4°C) and the total cell lysate was analyzed for ErbB3 and AKT phosphorylation using western blotting and immunodetection.

5.2.3.9 Cell-free γ-secretase assay

Homogenization buffer	0.25 M sucrose, 10 mM HEPES pH 7.4 in ddH$_2$O, supplemented with 1x complete Protease Inhibitor Cocktail (Roche)
Assay buffer	150 mM sodium citrate pH 6.4, 5 mM 1,10-phenantroline in ddH$_2$O, supplemented with 4x complete Protease Inhibitor Cocktail (Roche)
Lysis buffer	20 mM sodium citrate pH 6.4, 1 mM EDTA, 1% Triton X-100 in ddH$_2$O, supplemented with Protease Inhibitor Cocktail (Sigma)
Laemmli sample buffer (4x)	0.25 M Tris pH 6.8, 8% SDS, 40% glycerol, 1% DTT, bromphenol blue in ddH$_2$O

The cell-free γ-secretase assay used to generate the NRG1 intracellular domain (ICD) *in vitro* was modified from a protocol published previously (Fukumori et al., 2006). HEK293 cells

harvested from a 10 cm culture dish were resuspended in 750 µl of homogenization buffer and disrupted by passing the suspension through a needle (gauge 23, 0.6 mm, 1 ml syringe) for 15 times. Nuclei and cell debris were removed by centrifugation (10', 1000 g at 4°C) and the post nuclear supernatant was transferred to fresh tubes and centrifuged again (1 h, 100000 g at 4°C) to pellet cell membranes. The membrane pellet was resuspended in 100 µl of assay buffer by pipetting and then incubated at 37°C (with agitation) for up to 3.5 h. As control, the assay was either performed at 4°C or the γ-secretase inhibitor L-685,458 (5.1.4 Table 12) was added at a final concentration of 1 µM. The reaction was terminated by cooling the samples on ice and membranes (P100) and supernatant (S100) were separated by centrifugation (1 h, 100000 g at 4°C). To solubilize the membranes, the P100 pellet was resuspended in 200 µl of lysis buffer, laemmli sample buffer was added and the sample was incubated at 95°C for 5'. After centrifugation (5', 17000 g at RT) the solubilized membranes were analyzed by SDS-PAGE and immunoblotting. The soluble membrane fraction S100 containing the NRG1 ICD was either also subjected to SDS-PAGE immediately or further processed for mass spectrometric measurement by reduction and alkylation (5.2.4.3).

5.2.4 Mass spectrometry

5.2.4.1 Immunoprecipation for mass spectrometric analysis (IP-MS)

IP-MS buffer	10 mM Tris pH 8.0, 140 mM NaCl, 5 mM EDTA in ddH$_2$O, sterile filtered, then supplemented with 0.1% Octyl-β-D-glucopyranoside (Sigma)

Immunoprecipitation of samples to be analyzed by mass spectrometry was done similar as described before (5.2.3.4) with the following modifications: In order to allow for a small elution volume only 10-15 µl of antibody conjugated agarose beads and 20-30 µl of PGS were added for precipitation. After collection, beads were washed three times with 1 ml IP-MS buffer and three times with 1 ml ddH$_2$O and, after removal of residual liquid, were stored at -20°C or immediately processed for mass spectrometric analysis (5.2.4.4).

5.2.4.2 NRG1 β-peptide reduction prior to MS

NRG1 β-peptides were immunoprecipitated from cell supernatant as described above (5.2.4.1). 30 µl of 75 mM DTT were added to the agarose beads and reduction was performed for 1 h at 30°C (with agitation). After centrifugation (1', 17000 g at RT) the DTT solution was aspirated from the beads and evaporated using a centrifugal evaporator (15' at 45°C). The remaining dried protein was solubilized in 15 µl of the matrix used for mass

spectrometry (5.2.4.4). The agarose beads were eluted as described (5.2.4.4) and both samples were analyzed by mass spectrometry.

5.2.4.3 NRG1 ICD reduction and alkylation prior to MS

ABC buffer	250 mM NH$_4$HCO$_3$ pH 8.0 in ddH$_2$O
DTT	1 M DTT in ddH$_2$O
IAA solution	100 mM 2-Iodacetamide (IAA) in 50 mM ABC buffer, prepared immediately before use, protected from light
Cysteine solution	100 mM cysteine in 50 mM ABC buffer, prepared immediately before use
IP-MS buffer	10 mM Tris pH 8.0, 140 mM NaCl, 5 mM EDTA in ddH$_2$O, sterile filtered, then supplemented with 0.1% Octyl-β-D-glucopyranoside (Sigma)

NRG1 ICD was generated *in vitro* using the cell-free γ-secretase assay as described above (5.2.3.9). The S100 assay fraction was adjusted to a final concentration of 50 mM NH$_4$HCO$_3$ by addition of ABC buffer and a pH strip was used to confirm the solution's pH was between 7.5 and 8.5. For reduction, DTT was added to a final concentration of 5.5 mM and the sample was incubated for 45' at 37°C (with agitation). Afterwards IAA was added (10.5 mM final concentration) and alkylation was performed for 45' at 37°C (with agitation) in the dark. Excess IAA was quenched by 16 mM cysteine for 5' at RT (with agitation). Irreversible alkylation of the proteins' free SH groups generates S-carboxyamidomethylcysteine (CAM, -CH$_2$CONH$_2$) residues which prevent any further modification and add a specific mass of 57.02 Da per modified cysteine to the proteins' molecular weights. For immuno-precipitation, 1 ml of IP-MS buffer was added to the sample and precipitation was performed as described before (5.2.4.1).

5.2.4.4 MALDI-TOF MS analysis

Matrix	0.3% trifluoroacetic acid, 40% acetonitrile in ddH$_2$O, saturated with α-cyano-4-hydroxycinnamic acid

To elute the precipitated peptides (5.2.4.1) 15-20 µl of the matrix solution were added to the agarose beads, the sample was mixed gently and incubated at RT for 5'. Afterwards the beads were pelleted by centrifugation (1', 17000 g at RT) and 1-2 µl of the supernatant were directly transferred to the wells of the target plate (Assay sample plate, 96 well, coat, Applied Biosystems). The samples were allowed to dry at RT and sample spotting was repeated if necessary. After complete drying, the peptides were analyzed by MALDI-TOF mass

spectrometry using a Voyager DE STR (Applied Biosystems) mass spectrometer in the lab of Dr. Imhof (Center for Protein Analysis, Ludwig-Maximilians-University, Munich). All samples were measured with the mass spectrometer set to linear mode and samples containing small peptides (1000-5000 Da) were additionally analyzed in reflector mode. In general the preset parameters of the spectrometer were used and grid voltage and delay time were set to 90-95% and 100-300 ns for the linear mode and 60-65% and 150-250 ns for the reflector mode, respectively. Molecular masses were calibrated with the calibration mixture 2 of the Sequazyme Peptide Mass Standards Kit (Applied Biosystems) and the data were analyzed using Data Explorer 4.3 (Applied Biosystems) and GPMAW 5.02 (Lighthouse data) software.

5.2.5 Zebrafish techniques

5.2.5.1 General

E3 media	5 mM NaCl, 0.17 mM KCl, 0.33 mM CaCl2, 0.33 mM MgSO4 in ddH$_2$O

Zebrafish were provided and all zebrafish experiments were conducted by Dr. Frauke van Bebber and Dr. Bettina Schmid (German Center for Neurodegenerative Diseases, DZNE, Munich). All zebrafish were raised at 28°C in E3 media supplemented with methylene blue (10-15%) to prevent the growth of mold and were staged as previously described (Kimmel et al., 1995). Zebrafish of either sex were used for this work and all experiments were performed in accordance with animal protection standards of the Ludwig-Maximilians-University Munich and have been approved by the government of Upper Bavaria. In addition to the AB wt strain the transgenic claudin k:GFP zebrafish line was used in which the Schwann cell promoter claudin k drives the expression of a membrane-bound GFP (Münzel et al., 2012). To analyze the activity of soluble NRG1 EGF-like domains *in vivo*, this line was crossed with BACE1 mutant zebrafish (bace1-/-) (van Bebber et al., 2013) resulting in transgenic claudin k:GFP zebrafish lacking endogenous BACE1 activity.

5.2.5.2 mRNA injections and imaging

The mRNAs coding for the different NRG1 EGF-like domains were synthesized *in vitro* using the mMessage mMACHINE kit (Ambion) following the manufacturer's instructions. The mRNA was injected into fertilized eggs (one-cell stage) at a concentration of 425 ng/µl which was determined by titration in order to minimize toxic effects. Three days postfertilization (3 dpf) the zebrafish larvae were anesthetized with triacine (0.016%) and oriented in 2% methylcellulose on coverslips. Images were acquired using an LSM510 META inverted

confocal microscope (Zeiss) and assembled in Photoshop 8.0 (Adobe Systems). Contrast and brightness were adjusted with ImageJ.

5.2.6 Calculation of hydrophobicity and aggregation

The hydrophobicity and aggregation propensity of the NRG1 β-peptide and different Aβ species were calculated using web-based software tools. The hydropathy index number is a measure for the hydrophobic or hydrophilic properties of a peptide and was calculated with the tool PeptGen available at http://hcv.lanl.gov/content/sequence/PEPTGEN/ Explanation.html. The PeptGen algorithm assigns the Kyte-Doolittle hydropathy index (Kyte and Doolittle, 1982) to every amino acid residue of a given sequence and subsequently calculates the average for the whole peptide. The intrinsic aggregation propensity (Zagg) of peptides was predicted using the sequence-based software Zyggregator (Tartaglia and Vendruscolo, 2008; Tartaglia et al., 2008) available at http://www-vendruscolo.ch.cam.ac.uk/ zyggregator-all.php after registration. The calculation was performed for a pH value of 7.

5.2.7 Statistical analysis

The data obtained from western blot quantification were normalized and the respective control was set to 1.0 or 100% as indicated in the figures. All statistical data are represented as mean +/- standard deviation (SD) and the number of experiments is given in each figure. Statistical analysis was done using the two-tailed unpaired Student's t-test and results were considered significant for p-values below 0.05 (* $p<0.05$, ** $p<0.01$, *** $p<0.0001$). Calculations were performed with EXCEL 2010 (Microsoft).

6 References

Alfalah M, Jacob R, Preuss U, Zimmer K-P, Naim H, Naim HY (1999) O-linked glycans mediate apical sorting of human intestinal sucrase-isomaltase through association with lipid rafts. Curr Biol 9:593–596.

Alzheimer A (1907) Über eine eigenartige Erkrankung der Hirnrinde. Allg Z Psychiatr Psych-Gerichtl Med 64:146–148.

Alzheimer A (1911) Über eigenartige Krankheitsfälle des späteren Alters. Z Für Gesamte Neurol Psychiatr 4:356–385.

Atanasoski S, Scherer SS, Sirkowski E, Leone D, Garratt AN, Birchmeier C, Suter U (2006) ErbB2 Signaling in Schwann Cells Is Mostly Dispensable for Maintenance of Myelinated Peripheral Nerves and Proliferation of Adult Schwann Cells after Injury. J Neurosci 26:2124–2131.

Bao J, Lin H, Ouyang Y, Lei D, Osman A, Kim T-W, Mei L, Dai P, Ohlemiller KK, Ambron RT (2004) Activity-dependent transcription regulation of PSD-95 by neuregulin-1 and Eos. Nat Neurosci 7:1250–1258.

Bao J, Wolpowitz D, Role LW, Talmage DA (2003) Back signaling by the Nrg-1 intracellular domain. J Cell Biol 161:1133–1141.

Baumann N, Pham-Dinh D (2001) Biology of Oligodendrocyte and Myelin in the Mammalian Central Nervous System. Physiol Rev 81:871–927.

Beckett C, Nalivaeva NN, Belyaev ND, Turner AJ (2012) Nuclear signalling by membrane protein intracellular domains: The AICD enigma. Cell Signal 24:402–409.

Bettegazzi B, Mihailovich M, Di Cesare A, Consonni A, Macco R, Pelizzoni I, Codazzi F, Grohovaz F, Zacchetti D (2010) β-Secretase activity in rat astrocytes: translational block of BACE1 and modulation of BACE2 expression. Eur J Neurosci Available at: http://www.ncbi.nlm.nih.gov/pubmed/21073551 [Accessed December 8, 2010].

Birchmeier C, Nave K-A (2008) Neuregulin-1, a key axonal signal that drives Schwann cell growth and differentiation. Glia 56:1491–1497.

Bland CE, Kimberly P, Rand MD (2003) Notch-induced Proteolysis and Nuclear Localization of the Delta Ligand. J Biol Chem 278:13607–13610.

Blennow K, Zetterberg H, Haass C, Finucane T (2013) Semagacestat's fall: where next for AD therapies? Nat Med 19:1214–1215.

Boucher AA, Arnold JC, Duffy L, Schofield PR, Micheau J, Karl T (2007) Heterozygous neuregulin 1 mice are more sensitive to the behavioural effects of Δ9-tetrahydrocannabinol. Psychopharmacology (Berl) 192:325–336.

Bozkulak EC, Weinmaster G (2009) Selective Use of ADAM10 and ADAM17 in Activation of Notch1 Signaling. Mol Cell Biol 29:5679–5695.

Braak H, Braak E (1995) Staging of Alzheimer's disease-related neurofibrillary changes. Neurobiol Aging 16:271–278; discussion 278–284.

Brinkmann BG, Agarwal A, Sereda MW, Garratt AN, Müller T, Wende H, Stassart RM, Nawaz S, Humml C, Velanac V, Radyushkin K, Goebbels S, Fischer TM, Franklin RJ, Lai C, Ehrenreich H, Birchmeier C, Schwab MH, Nave KA (2008) Neuregulin-1/ErbB signaling serves distinct functions in myelination of the peripheral and central nervous system. Neuron 59:581–595.

Britsch S, Li L, Kirchhoff S, Theuring F, Brinkmann V, Birchmeier C, Riethmacher D (1998) The ErbB2 and ErbB3 receptors and their ligand, neuregulin-1, are essential for development of the sympathetic nervous system. Genes Dev 12:1825–1836.

Brookmeyer R, Johnson E, Ziegler-Graham K, Arrighi HM (2007) Forecasting the global burden of Alzheimer's disease. Alzheimers Dement J Alzheimers Assoc 3:186–191.

Brou C, Logeat F, Gupta N, Bessia C, LeBail O, Doedens JR, Cumano A, Roux P, Black RA, Israël A (2000) A Novel Proteolytic Cleavage Involved in Notch Signaling. Mol Cell 5:207–216.

Brown MS, Ye J, Rawson RB, Goldstein JL (2000) Regulated intramembrane proteolysis: a control mechanism conserved from bacteria to humans. Cell 100:391–398.

Bublil EM, Yarden Y (2007) The EGF receptor family: spearheading a merger of signaling and therapeutics. Curr Opin Cell Biol 19:124–134.

Buonanno A (2010) The neuregulin signaling pathway and schizophrenia: From genes to synapses and neural circuits. Brain Res Bull 83:122–131.

Buonanno A, Fischbach GD (2001) Neuregulin and ErbB receptor signaling pathways in the nervous system. Curr Opin Neurobiol 11:287–296.

Burgess TL, Ross SL, Qian Y, Brankow D, Hu S (1995) Biosynthetic Processing of neu Differentiation Factor GLYCOSYLATION, TRAFFICKING, AND REGULATED CLEAVAGE FROM THE CELL SURFACE. J Biol Chem 270:19188–19196.

Buser AM, Schmid D, Kern F, Erne B, Lazzati T, Schaeren-Wiemers N (2009) The myelin protein MAL affects peripheral nerve myelination: a new player influencing p75 neurotrophin receptor expression. Eur J Neurosci 29:2276–2290.

Busfield SJ, Michnick DA, Chickering TW, Revett TL, Ma J, Woolf EA, Comrack CA, Dussault BJ, Woolf J, Goodearl AD, Gearing DP (1997) Characterization of a neuregulin-related gene, Don-1, that is highly expressed in restricted regions of the cerebellum and hippocampus. Mol Cell Biol 17:4007–4014.

Buxbaum JD, Liu KN, Luo Y, Slack JL, Stocking KL, Peschon JJ, Johnson RS, Castner BJ, Cerretti DP, Black RA (1998) Evidence that tumor necrosis factor alpha converting enzyme is involved in regulated alpha-secretase cleavage of the Alzheimer amyloid protein precursor. J Biol Chem 273:27765–27767.

References

Cabedo H, Carteron C, Ferrer-Montiel A (2004) Oligomerization of the sensory and motor neuron-derived factor prevents protein O-glycosylation. J Biol Chem 279:33623–33629.

Caescu CI, Jeschke GR, Turk BE (2009) Active-site determinants of substrate recognition by the metalloproteinases TACE and ADAM10. Biochem J 424:79–88.

Cai H, Wang Y, McCarthy D, Wen H, Borchelt DR, Price DL, Wong PC (2001) BACE1 is the major beta-secretase for generation of Abeta peptides by neurons. Nat Neurosci 4:233–234.

Cai XD, Golde TE, Younkin SG (1993) Release of excess amyloid beta protein from a mutant amyloid beta protein precursor. Science 259:514–516.

Cao X, Südhof TC (2001) A Transcriptively Active Complex of APP with Fe65 and Histone Acetyltransferase Tip60. Science 293:115–120.

Cao X, Südhof TC (2004) Dissection of amyloid-beta precursor protein-dependent transcriptional transactivation. J Biol Chem 279:24601–24611.

Capell A, Beher D, Prokop S, Steiner H, Kaether C, Shearman MS, Haass C (2005) γ-Secretase Complex Assembly within the Early Secretory Pathway. J Biol Chem 280:6471–6478.

Carpenter G (2003) ErbB-4: mechanism of action and biology. Exp Cell Res 284:66–77.

Chang H, Riese DJ 2nd, Gilbert W, Stern DF, McMahan UJ (1997) Ligands for ErbB-family receptors encoded by a neuregulin-like gene. Nature 387:509–512.

Chávez-Gutiérrez L, Tolia A, Maes E, Li T, Wong PC, Strooper B de (2008) Glu332 in the Nicastrin Ectodomain Is Essential for γ-Secretase Complex Maturation but Not for Its Activity. J Biol Chem 283:20096–20105.

Chen S, Velardez MO, Warot X, Yu Z-X, Miller SJ, Cros D, Corfas G (2006) Neuregulin 1–erbB Signaling Is Necessary for Normal Myelination and Sensory Function. J Neurosci 26:3079–3086.

Chen Y, Hancock ML, Role LW, Talmage DA (2010a) Intramembranous valine linked to schizophrenia is required for neuregulin 1 regulation of the morphological development of cortical neurons. J Neurosci Off J Soc Neurosci 30:9199–9208.

Chen Y, Hancock ML, Role LW, Talmage DA (2010b) Intramembranous valine linked to schizophrenia is required for neuregulin 1 regulation of the morphological development of cortical neurons. J Neurosci Off J Soc Neurosci 30:9199–9208.

Cheret C, Willem M, Fricker FR, Wende H, Wulf-Goldenberg A, Tahirovic S, Nave K-A, Saftig P, Haass C, Garratt AN, Bennett DL, Birchmeier C (2013) Bace1 and Neuregulin-1 cooperate to control formation and maintenance of muscle spindles. EMBO J 32:2015–2028.

172

Citron M, Oltersdorf T, Haass C, McConlogue L, Hung AY, Seubert P, Vigo-Pelfrey C, Lieberburg I, Selkoe DJ (1992) Mutation of the beta-amyloid precursor protein in familial Alzheimer's disease increases beta-protein production. Nature 360:672–674.

Citron M, Teplow DB, Selkoe DJ (1995) Generation of amyloid beta protein from its precursor is sequence specific. Neuron 14:661–670.

Corfas G, Roy K, Buxbaum JD (2004) Neuregulin 1-erbB signaling and the molecular/cellular basis of schizophrenia. Nat Neurosci 7:575–580.

Cosgaya JM, Chan JR, Shooter EM (2002) The Neurotrophin Receptor p75NTR as a Positive Modulator of Myelination. Science 298:1245–1248.

Cruts M, Theuns J, Van Broeckhoven C (2012) Locus-specific mutation databases for neurodegenerative brain diseases. Hum Mutat 33:1340–1344.

Crystal AS, Morais VA, Pierson TC, Pijak DS, Carlin D, Lee VM-Y, Doms RW (2003) Membrane Topology of γ-Secretase Component PEN-2. J Biol Chem 278:20117–20123.

De Strooper B, Annaert W, Cupers P, Saftig P, Craessaerts K, Mumm JS, Schroeter EH, Schrijvers V, Wolfe MS, Ray WJ, Goate A, Kopan R (1999) A presenilin-1-dependent γ-secretase-like protease mediates release of Notch intracellular domain. Nature 398:518–522.

De Strooper B, Saftig P, Craessaerts K, Vanderstichele H, Guhde G, Annaert W, Von Figura K, Van Leuven F (1998) Deficiency of presenilin-1 inhibits the normal cleavage of amyloid precursor protein. Nature 391:387–390.

De Strooper B, Vassar R, Golde T (2010) The secretases: enzymes with therapeutic potential in Alzheimer disease. Nat Rev Neurol 6:99–107.

Dejaegere T, Serneels L, Schäfer MK, Van Biervliet J, Horré K, Depboylu C, Alvarez-Fischer D, Herreman A, Willem M, Haass C, Höglinger GU, D'Hooge R, De Strooper B (2008) Deficiency of Aph1B/C-gamma-secretase disturbs Nrg1 cleavage and sensorimotor gating that can be reversed with antipsychotic treatment. Proc Natl Acad Sci U S A 105:9775–9780.

Dislich B, Lichtenthaler SF (2012) The Membrane-Bound Aspartyl Protease BACE1: Molecular and Functional Properties in Alzheimer's Disease and Beyond. Front Physiol 3:8.

Dominguez D et al. (2005) Phenotypic and Biochemical Analyses of BACE1- and BACE2-deficient Mice. J Biol Chem 280:30797–30806.

Donoviel DB, Hadjantonakis A-K, Ikeda M, Zheng H, Hyslop PSG, Bernstein A (1999) Mice lacking both presenilin genes exhibitearlyembryonic patterningdefects. Genes Dev 13:2801–2810.

References

Doody RS, Raman R, Farlow M, Iwatsubo T, Vellas B, Joffe S, Kieburtz K, He F, Sun X, Thomas RG, Aisen PS, Siemers E, Sethuraman G, Mohs R (2013) A Phase 3 Trial of Semagacestat for Treatment of Alzheimer's Disease. N Engl J Med 369:341–350.

Dovey HF et al. (2001) Functional gamma-secretase inhibitors reduce beta-amyloid peptide levels in brain. J Neurochem 76:173–181.

Drebin JA, Stern DF, Link VC, Weinberg RA, Greene MI (1984) Monoclonal antibodies identify a cell-surface antigen associated with an activated cellular oncogene. Nature 312:545–548.

Drubin DG, Kirschner MW (1986) Tau protein function in living cells. J Cell Biol 103:2739–2746.

Duffy L, Cappas E, Lai D, Boucher AA, Karl T (2010) Cognition in transmembrane domain neuregulin 1 mutant mice. Neuroscience 170:800–807.

Edbauer D, Neilson JR, Foster KA, Wang C-F, Seeburg DP, Batterton MN, Tada T, Dolan BM, Sharp PA, Sheng M (2010) Regulation of Synaptic Structure and Function by FMRP-Associated MicroRNAs miR-125b and miR-132. Neuron 65:373–384.

Edbauer D, Willem M, Lammich S, Steiner H, Haass C (2002) Insulin-degrading enzyme rapidly removes the beta-amyloid precursor protein intracellular domain (AICD). J Biol Chem 277:13389–13393.

Edbauer D, Winkler E, Regula JT, Pesold B, Steiner H, Haass C (2003) Reconstitution of γ-secretase activity. Nat Cell Biol 5:486–488.

Eggert S, Paliga K, Soba P, Evin G, Masters CL, Weidemann A, Beyreuther K (2004) The Proteolytic Processing of the Amyloid Precursor Protein Gene Family Members APLP-1 and APLP-2 Involves α-, β-, γ-, and ε-Like Cleavages MODULATION OF APLP-1 PROCESSING BY N-GLYCOSYLATION. J Biol Chem 279:18146–18156.

Einheber S, Zanazzi G, Ching W, Scherer S, Milner TA, Peles E, Salzer JL (1997) The axonal membrane protein Caspr, a homologue of neurexin IV, is a component of the septate-like paranodal junctions that assemble during myelination. J Cell Biol 139:1495–1506.

Endres K, Fahrenholz F (2010) Upregulation of the α-secretase ADAM10 – risk or reason for hope? FEBS J 277:1585–1596.

Esch F, Keim P, Beattie E, Blacher R, Culwell A, Oltersdorf T, McClure D, Ward P (1990) Cleavage of amyloid beta peptide during constitutive processing of its precursor. Science 248:1122 –1124.

Fahrenholz F (2007) Alpha-secretase as a therapeutic target. Curr Alzheimer Res 4:412–417.

Falls DL (2003a) Neuregulins and the neuromuscular system: 10 years of answers and questions. J Neurocytol 32:619–647.

Falls DL (2003b) Neuregulins: functions, forms, and signaling strategies. Exp Cell Res 284:14–30.

Falls DL, Rosen KM, Corfas G, Lane WS, Fischbach GD (1993) ARIA, a protein that stimulates acetylcholine receptor synthesis, is a member of the neu ligand family. Cell 72:801–815.

Ferri CP, Prince M, Brayne C, Brodaty H, Fratiglioni L, Ganguli M, Hall K, Hasegawa K, Hendrie H, Huang Y, Jorm A, Mathers C, Menezes PR, Rimmer E, Scazufca M, Alzheimer's Disease International (2005) Global prevalence of dementia: a Delphi consensus study. Lancet 366:2112–2117.

Fiúza U-M, Arias AM (2007) Cell and molecular biology of Notch. J Endocrinol 194:459–474.

Fleck D, Garratt AN, Haass C, Willem M (2012) BACE1 dependent neuregulin processing: review. Curr Alzheimer Res 9:178–183.

Fluhrer R, Multhaup G, Schlicksupp A, Okochi M, Takeda M, Lammich S, Willem M, Westmeyer G, Bode W, Walter J, Haass C (2003) Identification of a β-Secretase Activity, Which Truncates Amyloid β-Peptide after Its Presenilin-dependent Generation. J Biol Chem 278:5531–5538.

Fluhrer R, Steiner H, Haass C (2009) Intramembrane Proteolysis by Signal Peptide Peptidases: A Comparative Discussion of GXGD-type Aspartyl Proteases. J Biol Chem 284:13975–13979.

Förstl H, Kurz A (1999) Clinical features of Alzheimer's disease. Eur Arch Psychiatry Clin Neurosci 249:288–290.

Fortini ME (2002) γ-Secretase-mediated proteolysis in cell-surface-receptor signalling. Nat Rev Mol Cell Biol 3:673–684.

Fortna RR, Crystal AS, Morais VA, Pijak DS, Lee VM-Y, Doms RW (2004) Membrane Topology and Nicastrin-enhanced Endoproteolysis of APH-1, a Component of the γ-Secretase Complex. J Biol Chem 279:3685–3693.

Freese C, Garratt AN, Fahrenholz F, Endres K (2009) The effects of α-secretase ADAM10 on the proteolysis of neuregulin-1. FEBS J 276:1568–1580.

Fricker FR, Lago N, Balarajah S, Tsantoulas C, Tanna S, Zhu N, Fageiry SK, Jenkins M, Garratt AN, Birchmeier C, Bennett DLH (2011) Axonally derived neuregulin-1 is required for remyelination and regeneration after nerve injury in adulthood. J Neurosci Off J Soc Neurosci 31:3225–3233.

Friedhoff P, von Bergen M, Mandelkow EM, Davies P, Mandelkow E (1998) A nucleated assembly mechanism of Alzheimer paired helical filaments. Proc Natl Acad Sci U S A 95:15712–15717.

Fukumori A, Fluhrer R, Steiner H, Haass C (2010) Three-amino acid spacing of presenilin endoproteolysis suggests a general stepwise cleavage of gamma-secretase-mediated intramembrane proteolysis. J Neurosci Off J Soc Neurosci 30:7853–7862.

References

Fukumori A, Okochi M, Tagami S, Jiang J, Itoh N, Nakayama T, Yanagida K, Ishizuka-Katsura Y, Morihara T, Kamino K, Tanaka T, Kudo T, Tanii H, Ikuta A, Haass C, Takeda M (2006) Presenilin-dependent gamma-secretase on plasma membrane and endosomes is functionally distinct. Biochemistry (Mosc) 45:4907–4914.

Furukawa K, Sopher BL, Rydel RE, Begley JG, Pham DG, Martin GM, Fox M, Mattson MP (1996) Increased Activity-Regulating and Neuroprotective Efficacy of α-Secretase-Derived Secreted Amyloid Precursor Protein Conferred by a C-Terminal Heparin-Binding Domain. J Neurochem 67:1882–1896.

Gadgil HS, Bondarenko PV, Pipes GD, Dillon TM, Banks D, Abel J, Kleemann GR, Treuheit MJ (2006) Identification of cysteinylation of a free cysteine in the Fab region of a recombinant monoclonal IgG1 antibody using Lys-C limited proteolysis coupled with LC/MS analysis. Anal Biochem 355:165–174.

Gall SML, Bobé P, Reiss K, Horiuchi K, Niu X-D, Lundell D, Gibb DR, Conrad D, Saftig P, Blobel CP (2009) ADAMs 10 and 17 Represent Differentially Regulated Components of a General Shedding Machinery for Membrane Proteins Such as Transforming Growth Factor α, L-Selectin, and Tumor Necrosis Factor α. Mol Biol Cell 20:1785–1794.

Garratt AN, Voiculescu O, Topilko P, Charnay P, Birchmeier C (2000) A Dual Role of erbB2 in Myelination and in Expansion of the Schwann Cell Precursor Pool. J Cell Biol 148:1035–1046.

Gassmann M, Casagranda F, Orioli D, Simon H, Lai C, Klein R, Lemke G (1995) Aberrant neural and cardiac development in mice lacking the ErbB4 neuregulin receptor. Nature 378:390–394.

Geling A, Steiner H, Willem M, Bally-Cuif L, Haass C (2002) A γ-secretase inhibitor blocks Notch signaling in vivo and causes a severe neurogenic phenotype in zebrafish. EMBO Rep 3:688–694.

Georgakopoulos A, Litterst C, Ghersi E, Baki L, Xu C, Serban G, Robakis NK (2006) Metalloproteinase/Presenilin1 processing of ephrinB regulates EphB-induced Src phosphorylation and signaling. EMBO J 25:1242–1252.

Goddard DR, Bunning RA, Woodroofe MN (2001) Astrocyte and endothelial cell expression of ADAM 17 (TACE) in adult human CNS. Glia 34:267–271.

Goedert M, Spillantini MG, Cairns NJ, Crowther RA (1992) Tau proteins of Alzheimer paired helical filaments: abnormal phosphorylation of all six brain isoforms. Neuron 8:159–168.

Golde TE, Petrucelli L, Lewis J (2010) Targeting Abeta and tau in Alzheimer's disease, an early interim report. Exp Neurol 223:252–266.

Golde TE, Schneider LS, Koo EH (2011) Anti-aβ therapeutics in Alzheimer's disease: the need for a paradigm shift. Neuron 69:203–213.

Goldgaber D, Lerman MI, McBride OW, Saffiotti U, Gajdusek DC (1987) Characterization and chromosomal localization of a cDNA encoding brain amyloid of Alzheimer's disease. Science 235:877–880.

Golding JP, Trainor P, Krumlauf R, Gassmann M (2000) Defects in pathfinding by cranial neural crest cells in mice lacking the neuregulin receptor ErbB4. Nat Cell Biol 2:103–109.

Goodearl AD, Davis JB, Mistry K, Minghetti L, Otsu M, Waterfield MD, Stroobant P (1993) Purification of multiple forms of glial growth factor. J Biol Chem 268:18095–18102.

Gu Y, Chen F, Sanjo N, Kawarai T, Hasegawa H, Duthie M, Li W, Ruan X, Luthra A, Mount HTJ, Tandon A, Fraser PE, George-Hyslop PS (2003) APH-1 Interacts with Mature and Immature Forms of Presenilins and Nicastrin and May Play a Role in Maturation of Presenilin·Nicastrin Complexes. J Biol Chem 278:7374–7380.

Gu Y, Misonou H, Sato T, Dohmae N, Takio K, Ihara Y (2001) Distinct intramembrane cleavage of the beta-amyloid precursor protein family resembling gamma-secretase-like cleavage of Notch. J Biol Chem 276:35235–35238.

Haapasalo A, Kovacs DM (2011) The Many Substrates of Presenilin/γ-Secretase. J Alzheimers Dis 25:3–28.

Haass C (2004) Take five--BACE and the gamma-secretase quartet conduct Alzheimer's amyloid beta-peptide generation. EMBO J 23:483–488.

Haass C, Hung AY, Schlossmacher MG, Oltersdorf T, Teplow DB, Selkoe DJ (1993) Normal Cellular Processing of the β-Amyloid Precursor Protein Results in the Secretion of the Amyloid β Peptide and Related Moleculesa. Ann N Y Acad Sci 695:109–116.

Haass C, Schlossmacher MG, Hung AY, Vigo-Pelfrey C, Mellon A, Ostaszewski BL, Lieberburg I, Koo EH, Schenk D, Teplow DB, Selkoe DJ (1992) Amyloid β-peptide is produced by cultured cells during normal metabolism. Nature 359:322–325.

Haass C, Selkoe DJ (2007) Soluble protein oligomers in neurodegeneration: lessons from the Alzheimer's amyloid beta-peptide. Nat Rev Mol Cell Biol 8:101–112.

Haass C, Steiner H (2002) Alzheimer disease gamma-secretase: a complex story of GxGD-type presenilin proteases. Trends Cell Biol 12:556–562.

Hancock ML, Canetta SE, Role LW, Talmage DA (2008) Presynaptic Type III Neuregulin1-ErbB signaling targets α7 nicotinic acetylcholine receptors to axons. J Cell Biol 181:511–521.

Harari D, Tzahar E, Romano J, Shelly M, Pierce JH, Andrews GC, Yarden Y (1999) Neuregulin-4: a novel growth factor that acts through the ErbB-4 receptor tyrosine kinase. Oncogene 18:2681–2689.

Hardy J (2009) The amyloid hypothesis for Alzheimer's disease: a critical reappraisal. J Neurochem 110:1129–1134.

References

Hardy JA, Higgins GA (1992) Alzheimer's disease: the amyloid cascade hypothesis. Science 256:184–185.

Harrisingh MC, Perez-Nadales E, Parkinson DB, Malcolm DS, Mudge AW, Lloyd AC (2004) The Ras/Raf/ERK signalling pathway drives Schwann cell dedifferentiation. EMBO J 23:3061–3071.

Harrison PJ, Weinberger DR (2005) Schizophrenia genes, gene expression, and neuropathology: on the matter of their convergence. Mol Psychiatry 10:40–68.

Harrison SM, Harper AJ, Hawkins J, Duddy G, Grau E, Pugh PL, Winter PH, Shilliam CS, Hughes ZA, Dawson LA, Gonzalez MI, Upton N, Pangalos MN, Dingwall C (2003) BACE1 (β-secretase) transgenic and knockout mice: identification of neurochemical deficits and behavioral changes. Mol Cell Neurosci 24:646–655.

Hartmann D, de Strooper B, Serneels L, Craessaerts K, Herreman A, Annaert W, Umans L, Lübke T, Lena Illert A, von Figura K, Saftig P (2002) The disintegrin/metalloprotease ADAM 10 is essential for Notch signalling but not for alpha-secretase activity in fibroblasts. Hum Mol Genet 11:2615–2624.

Hashimoto R, Straub RE, Weickert CS, Hyde TM, Kleinman JE, Weinberger DR (2003) Expression analysis of neuregulin-1 in the dorsolateral prefrontal cortex in schizophrenia. Mol Psychiatry 9:299–307.

Hemming ML, Elias JE, Gygi SP, Selkoe DJ (2008) Proteomic Profiling of γ-Secretase Substrates and Mapping of Substrate Requirements. PLoS Biol 6:e257.

Hemming ML, Elias JE, Gygi SP, Selkoe DJ (2009) Identification of beta-secretase (BACE1) substrates using quantitative proteomics. PloS One 4:e8477.

Herreman A, Serneels L, Annaert W, Collen D, Schoonjans L, De Strooper B (2000) Total inactivation of γ–secretase activity in presenilin-deficient embryonic stem cells. Nat Cell Biol 2:461–462.

Hippenmeyer S, Shneider NA, Birchmeier C, Burden SJ, Jessell TM, Arber S (2002) A role for neuregulin1 signaling in muscle spindle differentiation. Neuron 36:1035–1049.

Hitt BD, Jaramillo TC, Chetkovich DM, Vassar R (2010) BACE1-/- mice exhibit seizure activity that does not correlate with sodium channel level or axonal localization. Mol Neurodegener 5:31.

Ho WH, Armanini MP, Nuijens A, Phillips HS, Osheroff PL (1995) Sensory and motor neuron-derived factor. A novel heregulin variant highly expressed in sensory and motor neurons. J Biol Chem 270:14523–14532.

Hogl S, Kuhn P-H, Colombo A, Lichtenthaler SF (2011) Determination of the Proteolytic Cleavage Sites of the Amyloid Precursor-Like Protein 2 by the Proteases ADAM10, BACE1 and γ-Secretase. PLoS ONE 6:e21337.

Holmes WE, Sliwkowski MX, Akita RW, Henzel WJ, Lee J, Park JW, Yansura D, Abadi N, Raab H, Lewis GD (1992) Identification of heregulin, a specific activator of p185erbB2. Science 256:1205–1210.

Hong L, Koelsch G, Lin X, Wu S, Terzyan S, Ghosh AK, Zhang XC, Tang J (2000) Structure of the Protease Domain of Memapsin 2 (β-Secretase) Complexed with Inhibitor. Science 290:150–153.

Horiuchi K, Zhou H-M, Kelly K, Manova K, Blobel CP (2005) Evaluation of the contributions of ADAMs 9, 12, 15, 17, and 19 to heart development and ectodomain shedding of neuregulins beta1 and beta2. Dev Biol 283:459–471.

Hu X, He W, Diaconu C, Tang X, Kidd GJ, Macklin WB, Trapp BD, Yan R (2008) Genetic deletion of BACE1 in mice affects remyelination of sciatic nerves. FASEB J Off Publ Fed Am Soc Exp Biol 22:2970–2980.

Hu X, Hicks CW, He W, Wong P, Macklin WB, Trapp BD, Yan R (2006) Bace1 modulates myelination in the central and peripheral nervous system. Nat Neurosci 9:1520–1525.

Huppert SS, Le A, Schroeter EH, Mumm JS, Saxena MT, Milner LA, Kopan R (2000) Embryonic lethality in mice homozygous for a processing-deficient allele of Notch1. Nature 405:966–970.

Hussain I, Powell D, Howlett DR, Tew DG, Meek TD, Chapman C, Gloger IS, Murphy KE, Southan CD, Ryan DM, Smith TS, Simmons DL, Walsh FS, Dingwall C, Christie G (1999) Identification of a novel aspartic protease (Asp 2) as beta-secretase. Mol Cell Neurosci 14:419–427.

Ittner LM, Ke YD, Delerue F, Bi M, Gladbach A, van Eersel J, Wölfing H, Chieng BC, Christie MJ, Napier IA, Eckert A, Staufenbiel M, Hardeman E, Götz J (2010) Dendritic function of tau mediates amyloid-beta toxicity in Alzheimer's disease mouse models. Cell 142:387–397.

Iwatsubo T, Odaka A, Suzuki N, Mizusawa H, Nukina N, Ihara Y (1994) Visualization of A beta 42(43) and A beta 40 in senile plaques with end-specific A beta monoclonals: evidence that an initially deposited species is A beta 42(43). Neuron 13:45–53.

Jackson LF, Qiu TH, Sunnarborg SW, Chang A, Zhang C, Patterson C, Lee DC (2003) Defective valvulogenesis in HB-EGF and TACE-null mice is associated with aberrant BMP signaling. EMBO J 22:2704–2716.

Janes PW, Saha N, Barton WA, Kolev MV, Wimmer-Kleikamp SH, Nievergall E, Blobel CP, Himanen J-P, Lackmann M, Nikolov DB (2005) Adam Meets Eph: An ADAM Substrate Recognition Module Acts as a Molecular Switch for Ephrin Cleavage In trans. Cell 123:291–304.

Jessen KR, Mirsky R (2005) The origin and development of glial cells in peripheral nerves. Nat Rev Neurosci 6:671–682.

Jonsson T et al. (2012) A mutation in APP protects against Alzheimer/'s disease and age-related cognitive decline. Nature 488:96–99.

References

Jorissen E, Prox J, Bernreuther C, Weber S, Schwanbeck R, Serneels L, Snellinx A, Craessaerts K, Thathiah A, Tesseur I, Bartsch U, Weskamp G, Blobel CP, Glatzel M, De Strooper B, Saftig P (2010) The disintegrin/metalloproteinase ADAM10 is essential for the establishment of the brain cortex. J Neurosci Off J Soc Neurosci 30:4833–4844.

Kaden D, Harmeier A, Weise C, Munter LM, Althoff V, Rost BR, Hildebrand PW, Schmitz D, Schaefer M, Lurz R, Skodda S, Yamamoto R, Arlt S, Finckh U, Multhaup G (2012) Novel APP/Aβ mutation K16N produces highly toxic heteromeric Aβ oligomers. EMBO Mol Med 4:647–659.

Kaether C, Haass C, Steiner H (2006a) Assembly, Trafficking and Function of &gamma;-Secretase. Neurodegener Dis 3:275–283.

Kaether C, Schmitt S, Willem M, Haass C (2006b) Amyloid Precursor Protein and Notch Intracellular Domains are Generated after Transport of their Precursors to the Cell Surface. Traffic 7:408–415.

Kakuda N, Funamoto S, Yagishita S, Takami M, Osawa S, Dohmae N, Ihara Y (2006) Equimolar Production of Amyloid β-Protein and Amyloid Precursor Protein Intracellular Domain from β-Carboxyl-terminal Fragment by γ-Secretase. J Biol Chem 281:14776–14786.

Kang J, Lemaire HG, Unterbeck A, Salbaum JM, Masters CL, Grzeschik KH, Multhaup G, Beyreuther K, Müller-Hill B (1987) The precursor of Alzheimer's disease amyloid A4 protein resembles a cell-surface receptor. Nature 325:733–736.

Kärkkäinen I, Rybnikova E, Pelto-Huikko M, Huovila AP (2000) Metalloprotease-disintegrin (ADAM) genes are widely and differentially expressed in the adult CNS. Mol Cell Neurosci 15:547–560.

Karl T, Burne THJ, Van den Buuse M, Chesworth R (2011) Do transmembrane domain neuregulin 1 mutant mice exhibit a reliable sensorimotor gating deficit? Behav Brain Res 223:336–341.

Karl T, Duffy L, Scimone A, Harvey RP, Schofield PR (2007) Altered motor activity, exploration and anxiety in heterozygous neuregulin 1 mutant mice: implications for understanding schizophrenia. Genes Brain Behav 6:677–687.

Kiencke P, Daniel D, Grimm C, Rychlik R (2011) Direct costs of Alzheimer's disease in Germany. Eur J Health Econ HEPAC Health Econ Prev Care 12:533–539.

Kim S-H, Yin YI, Li Y-M, Sisodia SS (2004) Evidence That Assembly of an Active γ-Secretase Complex Occurs in the Early Compartments of the Secretory Pathway. J Biol Chem 279:48615–48619.

Kimberly WT, LaVoie MJ, Ostaszewski BL, Ye W, Wolfe MS, Selkoe DJ (2003) γ-Secretase is a membrane protein complex comprised of presenilin, nicastrin, aph-1, and pen-2. Proc Natl Acad Sci 100:6382–6387.

Kimmel CB, Ballard WW, Kimmel SR, Ullmann B, Schilling TF (1995) Stages of embryonic development of the zebrafish. Dev Dyn Off Publ Am Assoc Anat 203:253–310.

Kingsley DM, Kozarsky KF, Hobbie L, Krieger M (1986) Reversible defects in O-linked glycosylation and LDL receptor expression in a UDP-Gal/UDP-GalNAc 4-epimerase deficient mutant. Cell 44:749–759.

Koo EH, Squazzo SL (1994) Evidence that production and release of amyloid beta-protein involves the endocytic pathway. J Biol Chem 269:17386–17389.

Kopan R, Ilagan MXG (2009) The Canonical Notch Signaling Pathway: Unfolding the Activation Mechanism. Cell 137:216–233.

Kraus MH, Issing W, Miki T, Popescu NC, Aaronson SA (1989) Isolation and characterization of ERBB3, a third member of the ERBB/epidermal growth factor receptor family: evidence for overexpression in a subset of human mammary tumors. Proc Natl Acad Sci 86:9193–9197.

Kuhn P-H, Wang H, Dislich B, Colombo A, Zeitschel U, Ellwart JW, Kremmer E, Rossner S, Lichtenthaler SF (2010) ADAM10 is the physiologically relevant, constitutive alpha-secretase of the amyloid precursor protein in primary neurons. EMBO J 29:3020–3032.

Kurohara K, Komatsu K, Kurisaki T, Masuda A, Irie N, Asano M, Sudo K, Nabeshima Y, Iwakura Y, Sehara-Fujisawa A (2004) Essential roles of Meltrin β (ADAM19) in heart development. Dev Biol 267:14–28.

Kyte J, Doolittle RF (1982) A simple method for displaying the hydropathic character of a protein. J Mol Biol 157:105–132.

La Marca R, Cerri F, Horiuchi K, Bachi A, Feltri ML, Wrabetz L, Blobel CP, Quattrini A, Salzer JL, Taveggia C (2011) TACE (ADAM17) inhibits Schwann cell myelination. Nat Neurosci 14:857–865.

Laird FM, Cai H, Savonenko AV, Farah MH, He K, Melnikova T, Wen H, Chiang H-C, Xu G, Koliatsos VE, Borchelt DR, Price DL, Lee H-K, Wong PC (2005) BACE1, a Major Determinant of Selective Vulnerability of the Brain to Amyloid-β Amyloidogenesis, is Essential for Cognitive, Emotional, and Synaptic Functions. J Neurosci 25:11693–11709.

Lal M, Caplan M (2011) Regulated intramembrane proteolysis: signaling pathways and biological functions. Physiol Bethesda Md 26:34–44.

Lammich S, Kojro E, Postina R, Gilbert S, Pfeiffer R, Jasionowski M, Haass C, Fahrenholz F (1999) Constitutive and regulated α-secretase cleavage of Alzheimer's amyloid precursor protein by a disintegrin metalloprotease. Proc Natl Acad Sci U S A 96:3922–3927.

Lammich S, Okochi M, Takeda M, Kaether C, Capell A, Zimmer A-K, Edbauer D, Walter J, Steiner H, Haass C (2002) Presenilin-dependent Intramembrane Proteolysis of CD44

References

Leads to the Liberation of Its Intracellular Domain and the Secretion of an Aβ-like Peptide. J Biol Chem 277:44754–44759.

Landman N, Kim T-W (2004) Got RIP?: Presenilin-dependent intramembrane proteolysis in growth factor receptor signaling. Cytokine Growth Factor Rev 15:337–351.

Laudon H, Hansson EM, Melén K, Bergman A, Farmery MR, Winblad B, Lendahl U, Heijne G von, Näslund J (2005) A Nine-transmembrane Domain Topology for Presenilin 1. J Biol Chem 280:35352–35360.

LaVoie MJ, Fraering PC, Ostaszewski BL, Ye W, Kimberly WT, Wolfe MS, Selkoe DJ (2003) Assembly of the γ-Secretase Complex Involves Early Formation of an Intermediate Subcomplex of Aph-1 and Nicastrin. J Biol Chem 278:37213–37222.

LaVoie MJ, Selkoe DJ (2003) The Notch Ligands, Jagged and Delta, Are Sequentially Processed by α-Secretase and Presenilin/γ-Secretase and Release Signaling Fragments. J Biol Chem 278:34427–34437.

Law AJ, Kleinman JE, Weinberger DR, Weickert CS (2007) Disease-associated intronic variants in the ErbB4 gene are related to altered ErbB4 splice-variant expression in the brain in schizophrenia. Hum Mol Genet 16:129–141.

Law AJ, Lipska BK, Weickert CS, Hyde TM, Straub RE, Hashimoto R, Harrison PJ, Kleinman JE, Weinberger DR (2006) Neuregulin 1 transcripts are differentially expressed in schizophrenia and regulated by 5′ SNPs associated with the disease. Proc Natl Acad Sci 103:6747–6752.

Lee H-J, Jung K-M, Huang YZ, Bennett LB, Lee JS, Mei L, Kim T-W (2002) Presenilin-dependent γ-Secretase-like Intramembrane Cleavage of ErbB4. J Biol Chem 277:6318–6323.

Lee VM-Y, Goedert M, Trojanowski JQ (2001) Neurodegenerative Tauopathies. Annu Rev Neurosci 24:1121–1159.

Li B, Woo R-S, Mei L, Malinow R (2007) The Neuregulin-1 Receptor ErbB4 Controls Glutamatergic Synapse Maturation and Plasticity. Neuron 54:583–597.

Li H, Wang B, Wang Z, Guo Q, Tabuchi K, Hammer RE, Südhof TC, Zheng H (2010) Soluble amyloid precursor protein (APP) regulates transthyretin and Klotho gene expression without rescuing the essential function of APP. Proc Natl Acad Sci 107:17362–17367.

Li K-X, Lu Y-M, Xu Z-H, Zhang J, Zhu J-M, Zhang J-M, Cao S-X, Chen X-J, Chen Z, Luo J-H, Duan S, Li X-M (2012) Neuregulin 1 regulates excitability of fast-spiking neurons through Kv1.1 and acts in epilepsy. Nat Neurosci 15:267–273.

Li Q, Loeb JA (2001) Neuregulin-Heparan-sulfate Proteoglycan Interactions Produce Sustained erbB Receptor Activation Required for the Induction of Acetylcholine Receptors in Muscle. J Biol Chem 276:38068–38075.

Lichtenthaler SF (2011) Alpha-secretase in Alzheimer's disease: molecular identity, regulation and therapeutic potential. J Neurochem 116:10–21.

Lichtenthaler SF, Haass C, Steiner H (2011) Regulated intramembrane proteolysis--lessons from amyloid precursor protein processing. J Neurochem 117:779–796.

Lichtenthaler SF, Wang R, Grimm H, Uljon SN, Masters CL, Beyreuther K (1999) Mechanism of the cleavage specificity of Alzheimer's disease γ-secretase identified by phenylalanine-scanning mutagenesis of the transmembrane domain of the amyloid precursor protein. Proc Natl Acad Sci 96:3053–3058.

Lin X, Koelsch G, Wu S, Downs D, Dashti A, Tang J (2000) Human aspartic protease memapsin 2 cleaves the beta-secretase site of beta-amyloid precursor protein. Proc Natl Acad Sci U S A 97:1456–1460.

Liu X, Bates R, Yin D-M, Shen C, Wang F, Su N, Kirov SA, Luo Y, Wang J-Z, Xiong W-C, Mei L (2011) Specific Regulation of NRG1 Isoform Expression by Neuronal Activity. J Neurosci 31:8491–8501.

Liu X, Hwang H, Cao L, Buckland M, Cunningham A, Chen J, Chien KR, Graham RM, Zhou M (1998) Domain-specific gene disruption reveals critical regulation of neuregulin signaling by its cytoplasmic tail. Proc Natl Acad Sci 95:13024–13029.

Liu Y, Ford B, Mann MA, Fischbach GD (2001) Neuregulins Increase α7 Nicotinic Acetylcholine Receptors and Enhance Excitatory Synaptic Transmission in GABAergic Interneurons of the Hippocampus. J Neurosci 21:5660–5669.

Liu Y, Tao Y-M, Woo R-S, Xiong W-C, Mei L (2007) Stimulated ErbB4 internalization is necessary for neuregulin signaling in neurons. Biochem Biophys Res Commun 354:505–510.

Loeb JA, Khurana TS, Robbins JT, Yee AG, Fischbach GD (1999) Expression patterns of transmembrane and released forms of neuregulin during spinal cord and neuromuscular synapse development. Dev Camb Engl 126:781–791.

López-Otín C, Bond JS (2008) Proteases: Multifunctional Enzymes in Life and Disease. J Biol Chem 283:30433–30437.

Lu HS, Chang D, Philo JS, Zhang K, Narhi LO, Liu N, Zhang M, Sun J, Wen J, Yanagihara D, Karunagaran D, Yarden Y, Ratzkin B (1995a) Studies on the Structure and Function of Glycosylated and Nonglycosylated neu Differentiation Factors SIMILARITIES AND DIFFERENCES OF THE α AND β ISOFORMS. J Biol Chem 270:4784–4791.

Lu HS, Hara S, Wong LW-I, Jones MD, Katta V, Trail G, Zou A, Brankow D, Cole S, Hu S, Wen D (1995b) Post-translational Processing of Membrane-associated neu Differentiation Factor Proisoforms Expressed in Mammalian Cells. J Biol Chem 270:4775–4783.

Luo W, Wang H, Li H, Kim BS, Shah S, Lee H-J, Thinakaran G, Kim T-W, Yu G, Xu H (2003) PEN-2 and APH-1 Coordinately Regulate Proteolytic Processing of Presenilin 1. J Biol Chem 278:7850–7854.

References

Luo X, Prior M, He W, Hu X, Tang X, Shen W, Yadav S, Kiryu-Seo S, Miller R, Trapp BD, Yan R (2011) Cleavage of neuregulin-1 by BACE1 or ADAM10 protein produces differential effects on myelination. J Biol Chem 286:23967–23974.

Luo Y, Bolon B, Kahn S, Bennett BD, Babu-Khan S, Denis P, Fan W, Kha H, Zhang J, Gong Y, Martin L, Louis J-C, Yan Q, Richards WG, Citron M, Vassar R (2001) Mice deficient in BACE1, the Alzheimer's β-secretase, have normal phenotype and abolished β-amyloid generation. Nat Neurosci 4:231–232.

Lyons DA, Pogoda H-M, Voas MG, Woods IG, Diamond B, Nix R, Arana N, Jacobs J, Talbot WS (2005) erbb3 and erbb2 Are Essential for Schwann Cell Migration and Myelination in Zebrafish. Curr Biol 15:513–524.

Marchionni MA, Goodearl AD, Chen MS, Bermingham-McDonogh O, Kirk C, Hendricks M, Danehy F, Misumi D, Sudhalter J, Kobayashi K (1993) Glial growth factors are alternatively spliced erbB2 ligands expressed in the nervous system. Nature 362:312–318.

Marcinkiewicz M, Seidah NG (2000) Coordinated expression of beta-amyloid precursor protein and the putative beta-secretase BACE and alpha-secretase ADAM10 in mouse and human brain. J Neurochem 75:2133–2143.

McConlogue L, Buttini M, Anderson JP, Brigham EF, Chen KS, Freedman SB, Games D, Johnson-Wood K, Lee M, Zeller M, Liu W, Motter R, Sinha S (2007) Partial Reduction of BACE1 Has Dramatic Effects on Alzheimer Plaque and Synaptic Pathology in APP Transgenic Mice. J Biol Chem 282:26326–26334.

Meakin PJ, Harper AJ, Hamilton DL, Gallagher J, McNeilly AD, Burgess LA, Vaanholt LM, Bannon KA, Latcham J, Hussain I, Speakman JR, Howlett DR, Ashford MLJ (2012) Reduction in BACE1 decreases body weight, protects against diet-induced obesity and enhances insulin sensitivity in mice. Biochem J 441:285–296.

Mei L, Xiong W-C (2008) Neuregulin 1 in neural development, synaptic plasticity and schizophrenia. Nat Rev Neurosci 9:437–452.

Meyer D, Birchmeier C (1994) Distinct isoforms of neuregulin are expressed in mesenchymal and neuronal cells during mouse development. Proc Natl Acad Sci 91:1064–1068.

Meyer D, Birchmeier C (1995) Multiple essential functions of neuregulin in development. Nature 378:386–390.

Meyer D, Yamaai T, Garratt A, Riethmacher-Sonnenberg E, Kane D, Theill LE, Birchmeier C (1997) Isoform-specific expression and function of neuregulin. Dev Camb Engl 124:3575–3586.

Meziane H, Dodart J-C, Mathis C, Little S, Clemens J, Paul SM, Ungerer A (1998) Memory-enhancing effects of secreted forms of the β-amyloid precursor protein in normal and amnestic mice. Proc Natl Acad Sci 95:12683–12688.

Michailov GV, Sereda MW, Brinkmann BG, Fischer TM, Haug B, Birchmeier C, Role L, Lai C, Schwab MH, Nave K-A (2004) Axonal neuregulin-1 regulates myelin sheath thickness. Science 304:700–703.

Montero JC, Yuste L, Díaz-Rodríguez E, Esparís-Ogando A, Pandiella A (2000) Differential shedding of transmembrane neuregulin isoforms by the tumor necrosis factor-alpha-converting enzyme. Mol Cell Neurosci 16:631–648.

Morris JK, Lin W, Hauser C, Marchuk Y, Getman D, Lee K-F (1999) Rescue of the Cardiac Defect in ErbB2 Mutant Mice Reveals Essential Roles of ErbB2 in Peripheral Nervous System Development. Neuron 23:273–283.

Morris M, Maeda S, Vossel K, Mucke L (2011) The many faces of tau. Neuron 70:410–426.

Mullan M, Crawford F, Axelman K, Houlden H, Lilius L, Winblad B, Lannfelt L (1992) A pathogenic mutation for probable Alzheimer's disease in the APP gene at the N–terminus of β–amyloid. Nat Genet 1:345–347.

Mullane K, Williams M (2013) Alzheimer's therapeutics: Continued clinical failures question the validity of the amyloid hypothesis—but what lies beyond? Biochem Pharmacol 85:289–305.

Mumm JS, Kopan R (2000) Notch Signaling: From the Outside In. Dev Biol 228:151–165.

Mumm JS, Schroeter EH, Saxena MT, Griesemer A, Tian X, Pan D., Ray WJ, Kopan R (2000) A Ligand-Induced Extracellular Cleavage Regulates γ-Secretase-like Proteolytic Activation of Notch1. Mol Cell 5:197–206.

Münzel EJ, Schaefer K, Obirei B, Kremmer E, Burton EA, Kuscha V, Becker CG, Brösamle C, Williams A, Becker T (2012) Claudin k is specifically expressed in cells that form myelin during development of the nervous system and regeneration of the optic nerve in adult zebrafish. Glia 60:253–270.

Murphy MP, Hickman LJ, Eckman CB, Uljon SN, Wang R, Golde TE (1999) γ-Secretase, Evidence for Multiple Proteolytic Activities and Influence of Membrane Positioning of Substrate on Generation of Amyloid β Peptides of Varying Length. J Biol Chem 274:11914–11923.

Nave K-A (2010) Myelination and the trophic support of long axons. Nat Rev Neurosci 11:275–283.

Nave K-A, Salzer JL (2006) Axonal regulation of myelination by neuregulin 1. Curr Opin Neurobiol 16:492–500.

Newbern J, Birchmeier C (2010) Nrg1/ErbB signaling networks in Schwann cell development and myelination. Semin Cell Dev Biol 21:922–928.

Ni C-Y, Murphy MP, Golde TE, Carpenter G (2001) γ-Secretase Cleavage and Nuclear Localization of ErbB-4 Receptor Tyrosine Kinase. Science 294:2179–2181.

Nilsberth C, Westlind-Danielsson A, Eckman CB, Condron MM, Axelman K, Forsell C, Stenh C, Luthman J, Teplow DB, Younkin SG, Näslund J, Lannfelt L (2001) The "Arctic"

References

APP mutation (E693G) causes Alzheimer's disease by enhanced Aβ protofibril formation. Nat Neurosci 4:887–893.

O'Tuathaigh CM, O'Sullivan GJ, Kinsella A, Harvey RP, Tighe O, Croke DT, Waddington JL (2006) Sexually dimorphic changes in the exploratory and habituation profiles of heterozygous neuregulin-1 knockout mice. [Miscellaneous Article]. Neuroreport January 23 2006 17:79–83.

Oehlrich D, Berthelot DJ-C, Gijsen HJM (2011) γ-Secretase Modulators as Potential Disease Modifying Anti-Alzheimer's Drugs. J Med Chem 54:669–698.

Ogata T, Iijima S, Hoshikawa S, Miura T, Yamamoto S, Oda H, Nakamura K, Tanaka S (2004) Opposing Extracellular Signal-Regulated Kinase and Akt Pathways Control Schwann Cell Myelination. J Neurosci 24:6724–6732.

Okamoto I, Kawano Y, Murakami D, Sasayama T, Araki N, Miki T, Wong AJ, Saya H (2001) Proteolytic release of CD44 intracellular domain and its role in the CD44 signaling pathway. J Cell Biol 155:755–762.

Okochi M, Fukumori A, Jiang J, Itoh N, Kimura R, Steiner H, Haass C, Tagami S, Takeda M (2006) Secretion of the Notch-1 Aβ-like Peptide during Notch Signaling. J Biol Chem 281:7890–7898.

Okochi M, Steiner H, Fukumori A, Tanii H, Tomita T, Tanaka T, Iwatsubo T, Kudo T, Takeda M, Haass C (2002) Presenilins mediate a dual intramembranous γ-secretase cleavage of Notch-1. EMBO J 21:5408–5416.

Orr-Urtreger A, Trakhtenbrot L, Ben-Levy R, Wen D, Rechavi G, Lonai P, Yarden Y (1993) Neural expression and chromosomal mapping of Neu differentiation factor to 8p12-p21. Proc Natl Acad Sci U S A 90:1867–1871.

Ozaki M, Sasner M, Yano R, Lu HS, Buonanno A (1997) Neuregulin-β induces expression of an NMDA-receptor subunit. Nature 390:691–694.

Pasquale EB (2008) Eph-Ephrin Bidirectional Signaling in Physiology and Disease. Cell 133:38–52.

Peles E, Bacus SS, Koski RA, Lu HS, Wen D, Ogden SG, Levy RB, Yarden Y (1992) Isolation of the neu/HER-2 stimulatory ligand: a 44 kd glycoprotein that induces differentiation of mammary tumor cells. Cell 69:205–216.

Perlin JR, Lush ME, Stephens WZ, Piotrowski T, Talbot WS (2011) Neuronal Neuregulin 1 type III directs Schwann cell migration. Dev Camb Engl 138:4639–4648.

Peschon JJ, Slack JL, Reddy P, Stocking KL, Sunnarborg SW, Lee DC, Russell WE, Castner BJ, Johnson RS, Fitzner JN, Boyce RW, Nelson N, Kozlosky CJ, Wolfson MF, Rauch CT, Cerretti DP, Paxton RJ, March CJ, Black RA (1998) An essential role for ectodomain shedding in mammalian development. Science 282:1281–1284.

Pinnix I, Musunuru U, Tun H, Sridharan A, Golde T, Eckman C, Ziani-Cherif C, Onstead L, Sambamurti K (2001) A Novel γ-Secretase Assay Based on Detection of the Putative C-terminal Fragment-γ of Amyloid β Protein Precursor. J Biol Chem 276:481–487.

Plowman GD, Culouscou JM, Whitney GS, Green JM, Carlton GW, Foy L, Neubauer MG, Shoyab M (1993) Ligand-specific activation of HER4/p180erbB4, a fourth member of the epidermal growth factor receptor family. Proc Natl Acad Sci 90:1746–1750.

Prokop S, Shirotani K, Edbauer D, Haass C, Steiner H (2004) Requirement of PEN-2 for Stabilization of the Presenilin N-/C-terminal Fragment Heterodimer within the γ-Secretase Complex. J Biol Chem 279:23255–23261.

Puente XS, Sánchez LM, Overall CM, López-Otín C (2003) Human and mouse proteases: a comparative genomic approach. Nat Rev Genet 4:544–558.

Qi-Takahara Y, Morishima-Kawashima M, Tanimura Y, Dolios G, Hirotani N, Horikoshi Y, Kametani F, Maeda M, Saido TC, Wang R, Ihara Y (2005) Longer forms of amyloid beta protein: implications for the mechanism of intramembrane cleavage by gamma-secretase. J Neurosci Off J Soc Neurosci 25:436–445.

Querfurth HW, LaFerla FM (2010) Alzheimer's disease. N Engl J Med 362:329–344.

Reiss K, Saftig P (2009) The "a disintegrin and metalloprotease" (ADAM) family of sheddases: physiological and cellular functions. Semin Cell Dev Biol 20:126–137.

Rieff HI, Raetzman LT, Sapp DW, Yeh HH, Siegel RE, Corfas G (1999) Neuregulin Induces GABAA Receptor Subunit Expression and Neurite Outgrowth in Cerebellar Granule Cells. J Neurosci 19:10757–10766.

Riethmacher D, Sonnenberg-Riethmacher E, Brinkmann V, Yamaai T, Lewin GR, Birchmeier C (1997) Severe neuropathies in mice with targeted mutations in the ErbB3 receptor. Nature 389:725–730.

Ring S, Weyer SW, Kilian SB, Waldron E, Pietrzik CU, Filippov MA, Herms J, Buchholz C, Eckman CB, Korte M, Wolfer DP, Müller UC (2007) The Secreted β-Amyloid Precursor Protein Ectodomain APPsα Is Sufficient to Rescue the Anatomical, Behavioral, and Electrophysiological Abnormalities of APP-Deficient Mice. J Neurosci 27:7817–7826.

Rio C, Rieff HI, Qi P, Corfas G (1997) Neuregulin and erbB Receptors Play a Critical Role in Neuronal Migration. Neuron 19:39–50.

Roberds SL et al. (2001) BACE knockout mice are healthy despite lacking the primary beta-secretase activity in brain: implications for Alzheimer's disease therapeutics. Hum Mol Genet 10:1317–1324.

Roberson ED, Scearce-Levie K, Palop JJ, Yan F, Cheng IH, Wu T, Gerstein H, Yu G-Q, Mucke L (2007) Reducing endogenous tau ameliorates amyloid beta-induced deficits in an Alzheimer's disease mouse model. Science 316:750–754.

References

Saftig P, Reiss K (2011) The "A Disintegrin And Metalloproteases" ADAM10 and ADAM17: Novel drug targets with therapeutic potential? Eur J Cell Biol 90:527–535.

Sannerud R, Annaert W (2009) Trafficking, a key player in regulated intramembrane proteolysis. Semin Cell Dev Biol 20:183–190.

Sastre M, Steiner H, Fuchs K, Capell A, Multhaup G, Condron MM, Teplow DB, Haass C (2001) Presenilin-dependent γ-secretase processing of β-amyloid precursor protein at a site corresponding to the S3 cleavage of Notch. EMBO Rep 2:835–841.

Sato T, Diehl TS, Narayanan S, Funamoto S, Ihara Y, Strooper BD, Steiner H, Haass C, Wolfe MS (2007) Active γ-Secretase Complexes Contain Only One of Each Component. J Biol Chem 282:33985–33993.

Savonenko AV, Melnikova T, Laird FM, Stewart K-A, Price DL, Wong PC (2008) Alteration of BACE1-dependent NRG1/ErbB4 signaling and schizophrenia-like phenotypes in BACE1-null mice. Proc Natl Acad Sci U S A 105:5585–5590.

Schechter AL, Stern DF, Vaidyanathan L, Decker SJ, Drebin JA, Greene MI, Weinberg RA (1984) The neu oncogene: an erb-B-related gene encoding a 185,000-Mr tumour antigen. Nature 312:513–516.

Scheuner D et al. (1996) Secreted amyloid beta-protein similar to that in the senile plaques of Alzheimer's disease is increased in vivo by the presenilin 1 and 2 and APP mutations linked to familial Alzheimer's disease. Nat Med 2:864–870.

Schlöndorff J, Becherer JD, Blobel CP (2000) Intracellular maturation and localization of the tumour necrosis factor alpha convertase (TACE). Biochem J 347 Pt 1:131–138.

Schroeter EH, Kisslinger JA, Kopan R (1998) Notch-1 signalling requires ligand-induced proteolytic release of intracellular domain. Nature 393:382–386.

Selkoe DJ (1999) Translating cell biology into therapeutic advances in Alzheimer's disease. Nature 399:A23–31.

Selkoe DJ (2001) Alzheimer's disease: genes, proteins, and therapy. Physiol Rev 81:741–766.

Shah S, Lee S-F, Tabuchi K, Hao Y-H, Yu C, LaPlant Q, Ball H, Dann CE, Südhof T, Yu G (2005) Nicastrin Functions as a γ-Secretase-Substrate Receptor. Cell 122:435–447.

Sheng JG, Price DL, Koliatsos VE (2003) The β-amyloid-related proteins presenilin 1 and BACE1 are axonally transported to nerve terminals in the brain. Exp Neurol 184:1053–1057.

Shirakabe K, Wakatsuki S, Kurisaki T, Fujisawa-Sehara A (2001) Roles of Meltrin beta /ADAM19 in the processing of neuregulin. J Biol Chem 276:9352–9358.

Silberberg G, Darvasi A, Pinkas-Kramarski R, Navon R (2006) The involvement of ErbB4 with schizophrenia: Association and expression studies. Am J Med Genet B Neuropsychiatr Genet 141B:142–148.

Sinha S et al. (1999) Purification and cloning of amyloid precursor protein β-secretase from human brain. Nature 402:537–540.

Sisodia SS (1992) Beta-amyloid precursor protein cleavage by a membrane-bound protease. Proc Natl Acad Sci 89:6075–6079.

Sisodia SS, St George-Hyslop PH (2002) gamma-Secretase, Notch, Abeta and Alzheimer's disease: where do the presenilins fit in? Nat Rev Neurosci 3:281–290.

Six E, Ndiaye D, Laabi Y, Brou C, Gupta-Rossi N, Israel A, Logeat F (2003) The Notch ligand Delta1 is sequentially cleaved by an ADAM protease and ?-secretase. Proc Natl Acad Sci U S A 100:7638–7643.

Spasic D, Annaert W (2008) Building γ-secretase – the bits and pieces. J Cell Sci 121:413–420.

St George-Hyslop PH (2000) Molecular genetics of Alzheimer's disease. Biol Psychiatry 47:183–199.

Stefansson H et al. (2002) Neuregulin 1 and Susceptibility to Schizophrenia. Am J Hum Genet 71:877–892.

Steiner H, Fluhrer R, Haass C (2008) Intramembrane proteolysis by gamma-secretase. J Biol Chem 283:29627–29631.

Steiner H, Kostka M, Romig H, Basset G, Pesold B, Hardy J, Capell A, Meyn L, Grim ML, Baumeister R, Fechteler K, Haass C (2000) Glycine 384 is required for presenilin-1 function and is conserved in bacterial polytopic aspartyl proteases. Nat Cell Biol 2:848–851.

Steinthorsdottir V, Stefansson H, Ghosh S, Birgisdottir B, Bjornsdottir S, Fasquel AC, Olafsson O, Stefansson K, Gulcher JR (2004) Multiple novel transcription initiation sites for NRG1. Gene 342:97–105.

Sternlicht MD, Sunnarborg SW, Kouros-Mehr H, Yu Y, Lee DC, Werb Z (2005) Mammary ductal morphogenesis requires paracrine activation of stromal EGFR via ADAM17-dependent shedding of epithelial amphiregulin. Dev Camb Engl 132:3923–3933.

Stockley JH, O'Neill C (2008) Understanding BACE1: essential protease for amyloid-β production in Alzheimer's disease. Cell Mol Life Sci 65:3265–3289.

Strooper BD (2010) Proteases and Proteolysis in Alzheimer Disease: A Multifactorial View on the Disease Process. Physiol Rev 90:465–494.

Struhl G, Adachi A (2000) Requirements for Presenilin-Dependent Cleavage of Notch and Other Transmembrane Proteins. Mol Cell 6:625–636.

Suzuki N, Cheung TT, Cai XD, Odaka A, Otvos L Jr, Eckman C, Golde TE, Younkin SG (1994) An increased percentage of long amyloid beta protein secreted by familial amyloid beta protein precursor (beta APP717) mutants. Science 264:1336–1340.

References

Syed N, Reddy K, Yang DP, Taveggia C, Salzer JL, Maurel P, Kim HA (2010) Soluble neuregulin-1 has bifunctional, concentration-dependent effects on Schwann cell myelination. J Neurosci Off J Soc Neurosci 30:6122–6131.

Takami M, Nagashima Y, Sano Y, Ishihara S, Morishima-Kawashima M, Funamoto S, Ihara Y (2009) gamma-Secretase: successive tripeptide and tetrapeptide release from the transmembrane domain of beta-carboxyl terminal fragment. J Neurosci Off J Soc Neurosci 29:13042–13052.

Talmage DA (2008) Mechanisms of neuregulin action. Novartis Found Symp 289:74–93.

Tan G-H, Liu Y-Y, Hu X-L, Yin D-M, Mei L, Xiong Z-Q (2012) Neuregulin 1 represses limbic epileptogenesis through ErbB4 in parvalbumin-expressing interneurons. Nat Neurosci 15:258–266.

Tartaglia GG, Pawar AP, Campioni S, Dobson CM, Chiti F, Vendruscolo M (2008) Prediction of Aggregation-Prone Regions in Structured Proteins. J Mol Biol 380:425–436.

Tartaglia GG, Vendruscolo M (2008) The Zyggregator method for predicting protein aggregation propensities. Chem Soc Rev 37:1395–1401.

Taveggia C, Feltri ML, Wrabetz L (2010) Signals to promote myelin formation and repair. Nat Rev Neurol 6:276–287.

Taveggia C, Zanazzi G, Petrylak A, Yano H, Rosenbluth J, Einheber S, Xu X, Esper RM, Loeb JA, Shrager P, Chao MV, Falls DL, Role L, Salzer JL (2005) Neuregulin-1 type III determines the ensheathment fate of axons. Neuron 47:681–694.

Thinakaran G, Borchelt DR, Lee MK, Slunt HH, Spitzer L, Kim G, Ratovitsky T, Davenport F, Nordstedt C, Seeger M, Hardy J, Levey AI, Gandy SE, Jenkins NA, Copeland NG, Price DL, Sisodia SS (1996) Endoproteolysis of Presenilin 1 and Accumulation of Processed Derivatives In Vivo. Neuron 17:181–190.

Thind K, Sabbagh MN (2007) Pathological correlates of cognitive decline in Alzheimer's disease. Panminerva Med 49:191–195.

Tiscornia G, Singer O, Verma IM (2006) Production and purification of lentiviral vectors. Nat Protoc 1:241–245.

Tomita T (2009) Secretase inhibitors and modulators for Alzheimer's disease treatment. Expert Rev Neurother 9:661–679.

Tsuang MT, Stone WS, Faraone SV (2001) Genes, environment and schizophrenia. Br J Psychiatry 178:s18–s24.

Turk B (2006) Targeting proteases: successes, failures and future prospects. Nat Rev Drug Discov 5:785–799.

Turk B, Turk DSA, Turk V (2012) Protease signalling: the cutting edge. EMBO J 31:1630–1643.

Van Bebber F, Hruscha A, Willem M, Schmid B, Haass C (2013) Loss of Bace2 in zebrafish affects melanocyte migration and is distinct from Bace1 knock out phenotypes. J Neurochem.

Vassar R et al. (1999) β-Secretase Cleavage of Alzheimer's Amyloid Precursor Protein by the Transmembrane Aspartic Protease BACE. Science 286:735–741.

Vassar R, Kandalepas PC (2011) The β-secretase enzyme BACE1 as a therapeutic target for Alzheimer's disease. Alzheimers Res Ther 3:20.

Velanac V, Unterbarnscheidt T, Hinrichs W, Gummert MN, Fischer TM, Rossner MJ, Trimarco A, Brivio V, Taveggia C, Willem M, Haass C, Möbius W, Nave K-A, Schwab MH (2012) Bace1 processing of NRG1 type III produces a myelin-inducing signal but is not essential for the stimulation of myelination. Glia 60:203–217.

Vidal GA, Naresh A, Marrero L, Jones FE (2005) Presenilin-dependent γ-Secretase Processing Regulates Multiple ERBB4/HER4 Activities. J Biol Chem 280:19777–19783.

Vigo-Pelfrey C, Lee D, Keim P, Lieberburg I, Schenk DB (1993) Characterization of beta-amyloid peptide from human cerebrospinal fluid. J Neurochem 61:1965–1968.

Walsh DM, Klyubin I, Fadeeva JV, Cullen WK, Anwyl R, Wolfe MS, Rowan MJ, Selkoe DJ (2002) Naturally secreted oligomers of amyloid beta protein potently inhibit hippocampal long-term potentiation in vivo. Nature 416:535–539.

Walsh T et al. (2008) Rare Structural Variants Disrupt Multiple Genes in Neurodevelopmental Pathways in Schizophrenia. Science 320:539–543.

Walss-Bass C, Liu W, Lew DF, Villegas R, Montero P, Dassori A, Leach RJ, Almasy L, Escamilla M, Raventos H (2006) A novel missense mutation in the transmembrane domain of neuregulin 1 is associated with schizophrenia. Biol Psychiatry 60:548–553.

Wang JY, Miller SJ, Falls DL (2001) The N-terminal region of neuregulin isoforms determines the accumulation of cell surface and released neuregulin ectodomain. J Biol Chem 276:2841–2851.

Wang R, Sweeney D, Gandy SE, Sisodia SS (1996) The Profile of Soluble Amyloid β Protein in Cultured Cell Media. J Biol Chem 271:31894 –31902.

Weggen S, Eriksen JL, Das P, Sagi SA, Wang R, Pietrzik CU, Findlay KA, Smith TE, Murphy MP, Bulter T, Kang DE, Marquez-Sterling N, Golde TE, Koo EH (2001) A subset of NSAIDs lower amyloidogenic Abeta42 independently of cyclooxygenase activity. Nature 414:212–216.

Weidemann A, Eggert S, Reinhard FBM, Vogel M, Paliga K, Baier G, Masters CL, Beyreuther K, Evin G (2002) A Novel ε-Cleavage within the Transmembrane Domain of the Alzheimer Amyloid Precursor Protein Demonstrates Homology with Notch Processing†. Biochemistry (Mosc) 41:2825–2835.

References

Weihofen A, Martoglio B (2003) Intramembrane-cleaving proteases: controlled liberation of proteins and bioactive peptides. Trends Cell Biol 13:71–78.

Wen D, Peles E, Cupples R, Suggs SV, Bacus SS, Luo Y, Trail G, Hu S, Silbiger SM, Levy RB (1992) Neu differentiation factor: a transmembrane glycoprotein containing an EGF domain and an immunoglobulin homology unit. Cell 69:559–572.

Wen D, Suggs SV, Karunagaran D, Liu N, Cupples RL, Luo Y, Janssen AM, Ben-Baruch N, Trollinger DB, Jacobsen VL (1994) Structural and functional aspects of the multiplicity of Neu differentiation factors. Mol Cell Biol 14:1909–1919.

Weskamp G, Schlöndorff J, Lum L, Becherer JD, Kim T-W, Saftig P, Hartmann D, Murphy G, Blobel CP (2004) Evidence for a Critical Role of the Tumor Necrosis Factor α Convertase (TACE) in Ectodomain Shedding of the p75 Neurotrophin Receptor (p75NTR). J Biol Chem 279:4241–4249.

Westmeyer GG, Willem M, Lichtenthaler SF, Lurman G, Multhaup G, Assfalg-Machleidt I, Reiss K, Saftig P, Haass C (2004) Dimerization of β-Site β-Amyloid Precursor Protein-cleaving Enzyme. J Biol Chem 279:53205–53212.

Willem M, Garratt AN, Novak B, Citron M, Kaufmann S, Rittger A, DeStrooper B, Saftig P, Birchmeier C, Haass C (2006) Control of peripheral nerve myelination by the beta-secretase BACE1. Science 314:664–666.

Willem M, Lammich S, Haass C (2009) Function, regulation and therapeutic properties of beta-secretase (BACE1). Semin Cell Dev Biol 20:175–182.

Wimo A, Prince M (2010) World Alzheimer Report 2010: The Global Economic Impact of Dementia. Lond Alzheimer's Dis Int:1–56.

Woldeyesus MT, Britsch S, Riethmacher D, Xu L, Sonnenberg-Riethmacher E, Abou-Rebyeh F, Harvey R, Caroni P, Birchmeier C (1999) Peripheral nervous system defects in erbB2 mutants following genetic rescue of heart development. Genes Dev 13:2538–2548.

Wolfe MS (2009) Intramembrane Proteolysis. Chem Rev 109:1599–1612.

Wolfe MS, De Los Angeles J, Miller DD, Xia W, Selkoe DJ (1999a) Are Presenilins Intramembrane-Cleaving Proteases? Implications for the Molecular Mechanism of Alzheimer's Disease†. Biochemistry (Mosc) 38:11223–11230.

Wolfe MS, Xia W, Ostaszewski BL, Diehl TS, Kimberly WT, Selkoe DJ (1999b) Two transmembrane aspartates in presenilin-1 required for presenilin endoproteolysis and γ-secretase activity. Nature 398:513–517.

Wolpowitz D, Mason TB, Dietrich P, Mendelsohn M, Talmage DA, Role LW (2000) Cysteine-rich domain isoforms of the neuregulin-1 gene are required for maintenance of peripheral synapses. Neuron 25:79–91.

Wong GT, Manfra D, Poulet FM, Zhang Q, Josien H, Bara T, Engstrom L, Pinzon-Ortiz M, Fine JS, Lee H-JJ, Zhang L, Higgins GA, Parker EM (2004) Chronic Treatment with

the γ-Secretase Inhibitor LY-411,575 Inhibits β-Amyloid Peptide Production and Alters Lymphopoiesis and Intestinal Cell Differentiation. J Biol Chem 279:12876–12882.

Woo R-S, Li X-M, Tao Y, Carpenter-Hyland E, Huang YZ, Weber J, Neiswender H, Dong X-P, Wu J, Gassmann M, Lai C, Xiong W-C, Gao T-M, Mei L (2007) Neuregulin-1 Enhances Depolarization-Induced GABA Release. Neuron 54:599–610.

Woodhoo A, Alonso MBD, Droggiti A, Turmaine M, D'Antonio M, Parkinson DB, Wilton DK, Al-Shawi R, Simons P, Shen J, Guillemot F, Radtke F, Meijer D, Feltri ML, Wrabetz L, Mirsky R, Jessen KR (2009) Notch controls embryonic Schwann cell differentiation, postnatal myelination and adult plasticity. Nat Neurosci 12:839–847.

Woodhoo A, Sommer L (2008) Development of the Schwann cell lineage: From the neural crest to the myelinated nerve. Glia 56:1481–1490.

Yan R, Bienkowski MJ, Shuck ME, Miao H, Tory MC, Pauley AM, Brashler JR, Stratman NC, Mathews WR, Buhl AE, Carter DB, Tomasselli AG, Parodi LA, Heinrikson RL, Gurney ME (1999) Membrane-anchored aspartyl protease with Alzheimer's disease β-secretase activity. Nature 402:533–537.

Yang X-L, Huang YZ, Xiong WC, Mei L (2005) Neuregulin-induced expression of the acetylcholine receptor requires endocytosis of ErbB receptors. Mol Cell Neurosci 28:335–346.

Yarden Y, Sliwkowski MX (2001) Untangling the ErbB signalling network. Nat Rev Mol Cell Biol 2:127–137.

Yu C, Kim SH, Ikeuchi T, Xu H, Gasparini L, Wang R, Sisodia SS (2001) Characterization of a presenilin-mediated amyloid precursor protein carboxyl-terminal fragment gamma. Evidence for distinct mechanisms involved in gamma -secretase processing of the APP and Notch1 transmembrane domains. J Biol Chem 276:43756–43760.

Yu G et al. (2000) Nicastrin modulates presenilin-mediated notch/glp-1 signal transduction and βAPP processing. Nature 407:48–54.

Zhang D, Sliwkowski MX, Mark M, Frantz G, Akita R, Sun Y, Hillan K, Crowley C, Brush J, Godowski PJ (1997) Neuregulin-3 (NRG3): A Novel Neural Tissue-Enriched Protein that Binds and Activates ErbB4. Proc Natl Acad Sci U S A 94:9562–9567.

Zhang H, Berezov A, Wang Q, Zhang G, Drebin J, Murali R, Greene MI (2007) ErbB receptors: from oncogenes to targeted cancer therapies. J Clin Invest 117:2051–2058.

Zhang Z, Nadeau P, Song W, Donoviel D, Yuan M, Bernstein A, Yankner BA (2000) Presenilins are required for γ-secretase cleavage of β-APP and transmembrane cleavage of Notch-1. Nat Cell Biol 2:463–465.

Zhao G, Cui M-Z, Mao G, Dong Y, Tan J, Sun L, Xu X (2005) γ-Cleavage Is Dependent on ζ-Cleavage during the Proteolytic Processing of Amyloid Precursor Protein within Its Transmembrane Domain. J Biol Chem 280:37689–37697.

References

Zheng H, Koo EH (2011) Biology and pathophysiology of the amyloid precursor protein. Mol Neurodegener 6:27.

Zhou H-M, Weskamp G, Chesneau V, Sahin U, Vortkamp A, Horiuchi K, Chiusaroli R, Hahn R, Wilkes D, Fisher P, Baron R, Manova K, Basson CT, Hempstead B, Blobel CP (2004) Essential Role for ADAM19 in Cardiovascular Morphogenesis. Mol Cell Biol 24:96–104.

Zhou W, Carpenter G (2000) Heregulin-dependent Trafficking and Cleavage of ErbB-4. J Biol Chem 275:34737–34743.

7   Acknowledgements

First and foremost I thank **Prof. Dr. Christian Haass** for being my mentor and giving me the chance to work in his lab and under his supervision. I am deeply grateful for his advice, his enthusiasm, his constant support and the many contributions he made to my projects. I am especially thankful for his dedication and help in publishing my findings. He taught me how to write a scientific publication. Above all I thank him for his exceptional support and mentoring in finding a postdoc position. I will never forget whose help brought me to San Francisco.

I am also extremely grateful to **Dr. Michael Willem** who directly supervised not only my PhD thesis but also my Master thesis and before that my internship in the lab. Without his support and his trust in my abilities I would not have gotten the chance to do my Master and PhD thesis in this laboratory. He taught me most of what I know about the practical work at the bench, trained me as a scientist and encouraged me to think critically. His great knowledge of the scientific literature, his ability to recognize hidden details in experimental results and his willingness to challenge existing theories laid the foundations of the projects I worked on.

Chiara Galante was the first master student I directly supervised in the lab. I thank her for making this experience so pleasurable, for all the hard work she contributed to my projects and for the great trip to Italy and her hospitality.

I also thank **Barbara Bettegazzi** for being a great PhD colleague in the α- and β-group, for teaching me a lot of techniques and for being so knowledgeable and helpful. Most of all I thank her and her family for becoming such good friends.

Without the help and support of the following collaborators the NRG1 type III ectodomain processing project would not have been possible: **Dr. Frauke van Bebber, Dr. Bettina Schmid, Dr. Dieter Edbauer, Dr. Alessio Colombo, Dr. Sabina Tahirovic and Prof. Dr. Stefan Lichtenthaler.** I thank them for sharing their technical expertise and their time. I am also grateful to **Akio Fukumori** who introduced me to the basics of mass spectrometry and taught me how to use the MALDI-TOF.

I thank the present and past members of the α- and β-group, especially **Bozidar Novak** and **Ann-Katrin Ludwig** who taught me a lot of basic experimental techniques and were patient with me when I first arrived in the lab. I also thank **Dr. Sven Lammich**, **Heike Hampel** and **Veronika Müller**.

I thank **Dr. Anja Capell** and her group for being such nice lab neighbors and especially **Katrin Fellerer** and **Julia Goetzl** for their help and many fun conversations.

Acknowledgements

During my time in the lab I have had the pleasure of meeting and working with some truly exceptional people, many of whom have become good friends. I especially thank the following for all the great times both inside and outside of the lab: **Julia Schlehe, Lena Bouman, Ulf Dettmer, Aaron Carlson, Manuel Lehm, Peer-Hendrik Kuhn, Alexander Hruscha, Richard Page, Anna Pilsl, Mara Taverna, Amelie Ebke, Benedikt Kretner, Jasmin Sydow, Joanna McCarter, Teresa Bachhuber and Gernot Kleinberger.**

I am especially grateful to the George Clooney fan club for the countless fantastic lunches with hilarious conversations and discussions about topics inside and outside of science. **Kathrin Müller-Rischart, Carolin Schweimer, Maria Sadic, Eva Bentmann, Benjamin Schwenk and Matthias Voss** thank you for knowing me in both my two (!) moods and for making my time in the lab a great and memorable one.

I thank **Sabine Odoy** for the perfect lab management and all the past and present members of the Haass lab who were excellent colleagues and contributed to the nice atmosphere in the lab.

I am indebted to the **Hans and Ilse Breuer Foundation** for their financial support and their invitations to the Eibsee Meetings.

I also thank all the members of the book club, especially **Alice Suelzen**, for broadening my horizon, all the nice meetings and the stimulating discussions about literature.

Finally, I thank my family, my parents **Marta** and **Karl-Heinz** and my brothers **Simon** and **Johannes** for their unlimited support and encouragement and for knowing the real me.

Last but not least I thank **Katja**, my Lebensmensch, for being at my side every step of the way.

8 Abbreviations

3 dpf	3 days postfertilization
Aβ	Amyloid β-peptide
AChR	Acetylcholine receptor
AD	Alzheimer's disease
ADAM	A disintegrin and metalloproteinase
AICD	Amyloid precursor protein intracellular domain
AMPA	2-amino-3-(3-hydroxy-5-methyl-isoxazol-4-yl)propanoic acid)
APH-1	Anterior pharynx-defective-1
APP	Amyloid precursor protein
ARIA	Acetylcholine receptor inducing activity
B4-ICD	ErbB4 intracellular domain
BACE1	β-site APP cleaving enzyme 1
CNS	Central nervous system
CRD	Cysteine-rich domain
CTF	C-terminal fragment
DRG	Dorsal root ganglia
EGF	Epidermal growth factor
EGFR	Epidermal growth factor receptor
ELISA	Enzyme-linked immunosorbent assay
Erk	Extracellular signal-regulated kinase
FAD	Familial Alzheimer's disease
GABA	γ-Aminobutyric acid
GGF	Glial growth factor
GSI	γ-Secretase inhibitors
GSM	γ-Secretase modulator
HRG	Heregulin
ICD	Intracellular domain
IP-MS	Immunoprecipitation mass spectrometry
KO	Knockout
MALDI-TOF	Matrix-assisted laser desorption/ionization time of flight mass spectrometry
MAPK	Mitogen-activated kinase
MS	Mass spectrometry

Abbreviations

NCSC	Neural crest stem cell
NCT	Nicastrin
NDF	Neu differentiation factor
NEXT	Notch extracellular truncated
NICD	Notch intracellular domain
NMDA	N-Methyl-D-Aspartic acid
NRG1	Neuregulin-1
NRG1-ICD	Neuregulin-1 intracellular domain
NTF	N-terminal fragment
o/n	Overnight
PEN2	Presenilin enhancer-2
PI3K	Phosphatidylinositol 3 kinase
PKB or AKT	Protein kinase B
PNS	Peripheral nervous system
PS	Presenilin
PSD-95	Post synaptic density protein 95
RIP	Regulated intramembrane proteolysis
RTK	ErbB receptor tyrosine kinase
sAPP	Soluble amyloid precursor protein
sEGF	Soluble EGF-like domain
SCP	Schwann cell precursor
siRNA	Small interfering RNA
SMDF	Sensory motor neuron-derived factor
ST6Gal-1	α-2,6 sialyltransferase
TACE	Tumor necrosis factor α converting enzyme
TGFα	Transforming growth factor α
Tm	Melting temperature
TMD	Transmembrane domain
TNFα	Tumor necrosis factor α
VGSC	Voltage-gated sodium channel
wt	Wild-type

9 Publications

The results of this study have partly been published in the following publication:

> **Fleck D**, van Bebber F, Colombo A, Galante C, Schwenk BM, Rabe L, Hampel H, Novak B, Kremmer E, Tahirovic S, Edbauer D, Lichtenthaler SF, Schmid B, Willem M, Haass C. Dual cleavage of neuregulin 1 type III by BACE1 and ADAM17 liberates its EGF-like domain and allows paracrine signaling. *J Neurosci.* **2013** May 1;33(18):7856-69.

Review article:

> **Fleck D**, Garratt AN, Haass C, Willem M. BACE1 dependent neuregulin processing. *Curr Alzheimer Res.* **2012** Feb;9(2):178-83.

Neurobiology of Disease

Dual Cleavage of Neuregulin 1 Type III by BACE1 and ADAM17 Liberates Its EGF-Like Domain and Allows Paracrine Signaling

Daniel Fleck,[1] Frauke van Bebber,[2] Alessio Colombo,[2,5] Chiara Galante,[1] Benjamin M. Schwenk,[2] Linnea Rabe,[1] Heike Hampel,[1] Bozidar Novak,[1] Elisabeth Kremmer,[3] Sabina Tahirovic,[2] Dieter Edbauer,[1,2,4] Stefan F. Lichtenthaler,[2,4,5] Bettina Schmid,[2,4] Michael Willem,[1] and Christian Haass[1,2,4]

[1]Adolf-Butenandt-Institute, Biochemistry, Ludwig-Maximilians-University, 80336 Munich, [2]German Center for Neurodegenerative Diseases (DZNE), 80336 Munich, Germany, [3]Institute of Molecular Immunology, Helmholtz Center Munich, 81377 Munich, Germany, [4]Munich Cluster for Systems Neurology (SyNergy), 80336 Munich, Germany, and [5]Neuroproteomics, Technical University of Munich, 81377 Munich, Germany

Proteolytic shedding of cell surface proteins generates paracrine signals involved in numerous signaling pathways. Neuregulin 1 (NRG1) type III is involved in myelination of the peripheral nervous system, for which it requires proteolytic activation by proteases of the ADAM family and BACE1. These proteases are major therapeutic targets for the prevention of Alzheimer's disease because they are also involved in the proteolytic generation of the neurotoxic amyloid β-peptide. Identification and functional investigation of their physiological substrates is therefore of greatest importance in preventing unwanted side effects. Here we investigated proteolytic processing of NRG1 type III and demonstrate that the ectodomain can be cleaved by three different sheddases, namely ADAM10, ADAM17, and BACE1. Surprisingly, we not only found cleavage by ADAM10, ADAM17, and BACE1 C-terminal to the epidermal growth factor (EGF)-like domain, which is believed to play a pivotal role in signaling, but also additional cleavage sites for ADAM17 and BACE1 N-terminal to that domain. Proteolytic processing at N- and C-terminal sites of the EGF-like domain results in the secretion of this domain from NRG1 type III. The soluble EGF-like domain is functionally active and stimulates ErbB3 signaling in tissue culture assays. Moreover, the soluble EGF-like domain is capable of rescuing hypomyelination in a zebrafish mutant lacking BACE1. Our data suggest that NRG1 type III-dependent myelination is not only controlled by membrane-retained NRG1 type III, but also in a paracrine manner via proteolytic liberation of the EGF-like domain.

Introduction

Protease signaling is an important cellular mechanism in health and disease, and sheddases often liberate membrane-bound substrates for paracrine signaling (Turk et al., 2012). Sheddases are also involved in the generation of the Alzheimer's disease-associated amyloid β-peptide from the amyloid precursor pro-

tein (APP) (Lichtenthaler et al., 2011). Production of amyloid β-peptide is initiated by the β-site APP-cleaving enzyme (BACE1 or β-secretase) (Haass, 2004), which is therefore a promising drug target for the treatment of Alzheimer's disease (De Strooper et al., 2010). Physiologically, BACE1 is required to process Neuregulin 1 (NRG1) type III, a key regulator of myelination in the peripheral nervous system (PNS; Hu et al., 2006; Willem et al., 2006; Birchmeier and Nave, 2008; Brinkmann et al., 2008). Therefore, understanding the precise function of BACE1 in NRG1 type III processing and signaling is crucial to avoid side effects upon therapeutic inhibition of BACE1. NRG1 is predominantly expressed in neurons and multiple variants are generated by alternative splicing. All NRG1 isoforms contain an epidermal growth factor (EGF)-like domain, which binds and activates ErbB receptor tyrosine kinases (Falls, 2003; Mei and Xiong, 2008). Although most isoforms are single transmembrane domain (TMD) proteins, NRG1 type III contains two TMDs and forms a hairpin-like protein with the EGF-like domain in its extracellular loop (Fig. 1A; Wang et al., 2001).

NRG1 type III is essential for Schwann cell development in both mouse and zebrafish and determines myelin sheath thickness (Wolpowitz et al., 2000; Michailov et al., 2004; Taveggia et al., 2005; Monk and Talbot, 2009; Perlin et al., 2011). BACE1
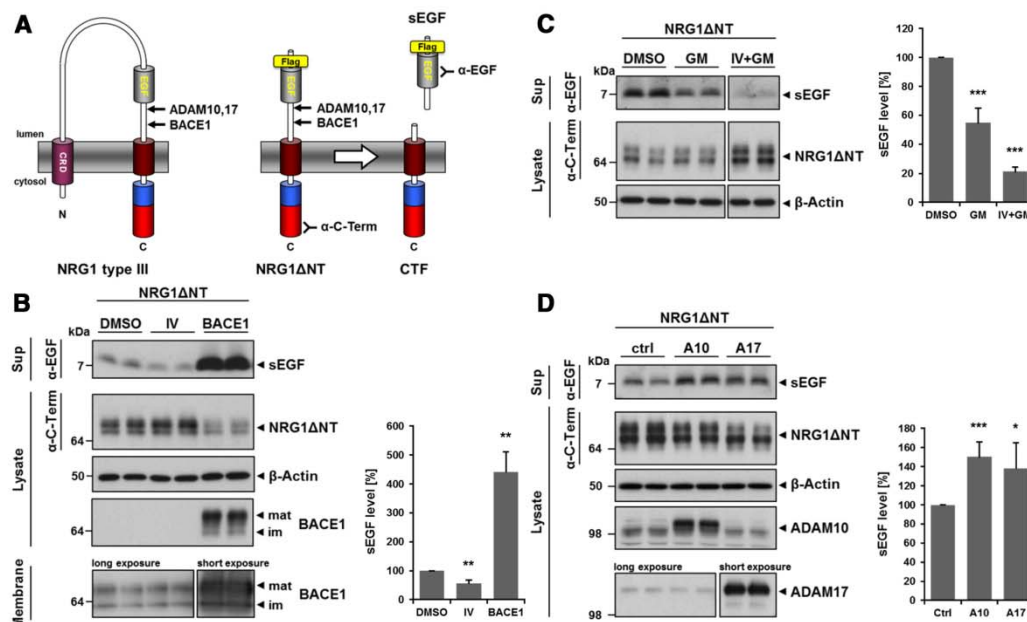
Figure 1. BACE1, ADAM10, and ADAM17 cleave in the stalk region of NRG1 type III. **A**, Schematic representation of NRG1ΔNT. NRG1ΔNT comprises the EGF-like domain and the C terminus but lacks the N terminus of NRG1 type III. A Flag-tag was inserted immediately N-terminal of the EGF-like domain to facilitate immunoprecipitation for MS analysis. Shedding of NRG1ΔNT by BACE1, ADAM10, or ADAM17 releases an sEGF domain that was detected directly in the supernatant using an EGF antibody. NRG1ΔNT was detected in the cell lysate with a C-terminal antibody. CRD indicates cysteine-rich domain. **B**, BACE1 is shedding NRG1 type III in the stalk region. HEK293 cells transfected with NRG1ΔNT were treated with the specific BACE1 inhibitor IV (10 μM) or cotransfected with BACE1. Note that, due to its rapid turnover, the CTF generated by shedding can only be detected upon γ-secretase inhibition (data not shown). Expression of transfected and endogenous BACE1 was confirmed in cell lysates and isolated membranes (bottom). mat indicates mature; im, immature. Bar graph: Quantification of experiments (mean ± SD; *$p < 0.05$, **$p < 0.01$, ***$p < 0.001$, two-tailed unpaired Student's t test, inhibitor: $n = 5$, overexpression: $n = 6$). **C, D**, ADAM10 and ADAM17 contribute to the shedding of NRG1 type III in the stalk region. **C**, Cells expressing NRG1ΔNT were treated with the broad-spectrum ADAM inhibitor GM6001 (GM, 25 μM). Coinhibition of ADAMs and BACE1 was achieved by combined treatment with GM and inhibitor IV (25 and 10 μM, respectively). **D**, Coexpression of NRG1ΔNT with ADAM10 (A10) or ADAM17 (A17). Bar graphs in **C, D**: Quantification of experiments (mean ± SD; *$p < 0.05$, **$p < 0.01$, ***$p < 0.001$, two-tailed unpaired Student's t test, in **C**, $n = 5$; in **D**, $n = 6$).

knock-out mice exhibit severe hypomyelination and accumulation of uncleaved NRG1 type III, demonstrating that NRG1 type III is a natural BACE1 substrate (Hu et al., 2006; Willem et al., 2006). NRG1-mediated signaling requires proteolytic processing and shedding in the stalk (juxtamembrane) region of NRG1 type I, and NRG1 type II releases the ectodomain as a paracrine signal. Conversely, shedding of NRG1 type III generates a membrane-tethered N-terminal fragment (NTF), which presents the EGF-like domain as juxtacrine signal (Falls, 2003). Because BACE1 knock-out mice still show some degree of myelination, other proteases may compensate for the loss of BACE1 (Velanac et al., 2012). Indeed, members of the ADAM (a disintegrin and metalloproteinase) family also cleave NRG1 (Montero et al., 2000; Shirakabe et al., 2001; Horiuchi et al., 2005; La Marca et al., 2011; Luo et al., 2011), and the NRG1 type III NTF generated by ADAM10 activates ErbB receptors similar to the BACE1-processed fragment (Luo et al., 2011).

Based on the finding that recombinant soluble NRG1 type III NTFs are sufficient for signaling *in vitro* (Syed et al., 2010), we searched for a proteolytic pathway that would physiologically liberate a signaling-competent EGF-like domain from NRG1 type III. We found that the EGF-like domain of NRG1 type III is liberated by a dual BACE1 or ADAM17 cleavage. Moreover, the soluble EGF-like (sEGF) domain not only stimulates ErbB3 re-

ceptor phosphorylation, but also rescues hypomyelination in a *bace1* mutant zebrafish.

Materials and Methods

cDNA constructs, primers, and lentivirus production. NRG1 type III β1a (GenBank: AF194438.1) cDNA was cloned into the pcDNA4-myc-HisA vector (Invitrogen) using EcoRI and XhoI restriction sites. For the construct V5-IIINRG1, a V5-tag (GKPIPNPLLGLDST) was inserted directly after M1 by fusion PCR. The V5-IIINRG1-HA construct was generated by introduction of an HA-tag (YPYDVPDYA) between V281 and M282. For the truncated construct NRG1ΔNT, the respective NRG1 type III sequence was subcloned into the pSecTag2A (Invitrogen) vector that features an N-terminal secretion signal. A suboptimal Furin cleavage site (RAVRSL) after the secretion signal sequence was optimized (RARRSV) by QuikChange mutagenesis (Stratagene) and a Flag-tag (DYKDDDDK) was inserted N-terminal of I236. The constructs α- and β-sEGF were generated by subcloning the respective sequences from V5-IIINRG1-HA into the modified pSecTag2A vector using the SfiI and XhoI restriction sites. BACE1 and ADAM10 expression constructs have been described previously (Capell et al., 2000; Wild-Bode et al., 2006). The construct expressing ADAM17 was kindly provided by Dr. R.A. Black at Amgen and has been described previously (Black et al., 1997). For expression in primary neurons, V5-IIINRG1-HA was cloned into a lentiviral expression vector AD149FhSynW2 under control of the human synapsin promoter using the NheI and EcoRI restriction sites. Lentiviral particles were produced in HEK293FT cells as described previously (Orozco et al.,

2012). Briefly, HEK293FT cells were cotransfected with the lentiviral expression construct psPAX2 and pVSVg for 24 h. After another 24 h, supernatant was collected and virus particles were concentrated by ultracentrifugation and resuspended in neurobasal medium. The sequences of all constructs were verified by sequencing. Construct and oligonucleotide sequences are available upon request.

Stable cell lines, transfection, and inhibitor treatment. HEK293T cells (Invitrogen) and MCF-7 cells (Karey and Sirbasku, 1988) were cultured in DMEM with Glutamax (Invitrogen) supplemented with 10% fetal calf serum (Invitrogen). CHO IdlD cells deficient in *O*-linked glycosylation were a kind gift from Monty Krieger and have been described previously (Kingsley et al., 1986). CHO wild-type (wt) and IdlD cells were cultured in DMEM with 10% fetal calf serum and nonessential amino acids. Transfections were performed using Lipofectamine 2000 (Invitrogen) according to the manufacturer's instructions. The following inhibitors were dissolved in DMSO and used at the indicated final concentrations for 12–24 h: BACE1 inhibitor IV (5 or 10 μM; Calbiochem); GM6001, a broad-spectrum inhibitor of matrix metalloproteinases and ADAMs (25 μM; Enzo Life Sciences), the ADAM10-specific inhibitor GI254023X (5 μM; a kind gift from Dr. Schmidt, Technical University of Darmstadt, described previously by Ludwig et al., 2005), and the ADAM17-specific inhibitor GL 506–3 (5 μM; a kind gift from Galderma). *O*-linked glycosylation was blocked with benzyl-2-acetamido-2-deoxy-α-D-galactopyranoside (4 mM; Merck).

Primary neuronal culture, transduction, and inhibitor treatment. Hippocampal neurons were prepared from embryonic day 18 Sprague-Dawley rat embryos as described previously (Orozco et al., 2012) and cultured in neurobasal medium (Invitrogen) supplemented with 2% B27 (Invitrogen), Pen/Strep, and 2 mM L-glutamine. After 4 d *in vitro*, cells were incubated with lentiviral particles for 8 h, and after 2 d, transduction inhibitor treatment was performed for 16 h. Supernatants and cells were collected and analyzed by immunoblotting.

Primary Schwann cell culture. Primary rat Schwann cells were prepared as described previously (Einheber et al., 1997) and proliferation was induced using high-glucose DMEM with Glutamax (Invitrogen), 10% FBS, 2 mM L-glutamine (Invitrogen), 2 μM forskolin (Sigma-Aldrich), and 10 μg/ml pituitary extract (Sigma-Aldrich). One day before the experiment, cells were washed twice with HBSS (Invitrogen) and proliferation was stopped by maintaining the cells in DMEM with Glutamax, 10% FBS, and 2 mM L-glutamine.

Antibodies. The following monoclonal neoepitope-specific antibodies were generated by immunization with the respective peptides: 4F10: rat, SFYKHLGIEF; 10E8: mouse, MEAEELYQKR; 7E6: mouse, QTAP-KLSTS. Hybridoma supernatants were used 1:40 for immunoblotting. The following antibodies were used for immunoblotting: antibody to NRG1 C terminus (pRb, 1:10000; SC348; Santa Cruz Biotechnology), to NRG1 EGF-like domain (HRGβ pRb, 1:2000, Ab-2; Thermo Scientific), to β-actin (1:5000; Sigma-Aldrich), to BACE1 (pRb, 1:1000, AB5940; Millipore), to ADAM17/TACE (pRb, 1:1000, ab39162; Abcam), to ADAM10 (pRb, 1:5000, 422751; Calbiochem), to Calnexin (pRb, 1:10000; Stressgen), to V5-tag (1:5000; Invitrogen), to HA-tag (HRP-conjugated mRat, 1:2000, 3F10; Roche), to ErbB3 (pRb, 1:1000, sc-285, C-17; Santa Cruz Biotechnology), to p-ErbB3 (pRb, 1:1000, sc-135654, Tyr1328; Santa Cruz Biotechnology), to AKT (mRb, 1:4000, C67E7; Cell Signaling Technology), and to p-AKT (mRb, 1:3000, D9E XP Ser473; Cell Signaling Technology). Secondary antibodies were HRP-conjugated anti-mouse and anti-rabbit IgG (pGoat, 1:10000; Promega) or anti-rat IgG (pGoat, 1:4000, sc-2006; Santa Cruz Biotechnology).

Sample preparation and immunoblotting. Medium was conditioned overnight, immediately cooled upon collection, and supplemented with protease inhibitor mixture (Sigma-Aldrich). Cell debris was removed by centrifugation (5 min, 5500 $\times$ g, 4°C) and the supernatant was subjected directly to standard SDS-PAGE. For total cell lysates, cells were washed with ice-cold PBS, scraped off, and pelleted by centrifugation (5 min, 1000 $\times$ g, 4°C). Cells were lysed in lysis buffer (20 mM citrate, pH 6.4, 1 mM EDTA, 1% Triton X-100) freshly supplemented with protease inhibitor mixture for 30 min on ice. After clarification (15 min, 10000 $\times$ g, 4°C), protein concentration was determined with the BCA protein assay (Pierce) and equal amounts of protein were subjected to SDS-PAGE.

Proteins were transferred onto PVDF (Immobilon-P; Millipore) or nitrocellulose (Protran; Whatman) membranes and the indicated antibodies were used for immunodetection. Bound antibodies were detected with HRP-conjugated secondary antibodies using the chemiluminescence detection reagents ECL and ECL Plus (GE Healthcare). For quantification, images were acquired with a Luminescent Image Analyzer LAS-4000 (Fujifilm) and analyzed with the Multi Gauge V3.0 software.

siRNA-mediated knock-down and membrane preparation. For RNA interference, cells were plated in polylysine-coated dishes and reverse transfected with siGENOME pool targeting ADAM10 (10 nM; Thermo Scientific), ON-TARGETplus SMARTpool targeting ADAM17 (15 nM; Dharmacon) or respective controls using Lipofectamine 2000 (Invitrogen). Fresh medium was added 24 h after transfection and (if applicable) substrate cDNA was transfected 48 h after initial transfection. Medium was conditioned starting 68 h after siRNA transfection and cells were harvested 12–24 h later. For detection of endogenous BACE1, ADAM10 and ADAM17 cell membranes were prepared as described previously (Sastre et al., 2001).

MS analysis after immunoprecipitation. Conditioned medium was prepared as described above and incubated with anti-Flag M2 or anti-HA (Sigma-Aldrich) agarose beads overnight (rotation, 4°C). Beads where washed three times with IP/MS buffer (0.1% *N*-octylglucoside, 10 mM Tris-HCl, pH 8.0, 5 mM EDTA, 140 mM NaCl) and two times with water. Immunoprecipitated proteins were eluted with trifluoroacetic acid/acetonitrile/water (0.3%/40%) saturated with α-cyano-4-hydroxycinnamic acid and matrix-assisted laser desorption/ionization–time of flight (MALDI-TOF) analysis was performed as described previously (Okochi et al., 2002) using Voyager DE STR (Applied Biosystems). Molecular masses were calibrated using the Sequazyme Peptide Mass Standards Kit (Applied Biosystems).

Preparation of sEGF domains and phosphorylation assays. sEGF domains were expressed in CHO wt and CHO IdlD cells and supernatants were conditioned for 24 h. After quantification of their initial abundance by Western blotting, medium from control cells was used to adjust the concentrations of the EGF-like domains in the supernatants by dilution. Equal concentrations were controlled by Western blotting again (and further adjustment was done if necessary) and the adjusted supernatants were used for phosphorylation assays. The assay was performed as follows: subconfluent MCF-7 or purified primary Schwann cells were incubated with conditioned media containing equal amounts of EGF-like domains for 30 min. Medium from cells expressing an empty vector was used as negative control and incubation with 0.5 nM recombinant NRG1 EGF-like domain (NRG1-β1, 396-HB/CF; R&D Systems) served as a positive control. Cells were then washed with ice-cold PBS and lysates were prepared as described above using a modified RIPA buffer supplemented with phosphatase inhibitor mixture (PhosSTOP; Roche). Eventually, the phosphoprotein/total protein readout of the assay was normalized to the Western blot intensities of the EGF-like domains in the media used for stimulation.

Zebrafish maintenance and transgenic lines used. All zebrafish embryos were raised at 28°C in E3 media (5 mM NaCl, 0.17 mM KCl, 0.33 mM CaCl$_2$, 0.33 mM MgSO$_4$) and were staged as described previously (Kimmel et al., 1995). To suppress the growth of mold, methylene blue (10^{-5}%) was added to E3 media. Animals of either sex were used for this study. All experiments were performed in accordance with animal protection standards of the Ludwig-Maximilians University Munich and have been approved by the government of Upper Bavaria (Regierung von Oberbayern, München, Germany). In addition to the AB wt strain, a transgenic zebrafish line, Tg(*claudin k*:GFP) in which the *claudin k* promoter drives expression of a membrane-bound GFP (Münzel et al., 2012), was also used. This transgenic line is hereafter referred to as *claudin k*:GFP. Furthermore, a newly generated *bace1* mutant (van Bebber et al., 2013) was crossed to *claudin k*:GFP, and *bace1* homozygous mutants carrying the *claudin k*:GFP were used to analyze the activity of NRG1 type III-derived β-sEGF *in vivo*.

mRNA injections and image acquisition. β-sEGF mRNA was synthesized *in vitro* using the mMessage mMACHINE kit (Ambion) according to standard protocols. β-sEGF mRNA was injected at a concentration of 425 ng/μl in fertilized eggs at the one-cell stage. Zebrafish larvae were
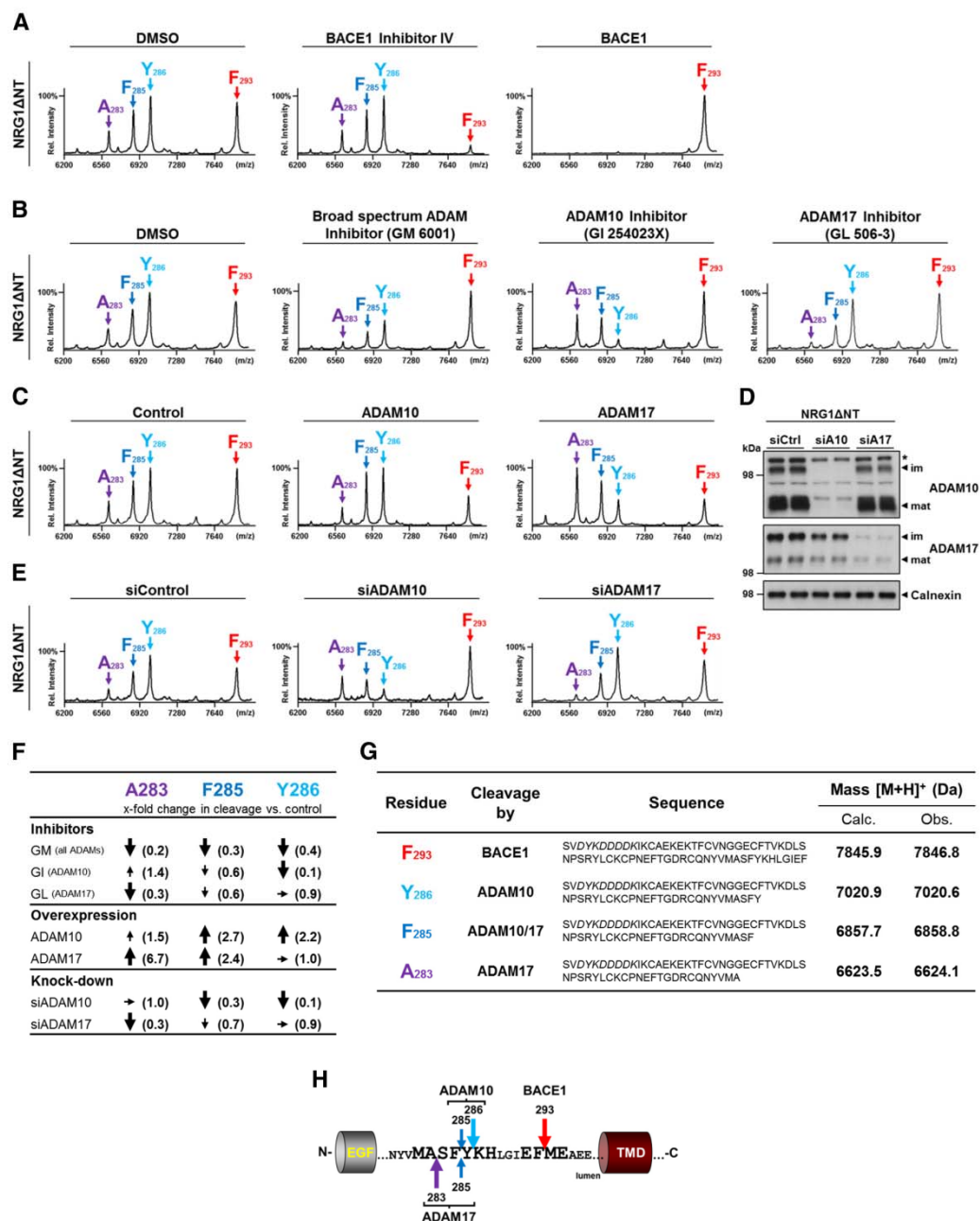
Figure 2. Identification of shedding sites of BACE1, ADAM10, and ADAM17 in the stalk region of NRG1 type III. *A*, BACE1 cleaves NRG1 type III after F293. Supernatants of Figure 1*B* were immunoprecipitated with Flag-agarose beads and precipitated sEGF peptides were analyzed by MALDI-TOF MS. The peptide corresponding to a cleavage after F293 is generated by BACE1 (red arrow). Note that with overexpression of BACE1, the other peaks are below detection limit. *B*, *C*, ADAM10 and ADAM17 shed NRG1 type III after A283, F285, and Y286. Cells expressing NRG1ΔNT were either treated with indicated inhibitors (GM6001, 25 μM; GI254023X and GL506−3, 5 μM) or cotransfected with indicated proteases and supernatants were analyzed as in *A*. ADAM-specific peaks were compared with the peak caused by BACE1 in each spectrum. Broad-spectrum ADAM inhibition (GM6001) reduced cleavage at all ADAM cleavage sites. Inhibition and overexpression of ADAM10 revealed its main cleavage sites to be after Y286 and F285 (light blue and blue arrows, respectively). Conversely, ADAM17 cleaved NRG1ΔNT mainly after A283 (*Figure legend continues.*)

anesthetized with tricaine (0.016% w/v) at 3 d postfertilization (dpf) and oriented in 3% methylcellulose on coverslips. Fluorescence of *claudin k*:GFP was imaged with an LSM510 META inverted confocal microscope (Zeiss). Pictures were assembled in Photoshop 8.0 (Adobe Systems). Brightness and contrast were adjusted with ImageJ.

Results

Juxtamembrane cleavage of NRG1 type III by ADAM10, ADAM17, and BACE1

To investigate NRG1 type III processing in living cells, we generated a truncated Flag-tagged NRG1 type III construct comprising the C-terminal region, the transmembrane domain, the juxtamembrane region, and the EGF-like domain (NRG1ΔNT; Fig. 1A). Expression of the truncated protein not only facilitates the analysis of proteolytic processing within living cells, but also allows the determination of potential cleavage sites by MS. We coexpressed three different sheddases suggested to be involved in NRG1 type III processing, BACE1, ADAM10, and ADAM17 (Montero et al., 2000; Hu et al., 2006; Willem et al., 2006; La Marca et al., 2011; Luo et al., 2011), or repressed their endogenous activities with inhibitors. Inhibition of endogenous BACE1 (by the BACE1 inhibitor IV) resulted in reduced liberation of the EGF-like domain into the supernatant (Fig. 1B). Conversely, ectopic BACE1 expression strongly enhanced shedding reflected by significantly increased amounts of the sEGF domain in the supernatant and reduced substrate levels in the cell lysate (Fig. 1B). Due to its rapid turnover by the γ-secretase (Bao et al., 2003, 2004), the C-terminal fragment (CTF) resulting from shedding could only be detected upon γ-secretase inhibition (data not shown).

We then investigated whether both ADAM10 and ADAM17 were also able to cleave NRG1ΔNT. The broad-spectrum ADAM inhibitor GM6001 significantly reduced the amount of sEGF detected in the supernatant. Combined inhibition of BACE1 and ADAMs by treatment with both inhibitor IV and GM6001 almost completely abolished endogenous shedding activity, as reflected by strongly reduced amounts of sEGF in the supernatant and the accumulation of NRG1ΔNT substrate within the cell lysate (Fig. 1C). Consistent with these findings, ectopic expression of either ADAM10 or ADAM17 resulted in enhanced shedding of NRG1ΔNT and subsequent sEGF accumulation in the conditioned media (Fig. 1D). These results suggest that BACE1, ADAM10, and ADAM17 are able to cleave NRG1 type III between the extracellular EGF-like domain and the C-terminal transmembrane domain.

←

(*Figure legend continued.*)   (purple arrows). **D, E,** Knock-down of ADAM10 and ADAM17 confirms shedding sites. Cells expressing NRG1ΔNT were transfected with siRNA (10 nM) against ADAM10 (siA10) or ADAM17 (siA17) and a nontargeting siRNA as a control (siCtrl). **D,** Western blot analysis of membrane preparations confirmed efficient downregulation of both the immature (im) and mature (mat) form of ADAM10 and ADAM17. **E,** sEGF peptides were isolated from the supernatant and analyzed as in **B. F,** Summary of MS data for ADAM10 and ADAM17 cleavage after A283, F285, and Y286. Peak intensities (areas) of ADAM-specific peaks were normalized to the signal generated by BACE1 in each spectrum (mean ± SD; $n = 3$). The normalized peak intensities then were compared with the respective controls. Changes of cleavage (fold) under different conditions (inhibition, overexpression, and knock-down of ADAM10 and ADAM17) are summarized as follows: increased: >1.6× (↑ , big arrows), mildly increased: 1.5–1.2× (↑ , small arrows) unchanged: 1.1–0.9× (→), mildly decreased: 0.8–0.5× (↓ , small arrows), or decreased: <0.4× (↓ , big arrows). **G,** List of peptides identified by MS. Peptide sequences with corresponding protease(s) are given and observed (Obs.) peptide masses are compared with calculated (Calc.) masses. Italic letters indicate Flag-tag: $[M+H]^+$, a singly charged peptide. **H,** Graphic representation of shedding sites in the stalk region of NRG1 type III. Cleavage sites of BACE1, ADAM10, and ADAM17 are shown and preferred cleavage positions of ADAM10 and ADAM17 are indicated by longer arrows, respectively.

Identification of BACE1, ADAM10, and ADAM17 cleavage sites within the juxtamembrane region of NRG1 type III

To map the cleavage sites of the respective proteases, we immunoprecipitated the sEGF domain from the supernatants of NRG1ΔNT-expressing HEK293 cells using antibodies to the Flag epitope (Fig. 1A). Isolated peptides were analyzed using MALDI-TOF MS. Mass spectra derived from the supernatant of control cells revealed four prominent peptide species corresponding to cleavages after A283, F285, Y286, and F293 (Fig. 2A, G). To identify the specific cleavage sites of the three sheddases shown to be involved in processing of NRG1ΔNT, we inhibited their endogenous activities with selective inhibitors or enhanced their cleavage by overexpression of the corresponding protease. This revealed that the peptide peak at 7846.8 kDa corresponding to a cleavage site after F293 was strongly reduced upon inhibition of endogenous BACE1 (Fig. 2A). Conversely, production of the same peptide was greatly enhanced to the expense of all other cleavage products upon BACE1 overexpression (Fig. 2A), indicating competing shedding activities.

Similarly, we analyzed the secreted EGF-like domains upon overexpression or inhibition of ADAM proteases. Inhibition of ADAMs with the broad-spectrum ADAM inhibitor GM6001 decreased the abundance of the three peptides A283, F285, and Y286 compared with the peptide generated by BACE1, suggesting that these peptides are indeed generated by protease activities associated with members of the ADAM family (Fig. 2B,F). To identify the cleavage sites of ADAM10 and ADAM17, we used inhibitors that preferentially inhibit either ADAM10 (GI254023X) or ADAM17 (GL506–3). Inhibition of ADAM10 reduced the intensity of peaks corresponding to cleavages after F285 and Y286 but increased cleavage after A283. Conversely, blocking ADAM17 resulted in reduced cleavage after A283 (and, to a minor extent, after F285), whereas cleavage after Y286 remained unaffected (Fig. 2B,F). Consistent with these findings, overexpression of either protease caused increased cleavage after the sites affected by their respective inhibitors (Fig. 2C,F). Therefore, ADAM10 expression leads to enhanced cleavage after residues F285 and Y286, whereas expression of ADAM17 increases cleavage after residues A283 and F285 (Fig. 2C).

To verify these cleavage sites under endogenous conditions, we knocked down ADAM10 and ADAM17 in HEK293 cells expressing NRG1ΔNT. The siRNA pools efficiently reduced the protein levels of ADAM10 and ADAM17 (Fig. 2D). As before, sEGF peptides were isolated from the conditioned medium and analyzed by MALDI-TOF MS (Fig. 2E). Knock-down of ADAM10 dramatically reduced cleavage after Y286 and F285, whereas cleavage after A283 was unaffected. Conversely, reduction of ADAM17 strongly impaired cleavage after A283 and reduced cleavage after F285 to some extent, whereas cleavage after Y286 was not affected (Fig. 2E,F). These findings suggest that BACE1 specifically cleaves NRG1 type III after F293, whereas ADAM17 cleaves after A283 and, to some extent, also after F285. ADAM10 processes NRG1 type III after Y286, but also shares the minor cleavage site after F285 with ADAM 17 (Fig. 2H).

Processing of NRG1 type III liberates the EGF-like domain

Shedding is thought to activate NRG1 type III by generating a membrane-tethered NTF comprising the EGF-like domain (Falls, 2003; Fig. 3A). However, we hypothesized that the resulting NTF may even be further processed by sheddases to liberate an sEGF domain (Fig. 3A). To examine this possibility, we expressed full-length NRG1 type III with an N-terminal V5-tag (V5-IIINRG1) in HEK293 cells and coexpressed BACE1,
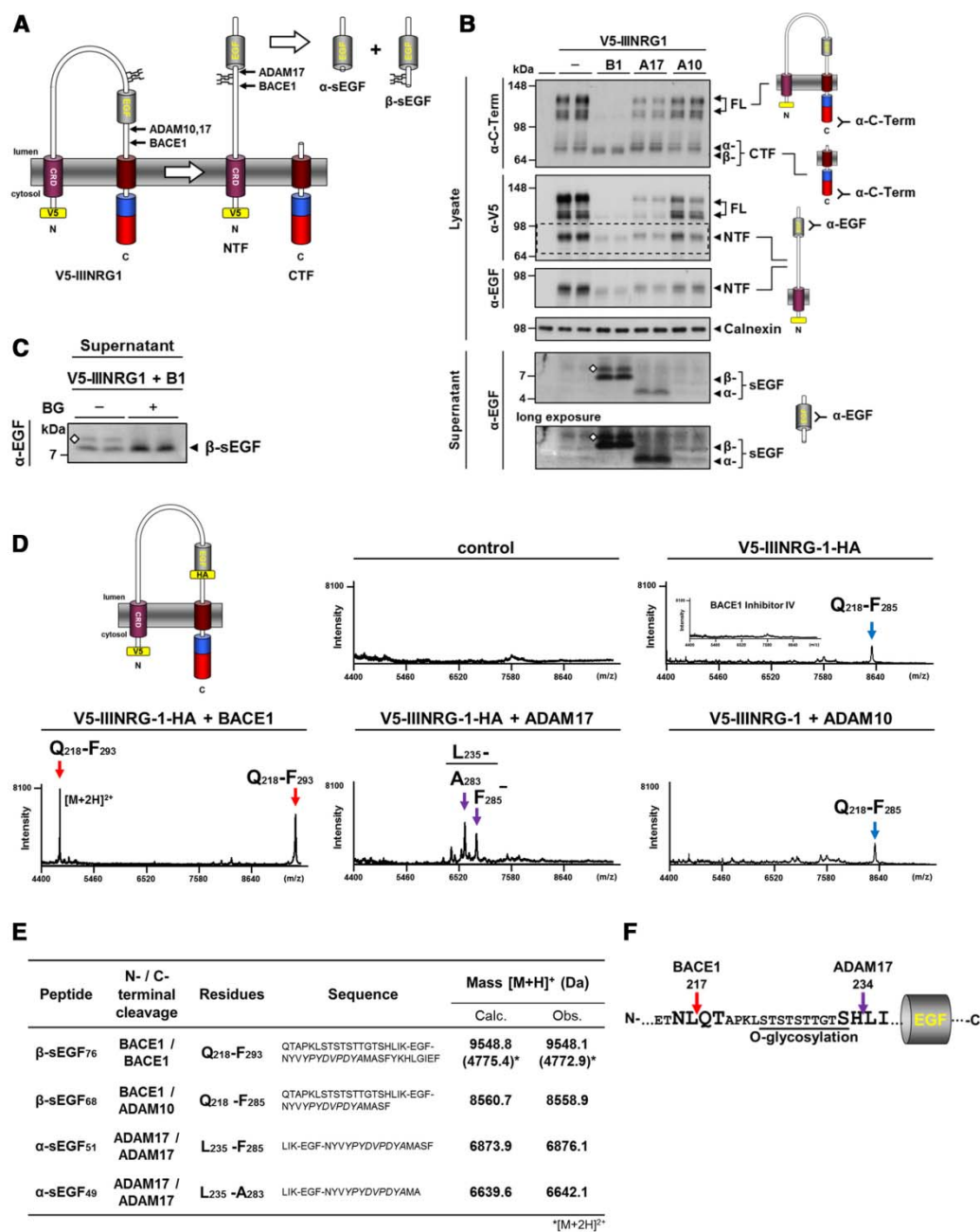
E

Peptide	N- / C-terminal cleavage	Residues	Sequence	Mass [M+H]⁺ (Da)	
				Calc.	Obs.
β-sEGF$_{76}$	BACE1 / BACE1	Q$_{218}$-F$_{293}$	QTAPKLSTSTSTTGTSHLIK-EGF-NYVV*PYDVPDY*AMASFYKHLGIEF	9548.8 (4775.4)*	9548.1 (4772.9)*
β-sEGF$_{68}$	BACE1 / ADAM10	Q$_{218}$ -F$_{285}$	QTAPKLSTSTSTTGTSHLIK-EGF-NYVV*PYDVPDY*AMASF	8560.7	8558.9
α-sEGF$_{51}$	ADAM17 / ADAM17	L$_{235}$ -F$_{285}$	LIK-EGF-NYV*VPYDVPDY*AMASF	6873.9	6876.1
α-sEGF$_{49}$	ADAM17 / ADAM17	L$_{235}$ -A$_{283}$	LIK-EGF-NYV*VPYDVPDY*AMA	6639.6	6642.1

*[M+2H]²⁺

Figure 3. BACE1 and ADAM17 liberate an sEGF domain from NRG1 type III. *A*, Model depicting NRG1 type III processing and EGF liberation. Shedding of the V5-tagged NRG1 type III (V5-IIINRG1) in the C-terminal stalk region generates an NTF and CTF. Further cleavage of the NTF by ADAM17 and BACE1 liberates the EGF-like domain into the lumen (α- and β-sEGF). Glycosylation N-terminal of the EGF-like domain is indicated. *B*, Processing of NRG1 type III generates both a membrane-tethered and an sEGF domain. V5-IIINRG1 was coexpressed with BACE1 (B1), ADAM17 (A17), and ADAM10 (A10), and membrane-tethered fragments were detected in the cell lysate by Western blotting. Due to the different shedding sites in the stalk region of NRG1 type III, the CTFs generated by BACE1 and ADAMs differ in size (β-CTF and α-CTF, respectively). The observed NTFs contained the EGF-like domain, as confirmed by reprobing of the membrane with (*Figure legend continues.*)

ADAM10, or ADAM17 (Fig. 3B). Expression of either protease was controlled as before (Fig. 1) and comparable amounts were observed (data not shown). Full-length V5-IIINRG1 was detected as multiple bands, suggesting intensive posttranslational modification such as glycosylation (Fig. 3B). Decreased full-length protein was present in the lysate upon coexpression of either protease. This was most apparent when BACE1 was overexpressed (Fig. 3B). The CTF generated upon BACE1 overexpression (β-CTF) migrated slightly faster than the CTFs generated by either ADAM (α-CTF; Fig. 3B). This is consistent with the BACE1 cleavage site being closer to the transmembrane domain than the cleavage sites identified for ADAM10 and ADAM17 (Fig. 2H). We also analyzed the cell lysate for the NTF generated upon shedding of NRG1 type III. Detection with an antibody against the N-terminal V5-tag and reprobing with an anti-EGF antibody confirmed that the observed NTF still contained the EGF-like domain (Fig. 3B, dashed box).

Enhanced proteolytic cleavage of the full-length V5-IIINRG1 should lead to the accumulation of the NTF as cleavage product. However, we did not detect higher amounts of NTF in cells coexpressing one of the three sheddases, but rather observed reduced NTF levels especially upon BACE1 or ADAM17 coexpression (Fig. 3B). Because this may be indicative of further NTF processing by these proteases, we analyzed the supernatants for soluble peptides liberated from the membrane-bound NTF. Both BACE1 and ADAM17 were found to liberate sEGF domains of different sizes (β-sEGF and α-sEGF) into the medium (Fig. 3B). Moreover, processing of V5-IIINRG1 by endogenous proteases also resulted in the secretion of a β-sEGF, albeit to a much smaller extent (Fig. 3B, long exposure). β-sEGF, but not α-sEGF, migrated as a double band, suggesting posttranslational modifications (Fig. 3B). A serine/threonine-rich stretch, which may be a site for O-linked glycosylation, is located close to the N terminus of the EGF-like domain (Fig. 3A). We treated cells expressing V5-IIINRG1 and BACE1 with benzyl-2-acetamido-2-deoxy-α-D-galactopyranoside, a specific blocker of O-linked glycosylation. Western blot analysis of supernatants using an antibody against the EGF-like domain revealed that inhibition of O-glycosylation abolished formation of the higher-molecular-weight band and caused β-sEGF to appear as a single peptide (Fig. 3C). This dem-

onstrates that, in contrast to α-sEGF, β-sEGF is subject to O-linked glycosylation.

A second BACE1 and ADAM17 cleavage N-terminal of the EGF-like domain

The results described above suggest that the EGF-like domain is released by cleavages that occur both N-terminal and C-terminal of the EGF-like domain. To identify the putative cleavage site(s), we used a combined immunoprecipitation/MALDI-TOF MS approach. An HA-tag was inserted immediately after the EGF-like domain to enable immunoprecipitation. This construct (V5-IIINRG1-HA; Fig. 3D) was transiently expressed in HEK293 cells with and without BACE1, ADAM10, or ADAM17. Western blot analysis of lysates and supernatants confirmed the generation of membrane-tethered and soluble fragments from this construct in a similar fashion to the untagged construct (data not shown). MS analysis of peptides secreted from cells expressing V5-IIINRG1-HA yielded one major peak at 8558.9 kDa (Fig. 3D). This corresponds to a peptide (β-sEGF$_{68}$) having Q218 as an N-terminal residue and F285 as a C-terminal residue (Fig. 3E). Although the C terminus is the result of endogenous ADAM-mediated shedding in the stalk region after F285 (Fig. 2H), the N terminus results from a novel cleavage after L217, 16 residues N-terminal of the EGF-like domain. Inhibition of endogenous BACE1 activity with the specific inhibitor IV abolished generation of the peptide, suggesting BACE1-mediated processing after L217 (Fig. 3D, inset). Strikingly, this novel cleavage site (ETNL|QTAP) resembles that of the Swedish mutation of APP (EVNL|DAEF), which strongly increases BACE1-mediated processing (Citron et al., 1992, 1995; Cai et al., 1993). Consistent with this, coexpression of BACE1 strongly enhanced cleavage at this novel site and, in agreement with the shedding data shown above (Fig. 2H), produced a slightly larger peptide (β-sEGF$_{76}$) ending with the BACE1 shedding site F293 at its C terminus (Fig. 3D,E).

Expression of ADAM17 liberated a shorter sEGF from V5-IIINRG1-HA beginning with L235 and ending after either A283 or F285, respectively (α-sEGF$_{49}$ and $_{51}$; Fig. 3D,E). This is consistent with the data obtained for ADAM17-mediated processing of NRG1-ΔNT (Fig. 2H). The newly identified ADAM17 cleavage site after H234 is located immediately N-terminal of the EGF-like domain and is therefore responsible for the observed size difference of α-sEGF and β-sEGF (Fig. 3F). Cleavage at this site excludes the serine/threonine-rich stretch from α-sEGF and explains why, in contrast to β-sEGF, α-sEGF is not subject to O-linked glycosylation (Fig. 3B,C,F). These findings demonstrate that BACE1 and ADAM17, but not ADAM10, are capable of liberating the EGF-like domain from NRG1 type III by dual cleavage (Fig. 3A).

Membrane-bound and soluble fragments of NRG1 type III are detected by neo-epitope-specific antibodies to BACE1 cleavage sites

To further validate and facilitate detection of NRG1 type III fragments, we generated neo-epitope-specific antibodies against the above identified cleavage sites. Monoclonal antibodies 10E8 and 4F10 were raised against the neo-epitopes generated by BACE1-mediated shedding in the stalk region (epitopes M$_{294}$EAEELYQKR and SFYKHLGIEF$_{293}$, respectively). An additional antibody was raised against the novel BACE1 cleavage site N-terminal of the EGF-like domain (7E6, epitope Q$_{218}$TAPKLSTS; Fig. 4A). We then investigated whether these antibodies are suitable as sensitive tools for the

---

(Figure legend continued.) an EGF antibody (dashed box). Analysis of the supernatants revealed that BACE1 and ADAM17 liberate sEGF domains of different sizes (β-sEGF and α-sEGF, respectively). The diamonds denote posttranslational modification. C, The β-sEGF is subject to O-linked glycosylation. Cells expressing V5-IIINRG1 and BACE1 were treated or not with a blocker of O-glycosylation (benzyl-2-acetamido-2-deoxy-α-D-galactopyranoside, BG, 4 mM). Soluble β-sEGF was detected with an antibody against the EGF-like domain. The diamond denotes O-linked glycosylation. D, Cleavage of NRG1 type III NTF before Q218 by BACE1 and before L235 by ADAM17 liberates an EGF-like domain. For immunoprecipitation, an HA-tag was inserted immediately after the EGF-like domain into the construct shown in A. To determine the exact cleavage sites, fragments were isolated from supernatants by IP with HA agarose and analyzed by MALDI-TOF MS. BACE1 liberated a fragment comprising residues Q218-F293, whereas ADAM17 generated smaller fragments containing residues L235-F285 and L235-A283. Processing by endogenous proteases or by coexpressed ADAM10 caused low level secretion of a fragment with a BACE1-cleaved N terminus and an ADAM-cleaved C terminus (Q218-F285). Inhibition of BACE1 (BACE1 inhibitor IV, 10 μM) abolished secretion of the EGF-like domain completely (inset in second panel). E, List of peptides identified by MS. Peptide sequences (without residues of the EGF-like domain) and corresponding proteases are listed. Observed masses (Obs.) are compared with calculated (Calc.) masses. Peptide numbers indicate number of residues comprised by each peptide (excluding the HA-tag). [M+H]$^+$ indicates singly charged peptide; [M+2H]$^{2+}$, a doubly charged peptide; italic letters, HA-tag. F, Graphic representation of BACE1 and ADAM17 cleavage sites N-terminal of the EGF-like domain. Cleavage sites and the serine/threonine-rich region where O-linked glycosylation occurs are indicated.
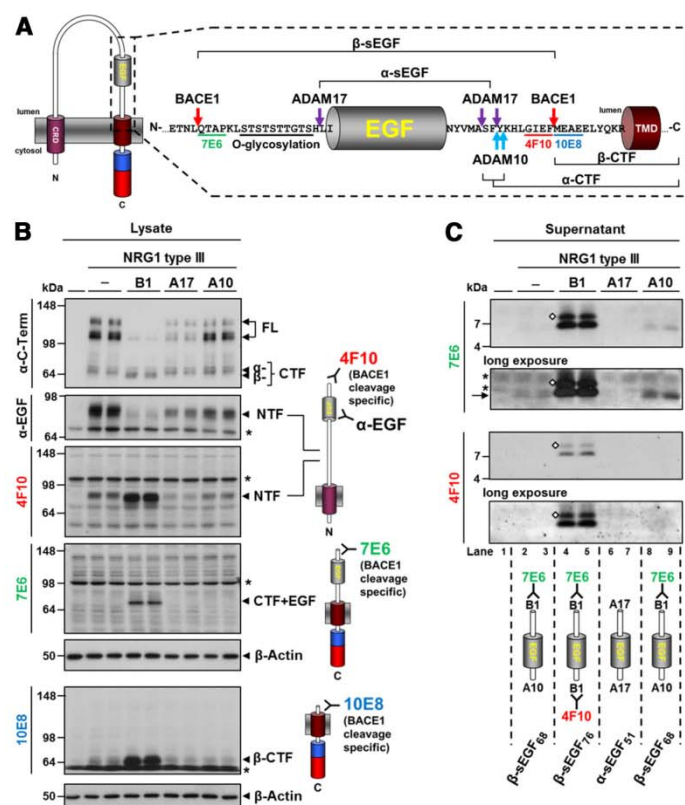
Figure 4. Monoclonal antibodies generated against BACE1 cleavage sites in NRG1 type III detect membrane-bound and soluble fragments. **A**, Scheme summarizing identified cleavage sites in NRG1 type III. Cleavage sites of respective proteases are marked by arrows and α-sEGF and β-sEGF and α-CTF and β-CTF are indicated. Epitopes of the generated antibodies and the site of glycosylation are shown. **B**, Membrane-tethered NRG1 type III fragments are recognized by antibodies raised against BACE1 cleavage sites. Total lysates of cells expressing untagged NRG1 type III and BACE1 (B1), ADAM17 (A17), or ADAM10 (A10) were analyzed by Western blotting. BACE1-cleaved fragments were detected with the indicated antibodies. **C**, Antibodies 7E6 and 4F10 recognize β-sEGF. Media from **B** were analyzed by Western blot. The N terminus of β-sEGF was detected using 7E6 and the C terminus was detected with 4F10. Note that in the case of endogenous processing or ADAM10 overexpression, the β-sEGF is liberated by N-terminal BACE1 cleavage (7E6 signal in lanes 2 and 3 and lanes 8 and 9, indicated by an arrow) but not C-terminal BACE1 shedding (no 4F10 signal in lanes 2 and 3 and lanes 8 and 9). Overexpression of ADAM17 prevents formation of β-sEGF (no signals for either antibody in lanes 6 and 7). Diamonds indicate glycosylation. Asterisks indicate unspecific background bands that are also present in the untransfected control (lane 1).

detection of the different processing products generated by BACE1, ADAM10, and ADAM17.

In cell lysates of HEK293 cells coexpressing NRG1 type III and either protease, antibody 4F10 selectively detected NTFs generated by BACE1- but not ADAM-mediated shedding (Fig. 4B). Upon coexpression of BACE1, the 7E6 antibody detected the CTF (comprising the EGF-like domain) resulting from BACE1 cleavage after L216 (Fig. 4B). This indicates that, upon elevated BACE1 expression, cleavage may first occur N-terminal of the EGF-like domain. Antibody 10E8 confirmed the generation of the β-CTF upon shedding of NRG1 type III by BACE1, but not by ADAMs (Fig. 4B). Being specific for the BACE1-generated neo-epitopes, the antibodies did not recognize the full-length NRG1 type III.

Western blot analysis of supernatants with antibodies 7E6 and 4F10 (specific to the BACE1 cleaved N and C terminus of the EGF-like domain, respectively) revealed robust amounts of soluble β-sEGF$_{76}$ upon expression of BACE1 (Fig. 4C, lanes 4 and 5). As determined by MS (Fig. 3D, E), endogenous protease activity in HEK293 cells generates β-sEGF$_{68}$ through ADAM10-mediated (C-terminal) shedding and BACE1-mediated (N-terminal) cleavage. Consistent with this, we detected low amounts of β-sEGF$_{68}$ with the 7E6 antibody (Fig. 4C, lanes 2 and 3, arrow), whereas the 4F10 antibody did not recognize this fragment due to the absence of a BACE1-generated C-terminal epitope. Accordingly, enhanced shedding by ectopic expression of ADAM10 further increased the amounts of β-sEGF$_{68}$ in the supernatant (Fig. 4C, compare lanes 8 and 9 with lanes 2 and 3). ADAM17-mediated cleavage N- and C-terminal of the EGF-like domain releases α-sEGF$_{49}$ (Fig. 3D, E), which does not contain the epitopes recognized by 7E6 or 4F10 (Fig. 4A). Consistent with that, overexpression of ADAM17 prevented endogenous formation of β-sEGF$_{68}$, and no 7E6 signal is observed in lanes 6 and 7 in Figure 4C. Therefore, the neo-epitope-specific antibodies are sensitive and selective tools for the investigation of NRG1 type III processing, and their specific immunoreactivity with defined processing products confirms the cleavage sites described above.

Dual cleavage of NRG1 type III in primary neurons releases the EGF-like domain

The neo-epitope-specific antibodies characterized in Figure 4 were used to investigate proteolytic processing of NRG1 type III in primary hippocampal neurons. To allow detection of NRG1 proteolytic fragments in neurons, we expressed V5-IIINRG1-HA using lentiviral transduction and studied its processing by endogenous secretases (Fig. 5). As revealed by Western blot analysis of lysates, shedding of V5-IIINRG1-HA in neurons generated a CTF and an NTF containing the EGF-like domain (Fig. 5A). Inhibition of BACE1 activity (by the BACE inhibitor IV) decreased the overall turnover of the full-length protein, as shown by the accumulation of the full-length precursor and decreased generation of the CTF. This was amplified by concomitant inhibition of ADAM proteases (by IV + GM6001), supporting the idea that BACE1 and ADMAs can compete for shedding in the stalk region of NRG1 type III under physiological conditions. CTFs and NTFs resulting from BACE1 shedding only were specifically detected with antibodies 10E8 and 4F10 and their generation was completely abolished upon inhibition of BACE1. Using antibody 7E6 for immunodetection, we did not observe a CTF containing the EGF-like domain (CTF+EGF; Fig. 4B) that would be generated by a single BACE1 cleavage of NRG1 type III after L216
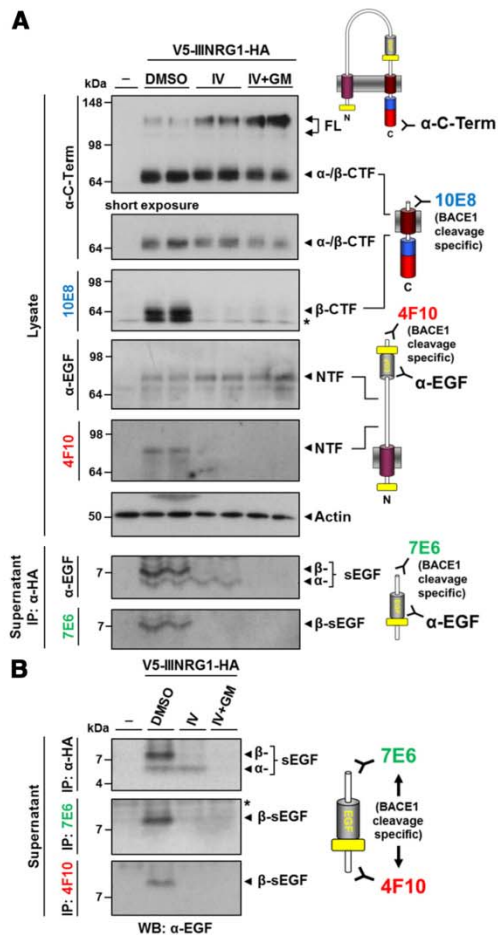
Publications

Figure 5. Cleavage of NRG1 type III in primary neurons releases the EGF-like domain. **A,** Processing of NRG1 type III in primary neurons generates both a membrane-tethered and an sEGF domain. V5-IIINRG1-HA was expressed in primary hippocampal neurons and cells were treated with indicated inhibitors (BACE1 inhibitor IV, 5 μM; ADAM inhibitor GM6001, 25 μM) for 16 h. Cells were lysed, conditioned supernatants were immunoprecipitated with HA-agarose beads, and protein levels were determined by immunoblotting with indicated antibodies. β-CTFs and NTFs generated by BACE1 cleavage were specifically detected by antibodies 10E8 and 4F10, respectively. Additional cleavages N-terminal of the EGF-like domain by BACE1 and ADAMs liberated β-sEGF and α-sEGF into the supernatant, respectively. **B,** BACE1 cleavage N- and C-terminal of the EGF-like domain liberates β-sEGF from neurons. Supernatants from neurons as described in **A** were immunoprecipitated with antibodies against the HA-tag or previously identified BACE1 cleavage sites (7E6 and 4F10). Purified peptides were detected using an α-EGF antibody.

(data not shown). This is consistent with the concept that, physiologically, the EGF-like domain of NRG1 type III is tethered to the membrane via its NTF (Taveggia et al., 2005). As observed in non-neuronal cells (Fig. 3), additional N-terminal cleavages release the EGF-like domain into the supernatant (β-sEGF and α-sEGF, respectively; Fig. 5A). Blocking BACE1 activity selectively prevented generation of the slightly larger β-sEGF, whereas the shorter α-sEGF was abolished upon ADAM inhibition. Reprobing of the membrane

with the 7E6 antibody (Fig. 5A) revealed that the β-sEGF contains a BACE1-generated N terminus. We then performed immunoprecipitations from supernatants of neurons expressing V5-IIINRG1-HA using the neo-epitope-specific antibodies 7E6 and 4F10 (Fig. 5B). With both antibodies, the slightly larger β-sEGF, but not the smaller α-sEGF (lower band in upper panel of Fig. 5B), was detected, further confirming the identified BACE1 cleavage sites.

These findings demonstrate that processing of NRG1 type III by endogenous BACE1 and ADAM proteases in primary neurons results in the release of the EGF-like domain as β-sEGF and α-sEGF.

α-sEGF and β-sEGF activate ErbB3 receptors in a paracrine fashion

Myelination in the PNS is proposed to be regulated through the juxtacrine activation of ErbB receptors on Schwann cells by the NRG1 type III NTF-tethered EGF-like domain on axonal membranes (Wang et al., 2001; Birchmeier and Nave, 2008). In particular, stimulation of ErbB3 receptor phosphorylation and subsequent activation of the downstream PI3 kinase signaling pathway has been shown to promote PNS myelination (Newbern and Birchmeier, 2010). Because we were able to show that the EGF-like domain of NRG1 type III is liberated by BACE1 and ADAM17, we also investigated whether these small, sEGF domains were functional and if they could signal through ErbB3 receptors in a paracrine fashion. We expressed α-sEGF and β-sEGF in CHO wt cells and collected conditioned media (Fig. 6A). MCF-7 cells that express the ErbB3 receptor and are known to allow monitoring of NRG1 signaling via ErbB3 (Luo et al., 2011) were then incubated with the conditioned media containing equal concentrations of α-sEGF or β-sEGF or with supernatants from cells transfected with an empty vector. The ability of the sEGF domains to activate ErbB3 receptors and initiate PI3 kinase downstream signaling was monitored via phosphorylation of ErbB3 and AKT. Stimulation with 0.5 nM recombinant NRG1 EGF-like domain served as a positive control. Western blot analysis of total and phosphorylated levels of ErbB3 and AKT confirmed robust activation of both receptor and downstream signaling pathway upon stimulation with α-sEGF and β-sEGF (Fig. 6B, left). No significant differences between α-sEGF and β-sEGF in ErbB3 and AKT activation were observed (Fig. 6C).

In contrast to the smaller α-sEGF, β-sEGF contains a serine/threonine-rich sequence that can be O-glycosylated (Fig. 3C). To determine whether this difference in glycosylation affects activation of ErbB3 and AKT signaling we expressed α-sEGF and β-sEGF in CHO ldlD cells (Kingsley et al., 1986), which are deficient in O-linked glycosylation (Fig. 6A). Treatment of MCF-7 cells with conditioned media containing α-sEGF or nonglycosylated β-sEGF again stimulated activation of ErbB3 and AKT signaling in a very similar way (Fig. 6B, right; C). This suggests that O-linked glycosylation does not significantly alter the ability of β-sEGF to activate and signal through ErbB3 receptors.

Schwann cells are the recipient cells of NRG1 type III-mediated signaling during PNS myelination. Therefore, we repeated the experiments described above and incubated purified rat primary Schwann cells with α-sEGF and β-sEGF. Western blot analysis of phosphorylated ErbB3 and AKT levels in these cells confirmed our previous results. No difference in the activation of ErbB3 and AKT was observed upon stimulation with either α-sEGF or glycosylated or nonglycosylated β-sEGF (Fig. 6D).

These findings are in conflict with a recent study claiming an inhibitory effect of ADAM17-processed NRG1 type III on PNS
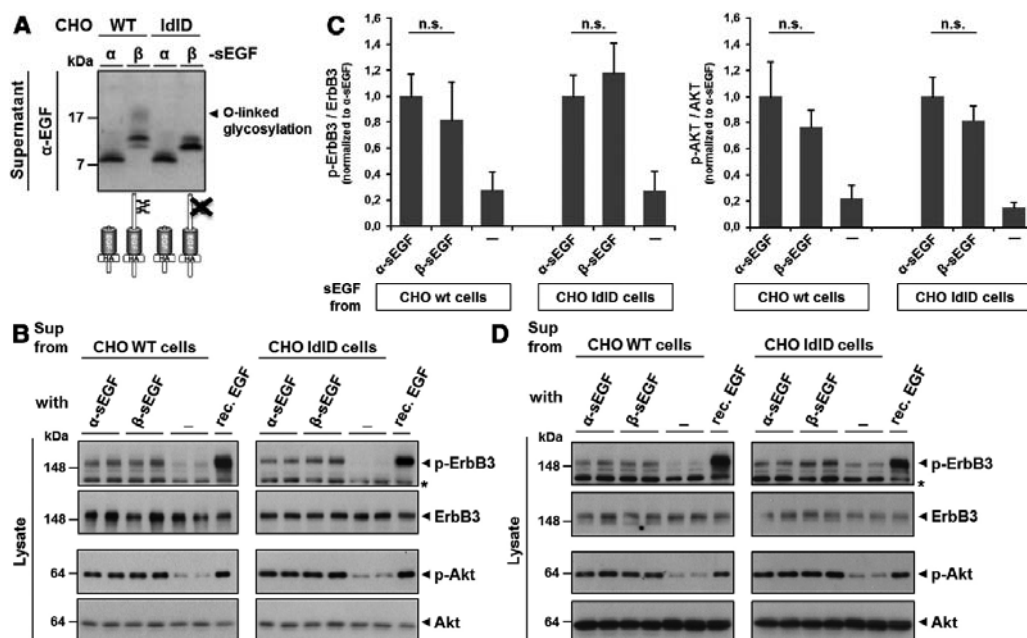
Figure 6. sEGF domains activate ErbB3 receptors on MCF-7 and Schwann cells and initiate AKT downstream signaling. *A*, Preparation of a-sEGF and glycosylated and nonglycosylated β-sEGF using CHO cells. α-sEGF and β-sEGF constructs were expressed in wt and *O*-glycosylation deficient (ldlD) CHO cells. Conditioned supernatants were analyzed by Western blotting and the concentrations of α-sEGF and β-sEGF were adjusted by dilution with medium from control cells. *O*-linked glycosylation causes β-sEGF to migrate as an additional and diffuse band of higher molecular weight, which is abolished in CHO ldlD cells. *B–D*, α-sEGF and β-sEGF activate ErbB3 receptors and AKT signaling in MCF-7 and primary Schwann cells independently of glycosylation. MCF-7 cells (*B*) and primary Schwann cells (*D*) were incubated with supernatants from *A* or from cells expressing an empty vector as a control. A recombinant NRG1 EGF-like domain (0.5 nM) was used as a positive control. After cell lysis, the levels of (phosphorylated) ErbB3 and AKT were determined by Western blotting. Quantification of phosphorylated protein/total protein ratio of experiments with MCF-7 cells is shown in *C* (mean ± SD; n.s., not significant, *$p < 0.05$, **$p < 0.01$, ***$p < 0.001$, two-tailed unpaired Student's t test, $n = 3$).

myelination (La Marca et al., 2011). In this study, a slightly different ADAM17 cleavage site (G290) was identified. Moreover, although a recombinant NRG1 EGF-like domain cleaved by BACE1 induced AKT signaling in Schwann cells, an ADAM17-cleaved fragment failed to do so. We therefore investigated whether the different cleavage sites found for ADAM17 (G290 and A283) may explain the discrepancy in signaling of ADAM17- and BACE1-generated sEGF. We constructed sEGF domains that only differ in their very C-terminal residues. β-sEGF-F was designed to end with F293, simulating BACE1 processing, whereas β-sEGF-G terminates at G290, mimicking the ADAM17 cleavage site proposed by La Marca et al. (2011). Conditioned media containing similar amounts of the peptides (Fig. 7A) were then used to stimulate MCF-7 (Fig. 7B,C) and rat primary Schwann cells (Fig. 7D) as before. No difference in ErbB3 activation or induction of downstream AKT signaling in these cells was observed upon stimulation with β-sEGF-F or β-sEGF-G.

These findings demonstrate that sEGF domains generated from NRG1 type III by BACE1 and ADAM17 are biologically active and signal through ErbB3 receptors on Schwann cells in a paracrine manner.

β-sEGF promotes PNS myelination *in vivo*

We also investigated whether the sEGF domain possesses signaling activity *in vivo*. We expressed the BACE1-derived β-sEGF in homozygous mutant *bace1* (*bace1⁻/⁻*) zebrafish (van Bebber et al., 2013) and investigated whether the β-sEGF could compensate for the lack of BACE1-mediated NRG1 type III processing. To visualize myelination *in vivo*, we generated *bace1⁻/⁻* mutants expressing GFP under the control of the *claudin k* promoter, which labels Schwann cells and oligodendrocytes (Fig. 8A,B; Münzel et al., 2012). Phenotypically, *bace1* homozygous zebrafish mutants become distinguishable from their wt siblings at 3 dpf due to severely reduced Schwann cell myelination (Fig. 8A,B). Myelination of lateral line axons by Schwann cells in the PNS is severely impaired, whereas myelination of Mauthner axons by oligodendrocytes in the CNS is unaffected (Fig. 8A,B). The observed selective hypomyelination in the PNS of *bace1⁻/⁻* zebrafish is consistent with the reduced myelination of BACE1 knock-out mice (Willem et al., 2006). To determine whether paracrine signaling could stimulate myelination, *bace1⁻/⁻* zebrafish carrying the *claudin k*:GFP transgene were injected with β-sEGF mRNA and analyzed at 3 dpf for rescued myelination. In 24 of 63 *bace1⁻/⁻* zebrafish, hypomyelination in the PNS was partially rescued upon expression of β-sEGF (Fig. 8B,C).

Finally, we used our zebrafish model to further test *in vivo* whether the C terminus of the EGF-like domain generated by ADAM17 cleavage abolishes its signaling capacity, as observed by La Marca et al. (2011). We injected mRNA encoding a NRG1 type III EGF-like domain terminating at either G290 (β-sEGF-G; La Marca et al., 2011) or A283 (β-sEGF-A; this study) into *bace1⁻/⁻* zebrafish. Both mRNAs partially rescued the PNS hypomyelina-
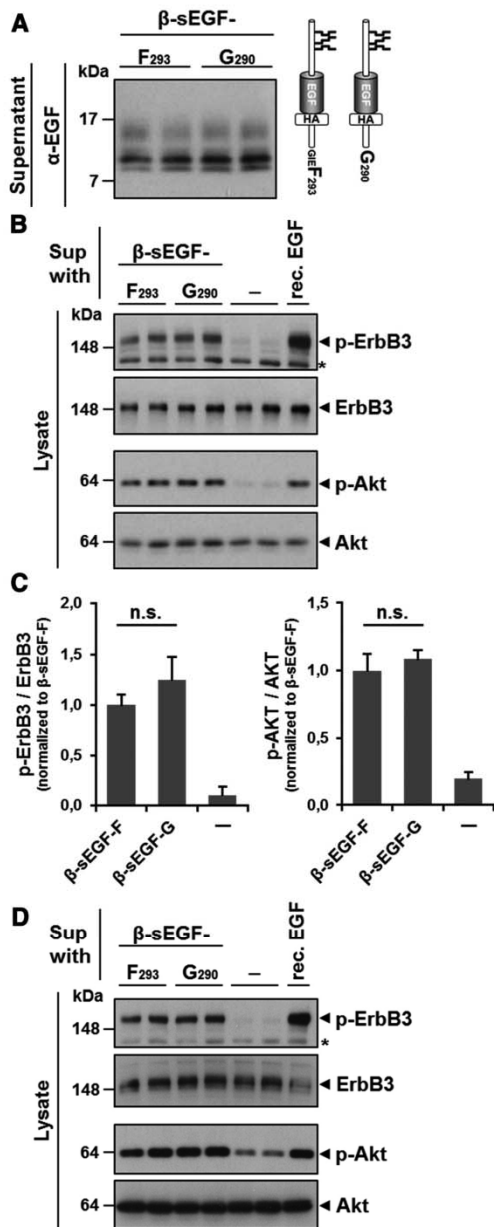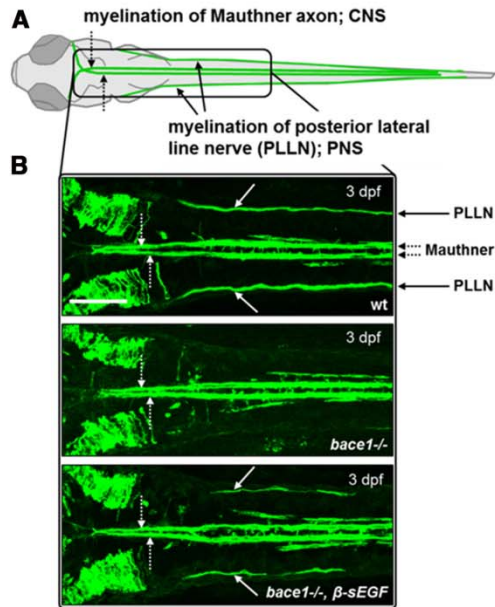
Figure 7. β-sEGF generated by BACE1- or ADAM17-mediated shedding similarly activates ErbB3 receptors and AKT downstream signaling *A*, β-sEGF-F and β-sEGF-G mimic shedding of NRG1 type III by BACE1 and ADAM17. The constructs β-sEGF-F and β-sEGF-G have identical N termini but comprise C termini generated by either BACE1- or ADAM17-mediated shedding: F293, BACE1 shedding; G290, ADAM17 shedding (see Results for details). Conditioned supernatant was collected from CHO wt cells and analyzed by Western blot. *B–D*, β-sEGF-F and β-sEGF-G activate ErbB3 receptors and AKT signaling in MCF-7 and primary Schwann cells. MCF-7 cells (*B*) and primary Schwann cells (*D*) were incubated with supernatants from *A* or from

Figure 8. The soluble NRG1 type III EGF-like domain liberated by BACE1 promotes PNS myelination *in vivo*. *A*, The transgenic *claudin k*:GFP line allows visualization of myelin sheaths in zebrafish larvae. Schematic view of *claudin k*:GFP labeled myelin around Mauthner axons (CNS, dotted arrows) and lateral line axons (PNS, arrows) at 3 dpf (dorsal view). *B*, The sEGF domain rescues PNS myelination defect in *bace1*$^{-/-}$ zebrafish carrying the *claudin k*:GFP transgene. Dorsal views of wt, uninjected *bace1* mutants (*bace1*$^{-/-}$) and *bace1* mutants injected with β-sEGF mRNA (*bace1*$^{-/-}$, β-sEGF). Middle: In *bace1*$^{-/-}$ mutants myelination of the Mauthner axons (dotted arrows) is not affected, whereas myelination of the lateral line axons is severely reduced to absent (arrows in other panels). Bottom: Upon injection of β-sEGF mRNA, *bace1*$^{-/-}$ mutants display a partial rescue of hypomyelination in the PNS. Scale bar, 100 μm. *C*, sEGF domains generated by ADAM17-mediated shedding of NRG1 type III also promote PNS myelination. In addition to β-sEGF (*B*), β-sEGF constructs with C termini mimicking ADAM17 mediated shedding (β-sEGF-G290 and β-sEGF-A283; see Results for details) were injected into *bace1*$^{-/-}$ mutant zebrafish. Regardless of their very C-terminal residues, all constructs partially rescued the hypomyelination phenotype.

←

cells expressing an empty vector as a control. Recombinant NRG1 EGF-like domain (0.5 nM) was used as a positive control. Cells were lysed and levels of (phosphorylated) ErbB3 and AKT were determined by Western blotting. Quantification of phosphorylated protein/total protein ratio of experiments with MCF-7 cells is shown in *C* (mean ± SD; n.s., not significant, *$p < 0.05$, **$p < 0.01$, ***$p < 0.001$, two-tailed unpaired Student's *t* test, $n = 3$).

tion, similar to the rescue observed with β-sEGF (Fig. 8C). Although it is not possible to compare quantitatively the extent of the rescue effects, the results nevertheless provide strong evidence that the ADAM17-cleaved C terminus of the EGF-like domain does not abolish its signaling ability, as was claimed previously (La Marca et al., 2011).

In conclusion, our findings demonstrate that the sEGF domain of NRG1 type III liberated by N-terminal BACE1 cleavage promotes PNS myelination *in vivo*.

Discussion

Release of growth factors by proteolytic processing has emerged as an important regulator of many signaling pathways. For example, shedding particularly regulates signaling of ErbB receptor ligands (Sanderson et al., 2006). Sheddases either generate signaling-competent, membrane-retained proteins or release ectodomains that subsequently signal in a paracrine manner. At the same time, ectodomain shortening also triggers intramembrane cleavage of the remaining membrane fragments by intramembrane-cleaving proteases, releasing the substrate's intracellular domains into the cytosol, which may then act as transcription factors (Blobel et al., 2009; Lal and Caplan, 2011).

NRG1 type III is subject to such processing, which is also called regulated intramembrane proteolysis (Brown et al., 2000). Shedding in its stalk region activates NRG1 type III by generating a membrane-anchored NTF that presents the EGF-like domain to the luminal space and signals to ErbB receptors in a juxtacrine/contact-dependent manner (Falls, 2003; Taveggia et al., 2005). In addition, the resulting NRG1 CTF is cleaved by the γ-secretase and regulates transcription in neurons (Bao et al., 2003, 2004; Chen et al., 2010). Analysis of knock-out mouse models established BACE1 and ADAM17 as important NRG1 type III sheddases that control myelination in the PNS. Although BACE1-mediated shedding of NRG1 type III promotes myelination (Hu et al., 2006; Willem et al., 2006), shedding by ADAM17 was shown to inhibit this process (La Marca et al., 2011). This differential regulation was suggested to be due to small differences in the C termini of the NRG1 type III NTFs generated after shedding by BACE1 or ADAM17 (La Marca et al., 2011).

Despite the proposed importance, most NRG1 type III cleavage sites have only been investigated *in vitro* using short recombinant peptides in cleavage assays. Moreover, although the CTF resulting from shedding is eventually turned over by the γ-secretase, little is known about further processing of the corresponding NTF. It has been suggested that cleavage close to its N-terminal cysteine-rich TMD could release a large, soluble fragment containing the EGF-like domain (Wang et al., 2001). However, it remained unclear which proteases could mediate such a second cleavage event and whether the resulting soluble protein would possess signaling activity. We have now analyzed proteolytic processing of NRG1 type III in living cells to investigate whether, indeed, an sEGF domain was generated. To confirm the biological activity of such an sEGF domain, we generated a zebrafish mutant that lacks BACE1 and allows *in vivo* rescuing assays.

We first investigated the cleavages occurring between the EGF-like domain and the C-terminal TMD. Consistent with Montero et al. (2000), who suggested that the region from methionine 282 to tyrosine 286 may be a site of ADAM-mediated cleavage, we now assigned the ADAM17 cleavage to alanine 283 and, to a minor extent, to phenylalanine 285. Cleavage between alanine 283 and serine 284 fits well with the substrate preference of ADAM 17, which is known to favor alanine residues at the P1

position and to cleave several substrates with serine at P1′ (Caescu et al., 2009). For BACE1 and ADAM10, we report cleavage sites after phenylalanine 293 and phenylalanine 285, respectively, thereby confirming previous data from assays with recombinant proteins (Hu et al., 2008, Luo et al., 2011). In the case of ADAM10, we also observed cleavage after tyrosine 286, which has not been reported previously. These findings demonstrate homogenous shedding of NRG1 type III by BACE1 10 residues N-terminal of the TMD and heterogeneous shedding by ADAM10 and ADAM17 at close but distinct sites 7–10 residues N-terminal of the BACE1 cleavage site. We note that the shedding sites reported here for ADAM10 (Y286) and ADAM17 (A283 and F285) differ from the sites reported by others (La Marca et al., 2011; Luo et al., 2011). For ADAM10, the difference is marginal and may be due to the different experimental setups, namely *in vitro* digest of recombinant peptides (Luo et al., 2011) and cellular expression system (this study). For ADAM17, it is currently unclear why Luo et al. (2011) and we could not observe cleavage after G290 as reported by La Marca et al. (2011). However, the fact that the cleavage site motifs of ADAM10 and ADAM17 are fairly similar to each other and that both enzymes can cleave peptides *in vitro* at the same peptide bonds (Caescu et al., 2009) support our finding of close cleavage sites for these proteases within the stalk region of NRG1 type III.

BACE1- and ADAM-mediated shedding of NRG1 type III was also detected under endogenous protease levels in primary neurons. Although we cannot compare the contribution of individual proteases quantitatively, we observed additive effects of BACE1 and ADAM inhibitors, supporting the idea that these enzymes compete for shedding in the stalk region of NRG1 type III in neurons.

In addition to the shedding events taking place C-terminal of the EGF-like domain, we observed proteolytic processing at novel sites located N-terminal of the EGF-like domain, which indicated that the EGF-like domain may be secreted. We observed liberation of the EGF-like domain from NRG1 type III by additional N-terminal cleavages in HEK cells and primary neurons generating α-sEGF and β-sEGF. Using MS and site-specific antibodies, we were able to demonstrate that BACE1 is responsible for the N-terminal cleavage generating β-sEGF in both cell types. Interestingly, the novel BACE1 cleavage site resembles the BACE1 cleavage site in APP with the Swedish mutation. This mutation dramatically increases the affinity of BACE1 to its substrate (Citron et al., 1992, 1995), strongly indicating that this site may be used efficiently *in vivo*. In addition to BACE1, ADAM17 (but not ADAM10) was also found to cleave at another novel site close to the N terminus of the EGF-like domain, thereby generating α-sEGF. The detection of a similar fragment in the supernatant of primary neurons expressing NRG1 type III suggests that α-sEGF is generated by ADAM17-mediated cleavage in these cells as well. However, due to the lack of antibodies against the novel ADAM17 cleavage site, we currently cannot exclude an additional contribution of other ADAMs.

Both α-sEGF and β-sEGF are functionally active and induce ErbB3 receptor phosphorylation and AKT downstream signaling in MCF-7 and Schwann cells. Moreover, we demonstrated the *in vivo* signaling potential of β-sEGF as an instructive factor in the process of peripheral myelination, because β-sEGF was able to rescue the peripheral hypomyelination in a *bace1* mutant zebrafish.

Our data are in agreement with a recent study reporting paracrine stimulation of Schwann cells and myelination by recombinant NRG1 type III (Syed et al., 2010). However, whereas this

study used a mixture of recombinant peptides comprising the entire NRG1 type III N terminus, we now provide evidence for the generation of signaling-competent, soluble NRG1 type III fragments by BACE1- and ADAM17-mediated proteolysis. Unfortunately, it is not possible to generate an N-terminally uncleavable NRG1 type III NTF, so we cannot investigate whether NRG1 type III signaling in the context of myelination occurs exclusively via the sEGF domain. However, our results, together with the data of others (Syed et al., 2010), suggest that this novel paracrine signaling pathway may at least partially contribute to NRG1 type III signaling.

We observed a similar activation of ErbB3 and AKT in Schwann cells after stimulation with ADAM17-generated α-sEGF (C terminus A283) and BACE1 generated β-sEGF (C terminus F293). In contrast, others did not detect such activation upon stimulation with an EGF-like domain cleaved by ADAM17 (C terminus G290, La Marca et al., 2011). Because this was attributed to the very C-terminal residues of the EGF-like domain, we sought to reconcile these controversial findings by investigating the impact of these residues on ErbB activation. However, we could not detect any difference regarding ErbB signaling between sEGF domains terminating at the identified BACE1 (F293) or the ADAM17 cleavage sites (A283 and G290). Likewise, neither C termini attributed to ADAM17 cleavage prevented rescue of the hypomyelination phenotype in a $bace1^{-/-}$ zebrafish model. Moreover, in support of our findings, another study recently found no difference in ErbB activation by the membrane-anchored EGF-like domain after BACE1 (C terminus F293) or ADAM10 (C terminus F285, which excludes G290) processing (Luo et al., 2011). We currently have no definite explanation for the observed discrepancies; however, in vitro digests with recombinant peptides and enzymes imply the risk of additional cleavages that would not occur in a cellular environment. Such an additional cleavage within the EGF-like domain might abolish its signaling capacity and could partially account for the observed differences.

In summary, we have shown here that cleavage of NRG1 type III by BACE1 and ADAM17 at as-yet-unknown sites releases the EGF-like domain from its membrane anchor and allows for paracrine signaling of NRG1 type III via ErbB receptors. The proteases involved in NRG1 type III processing are major drug targets in the prevention or therapy of Alzheimer's disease and cancer (Duffy et al., 2011; Vassar and Kandalepas, 2011). The fact that these proteases have multiple—and until now unappreciated— roles in NRG1 signaling calls for caution when manipulating their activities in the course of therapy.

References

Bao J, Wolpowitz D, Role LW, Talmage DA (2003) Back signaling by the Nrg-1 intracellular domain. J Cell Biol 161:1133–1141. CrossRef Medline

Bao J, Lin H, Ouyang Y, Lei D, Osman A, Kim TW, Mei L, Dai P, Ohlemiller KK, Ambron RT (2004) Activity-dependent transcription regulation of PSD-95 by neuregulin-1 and Eos. Nat Neurosci 7:1250–1258. CrossRef Medline

Birchmeier C, Nave KA (2008) Neuregulin-1, a key axonal signal that drives Schwann cell growth and differentiation. Glia 56:1491–1497. CrossRef Medline

Black RA, Rauch CT, Kozlosky CJ, Peschon JJ, Slack JL, Wolfson MF, Castner BJ, Stocking KL, Reddy P, Srinivasan S, Nelson N, Boiani N, Schooley KA, Gerhart M, Davis R, Fitzner JN, Johnson RS, Paxton RJ, March CJ, Cerretti DP. (1997) A metalloproteinase disintegrin that releases tumour-necrosis factor-alpha from cells. Nature 385:729–733. CrossRef Medline

Blobel CP, Carpenter G, Freeman M (2009) The role of protease activity in ErbB biology. Exp Cell Res 315:671–682. CrossRef Medline

Brinkmann BG, Agarwal A, Sereda MW, Garratt AN, Müller T, Wende H, Stassart RM, Nawaz S, Humml C, Velanac V, Radyushkin K, Goebbels S, Fischer TM, Franklin RJ, Lai C, Ehrenreich H, Birchmeier C, Schwab MH, Nave KA (2008) Neuregulin-1/ErbB signaling serves distinct functions in myelination of the peripheral and central nervous system. Neuron 59:581–595. CrossRef Medline

Brown MS, Ye J, Rawson RB, Goldstein JL (2000) Regulated intramembrane proteolysis: a control mechanism conserved from bacteria to humans. Cell 100:391–398. CrossRef Medline

Caescu CI, Jeschke GR, Turk BE (2009) Active-site determinants of substrate recognition by the metalloproteinases TACE and ADAM10. Biochem J 424:79–88. CrossRef Medline

Cai XD, Golde TE, Younkin SG (1993) Release of excess amyloid beta protein from a mutant amyloid beta protein precursor. Science 259:514–516. CrossRef Medline

Capell A, Steiner H, Willem M, Kaiser H, Meyer C, Walter J, Lammich S, Multhaup G, Haass C (2000) Maturation and propeptide cleavage of beta-secretase. J Biol Chem 275:30849–30854. CrossRef Medline

Chen Y, Hancock ML, Role LW, Talmage DA (2010) Intramembranous valine linked to schizophrenia is required for neuregulin 1 regulation of the morphological development of cortical neurons. J Neurosci 30:9199–9208. CrossRef Medline

Citron M, Oltersdorf T, Haass C, McConlogue L, Hung AY, Seubert P, Vigo-Pelfrey C, Lieberburg I, Selkoe DJ (1992) Mutation of the beta-amyloid precursor protein in familial Alzheimer's disease increases beta-protein production. Nature 360:672–674. CrossRef Medline

Citron M, Teplow DB, Selkoe DJ (1995) Generation of amyloid beta protein from its precursor is sequence specific. Neuron 14:661–670. CrossRef Medline

De Strooper B, Vassar R, Golde T (2010) The secretases: enzymes with therapeutic potential in Alzheimer disease. Nat Rev Neurol 6:99–107. CrossRef Medline

Duffy MJ, Mullooly M, O'Donovan N, Sukor S, Crown J, Pierce A, McGowan PM (2011) The ADAMs family of proteases: new biomarkers and therapeutic targets for cancer? Clin Proteomics 8:9. CrossRef Medline

Einheber S, Zanazzi G, Ching W, Scherer S, Milner TA, Peles E, Salzer JL (1997) The axonal membrane protein Caspr, a homologue of neurexin IV, is a component of the septate-like paranodal junctions that assemble during myelination. J Cell Biol 139:1495–1506. CrossRef Medline

Falls DL (2003) Neuregulins and the neuromuscular system: 10 years of answers and questions. J Neurocytol 32:619–647. CrossRef Medline

Haass C (2004) Take five-BACE and the gamma-secretase quartet conduct Alzheimer's amyloid beta-peptide generation. EMBO J 23:483–488. CrossRef Medline

Horiuchi K, Zhou HM, Kelly K, Manova K, Blobel CP (2005) Evaluation of the contributions of ADAMs 9, 12, 15, 17, and 19 to heart development and ectodomain shedding of neuregulins beta1 and beta2. Dev Biol 283:459–471. CrossRef Medline

Hu X, Hicks CW, He W, Wong P, Macklin WB, Trapp BD, Yan R (2006) Bace1 modulates myelination in the central and peripheral nervous system. Nat Neurosci 9:1520–1525. CrossRef Medline

Hu X, He W, Diaconu C, Tang X, Kidd GJ, Macklin WB, Trapp BD, Yan R (2008) Genetic deletion of BACE1 in mice affects remyelination of sciatic nerves. FASEB J 22:2970–2980. CrossRef Medline

Karey KP, Sirbasku DA (1988) Differential responsiveness of human breast cancer cell lines MCF-7 and T47D to growth factors and 17 beta-estradiol. Cancer Res 48:4083–4092. Medline

Kimmel CB, Ballard WW, Kimmel SR, Ullmann B, Schilling TF (1995) Stages of embryonic development of the zebrafish. Dev Dyn 203:253–310. CrossRef Medline

Kingsley DM, Kozarsky KF, Hobbie L, Krieger M (1986) Reversible defects in O-linked glycosylation and LDL receptor expression in a UDP-Gal/UDP-GalNAc 4-epimerase deficient mutant. Cell 44:749–759. CrossRef Medline

Lal M, Caplan M (2011) Regulated intramembrane proteolysis: signaling pathways and biological functions. Physiology (Bethesda) 26:34–44. CrossRef Medline

La Marca R, Cerri F, Horiuchi K, Bachi A, Feltri ML, Wrabetz L, Blobel CP, Quattrini A, Salzer JL, Taveggia C (2011) TACE (ADAM17) inhibits Schwann cell myelination. Nat Neurosci 14:857–865. CrossRef Medline

Lichtenthaler SF, Haass C, Steiner H (2011) Regulated intramembrane proteolysis–lessons from amyloid precursor protein processing. J Neurochem 117:779–796. CrossRef Medline

Ludwig A, Hundhausen C, Lambert MH, Broadway N, Andrews RC, Bickett DM, Leesnitzer MA, Becherer JD (2005) Metalloproteinase inhibitors for the disintegrin-like metalloproteinases ADAM10 and ADAM17 that differentially block constitutive and phorbol ester-inducible shedding of cell surface molecules. Comb Chem High Throughput Screen 8:161–171. CrossRef Medline

Luo X, Prior M, He W, Hu X, Tang X, Shen W, Yadav S, Kiryu-Seo S, Miller R, Trapp BD, Yan R (2011) Cleavage of neuregulin-1 by BACE1 or ADAM10 protein produces differential effects on myelination. J Biol Chem 286:23967–23974. CrossRef Medline

Mei L, Xiong WC (2008) Neuregulin 1 in neural development, synaptic plasticity and schizophrenia. Nat Rev Neurosci 9:437–452. CrossRef Medline

Michailov GV, Sereda MW, Brinkmann BG, Fischer TM, Haug B, Birchmeier C, Role L, Lai C, Schwab MH, Nave KA (2004) Axonal neuregulin-1 regulates myelin sheath thickness. Science 304:700–703. CrossRef Medline

Monk KR, Talbot WS (2009) Genetic dissection of myelinated axons in zebrafish. Curr Opin Neurobiol 19:486–490. CrossRef Medline

Montero JC, Yuste L, Díaz-Rodríguez E, Esparís-Ogando A, Pandiella A (2000) Differential shedding of transmembrane neuregulin isoforms by the tumor necrosis factor-alpha-converting enzyme. Mol Cell Neurosci 16:631–648. CrossRef Medline

Münzel EJ, Schaefer K, Obirei B, Kremmer E, Burton EA, Kuscha V, Becker CG, Brösamle C, Williams A, Becker T (2012) Claudin k is specifically expressed in cells that form myelin during development of the nervous system and regeneration of the optic nerve in adult zebrafish. Glia 60:253–270. CrossRef Medline

Newbern J, Birchmeier C (2010) Nrg1/ErbB signaling networks in Schwann cell development and myelination. Semin Cell Dev Biol 21:922–928. CrossRef Medline

Okochi M, Steiner H, Fukumori A, Tanii H, Tomita T, Tanaka T, Iwatsubo T, Kudo T, Takeda M, Haass C (2002) Presenilins mediate a dual intramembranous γ-secretase cleavage of Notch-1. EMBO J 21:5408–5416. CrossRef Medline

Orozco D, Tahirovic S, Rentzsch K, Schwenk BM, Haass C, Edbauer D (2012) Loss of fused in sarcoma (FUS) promotes pathological Tau splicing. EMBO Rep 13:759–764. CrossRef Medline

Perlin JR, Lush ME, Stephens WZ, Piotrowski T, Talbot WS (2011) Neuronal Neuregulin 1 type III directs Schwann cell migration. Development 138:4639–4648. CrossRef Medline

Sanderson MP, Dempsey PJ, Dunbar AJ (2006) Control of ErbB signaling through metalloprotease mediated ectodomain shedding of EGF-like factors. Growth Factors 24:121–136. CrossRef Medline

Sastre M, Steiner H, Fuchs K, Capell A, Multhaup G, Condron MM, Teplow DB, Haass C (2001) Presenilin-dependent gamma-secretase processing of beta-amyloid precursor protein at a site corresponding to the S3 cleavage of Notch. EMBO Rep 2:835–841. CrossRef Medline

Shirakabe K, Wakatsuki S, Kurisaki T, Fujisawa-Sehara A (2001) Roles of Meltrin beta /ADAM19 in the processing of neuregulin. J Biol Chem 276:9352–9358. CrossRef Medline

Syed N, Reddy K, Yang DP, Taveggia C, Salzer JL, Maurel P, Kim HA (2010) Soluble neuregulin-1 has bifunctional, concentration-dependent effects on Schwann cell myelination. J Neurosci 30:6122–6131. CrossRef Medline

Taveggia C, Zanazzi G, Petrylak A, Yano H, Rosenbluth J, Einheber S, Xu X, Esper RM, Loeb JA, Shrager P, Chao MV, Falls DL, Role L, Salzer JL (2005) Neuregulin-1 type III determines the ensheathment fate of axons. Neuron 47:681–694. CrossRef Medline

Turk B, Turk du SA, Turk V (2012) Protease signalling: the cutting edge. EMBO J 31:1630–1643. CrossRef Medline

van Bebber F, Hruscha A, Willem M, Schmid B, Haass C (2013) Loss of Bace2 in zebrafish affects melanocyte migration and is distinct from Bace1 knock out phenotypes. J Neurochem. Advance online publication. Retrieved February 14, 2013. doi:10.1111/jnc.12198. CrossRef Medline

Vassar R, Kandalepas PC (2011) The β-secretase enzyme BACE1 as a therapeutic target for Alzheimer's disease. Alzheimers Res Ther 3:20. CrossRef Medline

Velanac V, Unterbarnscheidt T, Hinrichs W, Gummert MN, Fischer TM, Rossner MJ, Trimarco A, Brivio V, Taveggia C, Willem M, Haass C, Möbius W, Nave KA, Schwab MH (2012) Bace1 processing of NRG1 type III produces a myelin-inducing signal but is not essential for the stimulation of myelination. Glia 60:203–217. CrossRef Medline

Wang JY, Miller SJ, Falls DL (2001) The N-terminal region of neuregulin isoforms determines the accumulation of cell surface and released neuregulin ectodomain. J Biol Chem 276:2841–2851. CrossRef Medline

Wild-Bode C, Fellerer K, Kugler J, Haass C, Capell A (2006) A basolateral sorting signal directs ADAM10 to adherens junctions and is required for its function in cell migration. J Biol Chem 281:23824–23829. CrossRef Medline

Willem M, Garratt AN, Novak B, Citron M, Kaufmann S, Rittger A, DeStrooper B, Saftig P, Birchmeier C, Haass C (2006) Control of peripheral nerve myelination by the beta-secretase BACE1. Science 314:664–666. CrossRef Medline

Wolpowitz D, Mason TB, Dietrich P, Mendelsohn M, Talmage DA, Role LW (2000) Cysteine-rich domain isoforms of the neuregulin-1 gene are required for maintenance of peripheral synapses. Neuron 25:79–91. CrossRef Medline

213